Characterization and elucidation of genomic modifiers of DJ-1 and LRRK2 animal models of Parkinson's disease

Paul C. Marcogliese

Thesis submitted to the

Faculty of Graduate and Postdoctoral Studies

in partial fulfillment of the requirements

for the Doctorate in Philosophy degree in Neuroscience

Department of Cellular and Molecular Medicine

Faculty of Medicine

University of Ottawa

Abstract:

Parkinson's disease (PD) is a common neurodegenerative disorder symptomatically characterized by motor dysfunction caused by the selective loss of nigral dopamine neurons within midbrain. The pathogenesis of PD remains unclear. Although, originally thought to be sporadic, about ten percent of PD is familial. The recent elucidation of mutations in genes linked to the disease has offered potential for new animal models and understanding of PD pathogenesis. DJ-1 and LRRK2 are genes linked to autosomal recessive juvenile-onset PD and autosomal-dominant late onset PD, respectively. How mutations in these two genes leads to PD remains uncertain and is plagued by poor murine models that do not recapitulate the human condition. The following dissertation attempts to characterize both mouse and fly models of DJ-1 and LRRK2 mediated PD and elucidate other genetic modifiers that may contribute to PD. Firstly, the DJ-1 null mouse model, which lacks cell death, was improved by backcrossing to a pure C57-Bl6 background. These DJ-1 null mice display a robust and progressive unilateral-to-bilateral loss of nigral neurons accompanied by motor deficits in aged mice. Secondly, a large scale screen was performed in *Drosophila* to determine genes that modify mutant LRRK2 toxicity in both the eye and dopaminergic neurons of the fly. The screen revealed 36 genetic interactors that either suppressed or enhanced LRRK2 induced cell death in the fly. One of these interactors was SCAR (human WAVE-2). Due to the role WAVE-2 is known to have in immune cell phagocytic function, we demonstrate that LRRK2 deficient/G2019S murine myeloid cells have impaired/enhanced phagocytic activity which is correlated with a decrease/increase in WAVE-2 protein, respectively. We furthermore suggest that LRRK2 and WAVE-2 may

bind directly and that LRRK2 phosphorylates WAVE-2 to maintain its stability. Finally, as a proof of concept, we constructed a novel animal model of LRRK2 in flies by limiting LRRK2 over expression to central phagocytes of the *Drosophila* brain. This causes lifespan deficits and motor dysfunction that can be rescued by down-regulation of SCAR. Collectively, this body of work helped create the first germ-line, genetic model of PD that recapitulates nigral loss and elucidated LRRK2 interactors in the fly. Furthermore, we demonstrate that one of these interactors mediated LRRK2's modulation of phagocytic activity that may contribute to the pathogenesis of PD.

Table of Contents: **Page Number**

List of Tables:

List of Figures:

List of Abbreviations:

+/+	Wild-type
+/-	Heterozygous
-/-	Homozygous
ΔFosB	ΔFBJ murine osteosarcoma viral oncogene homolog B
6-OHDA	6-hydroxydopamine
AV	Adeno Virus
ADP	Adenosine DiPhosphate
ANOVA	ANalyis Of VAriance
AD	Autosomal Dominant
ANK	Ankyrin
AO	Age at Onset
AR	Autosomal Recessive
ARM	Armadillo
ATP	Adenosine TriPhosphate
BAC	Bacterial Artificial Chromosome
BBB	Blood-brain barrier
Ca2+	Calcium
CCCP	Carbonyl Cyanide m-Chloro Phenyl hydrazine
CCW	Counter-clockwise
CD11b	Cluster of Differentiation 11b
CMA	Chaperone Mediated Autophagy
CME	Clathrin-mediated Endocytosis

CNS	Central Nervous System
COMT	Catechol-O-methyl transferase
COR	C-terminal of Roc
COX-2	Cyclooxygenase-2
CSF	Cerebral Spinal Fluid
CV	Cresyl Violet
CW	Clockwise
DAT	Dopamine Transporter
DBS	Deep Brain Stimulation
DIV	Days In Vitro
DNA	DeoxyriboNucleic Acid
Drp1	Dynamin-related protein 1
EO	Early onset
ER	Endoplasmic Reticulum
ERAD	Endoplasmic Reticulum Associated Degradation
ETC	Electron Transport Chain
FBS	Fetal Bovine Serum
GBA	β-GlucocereBrosidAse
GFP	Green Fluorescent Protein
GP	Globus Pallidus
GPe	Globus Pallidus external segment
GPi	Globus Pallidus internal segment
GST	Glutathione S-Transferase

GWAS	Genome Wide Association Studies
h	hour
H_2O_2	Hydrogen Peroxide
HEK293	Human Embryonic Kidney 293
Het	Heterozygous
Hom	Homozygous
Hz	Hertz
IFN-γ	Interferon gamma
iPD	Idiopathic Parkinson's disease
iPSC	induced Pluripotent Stem Cells
IL-1β	Interlukin-1β
IL-6	Interlukin-6
i.p.	Intraperitoneal
JO	Juvenile onset
KI	Knock-In
KifC5b	Kinesin family member C5b
KO	Knock-Out
LB	Lewy Body
LC	Locus Coeruleus
L-DOPA	Levodopa
LPS	Lipopolysaccharide
LRR	Leucine-rich repeats
LRRK1	Leucine-Rich Repeat Kinase 1

LRRK2	Leucine-Rich Repeat Kinase 2
LSD	Least significant difference
MAO	Monoamine Oxidase
MAPKKK	Mitogen-Activated Protein Kinase Kinase Kinase
MEF	Mouse Embryonic Fibroblast
mo	months
MPP+	1-Methyl-4-PhenylPyridinium ion
MPPP	1-Methyl-4-Phenyl-4-Propionoxy Piperidine
MPTP	1-Methyl-4-Phenyl-1,2,5,6-TetrahydroPyridine
MQC	Mitochondrial Quality Control
mRNA	messenger Ribosomal Nucleic Acid
mtDNA	mitochondrial Deoxyribonucleic acid
MTN	Medial Terminal Nucleus
NLRP3	NLR family, pyrin domain–containing 3
NNT	nicotinamide nucleotide transhydrogenase
NS	Not significant
NSAID	Non-Steroidal Anti-Inflammatory Drug
NSF	N-ethylmaleimide Sensitive Fusion
OMM	Outer Mitochondrial Membrane
PBS	Phosphate Buffered Saline
PD	Parkinson’s disease
PINK1	PTEN-induced putative kinase 1
PTEN	Phosphatase and Tensin homolog

REM	Rapid Eye Movement
RNAi	Ribonucleic acid interference
RNS	Reactive Nitrogen Species
Roc	Ras-like GTPase domain
ROS	Reactive Oxygen Species
s.c.	Subcutaneous
SDS	Sodium Dodecyl Sulfate
SEM	Standard Error of the Mean
Sfr1	SWI5-dependent recombination repair 1
shRNA	small hairpin Ribonucleic Acid
Sirbp1A	Signal Regulatory protein β1A
siRNA	small interfering Ribonucleic Acid
SNARE	Soluble NSF Attachment Protein Receptor
SNc	Substantia Nigra pars compacta
SNP	Single Nucleotide Polymorphisms
SNr	Substantia Nigra pars reticulata
SRY	Sex-determining region Y
SSRI	Selective Serotonin Reuptake Inhibitor
STN	SubThalamic Nucleus
STR	Striatum
TAG	Triacylglycerol
TFAM	Mitochondrial Transcription Factor A
Tg	Transgenic

TH+	Tyrosine Hydroxylase positive
TLR4	Toll-like Receptor 4
TNF-α	Tumor Necrosis Factor-α
UPR	Unfolded Protein Response
UPS	Ubiquitin-Proteasome System
VPS35	Vacuolar protein Sorting-associated Protein 35
VTA	Ventral Tegmental Area
WES	Whole-exome Sequencing
WGS	Whole-genome Sequencing
wk	Week
WT	Wild-type
Zswim6	zinc finger, SWIM domain containing 6

Acknowledgements:

As a student who only discovered the wonders of science after an Arts degree and then had to obtain high school science credits at the age of twenty-three to undertake a BSc, I am deeply grateful for the opportunity to conduct research in Dr. David Park's lab. I am thankful for over six years of support and guidance from Dr. Park. Our lab manager Steve Callaghan has been vital to my research over the years. I would like to personally thank my mentor, Dr. Maxime Rousseaux for his faith and patience. Deep thanks go to my advisory committee: Dr. Antonio Colavita, Dr. Diane Lagace and Dr. Michael Schlossmacher. I would like to thank Dr. Lagace for all of her, Mirela, and Chris' help with Behaviour Core. Also, I would like to thank Dr. Schlossmacher for the both scientific discussions and his kinship. I am grateful to everyone the Park lab. Particularly, I am indebted to Dr. Sarah Hewitt, Dr. Elizabeth Abdel-Messih, Katie Don-Carolis, Sameera Abuaish, Dr. Kwang Soo Kim, Dr. Jungwoo Yang, Dr. Yasmilde Rodriguez Gonzalez and Dr. Dianbo Qu. I have also been very lucky to mentor many undergrads including: Sarah Seang, Cindy Wei, Amanda Perozzo and Francis Lebrun, all of which were vital to completing the fly studies.

Thank you to the Departments of Neuroscience and Cellular & Molecular Medicine at uOttawa. I would also like to thank both the Parkinson's Research Consortium and Parkinson's Society of Canada for financial support throughout my studies.

Salute to my friends: Alem Berhane and Kwaku Boafo, we knew we'd all be doing 'big things'. I do owe thanks to a former partner, Ashley for her support was always appreciated. Thank you Moriah Trowell, you have helped me during my most

difficult time during this journey and I hope to spend my life making that up to you. I am privileged to have meet Shelby Hayter who has both motivated and inspired my work. Lastly, I would like to thank and dedicate this dissertation to my parents, Mark and Gail, whose never-ending support will always be remembered and is encouraging.

List of Manuscripts:

Chapter 2:

Rousseaux MW, **Marcogliese PC**, Qu D, Hewitt SJ, Seang S, Kim RH, Slack RS, Schlossmacher MG, Lagace DC, Mak TW, Park DS. Progressive dopaminergic cell loss with unilateral-to-bilateral progression in a genetic model of Parkinson disease. Proceedings of the National Academy of Sciences. 2012 Sep 25;109(39):15918-23.

Cited as "Very good" by F1000 Prime (Brundin P and Steiner J, 27 Mar 2013. F1000Prime.com/717979278#eval793471212)

Chapter 3:

Marcogliese PC, Abuaish S, Kabbach G, Abdel-Messih E, Seang S, Li G, Slack RS, Haque ME, Venderova K, Park DS. LRRK2-I2020T functional genetic interactors modifying eye degeneration and dopaminergic cell loss in Drosophila. *In prep to submit to PLOS Genetics.*

Chapter 4:

Kim KS*, **Marcogliese PC*,** Yang JW, LeBrun F, Abdel-Messih E, Kabbach G, Slack RS, Venderova K, Schlossmacher MG, Park, DS. LRRK2 regulates phagocytosis via direct phosphorylation of the actin-nucleating complex, WAVE-2. *In prep to submit to Nature Cell Biology.*

*contributed equally

Appended Manuscripts:

I. Rousseaux MW, **Marcogliese PC**, Qu D, Hewitt SJ, Seang S, Kim RH, Slack RS, Schlossmacher MG, Lagace DC, Mak TW, Park DS. Progressive

dopaminergic cell loss with unilateral-to-bilateral progression in a genetic model of Parkinson disease. Proceedings of the National Academy of Sciences. 2012 Sep 25;109(39):15918-23.

Cited as "Very good" by F1000 Prime (Brundin P and Steiner J, 27 Mar 2013. F1000Prime.com/717979278#eval793471212)

II. Aleyasin H, Rousseaux MW, **Marcogliese PC**, Hewitt SJ, Irrcher I, Joselin AP, Parsanejad M, Kim RH, Rizzu P, Callaghan SM, Slack RS. DJ-1 protects the nigrostriatal axis from the neurotoxin MPTP by modulation of the AKT pathway. Proceedings of the National Academy of Sciences. 2010 Feb 16;107(7):3186-91.

. *Cited as "Must Read" by F1000 Neuroscience (Thomas B, Beal M: 2010. F1000.com/1927965#eval1482064)*

III. Sanchez G, Varaschin RK, Büeler H, **Marcogliese PC**, Park DS, Trudeau LE. Unaltered striatal dopamine release levels in young Parkin knockout, Pink1 knockout, DJ-1 knockout and LRRK2 R1441G transgenic mice. PloS one. 2014 Apr 14;9(4):e94826.

IV. Qu D, Hage A, Don-Carolis K, Huang E, Joselin A, Safarpour F, **Marcogliese PC,** Rousseaux MW, Hewitt SJ, Huang T, Im DS. BAG2 Gene-mediated Regulation of PINK1 Protein Is Critical for Mitochondrial Translocation of PARKIN and Neuronal Survival. Journal of Biological Chemistry. 2015 Dec 18;290(51):30441-52.

Chapter 1: General Introduction to Parkinson's disease

1.1 - Parkinson's disease

Descriptions of an affliction causing tremulous motion, weakened strength and forward leaning posture were first documented in ancient Chinese and traditional Indian texts dating back to more than three thousand years ago. Aspects of this disease were then partially described in the 17th and 18th centuries in Europe (Goetz, 2011). However, it was the British physician Dr. James Parkinson who fully characterized this chronic and progressive disorder in the essay *'The Shaking Palsy'* (Parkinson, 1817). Parkinson's disease (PD) is the second most common neurodegenerative disorder, following Alzheimer's disease, and is the most common neurodegenerative disorder primarily affecting movement (de Lau and Breteler, 2006). Currently, PD affects over four million people worldwide (Huse et al., 2005). Aging is the largest risk factor for developing PD and there is a sizeable aging population entering the mid-21st century. Therefore, PD stands to cause a significant increase in burden to patients, caregivers and healthcare networks across the globe.

1.1.1 - Epidemiology

The age of onset of PD is typically negatively skewed, with a sharp increase of incidence at approximately 60 years of age (de Lau and Breteler, 2006). In Canada, the mean age at onset (AO) of symptoms is 64.4 and of diagnosis about 66.2 years old (Wong et al., 2014). The incidence of PD shows a 2:1 bias in males to females in cases with early onset (EO) (<50 years at diagnosis), but balances out after menopause, possibly due to the suggested neuroprotective actions of estrogen (de Lau and Breteler, 2006; Shulman, 2007). It was thought that rural living conferred increase risk to PD, however this remains controversial and seems to be significantly correlated other

variables such as farming or pesticide use (Wirdefeldt et al., 2011). Within Canada, there are approximately 55,000 current PD patients and a predicted increase with an aging population (Wong et al., 2014). Currently the socio-economic burden of PD costs Canadians over two hundred million dollars in direct costs and five hundred million dollars indirect costs annually (Brain, 2007; Findley, 2007). Consequently, determining new therapeutic avenues and understanding of PD is important to us all.

1.2 - Diagnosis and Symptomology of PD

PD is classically characterized by primary motor symptoms that include; bradykinesia, resting tremor, muscular rigidity and impaired gait (Jankovic, 2008). These motor symptoms are thought to be predominantly caused by the loss of dopaminergic neurons within the *Substantia Nigra pars compacta* (SNc) (to be further discussed in section 1.3.1). In fact, traditionally, diagnosis is only confirmed *post-mortem* after brain histology of nigral cell loss. However, a highly trained neurologist using a simple neurological exam can correctly diagnose PD over ninety percent of the time (Hughes et al., 2002). More recently, secondary non-motor symptoms, some of which are suggested to present prior to any motor disturbances, have been of increased study. Non-motor related symptoms may include: autonomic dysfunction, neuropsychiatric disorders, olfactory dysfunction, and sleep disruption. Although PD symptoms do not directly cause early death, people with PD do tend to succumb to early death in comparison to healthy individuals (Lang and Lozano, 1998). Common causes of death typically include choking, falls, or pneumonia.

1.2.1 - Motor symptoms

The symptomatic onset and presentation of particular motor symptoms may be heterogeneous in PD patients. The majority of patients (~70%) first notice a unilateral tremor that eventually spreads to a bilateral phenotype in more advanced stages of the disease. Many patients suffer from stiffness or rigidity as muscles feel tightened which is usually followed by slowness of movement known as bradykinesia. An additive effect of these symptoms can lead to postural dysfunction. This is typically a stooped posture. In very advanced cases of PD, swallowing and voluntary respiration may become extremely difficult (Jankovic, 2008).

1.2.2 - Non-motor symptoms

In recent decades, focus on non-motor related symptoms in PD has been of increased study. In part, this has been due to an effort to diagnose PD earlier and is complemented by more detailed patient history than in previous generations. PD patients are of increased risk of developing dementia compared to age-matched controls (Aarsland et al., 2001; 2003). Some cognitive impairment can also occur before PD diagnosis (Cooper et al., 1991). Similarly, there is an increase in mood disorders, anxiety, and depression in PD patients (Stein et al., 1990; Reijnders et al., 2008). Sleep disturbances, most commonly a failure to achieve adequate paralysis during the rapid eye movement (REM) sleep phase may also predict PD and future motoric dysfunction (Mouret, 1975; Stocchi et al., 1998; Gjerstad et al., 2007; Bjørnarå et al., 2015). The vast majority of patients succumb to some level of loss of smell. Olfactory dysfunction of some kind has been described in 98% of PD patients and typically presents itself prior to the onset of motor symptoms (Doty et al., 1988; Chaudhuri and Naidu, 2008; Haehner et al., 2011). Additionally, it is common for patients to suffer autonomic dysfunction prior

to motor symptoms. These usually present as gastrointestinal problems, typically constipation (Edwards et al., 1993; Adams-Carr et al., 2015).

1.3 - Pathophysiology of PD

Overwhelmingly, the focus of PD pathophysiology has been on the death of dopaminergic neurons within the SNc and subsequent motor symptoms. However, it is important to note other affected areas of the central nervous system (CNS) as well as the periphery (to be discussed in section 1.4.1). In the CNS, this is primarily a reduction of the three monoamines: dopamine (DA), noradrenaline (NA), and serotonin (5-HT) (Scatton et al., 1983).

1.3.1 - Dopaminergic loss in the Substantia nigra

Motor dysfunction in PD is predominantly characterized by the progressive loss of DA neurons within the SNc within the basal ganglia. These pigmented, neuromelanin-expressing and pace-making (2-4 Hz) neurons have cell bodies that reside in the SNc, while their axons project and innervate mostly interneurons in the caudate nucleus and putamen (humans) or collectively termed (particularly in rodents) striatum (STR) (Surmeier et al., 2010). Clinically, reports suggest that only after a loss of 50 to 70 percent of cells in the SNc, does the onset of PD motor symptoms occur in patients (Postuma et al., 2010). Consequently, evidence suggests that there are compensatory mechanisms at the level of the STR that may include dendritic sprouting of striatal interneurons (Tekumalla et al., 2001). However, eventually these potential mechanisms fail to innervate the nigrostriatal axis as DA output from the SNc decreases. Ultimately this results in decreased innervation of the motor cortex, which results in motor deficits. More specifically, there are both direct and indirect nigrostriatal pathways. These two

pathways are mediated by release of DA from the SNc to the STR. Within the STR, D_1 (direct pathway, excitatory) and D_2 (indirect pathway, inhibitory) receptors bind DA on mostly medium spiny neurons. The direct pathway sends inhibitory signals to the internal part of the Globus Pallidus (GPi), that in turn inhibits the thalamus; and in PD results in a subsequent decrease in activation of the motor cortex. The indirect pathway sends inhibitory signals to the external part of the Globus Pallidus (GPe) that results in inhibition of the Subthalamic Nucleus (STN) from GPi activation. However, in PD, inhibition of the STN is decreased which in turn activates the GPi that causes an increase in inhibition of the thalamus, and again a decrease in activation of the motor cortex (Graybiel, 2000)(See Figure 1.1). Interestingly, this loss of SNc neurons in PD is typically unilateral at symptom onset and will eventually affect both sides of the body at later stages of PD. It is unclear as to why differential loss of nigral neurons and subsequent symptomatic unilateralism exists (Hoehn and Yahr, 1967).

A remarkable feature of SNc loss observed in PD is the fact that the dopaminergic neurons of the Ventral Tegmental Area (VTA) are relatively spared. Accordingly, some research has focused on studying the differences between these two dopaminergic clusters (Surmeier et al., 2011; Pacelli et al., 2015). This resistance of the VTA is important as dopamine replacement therapy (see section 1.5) but may lead to VTA mediated side-effects in PD patients such as gambling or sex addiction as well as obsessive compulsive disorder (Ambermoon et al., 2011).

Figure 1.1: The nigrostriatal pathway in Parkinson's disease

Dopaminergic neurons in the SNc project to the dorsolateral putamen. Red arrows indicate inhibitory signals as green indicates excitatory signals. The thickness of each arrow indicates the relative strength of transmission. In sum, loss of SNc output to the STR results in an increase of inhibition of the thalamus via both indirect (D_2 mediated) and direct (D_1 mediated) pathways which in turn leads to diminished activation of the primary motor cortex in Parkinson's disease.

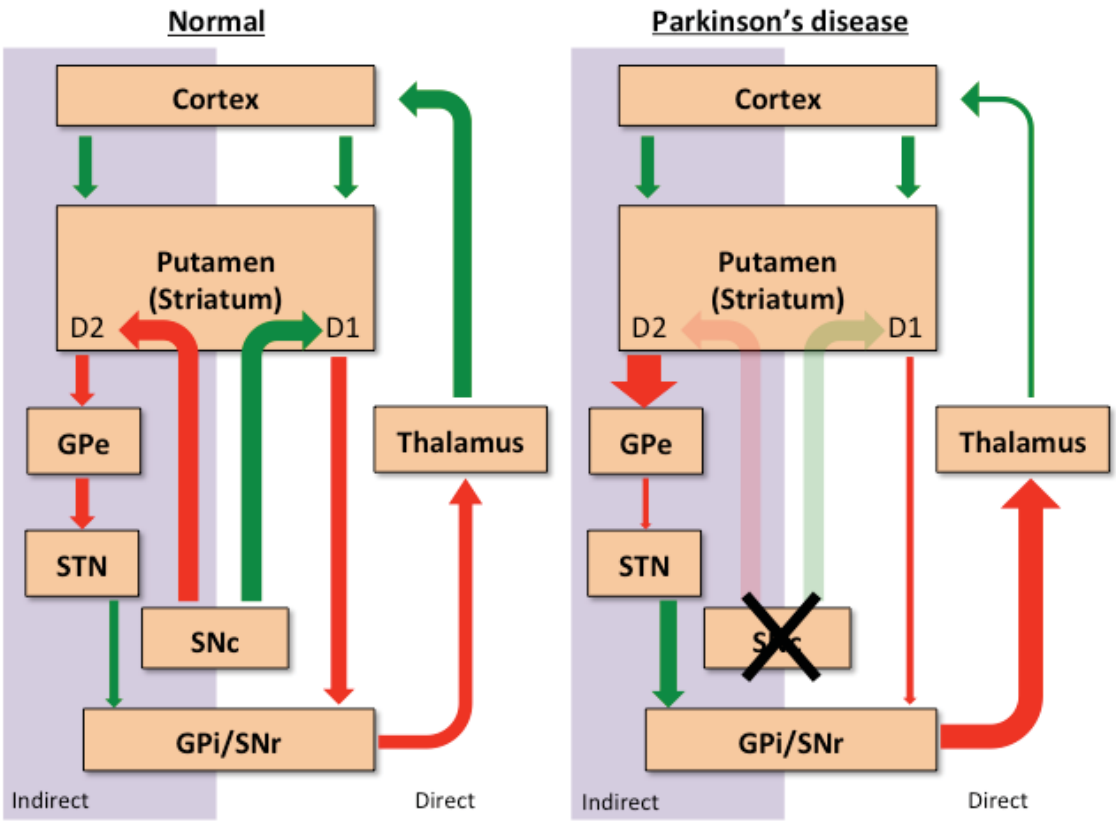
Normal
Cortex
Putamen
(Striatum)
D2
D1
GPe
STN
SNc
GPi/SNr
Thalamus
Indirect
Direct
Parkinson's disease
Cortex
Putamen
(Striatum)
D2
D1
GPe
STN
GPi/SNr
Thalamus
Indirect
Direct

1.3.2 - Noradrenergic loss in the Locus Coeruleus

Many PD patients also display loss of a subset of neuromelanin containing NA neurons within the *locus coeruleus* (LC) (Zweig et al., 1993; Zarow et al., 2003). While the pathology is described in more advanced cases, disturbances in this region correlate well with REM sleep problems observed many patients; and REM sleep patterns have been associated to the LC (Boeve et al., 2007). Additionally, the LC is associated with anxiety and its dysfunction in PD may at least partially explain the comorbidity of anxiety disorders with PD (Lauterbach et al., 2003).

1.3.3 - Serotonergic loss in the Raphe nucleus

An often-overlooked pathological observation in PD brains *post-mortem* is the loss of 5-HT neurons within the median raphe nucleus of the pons (Halliday et al., 1990). This correlates with the approximate 30-40% incidence of depression in PD patients (Blonder and Slevin, 2011). This secondary symptom to the primary motor symptoms of PD is commonly treated with both Selective Serotonin Reuptake Inhibitors (SSRIs) and cognitive behavioral therapy.

1.4 - Cellular Pathology in PD

A significant number of surviving DA neurons in the SNc contain cytoplasmic inclusions in both the soma and neurites, termed Lewy bodies or Lewy neurites, respectively. These inclusions are aggregates of misfolded proteins showing robust ubiquitin and α-synuclein (a familial PD gene) positive staining (Kuzuhara et al., 1988; Spillantini et al., 1997). It remains unclear as to the precise role that Lewy bodies play in PD. This has left the field somewhat divided between prion-like transmission of misfolded α-synuclein and Lewy bodies being a precursor to death (discussed further in

section 1.8.1), or observing Lewy bodies as potentially protective. However, it should be noted that not all PD patients display Lewy Body pathology (possibly due to Parkinsonism disorders) and that incidental Lewy Bodies do occur in 'healthy' individuals.

1.4.1 - The Braak Hypothesis

Lewy body pathology is not restricted to only the SNc and other rostral nuclei affected by PD. Efforts to stage the progression of PD has suggested that in fact Lewy bodies become present in other areas of the brain and body including the olfactory bulb and/or the enteric nervous system of the gut prior to midbrain pathology (Braak et al., 2002; 2003a). This pathology correlates well with the previously discussed loss of olfaction and gastrointestinal problems observed in many PD patients. While correlating clinical progression with pathology at time of death, Braak and colleagues have developed a hypothesis that Lewy body pathology may spread (possibly due to the a proposed prion-like nature of misfolded α-synuclein) from the enteric nervous system via the vagus nerve to eventually hit the midbrain. As PD progresses, pathology spreads in a rostral fashion throughout the brain. It should be noted that this pathological observation by Braak and colleagues may be an artifact of case selection and thus still remains controversial in the field (Dickson, 2012). However, the Braak hypothesis is supported by the extracellular propagation theory of α-synuclein (discussed further in section 1.8.1) that could be a mechanism for the seeding required for the spread of the pathology. Overall, the Braak hypothesis has peaked interest in the field as the nasal epithelium and the gastro-intestinal system both may provide an interface for a suspected environmental contribution to the pathogenesis of PD (Braak et al., 2003b).

1.5 - Current Therapy in PD

1.5.1 - Dopamine replacement

Unfortunately, therapies for PD have remained relatively unchanged for the past five decades. The gold standard treatment has been DA replacement by oral Levodopa (L-DOPA) intake (Fehling, 1966; Mercuri and Bernardi, 2005). L-DOPA is a precursor to DA that will provide DA to the nigrostriatal pathway. Used in conjunction with Carbidopa to increase L-DOPA bioavailability in the brain, many patients experience a reduction of motor symptoms for what has been termed the "honeymoon period". Over time patients notice a decrease in benefit from each dose and debilitating side-effects known as dyskinesias (Stocchi et al., 2010). Again, this treatment does not cease or slow PD progression and L-DOPA treatment is also associated with side-effects including mood changes, psychosis, and addictions (Evans and Lees, 2004). Determining the appropriate dose of L-DOPA has been a challenge due to its rapid metabolism and may require hourly intake. Usually in conjunction with L-DOPA therapy, DA agonists are used to achieve a similar goal of increasing DA bioavailability. This has also been accomplished via monoamine oxidase (MAO) inhibitors and catechol-O-methyl transferase (COMT) inhibitors.

1.5.2 - Deep brain stimulation

Although an invasive surgery, deep brain stimulation (DBS) has shown significant results in helping curb the motor symptoms of PD (Benabid et al., 2005). DBS involves the surgical insertion of bilateral electrodes to the GP or the STN. Once turned on, the electrodes stimulate these neurons to compensate for circuitry changes in the nigrostriatal pathway, and allow for appropriate motor function. There are a number of

screening criteria for choosing appropriate patients to undergo DBS that include: a correct idiopathic PD (iPD) diagnosis, advanced severity of illness, L-DOPA responsiveness, and absence of cognitive impairment (Marconi et al., 2008). It is still unclear how effective DBS may be for patients that do not fit the selection criteria.

1.5.3 - Other treatments

The potential therapeutic use of stem cells in neurodegenerative disease has been both exciting and marked with challenges. Exogenous fetal stem cell grafts have been shown to have potential in preliminary studies, however double blind studies carried out with sham surgeries revealed little benefit as well as graft-induced dyskinesias (Brundin et al., 2010). There may also be complications by tissue rejection by the patient's immune system. It is still unclear if these grafts lead to proper integration into the basal ganglia circuitry. Furthermore, it has been observed that Lewy body pathology spreads to grafted tissue and may, at best, only delay PD progression (Kordower et al., 2008).

One of the most effective, practical, and economical treatment methods that have been reported to increase quality of life in patients has been physiotherapy. While this therapy will not delay the symptoms of PD, the activity and exercise involved is suggested to make symptoms more manageable (Goodwin et al., 2008).

1.6 - Pathogenesis of PD

The underlying cause(s) of PD and nigral degeneration in general have remained elusive. However, insights from both epidemiological and genetic data has led to insight on the possible mechanism(s) involved. Epidemiological studies have implicated pesticide use and heavy metals as factors that may increase PD risk (Barbeau et al., 1987; Moretto and Colosio, 2013; Ward et al., 2014; Chen et al., 2015). Notably, in the early

1980s, an unfortunate group of drug users developed rapid (7-14 days) and advanced Parkinsonism caused by 1-methyl-4-phenyl-1,2,3,6-tetrahydropyridine (MPTP) contamination during synthetic heroin production (Langston et al., 1983). Both MPTP and pesticides such as rotenone and paraquat will be discussed further in detail as toxin models of PD.

The next landmark in PD research was twin-studies demonstrating a putative role for genetics in the disease. Up until this point PD was mainly thought to be idiopathic in nature. However, Tanner and colleagues showed that, at least with EO cases of PD, there was a significant concordance rate in monozygotic twins given their sample size (Tanner et al., 1999). A genetic component of the disease was furthermore confirmed in linkage analysis of families with apparent heritability (Polymeropoulos et al., 1996). It is now is estimated that about 10% of PD may be familial with a strong genetic component, however, it should be noted that not all pathogenic mutations in these genes display complete penetrance of the disease (Klein and Westenberger, 2012). The field now has 6 confirmed genes with pathogenic mutations linked to classical PD (to be discussed further in section 1.8). Additionally, 9 genes have been linked to atypical Parkinsonism that are typically from consanguineous families and display extrapyramidal symptoms (Verstraeten et al., 2015).

It has been thought that for the majority of PD cases that have no known family history, a genetic component may confer disease risk. More recent findings discovered so-called susceptibility genes by utilizing genome wide association studies (GWAS). This method examines data of both common and rare single nucleotide polymorphisms (SNPs) or most recently due to lowering costs, whole genome or whole exome

sequencing (WGS or WES, respectively). By examining associations between SNPs or rare variants in large populations of people with iPD compared to healthy age matched controls, we can determine what variants associate (or not) with the idiopathic disease. GWAS have determined over 25 candidate genes that may be involved in conferring risk of developing PD (Verstraeten et al., 2015).

The above milestones in PD research have allowed the field to begin elucidating what cellular pathways may be involved in PD, particularly, nigral death. Taking evidence from epidemiological, genetic and PD brain pathology, multiple cellular pathways have emerged as potential pathogenic mechanisms. These are: 1) protein quality control and recycling, 2) mitochondrial homeostasis, 3) oxidative stress, 4) neuroinflammation and, 5) vesicular trafficking (Cook et al., 2012; Esposito et al., 2012; Hirsch et al., 2012; Arena and Valente, 2015; Blesa et al., 2015).

1.6.1 - Protein quality control

One of the most striking pathological hallmarks of PD is the presence of Lewy bodies. These aggregates of misfolded proteins typically do not arise in a healthy cell as the unfolded protein response (UPR), ubiquitin-proteasome system (UPS) and autophagy pathways may be activated to remove deficient cellular components such as proteins and organelles as required.

Protein misfolded within the endoplasmic reticulum (ER) causes ER stress signals to activate the UPR pathway. UPR activation leads to activation of chaperones to ensure proper folding and may lead to activation of ER associated degradation (ERAD) to eliminate misfolded proteins. Extended ER stress may lead to activation of apoptotic pathways to perform programmed cell death. Evidence for both ER stress and UPR

activation has been observed in the SNc of PD patients *post-mortem* (Hoozemans et al., 2007). Parkinson's related pathogenic mutations in α-synuclein have been shown to increase UPR activation by increasing levels of classical UPR markers such as: CHOP and phosphorylated eIF2α leading to increased cell death (Smith et al., 2005). Additionally, pathogenic α-synuclein has further been shown to physically inhibit ATF6 that leads to disruption of the ERAD pathway (Credle et al., 2015).

Another classical method of maintaining proteostasis in the cell is via the ubiquitin-proteasome system (UPS). Briefly, this utilizes a network of broad-to-specific ubiquitin-activating (E1), -conjugating (E2), and – ligating (E3) enzymes to tag identified proteins with ubiquitin monomers for degradation by the proteasome. Parkinson's related mutations in the Parkin gene are responsible for a substantial portion of juvenile onset (JO) PD (Kitada et al., 1998; Lücking et al., 2000). Parkin is an E3 ligase responsible for sending target proteins to the proteasome. PD related Parkin mutations result in an accumulation of these proteins (Imai et al., 2000; Shimura et al., 2000). Furthermore, mice with conditional dopaminergic ablation of Psmc1, an essential component of the 26S proteasome, exhibit both neuronal death and α-synuclein positive inclusions (Bedford et al., 2008).

The cell also utilizes lipid membranes for a process called autophagy to sequester and degrade cellular components in the lysosome for recycling. This can be performed by lysosomal engulfment of material directly (microautophagy), the formation of a lipid bilayer called an autophagosome around the material to degrade prior to lysosomal fusion (microautophagy), and finally chaperone-mediated autophagy (CMA), which is highly selective and mediated by the hsc70 chaperone. The PD genes Parkin and PINK1 have

been associated with a subtype of macroautophagy that is specific for removal of damaged mitochondria termed mitophagy (Vives-Bauza et al., 2010). However, both of these genes as well as other PD genes including α-synuclein, LRRK2, and DJ-1 have all been associated with autophagy (Vogiatzi et al., 2008; Krebiehl et al., 2010; Tong et al., 2010; Winslow et al., 2010; Manzoni et al., 2013). While other studies have found α-synuclein, LRRK2, and Vacuolar protein sorting-associated protein 35 (VPS35) involved in CMA (Vogiatzi et al., 2008; Orenstein et al., 2013; Tang et al., 2015).

Taken together, there is a bulk of genetic evidence that the protein quality control pathways in the cell may be dysfunctional in PD. Interestingly, many PD toxin models of DA cell death, such as 1-methyl-4-phenylpyridinium ion (MPP+), 6-hydroxydopamine (6-OHDA), and rotenone also activate the ER stress and UPR pathways (Ryu et al., 2002). However, it is still unclear whether disruption of protein quality control is truly a pathogenic mechanism in PD or a secondary response to other cell death or damaging signals.

1.6.2 - Mitochondrial dysfunction

The evidence for mitochondria dysfunction in PD is compelling but remains controversial. *Post-mortem* analysis of PD brains reveals there is disruption of mitochondrial complex I (Mizuno et al., 1989; Schapira et al., 1989; 1990). PD patients also exhibit increased mitochondrial DNA (mtDNA) mutations specifically in the SNc compared to healthy controls (Bender et al., 2006). Furthermore, skin fibroblasts harvested from PD patients display mitochondrial abnormalities (Mortiboys et al., 2008; 2010). Toxins such as MPTP and rotenone, which may produce Parkinsonism in humans are suggested to inhibit mitochondrial complex I (OBERG, 1961; Mizuno et al., 1987;

Cleeter et al., 1992; Li et al., 2003). Conditional ablation of mitochondrial transcription factor A (TFAM) in dopaminergic neurons of mice causes both nigral DA loss and L-DOPA responsive motor deficits (Ekstrand et al., 2007). This reveals DA neurons are heavily relient on mitochondrial function for survival.

Autosomal recessive (AR) genes implicated in JO-PD: Parkin, PINK1 and DJ-1, have been implicated in mitochondrial homeostasis. Mitochondrial quality control involves Parkin dependent clearance of dysfunctional mitochondria and fission and fusion mechanisms to combat cellular stress (to be discussed in section 1.8). Dominant genes such as α-synuclein and LRRK2 have also been implicated in mitochondrial health as well (to be discussed in section 1.8). However, it should be noted that many of the cellular studies implicating impaired mitochondrial clearance (mitophagy) have not been performed in neurons and/or rely on overexpression paradigms (Parkin overexpression).

It has been suggested that the DA neurons of the SNc are one of the most energetically demanding cells of the CNS due to their pace-making requirements or relatively heavy axonal arborization (Surmeier et al., 2011; Pacelli et al., 2015). Therefore, it could be that subtle changes in mitochondrial homeostasis could eventually lead to the early death of these neurons due to intrinsic high metabolic demands of nigral DA neurons.

1.6.3 - Oxidative Stress

The generation and management of free radicals in the cell are thought to be important for redox signaling pathways in the cell. The free radical theory of aging suggests that maintenance of oxidants or any reactive oxygen species (ROS) may determine lifespan (Beckman and Ames, 1998). However, free radicals are also required

for the destruction of intracellular pathogens by immune cells. One of the main oxidants produced by the cell is superoxide. Superoxide may damage the cell when produced by the mitochondria during respiration (Brand et al., 2004). Oxidative damage may degrade many cellular components including nucleic acids, proteins and lipids, and may lead to apoptosis.

There is evidence of elevated oxidative damage in PD brains. The SNc displays increased peroxidation of lipids (Dexter et al., 1989), protein carbonylation (Alam et al., 1997) and DNA oxidation (Zhang et al., 1999) when compared to controls. Additionally, there are increased levels of free iron, which may lead to higher ROS, in the SNc of PD patients (Mann et al., 1994).

DA metabolism and DA itself can also increase oxidative stress in a cell. MAO degrades DA which produces hydrogen peroxide (H_2O_2) as a byproduct (Adams et al., 1972). This increase in H_2O_2 may lead to formation of hydroxyl radicals, by the Fenton reaction, that are highly toxic to cells (Youdim et al., 1989). Additionally, DA itself may be unstable and undergo auto-oxidation that produces DA quinones that also increase ROS (Muñoz et al., 2012).

Toxins that are associated with Parkinsonism in humans including MPTP and rotenone are associated with a robust increase in ROS (Sriram et al., 1997; Li et al., 2003). MPTP is a by-product and contaminate of synthetic heroin production and has since been shown to readily cross the blood brain barrier (BBB). Astrocytes then uptake MPTP and convert it to MPP+ via MAO-B which then enters DA neurons by the Dopamine Transporter (DAT) and subsequently causes nigral toxicity by inhibiting mitochondrial complex I of the electron transport chain (ETC). This then leads to both

ROS and reactive nitrogen species (RNS) via generation of superoxide and nitric oxide, respectively (Przedborski and Vila, 2003).

Finally, similar to the findings on mitochondrial abnormalities reviewed in section 1.6.2, mutations in familial PD genes are associated with increased oxidative stress (Lin and Beal, 2006; Henchcliffe and Beal, 2008; Hauser and Hastings, 2013). These will be discussed further in section 1.8 on familial PD.

1.6.4 - Neuroinflammation

The resident immune cells of the brain are the microglia. The origins of these "macrophages of the brain" remains controversial, however they are suggested to originate from myeloid progenitors in the periphery (Ginhoux and Prinz, 2015). In steady-state contexts, microglia survey the brain with filopodia-like processes to perform various roles in the brain including, but not limited to: synaptic pruning, destruction of pathogens that circumvent the BBB and removal of apoptotic corpses. The presence of neuroinflammation in many neurodegenerative diseases has long been thought to be a secondary pathogenesis to cell death which may exacerbate toxicity (Cappellano et al., 2013). However, recent advances in genetics, as well as the discovery of a discrete lymphatic system in the human CNS, have called for a re-examination of the role neuroinflammation may play in disease pathogenesis (Louveau et al., 2015).

Activated microglia are observed in PD brains *post-mortem* (McGeer et al., 1988; Hirsch et al., 2012). Patients with MPTP induced Parkinsonism also display activated microglia, even years after exposure (Langston et al., 1999). Prolonged activation of microglia generates elevated ROS, RNS, and cytokine release. Pro-inflammatory cytokines such as: interleukin-1β (IL-1β), interleukin-6 (IL-6), tumor necrosis factor-α

(TNF-α) and cyclooxygenase-2 (COX-2) are also elevated in PD brains (Teismann et al., 2003). Furthermore, many of these pro-inflammatory cytokines are elevated in PD patient cerebral spinal fluid (CSF) (Hirsch et al., 2012). Correlative data in humans suggests that daily ibuprofen, a non-steroidal anti-inflammatory drug (NSAID), may lower the risk of developing PD (Gao et al., 2011).

In animals models of PD, rotenone, MPTP, or paraquat cause microglia activation and an increase in pro-inflammatory cytokines (Członkowska et al., 1996; Sherer et al., 2003; Purisai et al., 2007; Ye et al., 2016). Inhibition of microglial activation via minocycline treatment can curb degeneration in the MPTP mouse model (Wu et al., 2002).

Furthermore, mice lacking interferon-gamma (IFN-γ), an immune specific gene that modulates the inflammatory response, are resistant to the MPTP toxin model of DA death (Mount et al., 2007).

Lipopolysaccharide (LPS), also known as endotoxin, is a molecule typically found on the cell wall of Gram-negative bacteria. LPS binds to toll-like receptor 4 (TLR4) which will elicit an immune response, including the release of pro-inflammatory cytokines. LPS mediated DA cell loss has been demonstrated in both cellular studies and in animals. The first studies suggested that direct injection of LPS into the SNc of rats causes microglia activation and subsequent degeneration of DA neurons (Bing et al., 1998; Castano et al., 1998). Similar studies have also been repeated in mice (Liu and Bing, 2011). One group suggested that degeneration of the SNc could occur 7-10 months after systemic LPS administration by intraperitoneal (i.p.) injection (Qin et al., 2007), however this remains controversial as it has failed to be reproduced (Jeong et al., 2010).

Interestingly, LPS is suggested to lack toxicity in other brain areas such as the hippocampus and cortex and indicates that DA neurons in the SNc may be more sensitive to microglial activation relative to other neural populations (Kim et al., 2000).

There is currently a lack of studies examining the role that familial PD genes may play in microglia activation or neuroinflammatory signaling. However, aggregated α-synuclein has been shown to activate microglia that may occur prior to any DA cell death (Su et al., 2008). Parkin null mice and LRRK2-G2019S mutant rats are hypersensitive to LPS treatment (Frank-Cannon et al., 2008; Moehle et al., 2015). In line with the mutant gain of hyper-kinase activity hypothesis of LRRK2-mediated death, LRRK2 null rats were found to be resistant to LPS (Daher et al., 2014)(Further discussed in section 1.8.6.7). Finally, DJ-1 may play a role in modulating the inflammatory response of astrocytes (Waak et al., 2009; Ashley et al., 2016). Overall, neuroinflammation may play a role in the pathogenesis of PD but evidence suggests that it may at least play a role in the progression of the disease and could be a modulatory target for therapy.

1.6.5 - Vesicular trafficking

A more recently identified potential mechanism contributing to the pathogenesis of PD has been disturbances in vesicular trafficking. Much of the evidence for vesicular trafficking deficits arises from genetic data across familial and sporadic PD. The normal function of PD-linked autosomal-dominant (AD) genes α-synuclein and VPS35 have both been implicated in vesicular formation and endosomal trafficking (Bonini and Giasson, 2005; Korolchuk et al., 2007; Munsie et al., 2015). Atypical forms of Parkinsonism have been linked to DNAJC6 and synaptojanin (SYNJ1) which both play a role in clathrin-mediated endocytosis (CME) (Edvardson et al., 2012; Quadri et al.,

2013). Lastly, GWAS studies have implicated GAK and TMEM175 to PD, which are suggested to have roles in this pathway way as well (Lee et al., 2006; Rhodes et al., 2011; Cang et al., 2015; Lill et al., 2015). However, it still remains unclear whether vesicle trafficking deficits underlie the cause of neurodegeneration in PD.

1.7 - Animals models of PD

Modeling PD has been a challenge in most model systems. As a disorder that typically affects the CNS of aged humans, research has been constrained by using animals that have much shorter lifespans. However, there are still a few avenues to explore DA cell death in vivo.

1.7.1 - Invertebrate models

The fruit fly (*Drosophila melanogaster*) has been a staple in both neurodevelopmental and neurodegenerative research. Exposure of rotenone in flies causes loss of DA clusters in the fly brain as well as locomotor deficits that are L-DOPA responsive (Coulom and Birman, 2004). Although flies lack any appropriate homolog to α-synuclein, the expression of α-synuclein mutants in the fly causes loss of DA neurons, Lewy body-like inclusions, and locomotor deficits (Feany and Bender, 2000). Similar loss of DA neurons and locomotor deficits have been seen in other Tg flies expressing LRRK2, Parkin, or VPS35 pathogenic mutants (Sang et al., 2007; Liu et al., 2008; Venderova et al., 2009; Wang et al., 2014a). Flies expressing DJ-1 mutations are sensitive to oxidative stress (Park et al., 2005), and flies missing the DJ-1 ortholog, dj-1β seem to have increased death when exposed to H_2O_2 (Menzies et al., 2005). The power and elegance of the *Drosophila* toolkit is that genes implicated in PD may be expressed in other tissues types via the well-established GAL4/Upstream Activation Sequence

(GAL4/UAS) system. This has allowed for *in vivo* suppression/enhancement screens to elucidate genetically interactions of PD genes.

The nematode (*Caenorhabditis elegans*) can also be a powerful and rapid tool for examining neuronal dysfunction related to PD. These worms are sensitive to MPP+, rotenone and 6-OHDA, which causes loss of DA neurons and locomotor deficits in the animal (Nass et al., 2001; Braungart et al., 2004; Ved et al., 2005). The expression of WT or mutant α-synuclein causes DA cell loss and locomotive defects in worms (Lakso et al., 2003). Lastly, knockdown of Parkin or DJ-1 orthologs cause increased sensitivity to oxidative stress (Ved et al., 2005). These models are consistent with PD models in *Drosophila.* Accordingly, the nematode provides another in vivo platform for studying whole gene networks that may be involved in toxin-induced or gene-mediated DA cell death.

1.7.2 - Vertebrate models

Zebrafish (*Danio rerio*) have allowed for modeling of DA cell death caused by toxins that can be merely added to the water in their environment. Novel technologies using the clustered regularly-interspaced short palindromic repeats - CRISPR associated protein 9 (CRISPR-Cas9) system of gene editing also allow for rapid generation of mutant zebrafish (Hwang et al., 2013). Zebrafish DA neurons are sensitive to MPTP and 6-OHDA and these fish display locomotor deficits (Anichtchik et al., 2004; Bretaud et al., 2004). Loss of function in PINK1, DJ-1, or Parkin orthologs causes PD-like DA cell death and motor disturbances (Bretaud et al., 2007; Flinn et al., 2009; Xi et al., 2010). LRRK2 deficiency in zebrafish was reported to causes loss of DA neurons and motor defects (Sheng et al., 2010) but failed to be reproduced (Ren et al., 2011). Loss of F-box

only protein 7 (Fbxo7), which is linked to atypical JO-PD in humans, also causes PD-like pathology in fish.

Mice are used for a multitude of toxin and genetic based models of PD. The MPTP model in mice is commonly a gold-standard approach to cause loss of DA neurons in mice. Different paradigms of MPTP exposure from acute to chronic treatment have been established in attempts to mimic death in humans (Gibrat et al., 2009). Intriguingly, rats are relatively resistant to selective DA loss with MPTP administration for reasons currently unknown (Bové et al., 2005). Direct injection of 6-OHDA causes cell loss and locomotor impairment in mice, rats, and monkeys (Mandel and Randall, 1985; Sauer and Oertel, 1994; Crofts et al., 2001; Ma et al., 2002). Models of rotenone and paraquat have been less consistent but may show future promise (Bové et al., 2005).

Mice have offered vast opportunities in genetic manipulation from gene knockouts (KOs), knock-in (KIs) and Tg over-expressors. Additionally, there are systems to conditionally KO a gene in a temporal and spatial manner. Unfortunately, the vast majority of PD models created based on genes discovered in the familial disease have failed to recapitulate the main aspects of the disease: nigral death and locomotor deficits. However, many genetic mouse models may display some intracellular abnormalities or are hypersensitive to PD toxins like MPTP (Lee et al., 2012). Conditional ablation of TFAM1, Psmc1, or sonic hedgehog (SHH) in result in DA cell loss in the SNc (Ekstrand et al., 2007; Bedford et al., 2008; Gonzalez-Reyes et al., 2012). There has also been some success causing DA cell loss using viral injection of PD related genes such as the A53T mutation of human α-synuclein (Kirik et al., 2002). However, recent genetic techniques

have allowed for Tg and KO rats to be developed which have recently showed both DA loss and motor deficits in both DJ-1 KO and PINK1 KO (Dave et al., 2014).

1.8 - Familial Parkinson's disease

It is currently estimated that about ten percent of PD is familial. There is evidence of a genetic component in iPD, but these risk alleles would not have a strong enough penetrance to display observable heritability in family pedigrees. The first discovered locus was PARK1, later to be linked to mutations in α-synuclein (SNCA) (Polymeropoulos et al., 1996). All loci found in linkage studies of families were termed PARK loci until segregating mutations in a specific gene were determined. However, currently employed strategies include WGS and WES in families has elucidated PD linked genes that fall outside previous linkage analysis. These same methods have been applied to sporadic PD in GWAS to elucidate risk alleles. There are now a total of 15 familial genes (classical and atypical). Furthermore, mutations in GBA are strongly associated with PD yet do not yet fit familial criteria. Lastly, GWAS has provided over 25 associated risk genes that may contribute to iPD.

Currently there are 6 PD linked genes that are attributed to classical PD. There are Parkin, PINK1, and DJ-1 that are linked to AR-PD and SNCA, LRRK2, and VPS35 linked to AD-PD. Additionally, there are mutations in ATP13A2, PLA2G6, FBXO7, DNAJC6, SYNJ1, EIF4G1 (may be linked to classical), ATP6AP2, COQ2, and DNAJC13 which are linked to atypical Parkinsonism (Verstraeten et al., 2015) (See Table 1.1). For the purposes of this dissertation, extended focus will be given to DJ-1 and LRRK2.

Table 1.1: Genetic of Parkinson's disease

A list of Mendelian genes linked to both classical and atypical familial PD with known age at onset and inheritance patterns. The table also described GBA, a strong risk allele for PD.

Mendelian Genes					
Gene	**Location**	**Inheritance**	**AoO**	**Primary Function**	**Reference**
SNCA	4q21	AD	EO - LO	Synaptic function	(Polymeropoulos et al., 1997)
PARKIN	6q25.2-q27	AR	JO	Mitochondrial function	(Kitada et al., 1998)
PINK1	1p36	AR	JO	Mitochondrial function	(Valente et al., 2004)
DJ-1	1p36	AR	JO	Response to oxidative stress	(Bonifati et al., 2003)
LRRK2	12q12	AD	LO	Trafficking	(Paisán-Ruiz et al., 2004)
VPS35	16q12	AD	LO	Vesicle Trafficking	(Zimprich et al., 2011)
Mendelian Genes - atypical PD					
PLA2G6	22q13.1	AR	JO	Mitochondrial function	(Paisán-Ruiz et al., 2009)
FBX07	22q12.3	AR	JO	Ubiquitination	(Shojaee et al., 2008)
ATP13A2	1p36	AR	JO	Mitochondrial function	(Ramirez et al., 2006)
DNAJC6	1p31.3	AR	JO	Synaptic function	(Edvardson et al., 2012)
SYNJ1	21q22.2	AR	JO	Synaptic function	(Quadri et al., 2013)
EIF4G1	3q27.1	AD	LO	Protein synthesis	(Chartier-Harlin et al., 2011)
ATP6AP2	Xp11.4	X-linked	JO-EO	Lysosome function	(Korvatska et al., 2013)
COQ2	4q21.23	AR	LO	Mitochondrial function	(Mitsui et al., 2013)
DNAJC13	3q22.1	AD	JO-LO	Vesicle Trafficking	(Vilariño-Güell et al., 2014)
Strongly Associated Risk Genes					
GBA	1q21	AD	LO	Lysosome function	(Tayebi et al., 2001)

1.8.1 - SNCA

Mutations in SNCA were first linked to PD in 1997 (Polymeropoulos et al., 1997). It is still unclear what function its encoded protein, α-synuclein, has in the cell. However, SNCA is ubiquitously expressed and strikingly, is a major component of Lewy Bodies. Not only have other mutations in SNCA been found in families with PD but even locus duplications, triplications, and quadruplications (Singleton et al., 2003; Chartier-Harlin et al., 2004). This suggests that not only can mutant SNCA contribute to PD, but an increase in dose of the WT SNCA may lead to PD in humans at earlier ages. These variations in SNCA may lead to either EO (dose dependently) or LO PD and are inherited in an AD fashion. SNCA also falls within a locus that is one of the shows the highest risk factor variants in sporadic PD by GWAS (Lill et al., 2012).

The prevailing thought on how SNCA may contribute to PD based on animal and cellular studies is that of SNCA stability and subsequent ability to spread an aggregate prone form of SNCA. It is suggested that in PD monomeric SNCA misfolds into oligomeric followed by fibrillar and finally aggregated beta sheet forms (Deleersnijder et al., 2013). Furthermore, it is suggested that the oligomeric and fibrillar forms may be the culprits for the spread of toxicity. Some studies suggest that these forms can cause changes to WT monomers in a prion-like manner, evidently spreading in cell-to-cell transmission (Luk et al., 2012; Volpicelli-Daley et al., 2014). SNCA remains a prominent research focus with many studies attempting to discern it's biological role in the cell and the potential mechanism underlying the spread of the fibrillar form.

1.8.2 – Parkin

Recessive mutations in the Parkin gene are responsible for approximately 50% of familial JO-PD and possibly 15% of JO sporadic PD (Abbas et al., 1999; Lücking et al., 2000). Parkin is a E3-ubiquitin ligase that has been heavily implicated in mitochondrial quality control and mitophagy. It has been proposed that another PD gene, PINK1 is stabilized at mitochondria that have lost membrane potential and recruits Parkin which then targets mitochondria for degradation (Vives-Bauza et al., 2010). Many of the studies performed *in vitro* rely on Parkin overexpression and the use of carbonyl cyanide m-chlorophenyl hydrazine (CCCP), a mitochondrial decoupler. Some suggest CCCP treatment of cells may not be physiologically relevant as other toxins tend to not produce Parkin recruitment to mitochondria (Scarffe et al., 2014). Interestingly, most PD brains that have been autopsied of patients with Parkin mutations exhibit minimal presence of Lewy bodies (Doherty and Hardy, 2013) . This suggests that there could be separate mechanisms that led to SNc death in humans.

1.8.3 - PINK1

Mutations in PINK1 are responsible for approximately 8 percent of EO familial PD (Valente et al., 2004; Mullin and Schapira, 2015). Seminal work in *Drosophila*, discovered that Parkin and PINK1 act in a similar pathway involved in mitochondrial fission/fusion and quality control. It was consistently found that Parkin expression could rescue PINK1 deficiency but not vice a versa (Park et al., 2006; Deng et al., 2008). Based on CCCP treatment studies in vitro, it thought that in a steady state PINK1 is consistently imported into the mitochondria, processed by various proteases and then released as a truncated form that is then degraded. While the model is criticized for failing to be evolutionarily parsimonious, evidence suggests that upon stress, the full length form of

PINK1 remains on the mitochondria to signal Parkin recruitment and mitophagy. It remains to be seen whether PINK1/Parkin mediated mitophagy is critical for SNc health. Lastly, although associated with Parkin, PINK1 PD brains do display some Lewy body pathology, adding to the complexity of interpreting PINK1 and Parkin in a linear pathway (Samaranch et al., 2010).

1.8.4 - VPS35

The most recent gene linked to familial LO-PD is VPS35. Mutations showing AD inheritance in VPS35 were elucidated using next generation sequencing techniques in 2011 (Vilariño-Güell et al., 2011; Zimprich et al., 2011). VPS35 is involved in retromer complex function that sorts and traffics endosomes to the trans Golgi network (Bonifacino and Hurley, 2008). However, it is still unclear how mutations in VPS35 may contribute to the pathogenesis of PD.

1.8.5 - DJ-1

Originally discovered as an a ras-dependant oncogene, mutations in *PARK7* (*DJ-1*) were linked to AR, JO-PD in 2003 (Bonifati et al., 2003). DJ-1 mutations are relatively rare and may be implicated in 1-2% of AR JO-PD (Heutink, 2006). These mutations are suggested to be loss of function, as the L166P point mutation (prevents dimer formation) (Miller et al., 2003) found in an Italian family and a 4kb genomic deletion (which removes the start codon) in a Dutch family (Clark et al., 2004). Highly oxidized DJ-1 has been found in the brains of sporadic PD patients (Choi et al., 2006).

1.8.5.1 - DJ-1 biology

The DJ-1 (PARK7) gene spans 8 exons on locus 1p36 in humans that encodes a protein of 189 amino acids. DJ-1 is part of the DJ-1/ThiJ/PfpI superfamily of proteins

that is heavily evolutionarily conserved across species (Bonifati et al., 2003; Fioravanti et al., 2008). Crystal structure studies of DJ-1 reveals that it consists of one folded domain with no quaternary structure (Wilson et al., 2003). DJ-1 forms a homodimer that is ubiquitous within the cell, as it has been found in the cytoplasm, nucleus and mitochondria.

DJ-1 is suggested to have a multitude of roles including: regulatory function in fertility, RNA binding, suppress phosphatase and tensin homolog (PTEN)-induced apoptosis, ROS scavenging and act as a molecular chaperone (Takahashi et al., 2001; Li et al., 2005; Yang et al., 2005; Shinbo et al., 2006; van der Brug et al., 2008).

1.8.5.2 - DJ-1 animal models

Similar to many other genetic PD mouse models, various DJ-1 nullizygous mice fail to display SNc or striatal terminal loss (Goldberg et al., 2005; Chen et al., 2005; Andres-Mateos et al., 2007; Manning-Boğ et al., 2007; Chandran et al., 2008; Pham et al., 2010; Ramsey et al., 2010). While some of these mice exhibited some abnormalities, it was breeding to a pure C57-Bl6 background, required for MPTP studies, that DJ-1 KO mice were hypersensitized to MPTP toxicity both in terms of DA counts in the SNc and striatal DA terminals (Kim et al., 2005).

Given the JO phenotype of DJ-1, PINK1, and Parkin mediated PD in humans, efforts were made to create a PD model by knocking out multiple genes in a mouse. A triple KO mouse characterized by Kitada and colleagues lacked any SNc degeneration (Kitada et al., 2009). At this time, the Park laboratory was conducting studies on DJ-1/PINK1 double KO mice and began to observe a striking SNc loss in a subset of DJ-1

KO controls and some double KO mice. This will be explored in Chapter 2 of this dissertation and led to the first germline genetic model of PD (Rousseaux et al., 2012).

1.8.5.3 - DJ-1: Oxidative stress

Multiple groups have reported that DJ-1 is implicated in the oxidative stress response and mitochondrial health (Aleyasin et al., 2010; Irrcher et al., 2010; Krebiehl et al., 2010; Joselin et al., 2012). In response to oxidative stress, the isoelectric point of DJ-1 shifts to more acidic forms as the sulfhydryl group of a highly conserved cysteine residue (C106 in humans) in the protein reacts with ROS forming a cysteine sulfinic acid (Taira et al., 2004; Mitsumoto et al., 2009). Similar to the hypersensitivity of DJ-1 KO mice to MPTP, primary cortical neurons lacking DJ-1 are hypersensitive to H_2O_2 treatment. Furthermore, exogenous expression of WT but not mutant DJ-1 increased survival of WT neurons following H_2O_2 treatment (Kim et al., 2005).

Several studies have shown that DJ-1 translocates to the mitochondria following oxidative stress (Canet-Avilés et al., 2004; Joselin et al., 2012). Additionally, in both mice and human lymphoblast cells derived from DJ-1 mutation carrying PD patients reveals aberrant fragmented mitochondrial morphology in which mitochondria undergo fission when under stress (Irrcher et al., 2010). Some have thought that DJ-1 can directly quench ROS via its atypical peroxiredoxin-like peroxidase activity. However, it is thought that DJ-1 is protective through other mechanism as abilities as a ROS scavengers were found to be relatively weak (Andres-Mateos et al., 2007).

DJ-1's protective role following stress has also been linked to the AKT pro-survival pathway and may be required and promote AKT phosphorylation (Aleyasin et al., 2010; Zhu et al., 2014; Jaramillo-Gómez et al., 2015; Tanti et al., 2015). Also, DJ-1

has been suggested to positively regulate the transcription of tyrosine hydroxylase (TH), the rate-limiting enzyme in DA synthesis (Ishikawa et al., 2009). The specific physiological role of DJ-1 remains unclear, however it's importance in ROS management and mitochondrial dynamics may be vital in understanding PD pathogenesis.

1.8.6 - LRRK2

Autosomal dominant (AD) mutations in the PARK8 locus on chromosome 12 were originally linked to familial PD in 2002 (Funayama et al., 2002). Two years later mutations within a gene in that locus, LRRK2 were linked to PD by two independent groups (Paisán-Ruiz et al., 2004; Zimprich et al., 2004). LRRK2 is thought to be a very important player in PD pathogenesis for a few reasons. Firstly, mutations in LRRK2 are the most commonly linked familial gene found to cause PD. Approximately 3-7% of all familial PD may be attributed to LRRK2 mutations (Lesage et al., 2005; Nichols et al., 2005). However, in certain populations, LRRK2 mutations can be responsible for upwards 20 to 40 percent of PD within Ashkenazi Jews and North African Berbers, respectively (Ozelius et al., 2006; Hulihan et al., 2008). Secondly, much of LRRK2-linked PD displays late-onset and has been noted to be clinically indistinguishable from iPD (Paisán-Ruiz, 2009). Lastly, GWAS studies have shown that variants in LRRK2 are associated with sporadic PD (Skipper et al., 2005). Consequently, understanding LRRK2s function within the cell and how pathogenic mutations lead to PD has been intensely pursued.

LRRK2 contains 41 exons and is located on chromosome 12 and 15 in the human and mouse genome respectively. The LRRK2 protein is a multi-domain protein spanning 2527 amino acids and runs at approximately at 245 kDa on SDS-PAGE gel. As a member

of the Roco superfamily of proteins, LRRK2 contains a characteristic Ras-like GTPase domain (Roc) and a C-terminal of Roc (COR) domain (Marín et al., 2008). Similar to other Roco proteins, LRRK2 also contains a serine/threonine kinase domain that shares a relatively low homology to the Mitogen-Activated Protein Kinase Kinase Kinase (MAPKKK) MAP–lineage(West et al., 2007). In addition to these catalytic domains, LRRK2 contains a number of protein-interacting domains including Armadillo (ARM), Ankyrin (ANK), Leucine rich repeats (LRR) n-terminal to the catalytic core with WD40 repeats c-terminal to the kinase domain (Gilsbach and Kortholt, 2014)(see Figure 1.2).

There are currently six known pathogenic mutations that are linked to PD. All six are contained within the catalytic core (refer to figure 1.2) of the protein which may indicate LRRK2 GTPase and/or kinase activity is important in PD. Zimprich and colleagues identified the first two families with mutations in the Roc (Y1699C) and COR (R1441C) domains respectively(Zimprich et al., 2004). In four separate families in Spain, the R1441G mutation (likely from the same founder) was found along with another family containing the Y1699C mutation(Paisán-Ruiz et al., 2004). A year later, a Japanese pedigree was found to have a mutation in the kinase domain (I2020T) (Funayama et al., 2005). This was then followed by another kinase mutation (G2019S) that was found in 13 families across North America and within PD patients with no known family history of the disease (Kachergus et al., 2005). Finally, the R1441H mutation has also been identified in PD patients (Ross et al., 2009). While these 6 pathogenic mutations have received the most study, there are many reports of risk variants in other families, including the G2385R in certain Asian populations

Figure 1.2: Schematic diagram of LRRK2 protein and pathogenic mutations in PD. The diagram depicts LRRK2 protein with multiple domains. The ARM, ANK, LRR, and WD40 domains are involved in protein-protein interactions. The Roc and COR form the GTPase. The known pathogenically linked mutations in LRRK2 fall within the GTPase or Kinase domain. Diagram adapted from (Cookson, 2010)

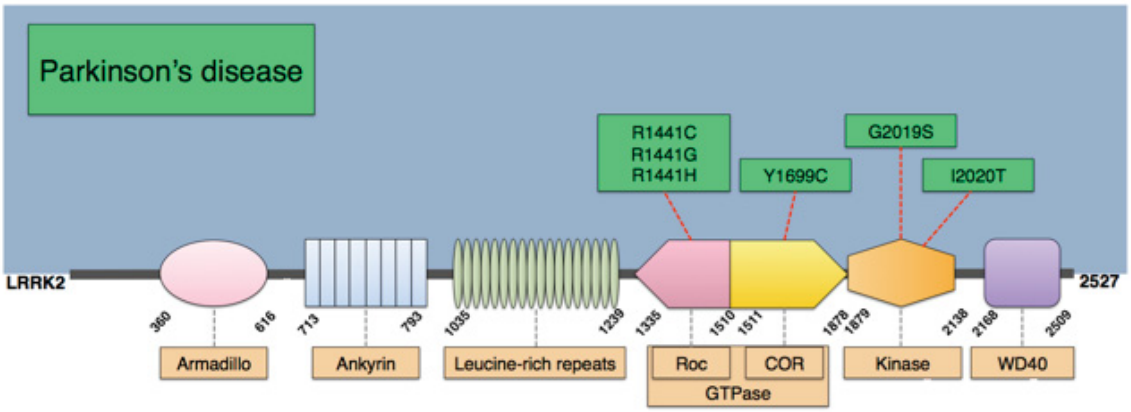
Parkinson's disease
R1441C
R1441G
R1441H
Y1699C
G2019S
I2020T
LRRK2
2527
360
616
713
793
1035
1239
1335
1510
1511
1878
1879
2138
2168
2509
Armadillo
Ankyrin
Leucine-rich repeats
Roc
COR
GTPase
Kinase
WD40

(Tan, 2006; Farrer et al., 2007; Funayama et al., 2007). After over a decade since discovering LRRK2 linked PD, the G2019S mutation has been the most commonly linked mutation found to segregate with PD in families. Although, the G2019S mutation is responsible for approximately 84 percent of LRRK2-linked PD, the overall penetrance of the disease phenotype is about 30 percent for G2019S carrier (Clark et al., 2006; Ozelius et al., 2006; Ferreira et al., 2007). This has led some to theorize that LRRK2 mutations may confer substantial risk to PD but may require an environmental or possibly another genetic risk factor to result in symptomatic presentation of the disease (Visanji et al., 2013). The neuropathology of LRRK2 linked PD is heterogeneous as many report diverse pathologies. This varies from minimal to diffuse Lewy bodies, TAU and amyloid pathology (Papapetropoulos et al., 2006; Poulopoulos et al., 2012).

1.8.6.1 - LRRK2 biology

It has been a challenge to determine the biological function of the LRRK2 protein, let alone it's role in PD pathogenesis. This is in part due to its large size, making it difficult to work with *in vitro*. LRRK2 is widely expressed throughout the body and in the brain. There are higher levels of LRRK2 within the SNc relative to the VTA, however levels in the SNc are low when compared to the striatum (as reviewed in Cookson, 2010). It is suggested that, sub-cellularly, LRRK2 is associated with membranous structures (Biskup et al., 2006). While mammals also possess LRRK1 which has been shown to be able to form a heterodimer with LRRK2 (Dächsel et al., 2010), the expression patterns of LRRK1 and LRRK2 seem to be discrete in at least the rat brain (Giesert et al., 2013).

LRRK2 studies in the past decade have implicated the protein to have a role in a breadth of cellular processing including: mitochondrial dysfunction, neuronal toxicity,

abnormal endocytosis of synaptic vesicles, autophagic dysfunction, translational regulation, and inflammatory response (MacLeod et al., 2006; Plowey et al., 2008; Shin et al., 2008; Mortiboys et al., 2010; Martin et al., 2014; Moehle et al., 2015). However, many of the LRRK2 cellular phenotypes remain subtle, have yet to be reproduced, or fail to shed insight on the selective loss of DA neurons in PD.

1.8.6.2 - LRRK2 animal models

A variety of LRRK2 mice have been created, including LRRK2 null, mutant knock in, and transgenic human expressing mice (see Table 1.2). Similar to most PD genetic mouse models, LRRK2 mice fail to recapitulate loss of DA neurons and motor deficits observed in humans. LRRK2 G2019S expressing via bacterial artificial chromosome (BAC) rats also fail to show loss of DA neurons, although have motor deficits (Lee et al., 2015). One explanation for lack a phenotype in rodents is that LRRK2 is minimally expressed in the murine SNc and is undetectable in the rat, possibly due to a lack of conservation between mammals of the transcriptional promoter region for LRRK2 (West et al., 2014). On the other hand, invertebrate models of LRRK2 induced neurodegeneration have been more successful in producing PD-like phenotypes. The nematode (*Caenorhabditis elegans*) and fruit fly (*Drosophila melanogaster*) contain one LRRK homolog, lrk-1 and lrrk, respectively. Ectopic expression of WT LRRK2 and its pathogeneic mutants, particulary the G2019S mutant produces loss of DA neurons in nemotodes (Yao et al., 2013) and flies (Liu et al., 2008). This has allowed for a platform for candidate screening in vivo, that has had some success translating to the mammalian system. For example, the ribsomal protein S15 was found to enhance dopaminergic loss

in G2019S flies upon RNAi. The same group then also demonstrated that S15 mediates dopaminergic death in mammalian cells (Martin et al., 2014).

Table 1.2: Murine models of LRRK2

The table displays the majority of LRRK2 mouse models including transgenic, knock-in, null, conditional, and viral delivery models. The vast majority of models fail to recapitulate PD. (CamKII = Ca^{2+}/calmodulin-dependent protein kinase II, HSV = herpes simplex virus, CMV = cytomegalovirus, CMVE-PDGFβ = CMV-enhanced human platelet-derived growth factor β-chain)

Model	Loss of TH+ neurons	Motor impairment	Reference
BAC human R1441G	No	Yes	(Li et al., 2009)
BAC human WT	No	No	(Melrose et al., 2010)
BAC human G2019S	No	No	
BAC human WT	No	No	(Li et al., 2010)
BAC human G2019S	No	No	
R1441C KI	No	No	(Tong et al., 2009)
LRRK2 KO (exon 29,30)	No	No	(Tong et al., 2010)
LRRK2 KO (exon 1)	No	No	
LRRK2 KO (exon 39-40)	No	No	(Andres-Mateos et al., 2009)
Conditional G2019S (CamKII)	ND	No	(Wang et al., 2008)
HSV delivery - G2019S	No	ND	(Lee et al., 2010)
HSV delivery - G2019S	Yes (21 DPI)	ND	
CMVE-PDGFβ -WT	No	No	(Ramonet et al., 2011)
CMVE-PDGFβ - R1441C	No	No	
CMVE-PDGFβ - G2019S	Yes (20 months old)	No	
CMVE-PDGFβ -WT	No	No	(Chen et al., 2012)
CMVE-PDGFβ - G2019S	Yes	Yes	
CMV I2020T	No	Yes	(Maekawa et al., 2012)
Conditional ROSA26 - R1441C	No	No	(Tsika et al., 2014)

1.8.6.3 - LRRK2: Cell death

Many early studies found that the expression of LRRK2 in cells was toxic. Both WT and pathogeneic LRRK2 transfection in cortical neurons causes an increase in cell death with most studies showing that pathogeneic LRRK2 causes enhanced death compared to WT expression (Iaccarino et al., 2007; Kanao et al., 2010; Cookson, 2012a). Some groups have shown that loss of LRRK2 may cause cell death as well. LRRK2 null mice display increased TUNEL positive neurons and activated caspase-3 in mouse kidneys (Tong et al., 2010). LRRK2 mediated neurotoxicity has been shown to be dependant on a variety of apoptotic related proteins including: caspase8, the death adaptor death adaptor protein FADD (Ho et al., 2009), Apaf1(Iaccarino et al., 2007) and chronic p38 activation (Yuan et al., 2011). LRRK2 induces expression of BIM and HID by phosphorylating the transcription factor FoxO (Kanao et al., 2010). Increased phosphorylated JNK and mRNA levels of pro-apoptotic markers such as: Bim, FasL, caspase-9, caspase-8 and caspase-3 have been observed in the SNc of G2019S-LRRK2-G2019S tg mice (Chen et al., 2012). However, there are some studies suggest that expression of LRRK2 is pro-survival and loss of LRRK2 function causes neuronal death (Chuang et al., 2014).

Some studies suggest less traditional pathways to LRRK2 induced cell death. Early studies suggested that pathogenic LRRK2 transfection in primary cortical cultures delays neurite outgrowth (MacLeod et al., 2006). However, this phenomenon has been suggested to be at best, transient, and has failed to be reproduced (Garcia-Miralles et al., 2015). Furthermore, there is currently no evidence of this phenotype in endogenous KI mice animals. Another study reported LRRK2 G2019S iPSCs to have nuclear envelope deficits that leads to cell death (Liu et al., 2012). It remains to be seen whether nuclear

envelope impairment in implicated in PD. Many overexpression studies also suggest that mutant LRRK2 causes an increase in phospho-TAU inclusions within the cell (Lin et al., 2010; Melrose et al., 2010; Bailey et al., 2013). This is notable as clinically, many LRRK2 mutant carriers display TAU pathology upon autopsy and in cerebrospinal fluid (Papapetropoulos et al., 2006; Aasly et al., 2012; Poulopoulos et al., 2012).

1.8.6.4 - LRRK2: Mitochondrial and oxidative stress

Multiple lines of evidence including: PD brain tissue post-mortem, autosomal recessive PD genes, and toxin models of dopaminergic death suggest that mitochondrial dysfunction and oxidative damage may contribute to the pathogenesis of PD. The examination of LRRK2 and its potential role in mitochondrial health and oxidative stress has remained arguably lacking when compared to the bulk of LRRK2 literature. However, one of the earliest studies to indicate that LRRK2 may play a role in mitochondrial homeostasis demonstrated that mutant LRRK2 expressing were sensitive to the mitochondrial complex I inhibitor, rotenone, which could be rescued by Parkin co-expression (Ng et al., 2009). Furthermore, Parkin expression can also rescue the enlarged mitochondria observed in the indirect flight muscles of G2019S-LRRK2 expressing flies (Ng et al., 2012). Mitochondrial abnormalities have been observed in flies expressing G2019S-LRRK2 within DA neurons as well (Hindle et al., 2013). Condensed mitochondria and mitochondrial clustering have been observed in both aged G2019S BAC transgenic and G2019S knock in mice (Ramonet et al., 2011; Yue et al., 2015). A decrease in mitochondrial membrane potential was observed in murine cortical cultures transfected with G2019S or R1441C constructs which also lead to an increase in mitochondrial clearance (mitophagy) (Cherra et al., 2013).In humans, two studies of skin

fibroblasts harvested from G2019S patients and healthy controls were examined for mitochondrial defects. Both mitochondrial membrane potential and ATP levels were decreased in the G2019S fibroblasts (Mortiboys et al., 2010; Papkovskaia et al., 2012). A decrease in mitochondrial respiration and an increase in mitochondrial mobility was observed in neural cells differentiated from patient induced pluripotent stem cells (iPSCs) (Cooper et al., 2012). LRRK2 may mediate these observed mitochondrial phenotypes via its suggested interaction with dynamin-related protein (Drp1). DRP1 is required for mitochondrial fission and DRP1 expression increases upon mutant LRRK2 expression which correlates with fragmented mitochondrial phenotypes (Niu et al., 2012; Wang et al., 2012).

1.8.6.5 - LRRK2: Endolysosomal and vesicular trafficking

A moderate amount of evidence in the field suggests that LRRK2 may have multiple roles involved in vesicle endocytosis, trafficking, autophagy, and lysosomal function. These connected pathways seem to relate to LRRK2s putative activity at membranes (Berger et al., 2010). The earliest work suggesting that LRRK2 may play a role in synaptic vesicle endocytosis was performed in yeast, identifying Rab5b as LRRK2 interactor and furthermore observering that LRRK2 and Rab5b co-localize in synaptic vesicles and is a LRRK2 kinase substrate (Shin et al., 2008; Yun et al., 2015). Electrophysiological recordings of cortical neurons after shRNA knock-down of LRRK2 suggests that LRRK2 is involved in vesicle recycling (Piccoli et al., 2011). Additionally, LRRK2 has been found to interact and phosphorylate Soluble NSF Attachment Protein Receptor (SNARE) related proteins in the synapse including N-ethylmaleimide sensitive fusion (NSF) protein and Snapin (Yun et al., 2013; Belluzzi et al., 2016). It has

been suggested that LRRK2 may bind many of these presynaptic proteins via its WD40 domain (Piccoli et al., 2014). This has led some to examine LRRK2s role in neurotransmitter release as inhibition of LRRK2 may decrease vesicle release as G2019S neurons display increased release (Migheli et al., 2013; Cirnaru et al., 2014). However, it should be noted that there is a lack of evidence that LRRK2 plays a role in DA release in mammals (Sanchez et al., 2014; Volta et al., 2015).

Studies of flies with mutations in the *Drosophila* lrrk homolog have observed defects in early endosomes, autophagosome accumulation, and enlarged lysosomes (Dodson et al., 2014). LRRK2s potential role in endocytosis has been supported by multiple interaction studies suggesting LRRK2 may: bind to Dynamin 1-3 (a mediator of membrane scission in clathrin-mediated endocytosis), phosphorylate EndophilinA (Critical for synaptic vesicle endocytosis), and interact with clathrin-light chains at endosomes (Matta et al., 2012; Stafa et al., 2013; Schreij et al., 2015). Another explanation for much of the evidence implicating LRRK2 in vesicle trafficking are studies associating LRRK2 with various Rab GTPase proteins known to be involved in cytoskeletal and trafficking networks. Specifically, LRRK2 may interact with Rab5b (Shin et al., 2008), Rab7 (Dodson et al., 2014), Rab7L1 (MacLeod et al., 2013), Rab9 (Dodson et al., 2012), Rab32 and Rab38 (Waschbüsch et al., 2014). Recent evidence has indicated that LRRK2s role in the endocytic pathway may be dependant on the Notch signalling pathway (Imai et al., 2015). Others have shown that LRRK2-associated downstream defects on the lysosome maybe suppressed by two-pore channel 2 (TPC2) inhibition (Hockey et al., 2015; Rivero-Ríos et al., 2015). It is still unclear, what precise role LRRK2 plays in trafficking and how that may lead to PD in humans.

1.8.6.6 - LRRK2: Autophagy

Autophagy is the broad term used for the intracellular recycling of proteins and organelles within the cell. Increasingly, LRRK2 has been implicated to have a role in the autophagy-lysosomal pathway. Deregulated macro-autophagy (from now referred to simply as autophagy) has been observed in both LRRK2 kinase (G2019S) and ROC (R1441C) pathogenic mutants *in vitro* (Plowey et al., 2008; Alegre-Abarrategui et al., 2009; Bravo-San Pedro et al., 2013). Furthermore, knock-down (KD) of LRRK2 by siRNA is suggested to increase autophagic flux (Alegre-Abarrategui et al., 2009). Similarly, LRRK2 kinase inhibition in human neuroblastoma cells also stimulates autophagy (Manzoni et al., 2013). Loss of function of lrrk in *Drosophila* is also associated with autophagic disturbances (Dodson et al., 2014). This is in line with work in *C. elegans* suggesting that both G2019S and R1441C mutant expression in these animals inhibits autophagy (Saha et al., 2014). LRRK2 involvement in autophagy is further evidenced by localization studies attributing LRRK2 localization at autophagic vacuoles (autophagosomes) and multi-vesicular bodies in both human brain and cultured cell lines (Alegre-Abarrategui et al., 2009; Schapansky et al., 2014). Autophagic abnormalities have been observed DA neurons derived from G2019S patient iPSCs (Sánchez-Danés et al., 2012). Multiple *in vivo* studies of different LRRK2 knock-out (KO) mice demonstrate autophagic disturbances in the kidney (Tong et al., 2010; Hinkle et al., 2012; Tong et al., 2012). Both G2019S and R1441G transgenic mice display autophagic abnormalities using Transmission Electron Microscopy (TEM) in the brain (Ramonet et al., 2011; Tagliaferro et al., 2015). While the bulk of the preceding work has been focused on generalized macro-autophagy, there is some evidence LRRK2 may be

involved with chaperone-mediated autophagy (CMA). LRRK2 is suggested to be degraded by CMA and mutant LRRK2 may also inhibit CMA activity (Orenstein et al., 2013).

1.8.6.7 - LRRK2: Regulatory elements

There is a portion of LRRK2 studies that have focused on LRRK2 role in translation particularly in global protein synthesis. This was originally sparked by studies that showed that human LRRK2 and Drosophila lrrk could phosphorylate the eIF4E-binding protein, 4E-BP (Imai et al., 2008). In consequence of 4E-BP hyperphosphorlyation by LRRK2, 4E-BP dissociates from eIF4E and allows uncontrollable 5' cap-dependent translation. However, other studies have shown that LRRK2 phosphorylation is weaker than LRRK2 autophosporylation and the interaction was not observed in mammalian cells (Kumar et al., 2010; Trancikova et al., 2012). More recently, further work in *Drosophila* has shown that LRRK2 stimulates both cap-dependent and cap-independent mRNA translation and increases global protein synthesis via phosphorylation of the ribosomal protein s15 (Martin et al., 2014). More studies in mammalian cells are needed to expand on these findings.

1.8.6.8 - LRRK2: Neuroinflammation

While neuroinflammation has been described in PD, it has mostly been thought as a secondary mechanism contributing to the pathogenesis of PD. However, recent evidence implicating LRRK2s role in the immune response and inflammatory signaling is potentially proving otherwise. Intriguingly, variants in LRRK2 may contribute to risk of the immune disorders: Crohn's disease and leprosy (Barrett et al., 2008; Marcinek et al., 2013). While LRRK2 is moderately expressed in neurons, LRRK2 is robustly expressed

in monocytes and macrophages but also has been shown to increase expression after toll-like receptor 4 (TLR4) agonist treatment with LPS (Hakimi et al., 2011; Moehle et al., 2012). Inhibition of LRRK2 kinase function has been shown to decrease phagocytic engulfment of HIV1 tat protein (Marker et al., 2012). The pro-inflammatory cytokine, IFN-γ has been shown to upregulate LRRK2 expression as LRRK2 may subsequently activate nuclear factor kappa-light-chain-enhancer of activated B cells (NF-κB) (Gardet et al., 2010; Thévenet et al., 2011). Furthermore, LRRK2 ablation or kinase inhibition has been shown to inhibit NF-κB signalling in microglia (Kim et al., 2012; Russo et al., 2015). In a collitis model of inflammatory bowel syndrome (IBS), LRRK2 KO mice were hypersensitive to experimental collitis and LRRK2 was shown to negatively regulate the transcription factor Nuclear factor of activated T-cells (NFAT)(Liu et al., 2011b). LRRK2s potential role in inflammation may be evolutionarily conserved in freshwater Hydra as it is upregulated following injury-induced immune response (Wenger et al., 2014). Recently it has been observed that LRRK2 null rats are resistant to DA cell death upon intra-nigral LPS injections into the SNc when compared to WT littermates (Daher et al., 2014) . Conversely, LRRK2-G2019S overexpressing rats are hypersensitive to LPS induced nigral death (Moehle et al., 2015). Furthermore, LRRK2 G2019S microglia from transgenic rats were shown to have enhanced chemotaxic response (Moehle et al., 2015). However, another group has shown a decrease in motility in similar assays with microglia derived from LRRK2 G2019S transgenic mice on a microglia reporter background (Choi et al., 2015). LRRK2 is easily studied in immune cells due to LRRK2s inducible response. However, it is unclear how LRRK2s role in immune cells could lead to DA cell death.

1.9 – Statement of research questions, hypothesis and objectives

The following three chapters encompass a body of work focused on two main overall objectives. These are to firstly, characterize DJ-1 null mice on a pure C57-Bl6 background (Chapter 2) and develop novel genetic animal models of PD by expressing LRRK2 in *Drosophila* central phagocytes (Chapter 4). The second is to determine genomic modifiers that can: 1) explain penetrance issues in DJ-1 animal models (Chapter 2); 2) determine genetic pathways that modify LRRK2 induced toxicity *in vivo* (Chapter 3); and 3) to explore one of the modifiers found in Chapter 3, SCAR/WAVE-2 and determine if LRRK2 plays a role in the phagocytic function of immune cells and may led to loss of TH+ cells through a WAVE-2 dependent mechanism (to be discussed further in Chapter 4).

1.9.1 - Hypothesis

Chapter 2: Progressive Dopaminergic Cell Loss With Unilateral-to-Bilateral Progression in a Genetic Model of Parkinson's Disease.

DJ-1 null mice on a pure C57-Bl6 background may exhibit dopaminergic cell loss and motor deficits and lack of phenotypic penetrance may be due to additional genetic modifiers within the colony.

Chapter 3: LRRK2 functional genetic interactors modifying eye degeneration and dopaminergic cell loss in Drosophila.

The elucidation of fly genes that enhance or suppress hLRRK2-mediated toxicity in the *Drosophila* eye and dopaminergic system will provide functional relevance of LRRK2 interacting pathways important in Parkinson's disease.

Chapter 4: LRRK2-G2019S phosphorylates and stabilizes WAVE-2 to increase phagocytic activity of myeloid cells leading to non-cell autonomous dopaminergic loss.

LRRK2 phosphorylates the actin assembly mediator WAVE-2 to mediate the phagocytic immune response of myeloid cells that leads to dopaminergic death in PD.

1.9.2 – Specific objectives

Chapter 2: DJ-1 C57-Bl6 mouse

Objective 1: Determine whether DJ-1 null mice backcrossed to a pure C57-Bl6 background results in a dopaminergic cell loss and PD relevant motor phenotypes.

Objective 2: Determine any potential genetic modifiers that may segregate with only DJ-1 null mice penetrant with PD-like pathology.

Chapter 3: LRRK2 Drosophila screen

Objective 1: Perform an unbiased screen for interacting gene regions using the Bloomington Deficiency line kit for chromosome two, three, and four of *D. melanogaster*.

Objective 2: Identify specific candidate genes from phenotype-modifying interacting regions.

2 i) Examine sub-regions and specific gene disruption lines for interacting regions to identify specific gene interactors.

2 ii) Confirm interactors using at least one other LRRK2 pathogenic mutant other than the kinase domain.

2 iii) Confirm specific gene interactors for modification of TH+ cell loss in the dopaminergic cell clusters of *Drosophila*.

Chapter 4: LRRK2 and WAVE-2

Objective 1: Determine if LRRK2 regulates phagocytic activity in mammalian immune cells.

Objective 2: Determine the mechanism by which if LRRK2 modulates WAVE2.

Objective 3: Determine if LRRK2 expression in *Drosophila* central phagocytes results in Parkinsonism that is mediated by SCAR/WAVE-2.

Chapter 2:

Progressive Dopaminergic Cell Loss With Unilateral-to-Bilateral Progression in a Genetic Model of Parkinson's Disease.

***Proceeding of the National Academy of Sciences USA*,**

2012 Sep 25; 109(39): 15918-23.

Maxime Rousseaux, **Paul C. Marcogliese**, Dianbo Qu, Sarah J. Hewitt, Sarah Seang, Raymond H. Kim, Ruth S. Slack, Diane C. Lagace, Michael G. Schlossmacher, Tak W. Mak, David S. Park

Statement of Author contribution:

The following manuscript was published in the Proceedings of the National Acadamey of Science USA (Rousseaux et al., 2012). We reported a novel pre-clinical model of PD in DJ-1 null mice fully back crossed on a C57-Bl6 background. This phenotype that affected approximately 20-40% of mice recapitulated many aspects of human PD including: progressive unilateral to bilateral loss of nigral neurons, degeneration in the LC, compensatory post-synaptic activity in the striatum of young mice and motor deficits in aged mice where striatal fiber density decreases. This was a significant finding as this phenotype occurred without any exogenous stressor and is the first whole germ-line model of PD that displays robust neuronal loss. We also conducted whole exome sequence on affected and unaffected DJ-1 KO mice and determine candidate modifiers that may explain the lack of full penetrance of the phenotype. This model may now act as a platform to study PD progression.

As second author for this study, Paul C. Marcogliese designed and performed all the behavioural experiments and assisted Maxime Rousseaux with histological characterization. Dr. David S. Park supervised the project. Dr. Raymond H. Kim generated the DJ-1 null mice. Dr. Diane C. Lagace provided access to the behavioural core facility and technical support. Maxime Rousseaux, Paul C. Marcogliese and Dr. David S. Park conducted data analysis and authored the manuscript.

Classification: BIOLOGICAL SCIENCES, Neuroscience

Progressive Dopaminergic Cell Loss With Unilateral-to-Bilateral Progression in a Genetic Model of Parkinson's Disease.

Maxime Rousseaux, **Paul C. Marcogliese**, Dianbo Qu, Sarah J. Hewitt, Sarah Seang, Raymond H. Kim, Ruth S. Slack, Diane C. Lagace, Michael G. Schlossmacher, Tak W. Mak, David S. Park

Number of text pages: 17

Number of figures: 6 main, 6 supplemental, 3 tables

Abstract:

DJ-1 mutations cause autosomal recessive early-onset Parkinson disease (PD). We report a model of PD pathology: the DJ1-C57 mouse. A subset of DJ-1–nullizygous mice, when fully backcrossed to a C57BL/6 background, display dramatic early-onset unilateral loss of dopaminergic (DA) neurons in their *substantia nigra pars compacta*, progressing to bilateral degeneration of the nigrostriatal axis with aging. In addition, these mice exhibit age-dependent bilateral degeneration at the *locus ceruleus* nucleus and display mild motor behavior deficits at aged time points. These findings effectively recapitulate the early stages of PD. Therefore, the DJ1-C57 mouse provides a tool to study the preclinical aspects of neurodegeneration. Importantly, by exome sequencing, we identify candidate modifying genes that segregate with the phenotype, providing potentially critical clues into how certain genes may influence the penetrance of DJ-1–related degeneration in mice.

Introduction:

Parkinson disease (PD) is a progressive neurodegenerative disorder with complex symptomology and etiology affecting an ever-increasing number of individuals. Although multifactorial in nature, increasing insight has been gained with regard to the pathogenesis of PD through investigation of genes linked to the disease. Because monogenic forms of PD can be modeled in a laboratory, numerous animal models have been created to recapitulate the disease. For instance, loss-of-function mutations in the *DJ-1* (*PARK7*) gene cause early-onset autosomal recessive PD (Bonifati et al., 2003; Hague et al., 2003). Patients harboring *DJ-1* mutations exhibit certain key characteristics principally in early-onset PD and may lack certain neuropathological attributes present in sporadic PD cases such as Lewy bodies (LBs)(Kitada et al., 2012). However, generation of DJ-1–nullizygous mice (DJ-$1^{-/-}$) on mixed background by various laboratories, including our own, failed to detect any basal levels of neurodegeneration even in aged mice (Goldberg et al., 2005; Chen et al., 2005; Kim et al., 2005; Andres-Mateos et al., 2007; Manning-Boğ et al., 2007; Chandran et al., 2008; Pham et al., 2010; Ramsey et al., 2010) (see Table 2.S1). Similarly, a number of PD-related, genetically manipulated mice have been created in attempts to recapitulate the disease process, whereas little or none has shown clear or robust neurodegeneration specific to the *substantia nigra pars compacta* (SNc) (reviewed in (Dawson et al., 2010)). Therefore, the creation of murine PD models that demonstrate significant dopaminergic (DA) loss remains an acute need in the field. The need for an early-onset model of PD is made more pressing given that no postmortem analyses of human DJ-1 mutant-carrying patients have been reported. This is

Table 2.S1. Comparison of previously generated DJ-1−/− mice. A comprehensive search of the literature is presented in this table to note the gross differences between the generation of these knockout animals. Specifically, we note that the number of backcrossings (at least published) remain very low for other DJ-1−/− mice. MPTP, 1-methyl-4-phenyl-1,2,3,6-tetrahydropyrindine. “6 for 2 mo” means six backcrosses for the MPTP study.

Gene Disruption	Background	Backcross # (to C57Bl/6)	Phenotype	Study author	Year
ΔExon 2-3	C57Bl/6 mixed	1	No gross behavioral or histological phenotype	Andres-Mateos *et al*.	2007
ΔExon 2	129/Sv/C57Bl/6 mixed	1	Mild decrease in motor performance.	Chandran *et al*.	2008
ΔExon 1-5 + promoter	129/C57Bl/6 mixed	1	Mild decrease in motor performance. Increase in striatal DA and its metabolites	Chen *et al*.	2005
ΔExon 2	B6/129	1	Mild decrease in motor performance. Reduced DA overflow/increased DA reuptake. Reduced response to DA.	Goldberg *et al*.	2004
ΔExon 3-5	129/Ola /C57Bl/6 mixed	1 (*6 for 2 months MPTP*)	No gross unstimulated behavioral or histological phenotype	Kim *et al*.	2005
Gene trap between exon 6-7	B6/129	1	Subtle locomotor deficit	Manning-Bog *et al.*	2007
Gene trap between exon 6-7	129P2/OlaHsd/ C57Bl/6 mixed	1	Mild decrease of TH+ cells in the VTA. Mild cognitive impairment	Pham *et al*.	2010
Gene trap between exon 6-7	129P2/OlaHsd/ C57Bl/6 mixed	1	No gross behavioral or histological phenotype	Ramsey *et al.*	2010

particularly critical if we are to understand how specific signaling pathways govern DA loss in monogenic forms of early-onset human PD. Presently, most mechanistic studies of DA loss rely on acute toxin models of Parkinsonism. However, the relevance of such studies to the human condition remains uncertain, because acute neurotoxins are rarely the culprit in the majority of PD cases. This potential discrepancy is highlighted by a number of failed clinical trials that have heavily relied on toxin models as preclinical evidence for efficacy (Waldmeier et al., 2006; Parkinson Study Group PRECEPT Investigators, 2007; Marks et al., 2010; Snow et al., 2010). A more representative model of DA loss that uses known factors in human PD is likely vital to develop better therapeutic outcomes.

Results:

In the course of our studies examining the effects of environmental perturbations in DJ-1$^{-/-}$ mice, we continued to examine the long-term effects of DJ-1 deficiency on DA neuron loss. Importantly, this was accomplished in animals completely backcrossed onto a C57BL/6 background (14× backcrossed, DJ-1$^{-/-}$; herein, referred to as DJ1-C57). Intriguingly, unilateral SNc degeneration in a subset of these DJ1-C57 knockout mice is observed as early as 2 mo of age (Fig. 2.1*A*, Fig. 2.S1, and Table 2.S2). This phenotype is not observed in animals younger than 2 mo (n = 8; Fig. 2.S1), thus indicating that this defect is unlikely to be developmental in origin. Moreover, this phenotype is not observed in any of the wild-type (WT) mice examined (n = 71). In addition, the ventral tegmental area (VTA) of these mice is mostly spared (Fig. 2.1*D*). This latter finding is particularly interesting given the observation that in postmortem brains from PD patients, VTA neurons remain relatively protected compared with their nigral counterparts (Perl, 2011).

Fig. 2.1: Young affected DJ1-C57 mice exhibit selective unilateral degeneration in their SNc. (*A*) Representative midbrain sections of DJ1-C57 affected (*Top*), DJ1-C57 Unaffected (*Middle*), and WT (*Bottom*) mice depicting TH staining in the SNc and VTA. (*B* and *C*) Quantification of *A* by stereology of total number of TH-positive cells in the SNc (*B*) and of CV-stained cells at the level of the MTN in the SNc (*C*). (*D*) Quantification of TH-positive neurons in the VTA of WT and DJ-1 affected mice. Note that WT, DJ1-C57 affected and DJ1-C57 unaffected are represented by blue, red, and yellow bars, respectively. Side A is depicted as solid shading and side B as hatched shading. NS, not significant ($P > 0.05$); ***$P < 0.001$; ANOVA, followed by Tukey's LSD post hoc tests. Data are represented as means (n = 7–80 per group) ± SEM.

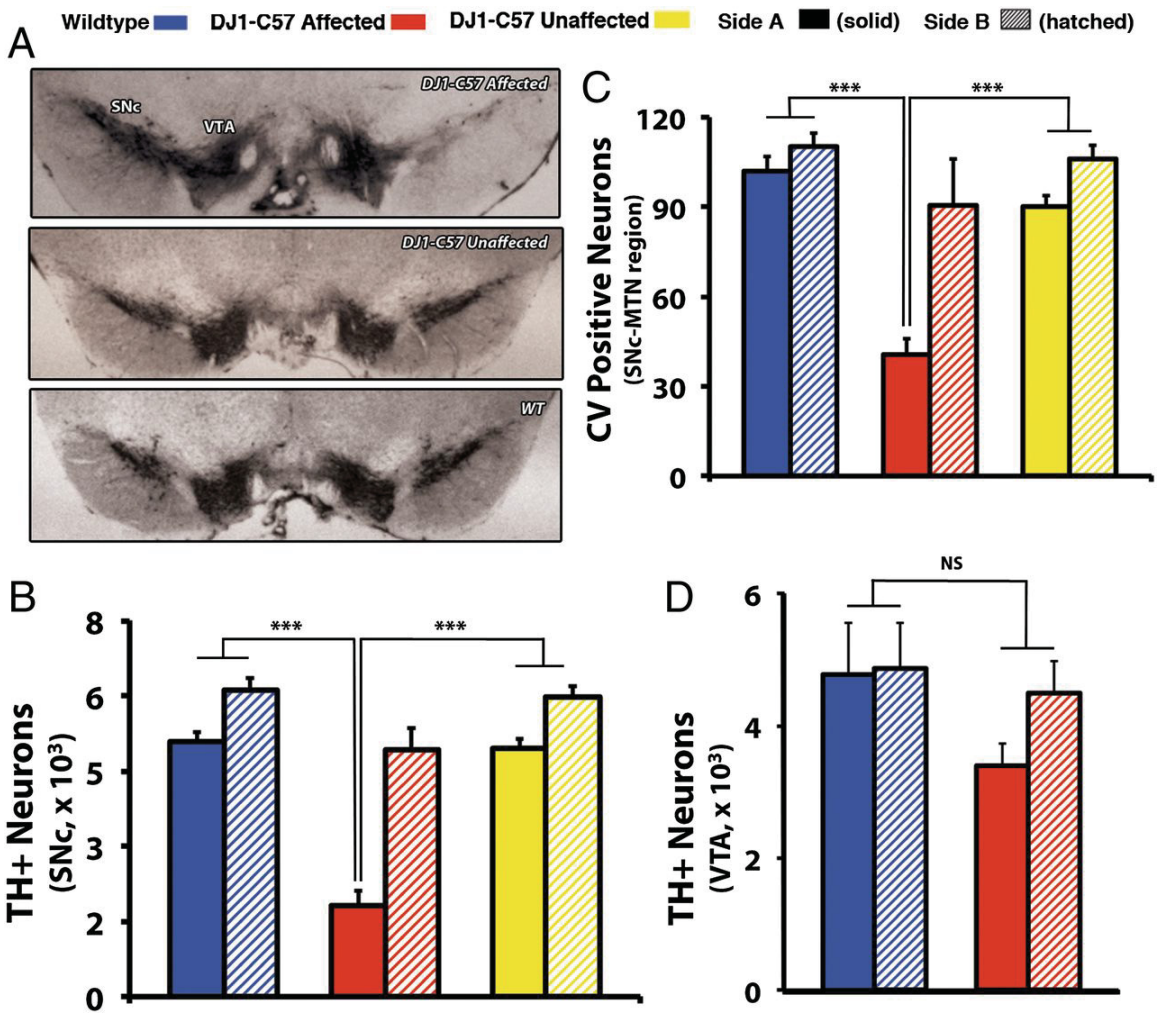
Wildtype
DJ1-C57 Affected
DJ1-C57 Unaffected
Side A (solid)
Side B (hatched)
A
SNc
VTA
DJ1-C57 Affected
DJ1-C57 Unaffected
WT
C
CV Positive Neurons
(SNc-MTN region)
120
90
60
30
0
***
***
B
TH+ Neurons
(SNc, x 10³)
8
6
5
3
2
0
***
***
D
TH+ Neurons
(VTA, x 10³)
6
4
2
0
NS

Fig. 2.S1: Unilateral DA cell loss in the SNc of a subset of DJ1-C57 mice as early as 2 mo of age. Stereological counts of TH-positive neurons in midbrain sections from WT and DJ1-C57 mice were performed at various time points. No mice were qualified as affected according to the >40% unilateral criteria in 6-wk-old mice. Each data point represents mean ± SEM (n = 1–37 per data point). **P < 0.01 by ANOVA, followed by Tukey's LSD post hoc test.

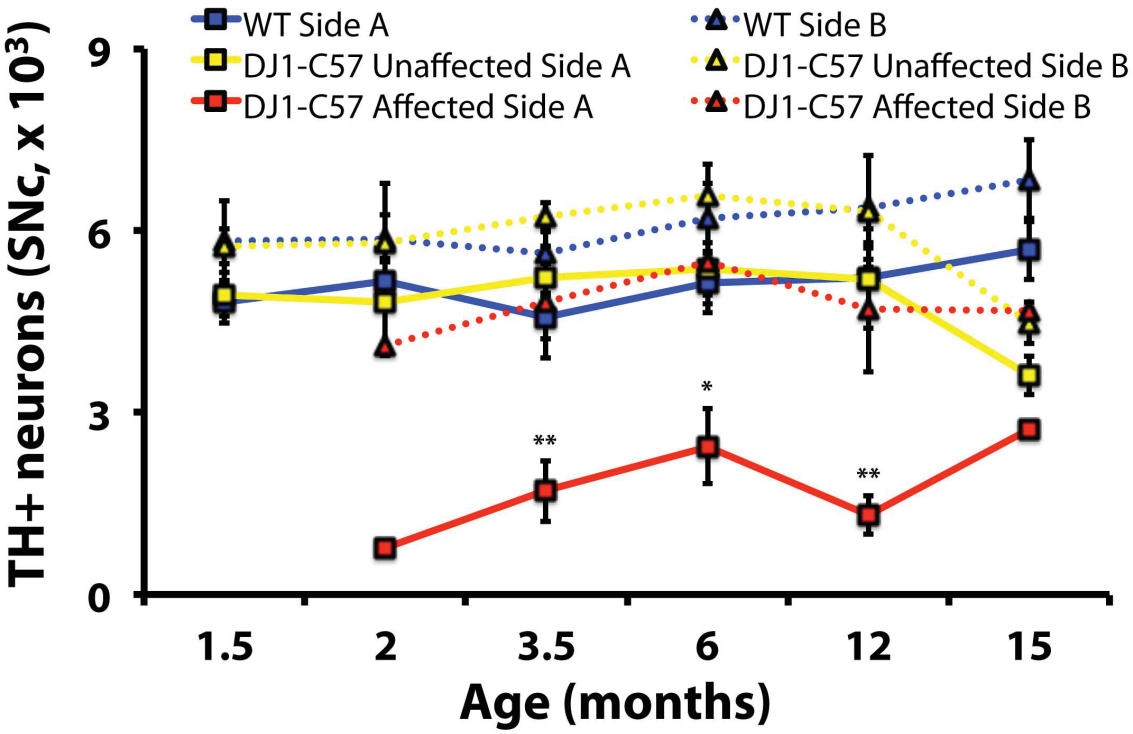
WT Side A
WT Side B
DJ1-C57 Unaffected Side A
DJ1-C57 Unaffected Side B
DJ1-C57 Affected Side A
DJ1-C57 Affected Side B
TH+ neurons (SNc, x 10³)
9
6
3
0
**
*
**
1.5
2
3.5
6
12
15
Age (months)

Table 2.S2: Penetrance of affected phenotype over time in DJ1-C57 and WT mice.

Penetrance was measured as an animal possessing a greater than 40% loss of neurons on one side of the SNc (side A) vs. the other side (side B). Samples were gathered at 1.5, 2, 3.5, 6, 12, and 15 mo. Sample sizes (n) for each group varied from 5 to 37. Only DJ1-C57 animals exhibited the phenotype that begins at 2 mo of age (n = 15 penetrant DJ1-C57 vs. n = 0 penetrant WT). Dashes represent not applicable.

Genotype	Age (mo)	Sample size (*n*)	Unilateral phenotype	Penetrance (%)
WT	1.5	5	No	0
	2	9	No	0
	3.5	19	No	0
	6	16	No	0
	12	10	No	0
	15	12	No	0
Total WT	—	71	No	0
DJ1-C57	1.5	8	No	0
	2	8	Yes	12.5
	3.5	37	Yes	16.2
	6	23	Yes	17.4
	12	7	Yes	42.9
	15	13	Yes	7.7
Total DJ1-C57	—	96	Yes	15.6

To objectively assess this phenotype, mice in this study are classified as either "affected" (unilateral phenotype: having a greater than 40% unilateral reduction of DA cells in the SNc compared with the other side) or "unaffected" (no unilateral phenotype: having similar bilateral DA cell numbers). No clear side or sex specificity is observed (right, 53%; female, 67%, respectively). Thus, to maintain consistency, "side A" is the term given for the side of the brain with the least number of neurons, regardless of the genotype (side B being the side with more DA neurons). When quantified, affected DJ1-C57 mice exhibit a dramatic reduction of neurons in their SNc, as visualized by tyrosine hydroxylase (TH) and cresyl violet (CV) staining (Fig. 2.1*B* and *C* and see Fig. 2.3*A*). Upon closer magnification of the SNc, the affected DJ1-C57 mice exhibit TH-positive fiber staining but with clear neuronal process disruption. When quantified, the remaining fibers at the level of the SNc in the affected DJ1-C57 mice display an elevated number of shortened processes with obvious neuritic beading (Fig. 2.2*A*) compared with unaffected DJ1-C57 or control mice. Consistent with this finding, an increase in CD11b-positive microglia is noted in young, affected animals (Fig. 2.3*B*), whereas no clear increase in astrocytosis on the affected side is observed (Fig. 2.S2).

Fig. 2.2: Widespread process disruption and aberrant striatal innervation in young affected DJ1-C57 mice. (A) Fiber sprouting in WT (Upper Left) and DJ1-C57 affected animals (Upper Right). Distribution of quantified uninterrupted process (TH+) length in a single vision plain (in microns) is presented (Lower). (B) Representative sections of striatum stained for ΔFosB in young WT (Left) and DJ1-C57 affected (Center) mice. (Right) Quantification of ΔFosB-positive puncta in the striatum. (C) Representative sections of the striatum stained for TH as in B. Quantification of striatal TH density is shown (Right). WT, DJ1-C57 affected, and DJ1-C57 unaffected are represented by blue, red, and yellow bars, respectively. Side A is depicted as solid shading and side B as hatched shading. NS, not significant ($P > 0.05$); *$P < 0.05$; **$P < 0.01$; ANOVA, followed by Tukey's LSD post hoc tests. Data are represented as means ($n = 3–11$ per group) ± SEM.

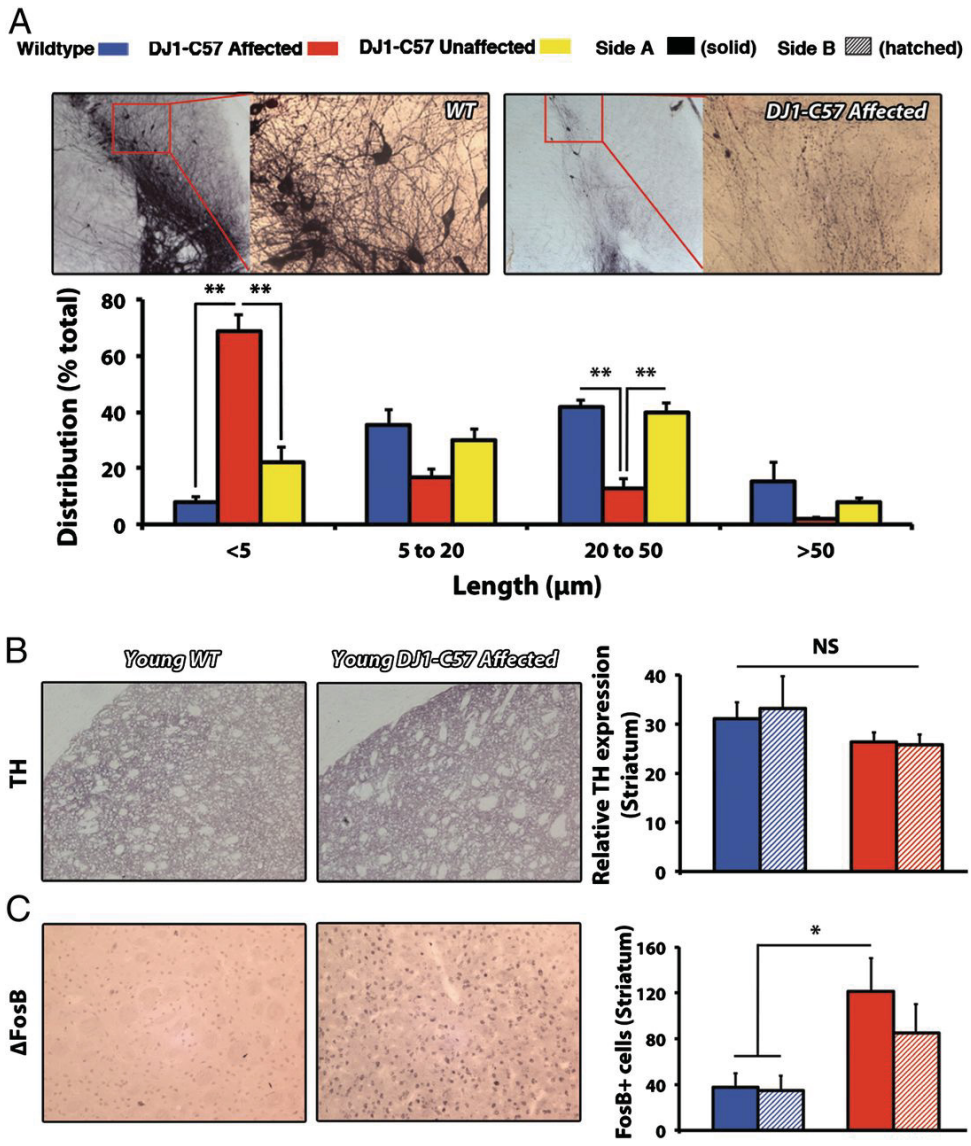
A
Wildtype
DJ1-C57 Affected
DJ1-C57 Unaffected
Side A (solid)
Side B (hatched)
WT
DJ1-C57 Affected
Distribution (% total)
80
60
40
20
0
**
**
**
**
<5
5 to 20
20 to 50
>50
Length (µm)
B
Young WT
Young DJ1-C57 Affected
TH
Relative TH expression (Striatum)
NS
40
30
20
10
0
C
ΔFosB
FosB+ cells (Striatum)
*
160
120
80
40
0

Fig. 2.3: Focal microgliosis in young affected DJ1-C57 mice. (*A*) Representative midbrain sections stained for CV in young WT and DJ1-C57 affected mice (1000× magnification). Thin arrows denote typical morphology of DA neurons of the SNc; thick arrows denote shrunken, dead nuclei; and arrowheads denote appearance of cells with altered morphology. (*B*) CD11b staining in the midbrain of young WT (*Left*) and DJ1-C57 affected (*Right*) mice was quantified and represented as the number of Cd11b-positive cells in the MTN region of the SNc. WT and DJ1-C57 affected are represented by blue and red bars, respectively. Side A is depicted as solid shading and side B as hatched shading. NS, not significant ($P > 0.05$); *$P < 0.05$; ANOVA, followed by Tukey's LSD post hoc tests. Data are represented as means ($n = 3–9$ per group) ± SEM.

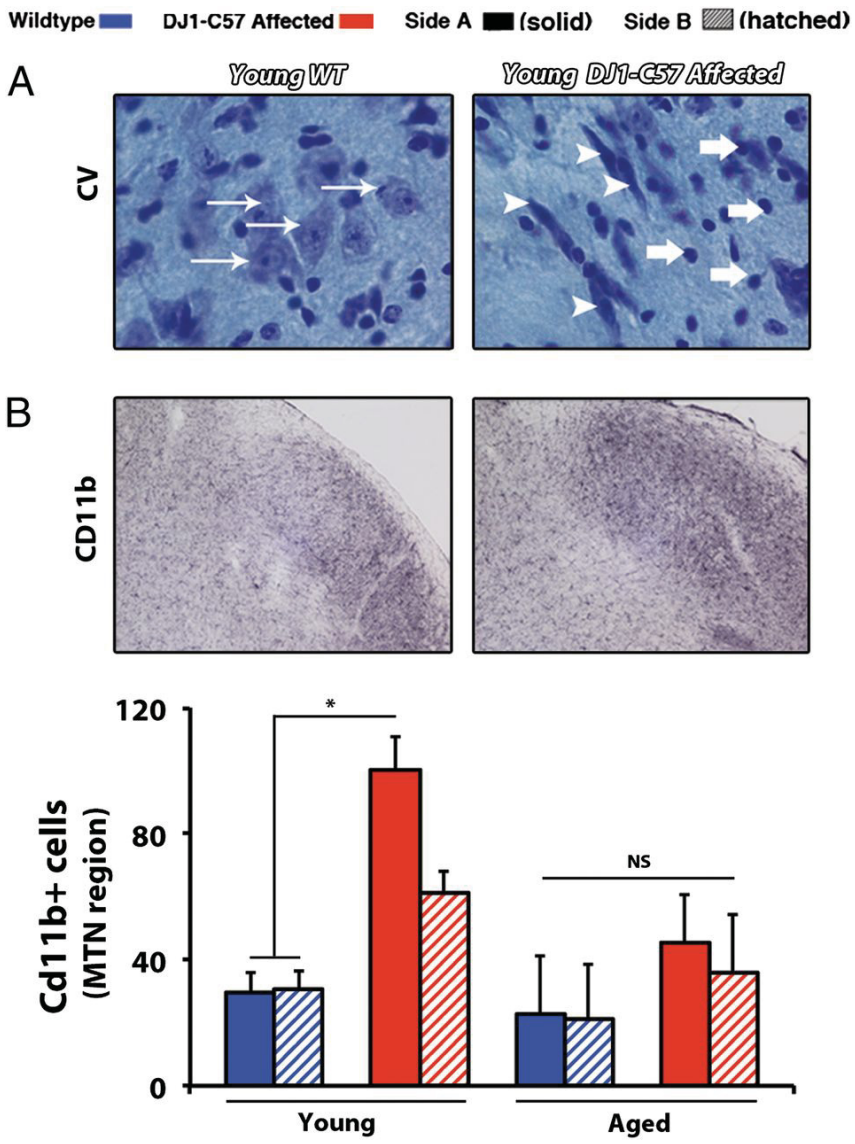
Wildtype
DJ1-C57 Affected
Side A (solid)
Side B (hatched)
A
Young WT
Young DJ1-C57 Affected
CV
B
CD11b
Cd11b+ cells
(MTN region)
120
80
40
0
*
NS
Young
Aged

Fig. 2.S2: No visible astrocytic aggregation in affected DJ1-C57 midbrain. (Upper) Midbrain sections from young WT (n = 6) and DJ1-C57 affected (n = 6) (Left) or aged WT (n = 4) and DJ1-C57 mice (n = 4) (Right) were costained for GFAP and TH. (Lower) GFAP-positive puncta in the SNc (MTN region) were quantified in three representative sections. NS denotes a nonsignificant difference by means of ANOVA.

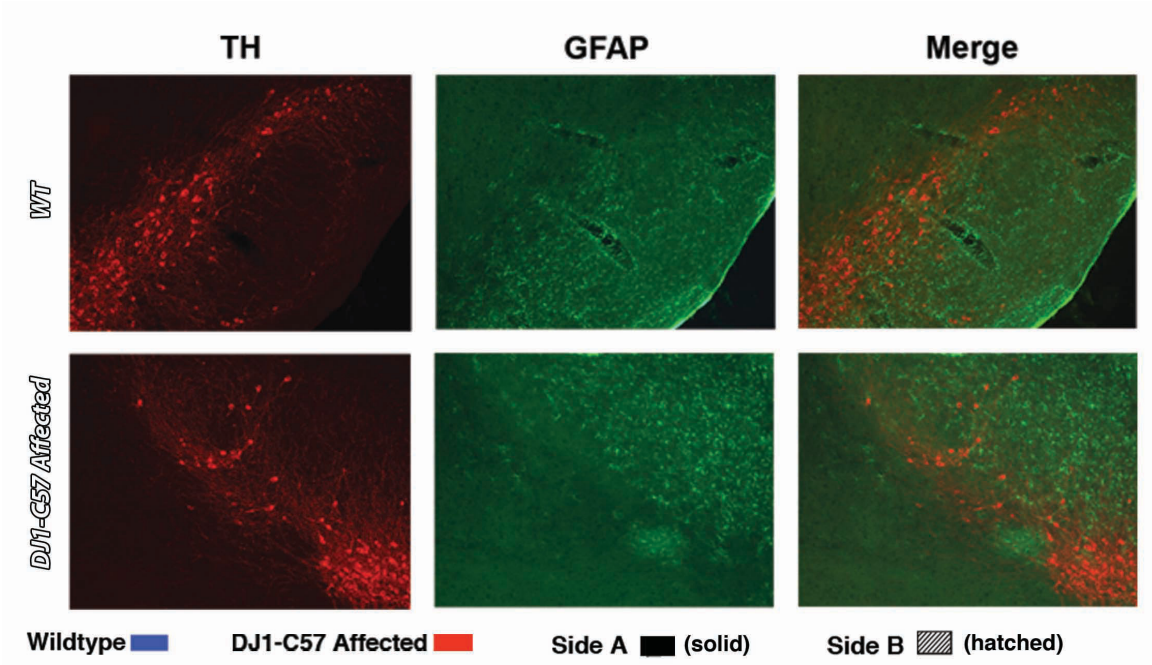
TH
GFAP
Merge
WT
DJ1-C57 Affected
Wildtype
DJ1-C57 Affected
Side A (solid)
Side B (hatched)

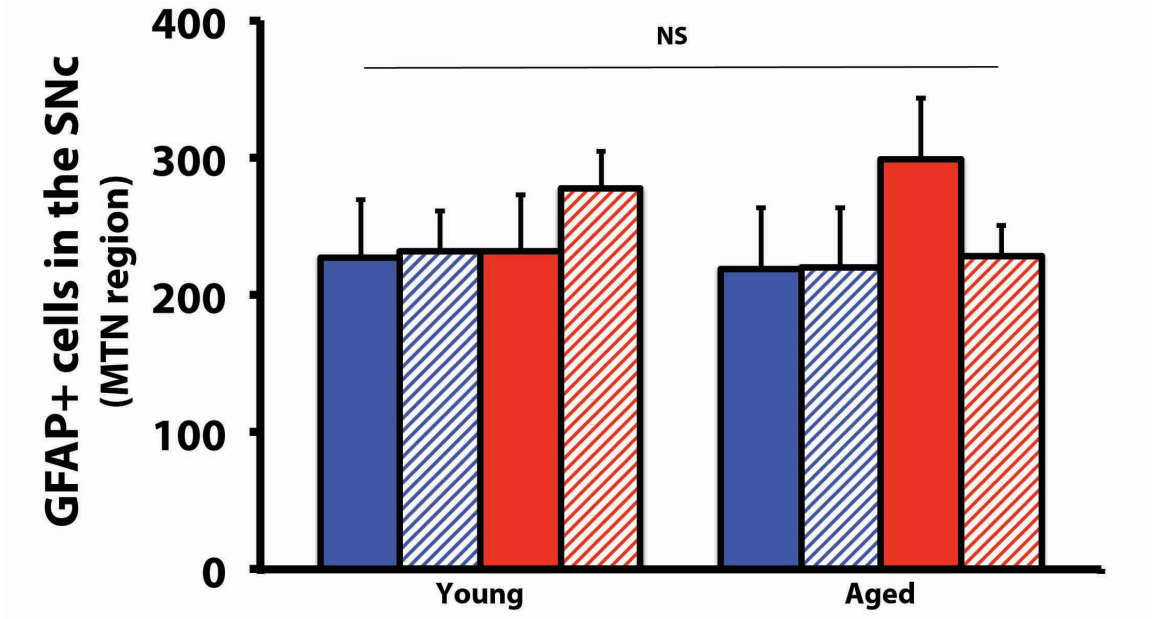
GFAP+ cells in the SNc
(MTN region)
400
300
200
100
0
NS
Young
Aged

To assess whether this histopathological phenotype corresponds with a functional outcome, we subjected animals to behavioral testing. However, DJ1-C57 affected mice do not exhibit a clear decrease in gross motor function at 2, 6, or 12 mo of age (Fig. 2.S3 *A–C*) or any differences in drug-induced rotational behavior (Fig. 2.S3*D*). The lack of behavioral differences may be accounted for by two observations. First, examination of the striatal DA terminals revealed no clear loss in striatal fibers in young animals (Fig. 2.2*B*). This finding raised the possibility that sprouting of neurites within the nigrostriatal pathway may be compensatory in young mice. This is of marked interest because we note significant sprouting of dysmorphic neurites (as seen in Fig. 2.2*A*) in the SNc, which may be compensating for the loss of cell bodies as reported previously (Pritzel et al., 1983; Song and Haber, 2000). Second, an increase in the striatal postsynaptic marker ΔFBJ murine osteosarcoma viral oncogene homolog B (ΔFosB) is observed in affected DJ1-C57 mice (Fig. 2.2*C*). PD patients have been shown to have up-regulated ΔFosB in their caudate/putamen (Tekumalla et al., 2001). Moreover, ΔFosB has been shown previously to be up-regulated in toxin models of neurodegeneration such as 1-methyl-4-phenyl-1,2,3,6-tetrahydropyrindine (MPTP) and 6-hydroxydopamine (6-OHDA) as a compensatory response to a loss of DA innervation (Doucet et al., 1996; Pérez-Otaño et al., 1998).

Fig. 2.S3: No visible motor behavior defects in young DJ1-C57 mice. (A–C) Littermate DJ1-C57 mice (n = 15) and WT (n = 12) controls were subjected to motor behavioral testing at 2, 6, and 12 mo. No significant differences were observed in either beam break (A), open field test (B), or rotorod (C). (D and E) Amphetamine- and apomorphine-induced rotational behavior was also performed at 6 mo. No significant differences in turn number or directionality was observed. Bars represent means ± SEM.

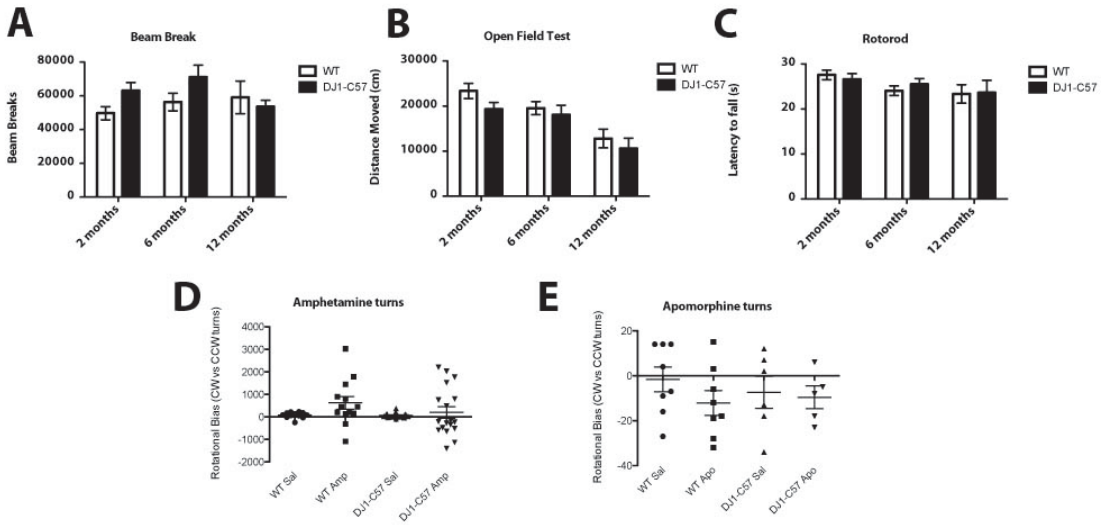
A
Beam Break
Beam Breaks
80000
60000
40000
20000
0
2 months
6 months
12 months
WT
DJ1-C57
B
Open Field Test
Distance Moved (cm)
30000
20000
10000
0
2 months
6 months
12 months
WT
DJ1-C57
C
Rotorod
Latency to fall (s)
30
20
10
0
2 months
6 months
12 months
WT
DJ1-C57
D
Amphetamine turns
Rotational Bias (CW vs CCW turns)
4000
3000
2000
1000
0
-1000
-2000
WT Sal
WT Amp
DJ1-C57 Sal
DJ1-C57 Amp
E
Apomorphine turns
Rotational Bias (CW vs CCW turns)
20
0
-20
-40
WT Sal
WT Apo
DJ1-C57 Sal
DJ1-C57 Apo

With aging of DJ-1–deficient animals, an increase in the prevalence of the DJ1-C57 affected unilateral phenotype was observed over time, peaking at 12 mo of age (42.9% penetrance, Fig. 2.4*A* and Table 2.S2). When only affected unilateral DJ1-C57 animals are considered, there was a clear loss in total number of SNc DA neurons even at early time points (Fig. 2.S4). However, if all (affected and unaffected) DJ-1–deficient animals were evaluated together, the total number of DA neurons was not significantly reduced until later aging stages (15 mo). At this time, the unilateral phenotype dissipated and a more bilateral phenotype of nerve cell loss was observed (Fig. 2.4 *A* and *B* and Table 2.S2). Interestingly, these aged mice, unlike at the earlier times, exhibited a decrease in DA-synthesizing TH-positive striatal terminals (Fig. 2.4*C*). Upon evaluation of any neuritic beading in these aged animals, we noted that although process length itself did not further change between young and aged DJ1-C57 mice (Fig. 2.S5 *A* and *B*), aged DJ1-C57 mice exhibited a decreased number of sprouting processes in the SNc region (Fig. 2.S5*C*). Moreover, long-term behavior testing revealed a mild motor defect in the aged (14–16 mo) DJ1-C57 mice when examined by both the grid test (Fig. 2.4*E*) and the pole test (males; Fig. 2.4*F*).

Fig. 2.4: Aged DJ1-C57 mice exhibit bilateral DA and noradrenergic denervation in the brainstem. (*A*) Penetrance of unilateral phenotype over time. Penetrant threshold: greater than 40% loss of DA neurons on one side (side A) vs. the other (side B). (*B*) Total stereological counts of DA neurons in the SNc of WT and DJ1-C57 aged (15-mo) animals. (*C*) Representative striatal sections of aged (12–15 mo) WT (*Upper Left*) and DJ1-C57 (*Lower Left*) mice stained for TH. Quantification of TH expression in the striatum relative to the *corpus callosum* was performed in young and aged animals (*Right*). (*D*) Representative micrographs of LC sections in the pons stained for TH for either aged WT (*Left*) or aged DJ1-C57 (*Center*). Quantification of TH-positive neurons for both young and aged animals is shown (*Right*). (*E*) The grip test evaluated the capacity of the mouse to stay on an inverted metal grid for 60 s. (*F*) The pole test evaluated the latency of mice to descend a gauze-wrapped pole (in seconds). NS, not significant ($P > 0.05$); *$P < 0.05$; ANOVA, followed by Tukey's LSD post hoc tests. Data are represented as means ($n = 3–13$ per group) ± SEM.

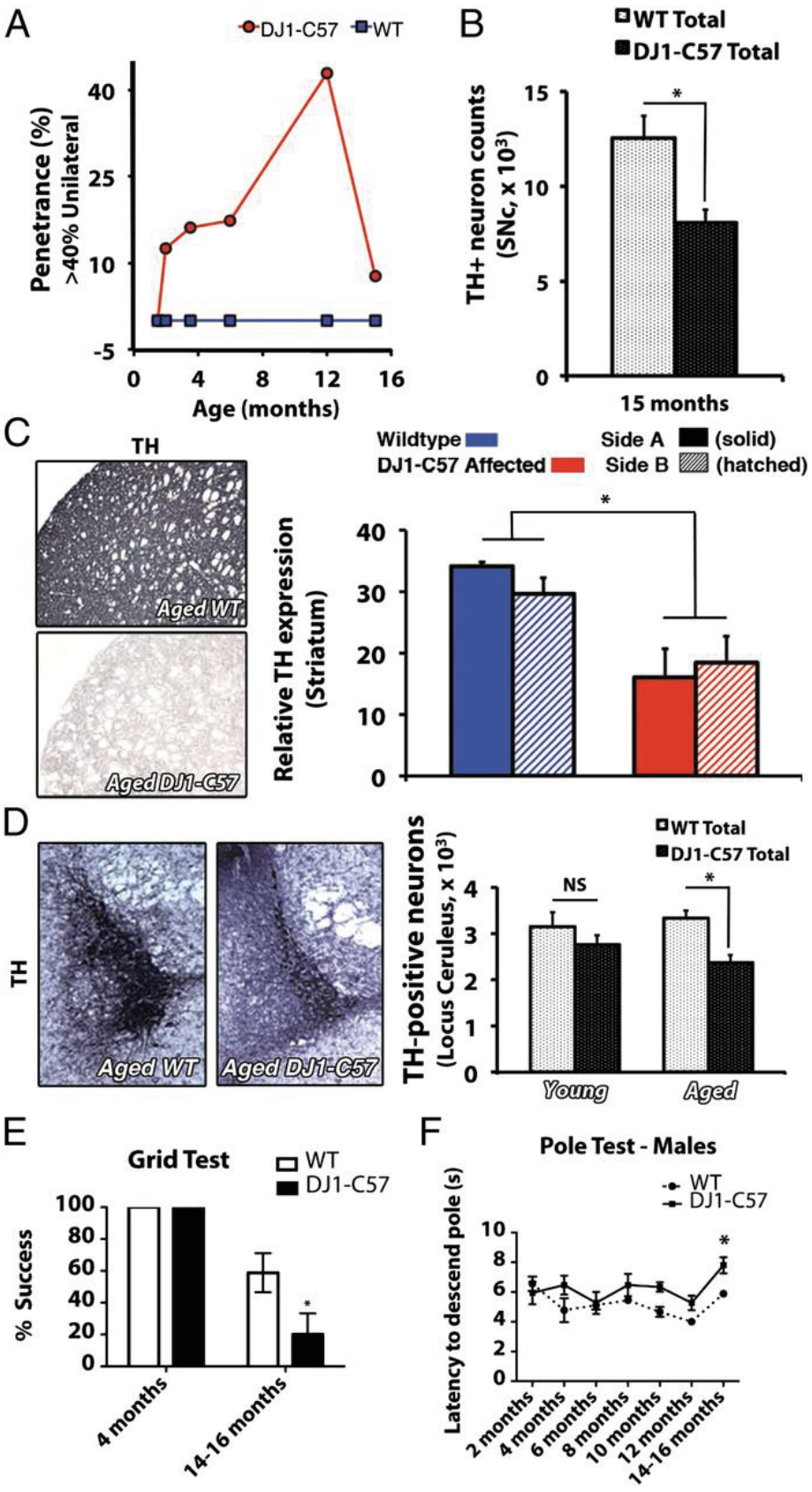
A
DJ1-C57
WT
Penetrance (%)
>40% Unilateral
40
25
10
-5
0
4
8
12
16
Age (months)
B
WT Total
DJ1-C57 Total
TH+ neuron counts
(SNc, x 10³)
15
10
5
0
*
15 months
C
TH
Aged WT
Aged DJ1-C57
Wildtype
DJ1-C57 Affected
Side A (solid)
Side B (hatched)
Relative TH expression
(Striatum)
40
30
20
10
0
*
D
TH
Aged WT
Aged DJ1-C57
TH-positive neurons
(Locus Ceruleus, x 10³)
WT Total
DJ1-C57 Total
4
3
2
1
0
NS
*
Young
Aged
E
Grid Test
WT
DJ1-C57
% Success
100
80
60
40
20
0
*
4 months
14-16 months
F
Pole Test - Males
WT
DJ1-C57
Latency to descend pole (s)
10
8
6
4
2
0
*
2 months
4 months
6 months
8 months
10 months
12 months
14-16 months

Fig. 2.S4: Bilateral DA cell loss in the SNc of aged DJ1-C57 mice. Stereological counts of TH-positive neurons in midbrain sections from WT and DJ1-C57 mice were performed at various time points. Each data point represents mean ± SEM (n = 1–37 per data point). *P < 0.05; **P < 0.01 by ANOVA, followed by Tukey's LSD post hoc test.

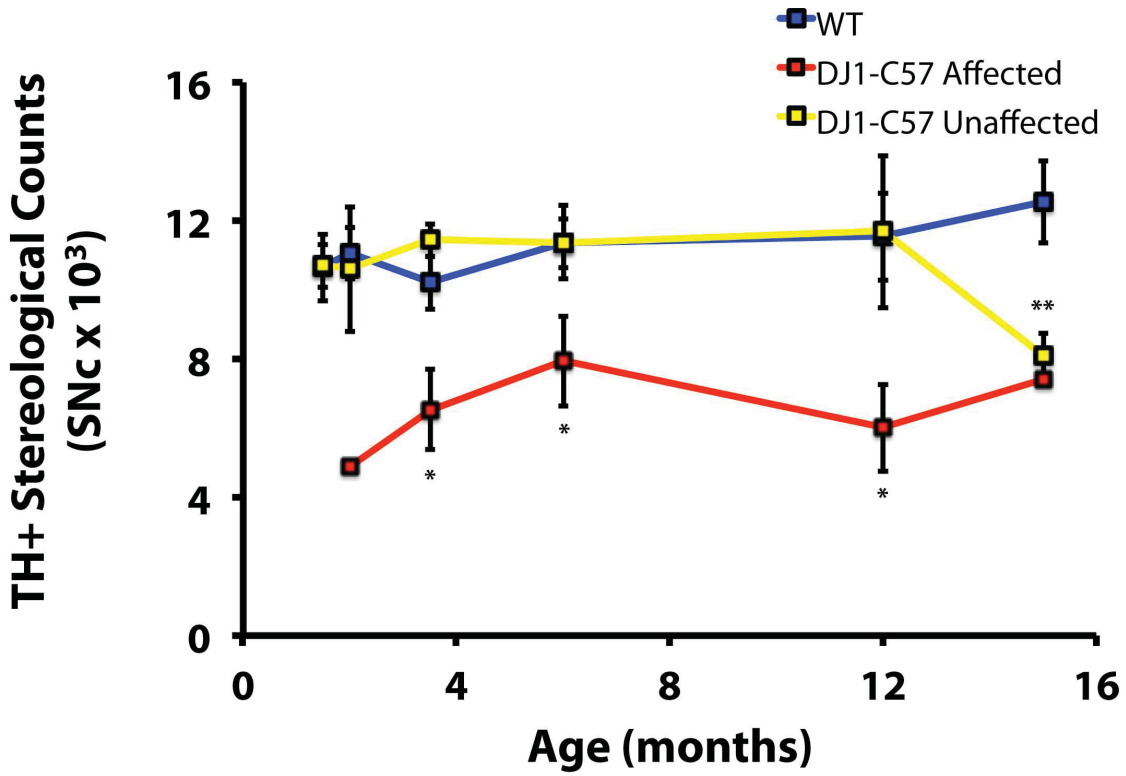
WT
DJ1-C57 Affected
DJ1-C57 Unaffected
TH+ Stereological Counts
(SNc x 10³)
16
12
8
4
0
0
4
8
12
16
Age (months)
*
*
*
**

Fig. 2.S5: DJ1-C57 affected mice exhibit neuritic beading in the SNc throughout their lifespan but show a marked decrease in fiber density with age. (A) Representative pictures of affected DJ1-C57 mice vs. WT animals. (B) Quantification of uninterrupted process length as in Fig. 2A. (C) Quantification of relative fiber density in the SNc. Each box represents mean ± SEM (n = 4–11 per data point). *P < 0.05; ***P < 0.001 by ANOVA, followed by Tukey's LSD post hoc test.

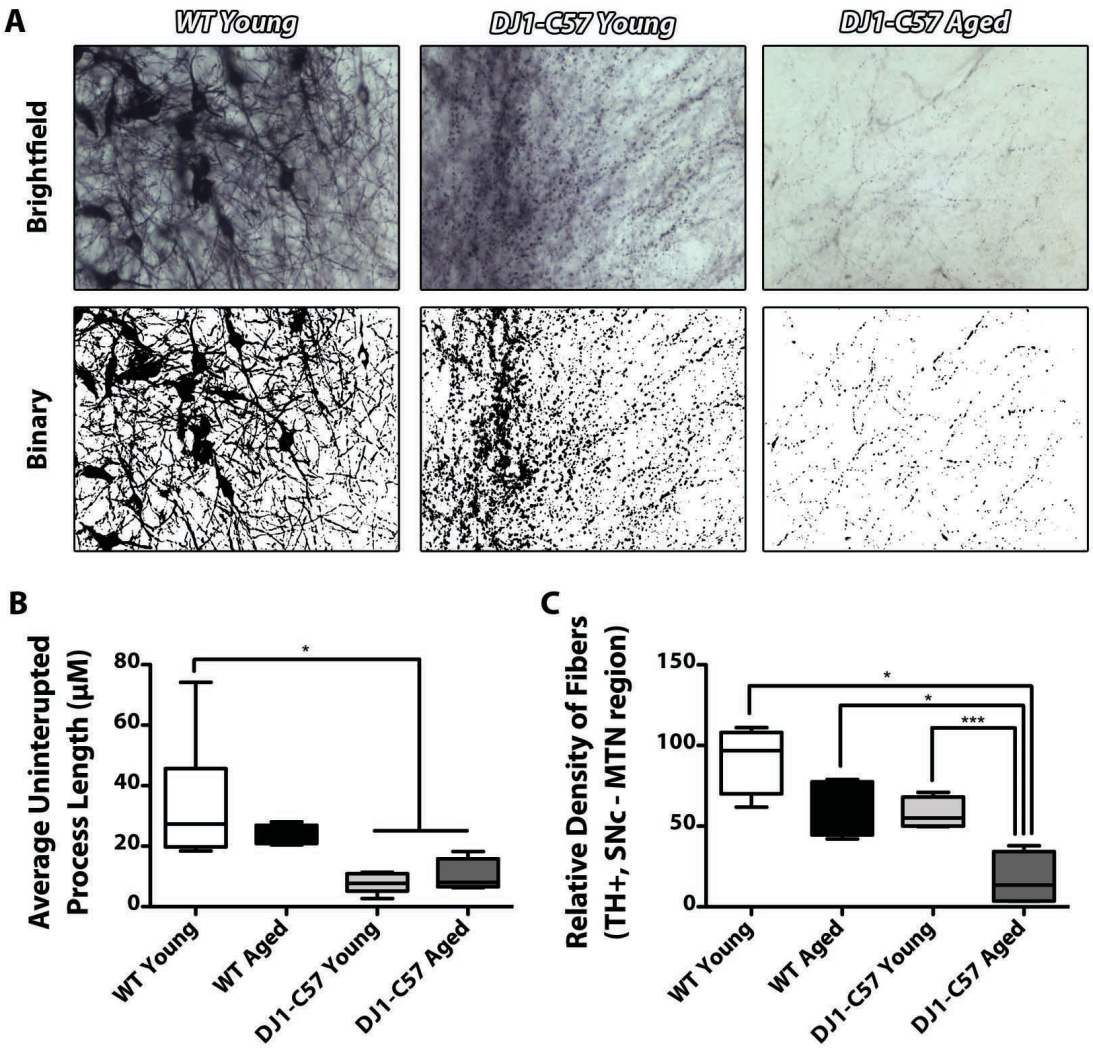
A
WT Young
DJ1-C57 Young
DJ1-C57 Aged
Brightfield
Binary
B
Average Uninterupted Process Length (µM)
80
60
40
20
0
*
WT Young
WT Aged
DJ1-C57 Young
DJ1-C57 Aged
C
Relative Density of Fibers (TH+, SNc - MTN region)
150
100
50
0
*
*
***
WT Young
WT Aged
DJ1-C57 Young
DJ1-C57 Aged

The neuropathology of PD encompasses degeneration not only of the SNc but also of other nuclei in the brainstem including the *locus ceruleus* (LC) (Forno and Alvord, 1974). Therefore, LC of DJ1-C57 mice were examined for TH-immunoreactive cell bodies. A significant reduction in TH-positive cells of the LC was observed in aged DJ1-C57 mice compared with WT controls (Fig. 2.4*D*). Furthermore, because α-synuclein aberrant processing is a hallmark of idiopathic PD, we examined whether our DJ1-C57 mice exhibited altered expression or localization of the protein. No visible changes were noted in the expression of endogenous α-synuclein between DJ1-C57 mice and littermate controls (Fig. 2.S6 *A* and *B*). In addition, upon examination of leucine-rich repeat kinase 2 (LRRK2) expression (another autosomal dominant PD-linked protein), we did not note any significant changes in expression or localization of the protein (Fig. 2.S6*B*).

Fig. 2.S6: DJ1-C57 affected mice do not show visible alterations in α-synuclein expression. (A) Representative midbrain sections stained for α-synuclein and LRRK2 at the level of the MTN. SNCA KO denotes α-synuclein–null animal tissue. (B) Changes in α-synuclein and LRRK2 expression were also determined by Western blot. Striatal punches were taken from SNCA KO, LRRK2 KO, DJ-1 KO, and WT animals to assess expression of α-synuclein and LRRK2, as well as confirm loss of DJ-1, in the brain.

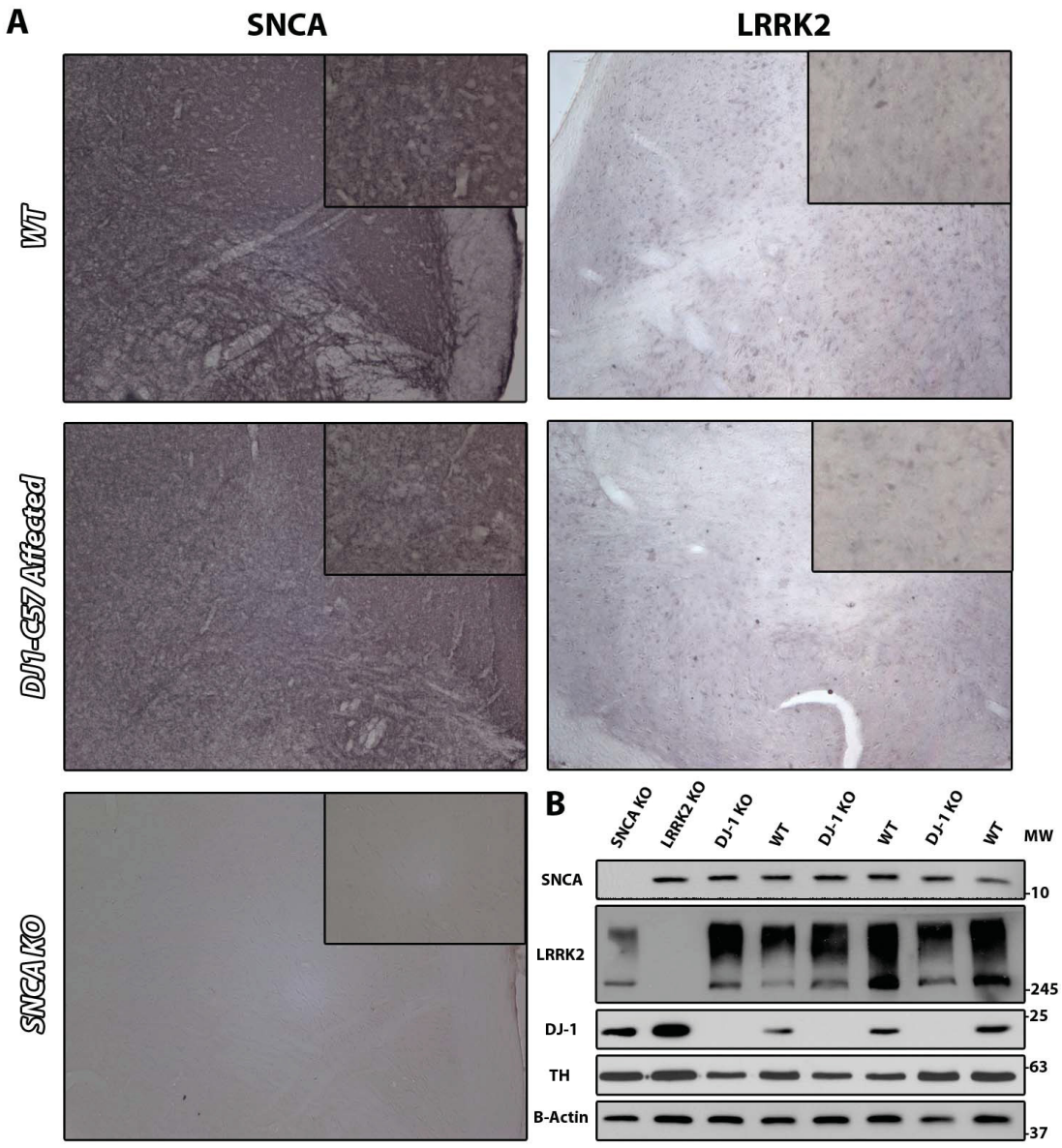
A
SNCA
LRRK2
WT
DJ1-C57 Affected
SNCA KO
B
SNCA KO
LRRK2 KO
DJ-1 KO
WT
DJ-1 KO
WT
DJ-1 KO
WT
MW
SNCA
LRRK2
DJ-1
TH
B-Actin
10
245
25
63
37

Finally, to elucidate potential mechanism(s) through which this selective neurodegeneration occurs in a subset of these DJ1-C57 mice, we performed whole-exome sequencing on affected (n = 3) and unaffected (n = 3) DJ-1-C57 mice as an approach to identify candidate modifiers (Fig. 2.5*A*). After filtering for coding regions and for variants found in all three affected but none of the three unaffected mice, only five candidates in coding regions were identified as potential modifiers of the phenotype [signal regulatory protein β (Sirbp)1A, 2610203C20Rik, zinc finger, SWIM domain containing 6 (Zswim6), kinesin family member (Kif) C5b, and SWI5-dependent recombination repair 1 (Sfr1); Fig. 2.5*B*]. Moreover, because exome sequencing also covers flanking intronic sequences, an additional 23 candidates were identified in noncoding regions (Table 2.S3), although none of these were in known intron–exon splice sites. Together, these results suggest the segregation of several genomic loci with the phenotype.

Fig. 2.5: List of exonic variants unique to affected DJ1-C57 mice. (*A*) Schematic workflow of exome sequencing to determine candidate mutations in affected DJ1-C57 mice (vs. unaffected littermate controls). (*B*) Table of variants present in all three examined affected animals and no unaffected littermates. See *Experimental Procedures* for selection criteria.

A

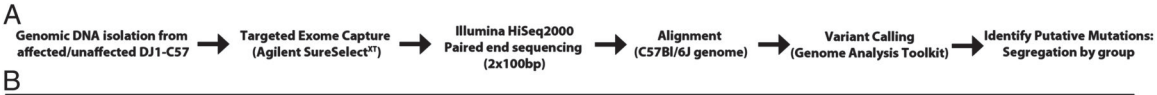

B

Gene name	Gene description	Position	Chromosome	Mutation type	Codon	Effect	Amino Acid	Function	Presence	
									Affected (/3)	Unaffected (/3)
Sirpb1a	signal-regulatory protein beta 1A	15,417,016	3	SNP	tCc/tTc	Missense Mutation	S84F	Phagocytosis	3	0
Sirpb1a	signal-regulatory protein beta 1A	15,417,020	3	SNP	Cat/Tat	Missense Mutation	H83Y	Phagocytosis	3	0
2610203C20Rik	RIKEN cDNA 2610203C20 gene	41,389,287	9	SNP	Acc/Ccc	Missense Mutation	T59P	Unknown	3	0
2610203C20Rik	RIKEN cDNA 2610203C20 gene	41,389,294	9	SNP	cAc/cCc	Missense Mutation	H61P	Unknown	3	0
Zswim6	zinc finger, SWIM domain containing 6	108,679,774	13	SNP	gCg/gGg	Missense Mutation	A157G	Unknown	3	0
Kifc5b	kinesin family member C5B	27,061,155	17	SNP	Gtc/Atc	Missense Mutation	V319I	Chromosomal segregation	3	0
Sfr1	SWI5 dependent recombination repair 1	47,807,383	19	SNP	Ccc/Acc	Missense Mutation	P93T	DNA recombination	3	0

Table 2.S3: Noncoding putative modifiers that segregate with the DJ1-C57 phenotype. The table shows variants present in all examined affected animals (n = 3) and no unaffected littermates (n = 3) as in Fig. 5. See Experimental Procedures for selection criteria. AKT, serine/threonine kinase; Het, heterozygous; Hom, homozygous; Kv channel, voltage-gated potassium channel; NLRP3, NLR family, pyrin domain–containing 3; ROS, reactive oxygen species; SRY, sex-determining region Y; TAG, triacylglycerol. Dash represents not defined.

Gene name	Gene description	Position	Chromo-some	Mutation type	Location	Genotype	Function	Presence	
								Affected (/3)	Unaffected (/3)
Pigt	phosphatidylinositol glycan anchor biosynthesis, class T	164,332,071	2	Indel	Intron	het	GPI-transfer to proteins	3	0
Sox2	SRY-box containing gene 2	34,549,323	3	SNP	UTR 5'	het	Transcription factor	3	0
Ptgr1	prostaglandin reductase 1	58,994,758	4	Indel	Intron	het	Metabolic inactivation of leukotriene B4	3	0
Gm13150	predicted gene 13150	146,356,934	4	SNP	Intron	het	Unknown	3	0
Sri	sorcin	8,062,470	5	Indel	Intron	het	Modulates calcium homeostasis by directly binding to it	3	0
RP24-449D6.1	-	15,032,507	5	SNP	Intron	het	Unknown	3	0
Plxnd1	plexin D1	115,920,073	6	SNP	Intron	het	Semaphorin signalling	3	0
Supt5h	suppressor of Ty 5 homolog (S. cerevisiae)	29,116,278	7	Indel	Intron	het	Homologue of "foggy", a zebrafish gene which shows DAergic degeneration when KOed, regulates transcriptional elongation	3	0
Myh14	myosin, heavy chain 7B, cardiac muscle, beta	51,894,551	7	SNP	Intron	het	Cardiac and skeletal muscle contraction	3	0
Trim30a	tripartite motif-containing 30A	111,578,560	7	Indel	Intron	het	Negatively regulates NLRP3 inflammasome activation and reduces ROS formation	3	0
Nucb2	nucleobindin 2	123,671,348	7	SNP	Intron	het	Calcium binding EF-hand protein	3	0
Gm10348	-	20,020,424	8	SNP	Upstream	het	Unknown	3	0
Thy1	thymus cell antigen 1, theta	43,855,093	9	SNP	Intron	het	Glycoprotein involved in cell-cell interactions in thymocytes and neurons	3	0
Snora62	small nucleolar RNA, H/ACA box 62	120,044,385	9	SNP	Downstream	het	Processing rRNA precursors	3	0
Dgka	diacylglycerol kinase, alpha	128,160,214	10	SNP	Intron	het	Phospholipid and TAG synthesis. Regulates RAS and RHO.	3	0
Kcnip1	Kv channel-interacting protein 1	33,545,464	11	Indel	Intron	het	Synaptic transmission regulation	3	0
Fam33a	family with sequence similarity 33, member A	86,929,722	11	SNP	Intron	het	Chromosomal segragation	3	0
Tecpr2	tectonin beta-propeller repeat containing 2	112,136,799	12	Indel	Intron	hom	Unknown	3	0
Slc34a1	solute carrier family 34 (sodium phosphate), member 1	55,504,541	13	Indel	Intron	het	Sodium-Phosphate co-transporter (Renal)	3	0
Atp8a2	ATPase, aminophospholipid transporter-like, class I, type 8A, member 2	60,392,606	14	Indel	Intron	het	Drive uphill transport of ions across membranes	3	0
1110020G09 Rik	RIKEN cDNA 1110020G09 gene	9,001,555	15	SNP	Intron	het	Unknown	3	0
Pdpk1	3-phosphoinositide dependent protein kinase 1	24,244,255	17	SNP	Intron	het	pAtes AKT at Thr308	3	0
Tcte1	t-complex-associated testis expressed 1	45,676,562	17	SNP	Intron	het	Testes specific of unclear function	3	0

Discussion:

In our DJ1-C57 mice, we have uncovered an early PD-type phenotype that progressed with age and showed incomplete penetrance. In backcrossing and extensively interbreeding DJ-1–null mice, we obtained a subset of DJ1-C57 mice that exhibited robust unilateral nigral degeneration as early as 8 wk of age: a finding potentially consistent with the early-onset pathogenicity of DJ-1 loss in human carriers of DJ-1 mutations (Bonifati et al., 2003). This cell loss was accompanied with compensatory sprouting and the appearance of dysmorphic and beading neurites, as well as microgliosis, a result congruent with the notion that microglia may induce neuritic beading during neuronal dysfunction (Takeuchi et al., 2005). Furthermore, findings of compensatory sprouting upon cell loss, dysmorphic neurites, and an increase in proinflammatory responses are all present in postmortem samples from PD patients (McGeer et al., 1988; Greenwood et al., 1991; Nagatsu and Sawada, 2005; Ouchi et al., 2005; Mount et al., 2007; Whitton, 2007). Therefore, given the early age of onset of degeneration in these mice, our findings are of particular significance and may correlate with features of autosomal recessive PD. This loss-of-function phenotype has not yet been modeled successfully in rodents, with the possible exception of a partial reduction in LC neurons in one *parkin*$^{-/-}$ mouse model (Coelln et al., 2004).

We also noted that although DJ-1 loss–mediated neurodegeneration will invariably lead to PD in humans, this might not be as dramatic in mice with a relatively short lifespan of ~24 mo. However, early pathological changes associated with this genetic form of PD are nonetheless observed. Thus, much like preclinical PD, where no clear clinicopathological correlate may be apparent until over 80% of the nigral cell

population has been lost, a compensatory mechanism such as neuritic sprouting or postsynaptic sensitization may account for the lack of motor defects in these young animals. Furthermore, the relevance of this model is made even more apparent as the DJ1-C57 mice age. Aged DJ1-C57 mice progressed to bilateral degeneration of their SNc, as well as of their nigrostriatal projections to the forebrain. Thus, this preclinical phenotype likely first occurs at 2 mo and progresses over the course of the following 10–12 mo. In addition, at this older stage, these mice exhibited cell loss at the level of the LC, a pathological characteristic of the human condition. Finally, aged mice beyond 12 mo start to show basal behavioral deficits. Therefore, our DJ1-C57 mouse model presents a potentially important role in filling the gap in our understanding of early-onset preclinical PD in humans.

The reason behind the observed phenotype remains unknown. To begin to explore this issue, we performed whole-exome sequencing to identify potential genes that may contain polymorphisms in affected but not unaffected mice. Surprisingly, the list of genes that met these criteria was limited to five candidates with exon-containing changes. One potential modifier gene candidate, *Sirbp1a*, was particularly interesting given the increase in microglial activation observed in the affected DJ1-C57 mice. SIRBP1A has been associated with a role in promoting phagocytosis in macrophages and monocytes (Hayashi et al., 2004). It is possible that disruption of this function may result in aberrant microglial activity. Future studies will seek to elucidate the putative relationship between DJ-1 and SIRBP1A, as well as with other coding modifiers. These exon candidates, although intriguing, are not the only factors that may account for the degenerative phenotype. Other possibilities include intron changes, particularly at loci-flanking exons.

In this regard, we observed that 23 intronic modifiers segregated with the phenotype. The specific role of these polymorphisms/indels remains unclear, because they do not correspond to splice donor/acceptor sites. Finally, it is possible that a combination of all of these factors may contribute to the phenotype. Therefore, more careful analyses must be performed to examine among these possibilities. What is important, however, is that our studies demonstrate that a defined group of polymorphisms can segregate with our phenotype. How these factors regulate DA loss in DJ-1–deficient mice will require further analyses.

Collectively, we present a murine model that reproduces a clinically detectable phenotype owing to the modification of a PD-related gene. Affected DJ1-C57 mice display: (*i*) unilateral DA cell loss with a predilection for the SNc versus VTA as early as 2 mo of age; (*ii*) development of aberrant neuritic processes with ensuing microgliosis in the SNc and increased ΔFosB staining in the striatum at a young age; and (*iii*) progression to bilateral degeneration of the nigrostriatal axis and of the LC at an older age (model; Fig. 2.6), which are associated with mild motoric changes. This progression to a bilateral phenotype is of particular interest to us given the typical unilateral-to-bilateral progression of the disease in humans (Pahwa et al., 2003). Interestingly, no significant changes were noted in α-synuclein or LRRK2 expression, suggesting a disease process independent of Lewy body generation. These results strongly suggest that this murine model of early parkinsonism mimics autosomal recessive early-onset PD pathology, rather than that of sporadic PD (Kitada et al., 2012). It, thus, provides a tool to elucidate the cascade of pathogenic changes that occurs in autosomal recessive, early-onset PD, as well as a platform to explore neuroprotective interventions in the future.

Fig. 2.6: DJ1-C57 preclinical model of DA neurodegeneration. (*A*) Altered representative micrographs reproduced with permission from the Mouse Brain Library [www.mbl.org; Rosen et al. (Rosen et al., 2003)] depicting healthy (red) SNc, striatum, and LC in 6-wk-old DJ1-C57 mice or all WT groups examined. (*B*) Affected DJ1-C57 mice demonstrate unilateral DA cell loss in the SNc but not in the LC. (*C*) Aged DJ1-C57 mice exhibit widespread degeneration in their nigrostriatal tract, as well as their LC.

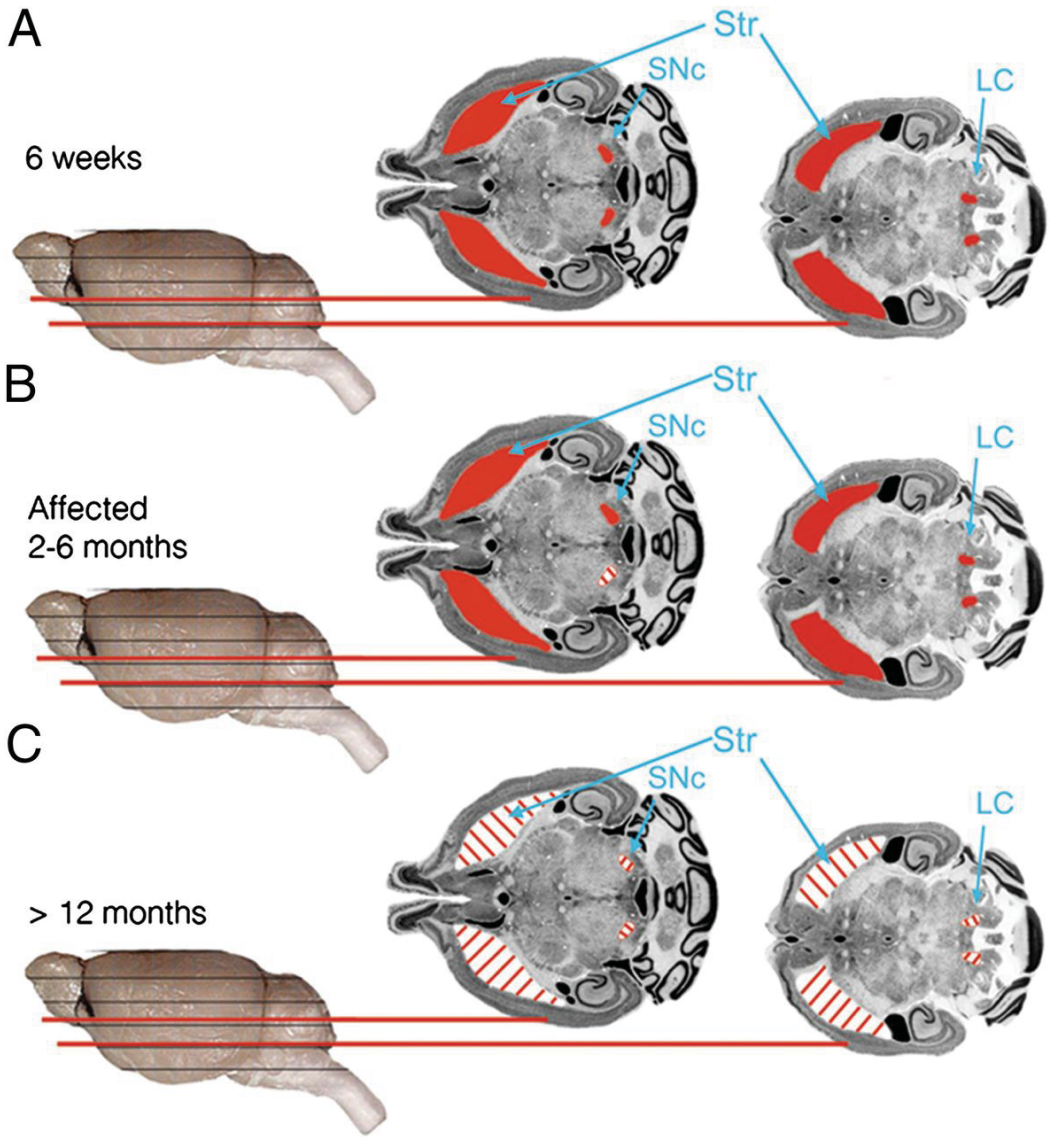
A
Str
SNc
LC
6 weeks
B
Str
SNc
LC
Affected
2-6 months
C
Str
SNc
LC
> 12 months

Experimental Procedures:

DJ1-C57 Mouse Creation: DJ-$1^{-/-}$ mice were generated as described previously (Kim et al., 2005). Mice were subsequently backcrossed 14 times onto a pure C57BL/6 background (Charles River) to obtain DJ1-C57 mice. Animals were then interbred extensively for colony maintenance and experimentation. Animals were kept at 25 °C on a light (12 h)/dark (12 h) cycle with ad libitum access to standard rodent laboratory chow and water. Animal care was carried out in accordance with the guidelines of the Canadian Council and Care of Animals in Research and the Canadian Institutes of Health Research and was approved by the University of Ottawa Animal Care Veterinary Services.

Histology: After being perfused transcardially, mouse brains were fixed in 4% paraformaldehyde and cryoprotected as described elsewhere (Crocker et al., 2001). Midbrain sections containing the SNc (40 μm), pontine sections containing LC (40 μμ), and striatal (14 μm) sections were immunostained via avidin–biotin complex staining as described previously (Mount et al., 2007).

DA Cell Survival Quantification: DA neuron survival in the SNc was blindly assessed by stereology using Stereo Investigator as described previously (Mount et al., 2007). Striatal TH quantification was performed at 200×. For each picture, five samples of striatum and one sample of corpus callosum were used for densitometric analysis. Relative intensity of immunodetection was calculated using ImageJ v.1.41o (National Institutes of Health). For each sample, three slices of striatum were used to calculate the mean striatal density.

Neuritic Beading Measurement: Neuritic beading was measured using ImageJ. Briefly, average length of uninterrupted process in a visually focused plane was measured as 20

measurements/section and measuring three sections per animal. Raw data were then binned into five categories of length and represented as percentage distribution.

ΔFosB and CD11b Measurement: Striatal (ΔFosB) and midbrain [cluster of differentiation (CD)11b] sections were stained, and three pictures were taken per animal, per side. Puncta in a given visual field were assessed blindly using ImageJ v1.41o.

Locus Ceruleus Neuron Quantification: Noradrenergic cell survival in the LC was measured by counting four representative sections and projecting their counts to a total value as described previously (German et al., 2000).

CV Quantification: CV staining and quantification were performed as described previously (Mount et al., 2007). Briefly, cell viability in the medial terminal nucleus (MTN) region of the midbrain was assessed as per the nuclear integrity of the cells present.

Antibodies Used: CD11b (1:200; AbD Serotec), FosB (1:250; Santa Cruz Biotechnologies), glial fibrillary acidic protein (GFAP) (1:1,000; Cell Signaling), DJ-1 (1:50,000; Abcam), α-synuclein (1:1,000; BD Transduction), LRRK2 (1:50,000; Epitomics), and TH (1:10,000; Immunostar or 1:2,000; Chemicon) were used for either avidin–biotin complex (ABC) visualization by 3,3′-diaminobenzidine (DAB) or via fluorophore-conjugated secondary antibody.

Motor Behavior Testing: The grid test was carried out by placing DJ1-C57 affected, unaffected, and WT mice on a metal grid (0.5-cm spacing between metal wires) and then turning the grid over for 60 s. If a mouse could hold on for the entire 60 s, it was scored as "success," whereas if it fell before the set time, it was scored as a "fail." The pole test was used to measure the latency to descent an 18-inch pole wrapped in gauze.

Exome Sequencing: Genomic DNA (6 μg) was isolated from ear samples of affected/unaffected mice using the DNeasy Blood and Tissue kit (Qiagen). Samples underwent targeted exome capture using the Agilent SureSelectXT Mouse All Exon kit and subsequently underwent next-generation sequencing via an Illumina HiSeq 2000 sequencer. Raw data were aligned to the mouse genome, and variants were called using the Broad Institute GATK (Genome Analysis ToolKit).

Statistical Analysis: Data throughout the paper are expressed as averages ± SEM for a given sample size (*n*). Statistical analysis for histological and behavioral data were performed by means of either a paired *t* test or one-way ANOVA, followed by Tukey's least significant difference (LSD) post hoc test, as indicated in *SI Text* and the figure legends.

Acknowledgments:

We thank the University of Ottawa Faculty of Medicine Behavior Core Facility for use of their equipment; Daniele Merico (Centre for Applied Genomics, Hospital for Sick Children) for assistance with bioinformatics analysis of the exome data; and Linda Jui, Mirela Hasu, Steve M. Callaghan, Carmen Estey, Elizabeth Abdel-Messih, and Hossein Aleyasin for technical assistance and scientific input. This work was supported by grants from Parkinson Society Canada; the Canadian Institutes of Health Research; the Centres of Excellence in Neurodegeneration (COEN); the Heart and Stroke Foundation of Ontario (HSFO); the Neuroscience Canada/Krembil Foundation; the Parkinson's Disease Foundation; The Michael J. Fox Foundation for Parkinson's Research; the Parkinson Research Consortium (PRC); the Canadian Stroke Network; the Heart and Stroke Foundation of Canada (HSFC) for Stroke Recovery; and the World Class University Program through the National Research Foundation of Korea, funded by Ministry of Education, Science, and Technology, South Korea Grant R31-2008-000-20004-0 (to D.S.P.). D.S.P. is a recipient of the HSFO Career Investigator Award. M.W.C.R. is a recipient of the HSFC Focus on Stroke Award, as well as the Canadian Institutes of Health Research (CIHR) Training Program in Neurodegenerative Lipidomics Supplement Scholarship. P.C.M. is a recipient of The PRC Toth Family Fellowship in Parkinson's Research.

Supplementary Information:

SI Experimental Procedures:

Additional Motor Behavior: In all behavior tests except for the pole test, mice were habituated to the testing room with white noise for an hour before testing. In the open field test (OFT), mice were placed in the corner of a novel (~45-cm3) box, and video was analyzed for 10 min. Total distance moved was measured in centimeters. In the rotorod test, mice were placed on an accelerating rotorod, and latency to fall of the rod was measured in seconds. In the beam break test, mice were subjected to a novel cage for 24 h, and total activity (beam breaks) was recorded. All video data were obtained and analyzed with the Noldus Ethnovision 8.0 software. Data analysis was carried out in age-matched littermates for 2, 6, and 12 mo. Amphetamine- and apomorphine-induced rotational behavior was performed in an open field environment (see open field test). Briefly, animals received an i.p. injection of amphetamine (2 mg/kg) or an s.c. injection of apomorphine (2 mg/kg) and were placed in the open field 5 min following the injection. Rotations [clockwise (CW) or counterclockwise (CCW)] were measured, and analysis was carried out post hoc using side A as the presumed affected side to compute net rotations.

Relative Density of Fibers in the SNc: Density of fibers in the SNc was performed using ImageJ. Briefly, pictures originally taken for the beading experiments were taken (at 40×) and subjected to the following processing. Background was reduced by selecting "subtract background" with a rolling ball radius of 15 pixels. Images were then converted into binary format, after which the area occupied by black within the field was measured as an indirect measurement of fiber density in the region of the SNc.

Chapter 3:

LRRK2-I2020T functional genetic interactors modifying eye degeneration and dopaminergic cell loss in Drosophila.

Paul C. Marcogliese, Sameera Abuaish, Ghassan Kabbach, Elizabeth Abdel-Messih, Sarah Seang, Gang Li, Ruth S. Slack, M. Emdadul Haque, Katerina Venderova, David S. Park

Statement of Author contribution:

The following manuscript follows the format for submission to the journal *PLOS Genetics* to which it will be submitted. This body of work encompasses an unbiased *in vivo* screen for LRRK2 genetic interactors in *Drosophila*. It was conducted based on LRRK2 mediated toxicity in the eye that the Park lab previously characterized (Venderova et al., 2009). Importantly, the 36 interactors elucidated from the screen were then examined in the fly dopaminergic system to determine if they could modify dopaminergic cell loss observed in LRRK2 expressing flies. Pathway analysis of interactors in the eye and dopamine system reveals potentially distinct pathways for LRRK2 mediated toxicity by cell type.

Initial screening efforts were primarily performed by Paul C Marcogliese (2nd and 4th chromosome) and Sameera Abuaish (3rd chromosome). Both PCM and SA performed dopaminergic characterization. Paul C. Marcogliese performed further studies including: locomotor assays, EGFR screening, and pathway analysis. Paul C. Marcogliese interpreted results and wrote the manuscript. David S Park edited the manuscript.

Classification: BIOLOGICAL SCIENCES, Neuroscience

LRRK2 functional genetic interactors modifying eye degeneration and dopaminergic cell loss in Drosophila.

Paul C. Marcogliese, Sameera Abuaish, Ghassan Kabbach, Elizabeth Abdel-Messih, Sarah Seang, Gang Li, Ruth S. Slack, M. Emdadul Haque, Katerina Venderova, David S. Park

Number of text pages: 15

Number of figures: 6 main, 1 supplemental, 6 tables

Abstract:

Progressive degeneration of dopaminergic neurons in the substantia nigra is the primary cause for motor symptoms observed in Parkinson's disease (PD). Mutations in leucine-rich repeat kinase 2 (LRRK2) are the most commonly linked contributor to familial PD. LRRK2 is suggested to be involved in a wide variety of cellular processes but deciphering its role in PD has been difficult. Modelling PD in rodents has been a persistent challenge for the field. However, the fruit fly has been utilized successfully to recapitulate PD gene related dopaminergic cell loss. Using the GAL4-UAS system and established models of hLRRK2 induced eye degeneration in *Drosophila*, we conducted a suppressor / enhancer screen to uncover genetic modifiers of LRRK2. We have identified 36 candidate interactors that modify LRRK2 toxicity in the eye. Importantly, we determined if these interactors also modified hLRRK2-I2020T induced dopaminergic cell loss in the fly brain and uncovered 17 genes that modify dopaminergic cell loss. Pathway analysis of eye and dopaminergic interactors reveals EGFR and ubiquitin signalling as a common pathway amongst the interactors, in the eye and DA neurons respectively. Our results offer critical targets for further study of LRRK2 function providing insight into PD pathogenesis.

Introduction:

Parkinson's disease (PD) is predominantly characterized by the progressive degeneration of the dopamine (DA) neurons of the nigrostriatal pathway. Motor symptoms arise typically after at least fifty percent of the DA neurons in the Substantia nigra pars compacta (SNc) have been lost. Currently, patients are treated symptomatically by DA replacement strategies. While the underlying etiology of PD has remained elusive, oxidative stress, mitochondrial damage, protein quality control and inflammatory processes have all been implicated in PD pathogenesis. Importantly, an increasing number of familial PD genes have been identified. LRRK2 mutations account for up to 42% of familial PD and potentially up to 10% of the sporadic disease making it the most commonly linked PD gene (Correia Guedes et al., 2010; Bardien et al., 2011). It encodes for a large, 2547 amino acid, multi-domain protein. Flanked by leucine-rich repeats and a WD40 domain at the N and C terminus respectively, the catalytic core of LRRK2 consists of a ROCO GTPase and a MAP-K like kinase domain (Mata et al., 2006). LRRK2 has been implicated in a wide variety of cellular process including: vesicular trafficking, mitochondrial dynamics, cytoskeleton dynamics, protein degradation pathways and autophagy, inflammatory response, and translational control (Shin et al., 2008; Mortiboys et al., 2010; Häbig et al., 2013; MacLeod et al., 2013; Martin et al., 2014). Unfortunately, there is an incomplete understanding of LRRK2 function as it relates to PD. LRRK2 mouse models, as with other PD genes, generally fail to recapitulate the primary characteristics of the disease. However, multiple groups have had success in modeling LRRK2 induced Parkinsonism in the fruit fly, *Drosophila melanogaster* (Liu et al., 2008; Venderova et al., 2009). Our previous work has shown

that human (h) LRRK2 mutant expression within the *Drosophila* tyrosine hydroxylase positive (TH+) neurons causes TH+ cell loss and locomotor deficits. We furthermore established a rapidly assessable model of degeneration by expressing the I2020T PD mutant in the compound eye of flies using the GMR-GAL4 promoter (Venderova et al., 2009). Using this model, we conducted a functional genetic screen for LRRK2 interacting genes that may enhance or suppress LRRK2 induced degeneration. Identified interacting genes were also confirmed in flies expressing the R1441C and Y1699C pathogenic mutants or the I1122V risk allele. Finally, in order to make our findings more relevant to PD, we determined if any identified candidates from the eye screen also modified TH+ cell loss in our hLRRK2-I2020T flies. Using this strategy we identified novel candidates that converged onto a distinctive genetic pathway than the interactors from the eye screen, supporting growing evidence in the field that LRRK2 may have diverse roles in different cell types.

Results:

The widely established GAL4-UAS (upstream activation sequence) system was utilized to first ectopically express I2020T-hLRRK2 in the retinal ganglion cells of the compound eye of *D. melanogaster*. We have previously shown that hLRRK2 expressing flies maintained at 29°C display retinal degeneration marked by loss of red pigmentation and occasional black spots (Venderova et al., 2009). To test if this phenotype could be suppressed or exacerbated by modifying other genes, we initially conducted an unbiased screen of chromosomes two, three, and four in the organism utilizing the Bloomington deficiency kit. This covers approximately 96% of the autosomal genes in the *Drosophila* genome. This consists of a total of 297 fly lines that have large hemizygous gene deletions that may range from usually 20-100 genes. Notably, taking advantage of the temperature dependency of the GAL4-UAS system, fly screening was conducted at both 29°C and 25°C. This was to ensure accurate sensitivity of the screen since hLRRK2 expressing flies at 25°C display a normal eye with no macroscopic degeneration (see Figure 3.1).

Figure 3.1: Schematic representation of the screen phenotypic readout, process and *Drosophila* genetics. Cartoon representation of parallel screen based on dose-dependent toxicity of LRRK2 expression in the eye due to the temperature dependency of the GAL4-UAS system (A). Diagram describing the screening process from large hemizygous deficiencies to narrowing with sub-region deficiencies and finally specific gene disruptions (B). Example of *Drosophila* genetics underlying the screening process including control and experimental crosses for a second chromosome deficiency (C).

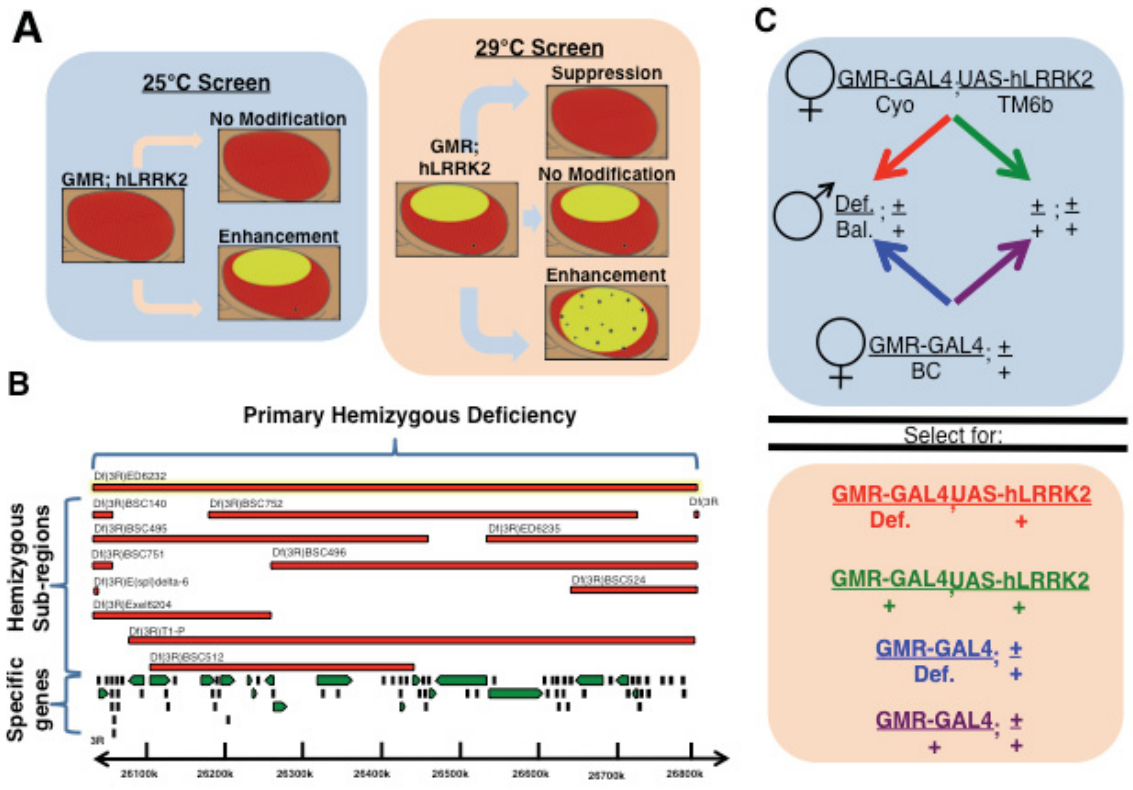
A
25°C Screen
GMR; hLRRK2
No Modification
Enhancement
29°C Screen
GMR; hLRRK2
Suppression
No Modification
Enhancement
B
Primary Hemizygous Deficiency
Hemizygous Sub-regions
Specific genes
C
GMR-GAL4 ♀
Cyo
UAS-hLRRK2
TM6b
Def. Bal. ♂
GMR-GAL4 BC ♀
Select for:
GMR-GAL4, UAS-hLRRK2 / Def. / +
GMR-GAL4, UAS-hLRRK2 / + / +
GMR-GAL4 / Def.
GMR-GAL4 / +

Eye screen:

Upon screening of the primary hemizygous deficiencies, we found 38 regions that phenotypically modified hLRRK2-I2020T expression under the GMR-GAL4 promoter (see Table 3.1). Of these, there were 9 lines on the second chromosome, 29 lines on the third and none found on the fourth. We found 7 deficiency lines that suppressed the loss of pigmentation, surface roughness and black lesions of the GMR-GAL4; UAS-hLRRK2-I2020T flies incubated at 29°C. There were no deficiencies found that led to an enhancement of the GMR-GAL4; UAS-hLRRK2-I2020T at 29°C. We did discover deficiencies that caused strongly defective eyes, however, these phenotypes were always found in the GMR-GAL4/deficiency control, and therefore not due to hLRRK2. Expression of UAS-hLRRK2-I2020T under the GMR-GAL4 does not produce any macroscopic degeneration of the eye at 25°C. We screened the deficiency kit at 25°C in parallel to the screen performed at 29°C. We found 31 deficiencies that produced an obvious loss of pigmentation and damage to the retina when crossed with UAS-hLRRK-I2020T at 25°C. For both temperatures and wherever possible, flies hemizygous for sub-regions within identified interacting primary regions were also analyzed to further narrow down candidate interacting regions (see Table 3.1). These are smaller deficiency regions not provided with the primary deficiency kit. All screened sub-regions that modified GMR-GAL4; UAS-hLRRK2-I2020T eyes displayed consistent phenotypes to the corresponding primary deficiency that they genetically reside within (see Table 3.1 - indents). Scanning electron microscope (SEM) images of deficiencies causing an enhancement or suppression at 25°C or 29°C were obtained for Df(3L)BSC20 and Df(2L)C144 respectively (see Figure 3.2). After the initial screening of the deficiency kit

and analyses of available sub-regions, we obtained 474 potentially interacting genes candidates that required further analyses. For screening these gene candidates, we utilized a) specific RNAi knock-down flies obtained from Vienna Drosophila RNAi Center (VDRC) b) disruption constructs (gene traps, mobile activating elements) and c) deletion generators from Bloomington when available. Overall, these are mostly loss of function or over-expression lines. Upon crossing over 1000 fly lines at 25°C and 29°C we identified 36 genes of the 474 that consistently modified the hLRRK2-I2020T eye phenotype (see Table 3.2). It is important to note that a specific gene was not necessarily identified for all 38 primary deficiency lines that modified the GMR-GAL4; UAS-hLRRK2-I2020T phenotype. There were 15 deficiencies where no specific gene disruption could be uncovered. There were 11 deficiencies where multiple LRRK2 genetic modifiers were found within the same primary deficiency. Of the 36 interactors, 13 fly lines caused a suppression of hLRRK2-I2020T toxicity at 29°C (7 down-regulated; 6 over-expressed). Again, there were no gene disruption lines that caused an enhancement of hLRRK2-I2020T induced damage at 29°C. There were 23 of 36 LRRK2 gene interactors that developed degeneration when crossed with the GMR-GAL4; UAS-hLRRK2-I2020T fly at 25°C (20 down-regulated; 3 over-expressed). Optical and SEM images of specific gene interactors causing an enhancement or suppression at 25°C or 29°C were obtained for the fly genes CBL and CathD respectively (see Figure 3.3). To confirm our results and test if phenotypic modification was mutation specific, we then crossed these 36 candidate genes with four other hLRRK2 expressing flies: wildtype (WT), two pathogenic mutants, R1441C and Y1699C, and a susceptibility mutation, I1122V (see Table 3.3). Screening specific gene disruptions with ectopic expression of

other hLRRK2 flies was fairly consistent in producing a similar modification (26/36 with at least one other LRRK2 line showing a consistent phenotype). There were 8 gene disruptions that did not modify hLRRK2-WT/I1122V/Y1699C or R1441C phenotypes. Finally, there were 2 gene disruptions (Hrs and CG10809) that suggested potential opposing effects in different hLRRK2 flies.

Table 3.1: List of primary hemizygous deficiencies with corresponding sub-regions that modify hLRRK2-I2020T toxicity in the compound eye. Hemizygous *Drosophila* lines from the Bloomington deficiency kit are crossed to GMR-GAL4; UAS-hLRRK2-I2020T and may cause no change, suppress or enhance hLRRK2-I2020T toxicity at 29°C or produce visible damage at 25°C. Flies were analyzed by a minimum of two independent researchers and at least 20 flies per line were examined.

Deficiency - Subregion	Deleted Segment	Temperature	Direction
Df(2L)dp-79b	22A2--22E1	25°C & 29°C	Enhancement
Df(2L)C144	22F4--23C3	29°C	Suppression
- Df(2L)BSC692	23B3--23B7	29°C	Suppression
- Df(2L)BSC180	23B7--23C3	29°C	Suppression
- Df(2L)Exel6008	22F4--23A3	29°C	Suppression
Df(2L)ED250	24F4--25A7	29°C	Enhancement
Df(2L)Mdh	30D--31F	29°C	Suppression
- Df(2L)BSC251	30F5--31A1	29°C	Suppression
Df(2L)BSC145	32C1--32C1	29°C	Suppression
Df(2L)BSC147	34C1--34C6	25°C	Enhancement
Df(2R)en-A	47D7--48B2	25°C	Enhancement
- Df(2R)BSC358	47E5--47F8	25°C	Enhancement
Df(2R)BSC40	48E1--48E10	25°C	Enhancement
Df(2R)Exel7131	50E4--50F6	25°C	Enhancement
Df(3L)ED50002	61A1--61B1	25°C	Enhancement
Df(3L)ED201	61B1--61C1	29°C	Suppression
- Df(3L)BSC128	61B2--61B2	29°C	Suppression
Df(3L)ED4287	62B4--62E5	25°C	Enhancement
Df(3L)BSC119	62E7--62F5	25°C	Enhancement
Df(3L)BSC23	62E8--63B6	25°C	Enhancement
Df(3L)M21	62F--63B10	25°C	Enhancement
Df(3L)ED208	63C1--63F5	25°C	Enhancement
Df(3L)ED210	64B9--64C13	25°C	Enhancement
Df(3L)Exel6109	65C3--65D3	25°C	Enhancement
Df(3L)BSC389	66C12--66D8	25°C	Enhancement
Df(3L)BSC35	66F1--67B3	29°C	Suppression
Df(3L)BSC392	67C4--67D1	29°C	Suppression
- Df(3L)BSC394	67C9--67D1	29°C	Suppression
Df(3L)BSC20	76A7--76B5	25°C	Enhancement
Df(3L)6B-29+Df(3R)6B-29	h53--h58	25°C	Enhancement
Df(3R)10-65	81F--81F	25°C	Enhancement
Df(3R)BSC633	84B2--84C3	25°C	Enhancement
Df(3R)BSC466	84E1--85A10	25°C	Enhancement
Df(3R)ED5428	85E1--85F8	25°C	Enhancement
Df(3R)BSC515	88F6--89A8	25°C	Enhancement
- Df(3R)BSC569	89A1--89A5	25°C	Enhancement
Df(3R)Ubx109	89E1--89E2	25°C	Enhancement
Df(3R)BSC517	92C1--92F13	25°C	Enhancement
Df(3R)BSC819	93A2--93B8	29°C	Suppression
Df(3R)BSC489	94F3--95D1	25°C	Enhancement
Df(3R)ED6232	96F10--97D2	25°C	Enhancement
- Df(3R)BSC495	96F6--97B4	25°C	Enhancement
- Df(3R)ED6235	97B9--97D12	25°C	Enhancement
Df(3R)L127	99B5--6;99F1	25°C & 29°C	Enhancement
Df(3R)BSC620	99C5--99D3	25°C	Enhancement
Df(3R)R133	99E1--5;3Rt	25°C	Enhancement
Df(3R)ED6361	100C7--100E3	25°C	Enhancement
Df(3R)ED50003	100E1--100E3	25°C	Enhancement

Figure 3.2: Representative deficiency suppression and enhancement of GMR-GAL4; UAS-hLRRK2-I2020T eyes.

Scanning electron microscope (SEM) images of GMR-GAL4; UAS-hLRRK2-I2020T /Df(3L)BSC20 causing an enhancement to hLRRK2-I2020T expression at 25°C (A) and GMR-GAL4/Df(2L)C144; UAS-hLRRK2-I2020T mediated suppression of bristle disorganization and structural abnormalities of the GMR-GAL4; UAS-hLRRK2-I2020T fly eye at 29°C (B).

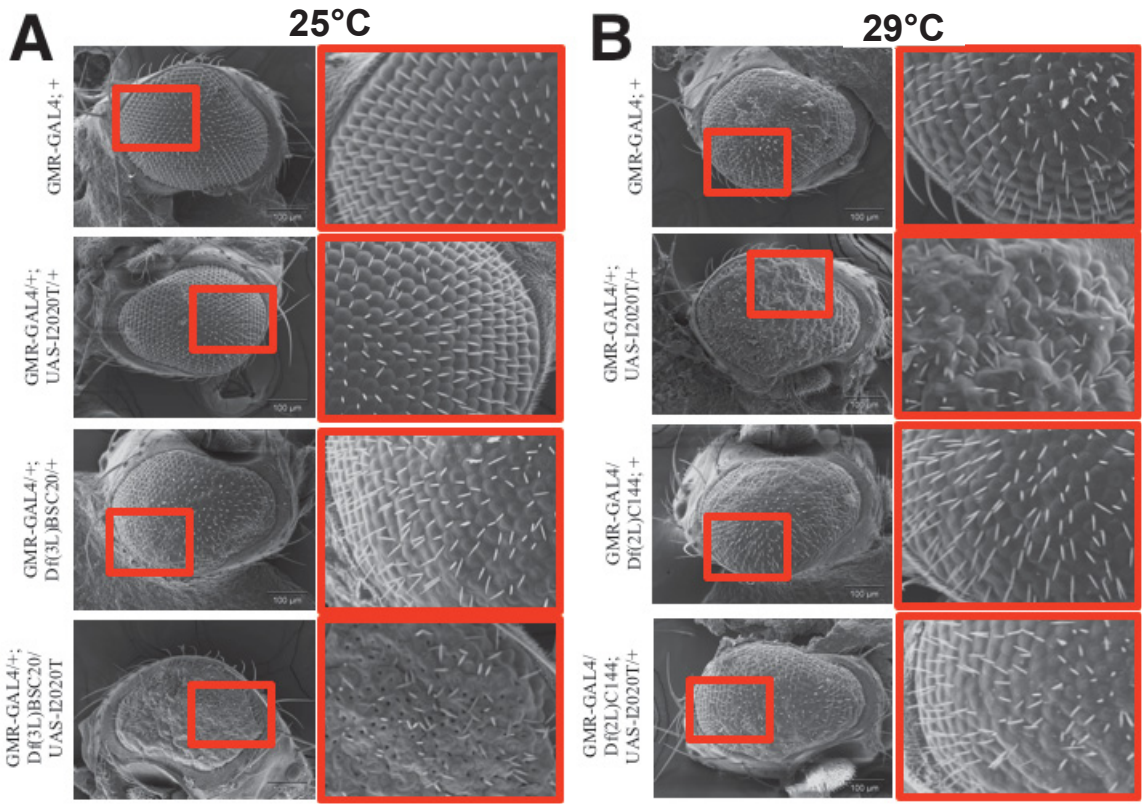
A
25°C
GMR-GAL4; +
GMR-GAL4/+;
UAS-I2020T/+
GMR-GAL4/+;
Df(3L)BSC20/+
GMR-GAL4/+;
Df(3L)BSC20/
UAS-I2020T
B
29°C
GMR-GAL4; +
GMR-GAL4/+;
UAS-I2020T/+
GMR-GAL4/
Df(2L)C144; +
GMR-GAL4/
Df(2L)C144;
UAS-I2020T/+

Table 3.2: List of specific genes that modify hLRRK2-I2020T toxicity in the compound eye.

Gene disruption lines for genes within the deficiency regions that modified hLRRK2-I2020T eye phenotypes were screened. Multiple gene disruption lines for 474 genes were crossed to GMR-GAL4; UAS-hLRRK2-I2020T and 36 genes were found to either suppress or enhance hLRRK2-I2020T toxicity at 29°C or produce damage at 25°C. Flies were analyzed by a minimum of two independent researchers with at least 20 flies per group.

Type of disruption	Gene	Deleted Segment	Location	Human Homolog	Temp.	Direction
			Down-regulated genes			
Deletion	CG31935	22A3-22A3	2L:1,594,822..1,611,157	RAB3GAP1	25°C	Enhancement
dsRNA	Hrs	23A3-23A3	2L:2,739,986..2,743,377	HGS	29°C	Suppression
Deletion	Rbp9	23C3-23C3	2L:2,954,762..2,968,434	ELAVL2	29°C	Suppression
dsRNA	SCAR	32C1-32C1	2L:10,976,772..10,982,395	WAVE1/2/3	25°C	Enhancement
dsRNA	CG8888	48D8-48E1	2R:12,064,565..12,079,543	BDH1	25°C	Enhancement
dsRNA	Hsc70-5	50E6-50E6	2R:14,252,598..14,256,192	HSPA9	29°C	Suppression
dsRNA	convoluted	50E6-50E6	2R:14,270,729..14,275,495	IGFALS	25°C	Enhancement
dsRNA	Mdr50	50E6-50E6	2R:14,246,966..14,252,597	ABCB1	25°C	Enhancement
dsRNA	CG7028	61B2-61B2	3L:207,184..211,457	PRPF4B	29°C	Suppression
dsRNA	aly	63A3-63A3	3L:3,024,129..3,026,521	LIN9	25°C	Enhancement
dsRNA	rasp	63B8-63B8	3L:3,162,180..3,163,852	HHAT	25°C	Enhancement
dsRNA	CG32266	63F1-63F1	3L:3,790,804..3,791,560	SORBS2	25°C	Enhancement
dsRNA	rpd3	64B12-64B12	3L:4,626,734..4,629,467	HDAC2	25°C	Enhancement
dsRNA	CG32236	64B13-64B13	3L:4,665,927..4,667,389	PPIA	25°C	Enhancement
dsRNA	gef64c	64B13-64B17	3L:4,692,783..4,796,253	ITSN1	25°C	Enhancement
dsRNA	Cbl	66C12-66C12	3L:8,424,954..8,432,246	CBL	25°C	Enhancement
Deletion	rdl	67A1-67A1	3L:9,145,838..9,182,149	GLRA3	29°C	Suppression
dsRNA	cdk8	67C10-67C10	3L:9,837,080..9,838,670	CDK8	29°C	Suppression
dsRNA	pipe	76A5-76A6	3L:19,298,623..19,337,609	HS2ST1	25°C	Enhancement
Deletion	vtd	80F-80F	3L:27,136,525..27,157,999	RAD21	25°C	Enhancement
dsRNA	CG1091	84B2-84B2	3R:7,083,225..7,086,083	ZCCHC6	25°C	Enhancement
dsRNA	αTub85E	85E6-85E6	3R:9,731,221..9,733,250	TUBA1C	25°C	Enhancement
dsRNA	CG5191	92F1-92F2	3R:20,560,865..20,573,000	FAAH	25°C	Enhancement
dsRNA	Atpα	93A4-93A4	3R:20,948,714..20,976,239	ATP1A3	29°C	Suppression
Deletion	CG6154	97A7-97A7	3R:26,262,662..26,277,050	DPEP1	25°C	Enhancement
dsRNA	tx	97B2-97F9	3R:26,440,778..26,448,991	ATOH1	25°C	Enhancement
dsRNA	Modulo	100E3-100E3	3R:32,052,060..32,054,974	RBM39	25°C	Enhancement
			Over-expressed genes			
Transgenic Transposon	CG2991	23B6-23B7	2L:2,857,164..2,868,548	MARCH3	29°C	Suppression
Elevated promoter	CG5846	30F2-30F2	2L:9,956,175..9,957,019	RFXANK	29°C	Suppression
Elevated promoter	CG13130	30F5-30F5	2L:9,983,671..9,984,743	UNC13b	29°C	Suppression
Elevated promoter	CG4747	30F5-30F5	2L:10,003,832..10,008,889	GLYR1	29°C	Suppression
Elevated promoter	cathD	43E18-43E18	2R:7,822,111..7,823,569	CTSD	29°C	Suppression
Elevated promoter	CG10809	67C11-67C11	3L:9,857,383..9,859,889	ANKRD54	29°C	Suppression
Enhancer Trap	mlp84b	84C1-84C1	3R:7,113,522..7,117,732	CSRP2	25°C	Enhancement
Gene Trap	beat-VII	97C3-97C4	3R:26,645,282..26,681,966	MUC18	25°C	Enhancement
Gene Trap	CG2003	100E1-100E1	3R:31,978,121..31,990,909	SLC17A7	25°C	Enhancement

Figure 3.3: Representative optical and SEM images of specific gene suppression and enhancement of hLRRK2-I2020T eyes. Down-regulation of CBL via RNAi combined with overexpression of hLRRK2-I2020T at 25°C produces a loss of pigmentation phenotype with further structural abnormalities observable under SEM (A). CathD overexpression at 29°C at least partially rescues loss of pigmentation and structural abnormalities of the hLRRK2-I2020T fly.

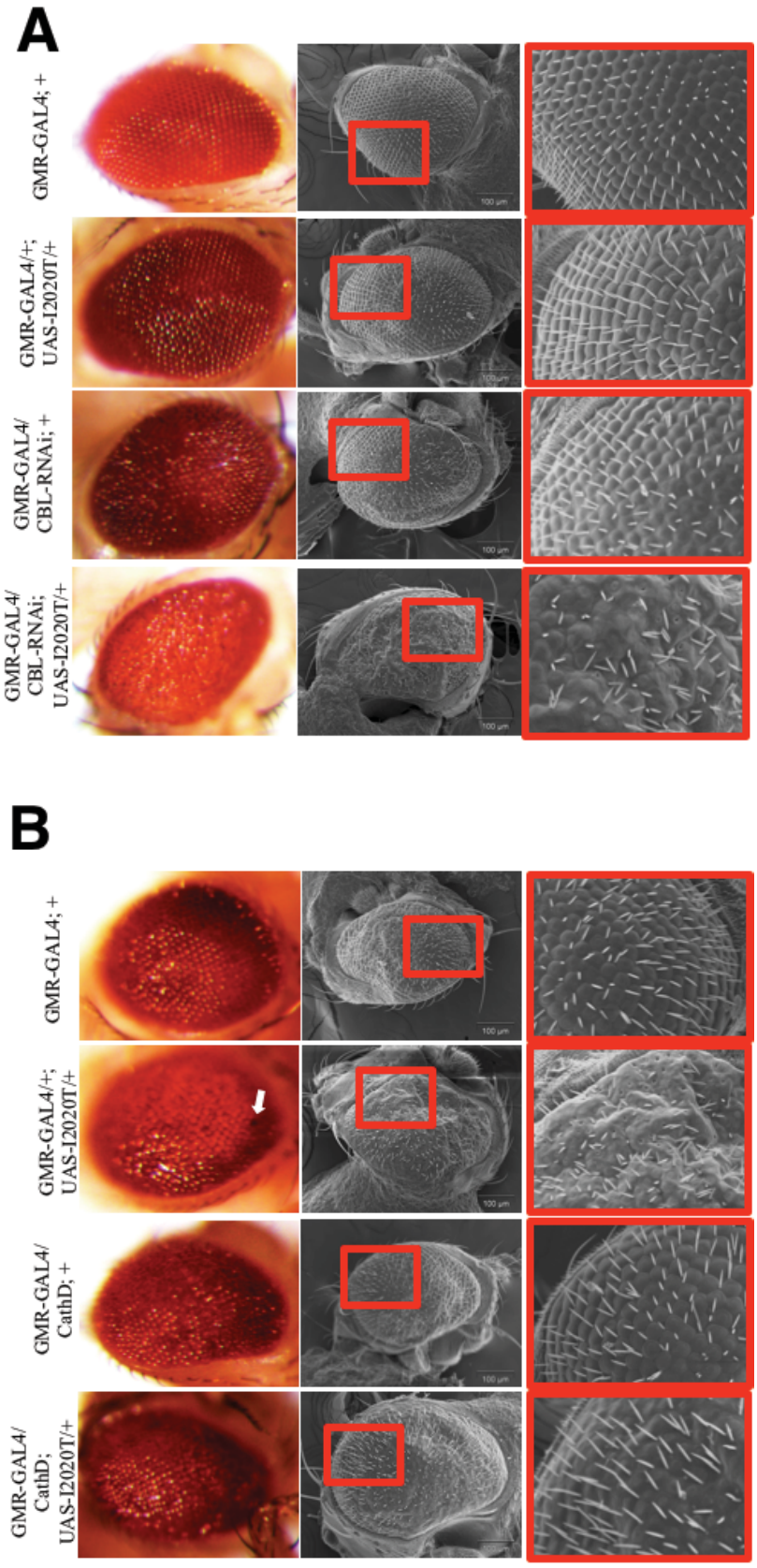
A
GMR-GAL4; +
GMR-GAL4/+; UAS-I2020T/+
GMR-GAL4/ CBL-RNAi; +
GMR-GAL4/ CBL-RNAi; UAS-I2020T/+
B
GMR-GAL4; +
GMR-GAL4/+; UAS-I2020T/+
GMR-GAL4/ CathD; +
GMR-GAL4/ CathD; UAS-I2020T/+

Table 3.3: Determination of phenotypic modulation of other hLRRK2 flies.

Specific gene disruption lines found to modify the GMR-GAL4; UAS-hLRRK2-I2020T eye phenotypes were crossed with other hLRRK2 constructs including: UAS-hLRRK2-WT, UAS-hLRRK2-I1122V, UAS-hLRRK2-Y1699C, and UAS-hLRRK2-R144C. (N = no phenotypic change). Analysis was conducted on at least 20 flies per group.

Type of disruption	Gene	Human Homolog	WT	I1122V	R1441C	Y1699C
Down-regulated genes causing I2020T Enhancement (25°C)						
Deletion	CG31935	RAB3GAP1	Enhancement	Enhancement	Enhancement	N
dsRNA	SCAR	WAVE1/2/3	Enhancement	Enhancement	Enhancement	Enhancement
dsRNA	CG8888	BDH1	N	N	N	N
dsRNA	convoluted	IGFALS	N	N	N	N
dsRNA	Mdr50	ABCB1	Enhancement	Enhancement	Enhancement	N
dsRNA	aly	LIN9	Enhancement	N	N	N
dsRNA	rasp	HHAT	N	Enhancement		N
dsRNA	CG32266	SORBS2	Enhancement	Enhancement	N	N
dsRNA	rpd3	HDAC2	N	N	N	N
dsRNA	CG32236	PPIA	Enhancement	Enhancement	Enhancement	N
dsRNA	gef64c	ITSN1	N	N	N	N
dsRNA	Cbl	CBL	Enhancement	Enhancement	Enhancement	Enhancement
dsRNA	pipe	HS2ST1	Enhancement	Enhancement	N	N
Deletion	vtd	RAD21	Enhancement	Enhancement	N	N
dsRNA	CG1091	ZCCHC6	N	N	N	N
dsRNA	αTub85E	TUBA1C	N	N	Enhancement	Enhancement
dsRNA	CG5191	FAAH	N	Enhancement	Enhancement	N
Deletion	CG6154	DPEP1	N	Enhancement	N	N
dsRNA	tx	ATOH1	Enhancement	Enhancement	Enhancement	N
dsRNA	Modulo	RBM39	N	N	N	N
Down-regulated genes causing I2020T Suppression (29°C)						
dsRNA	Hrs	HGS	Enhancement	N	N	N
Deletion	Rbp9	ELAVL2	Suppression	Suppression	Suppression	Suppression
dsRNA	Hsc70-5	HSPA9	Suppression	Suppression	Suppression	Suppression
dsRNA	CG7028	PRPF4B	Suppression	Suppression	Suppression	Suppression
Deletion	rdl	GLRA3	N	N	N	N
dsRNA	cdk8	CDK8	N	N	Suppression	Suppression
dsRNA	Atpα	ATP1A3	Suppression	N	N	N
Over-expressed genes causing I2020T enhancement (25°C)						
Enhancer	mlp84b	CSRP2	N	N	N	N
Gene Trap	beat-VII	MUC18	N	Enhancement	N	N
Gene Trap	CG2003	SLC17A7	Enhancement	N	N	N
Over-expressed genes causing I2020T suppression (29°C)						
Transgenic	CG2991	MARCH3	Suppression	Suppression	Suppression	Suppression
Elevated	CG5846	RFXANK	Suppression	Suppression	Suppression	Suppression
Elevated	CG13130	UNC13b	Suppression	Suppression	Suppression	Suppression
Elevated	CG4747	GLYR1	Suppression	Suppression	Suppression	Suppression
Elevated	cathD	CTSD	Suppression	Suppression	Suppression	Suppression
Elevated	CG10809	ANKRD54	N	Enhancement	Suppression	Suppression

Dopaminergic loss:

To extend our results from the eye to a more PD relevant model, we were able to screen 27 of our 36 candidates with expression of hLRRK2-I2020T with the dopamine decarboxylase (DDC-) GAL4 promoter. We were limited to screening 27 lines as our original DDC-GAL4 flies perished during our studies. We have previously shown that expression of the hLRRK2-I2020T mutation under the tyrosine hydroxylase (TH-GAL4) promoter causes both a loss of TH+ staining and locomotor deficits in the flies (Venderova et al., 2009). We were able to reproduce loss of TH+ staining in 10 day old DDC-GAL4; UAS- hLRRK2-I2020T adult flies as quantified by confocal microscopy (see Figure 3.4A-C). Furthermore, we confirmed that overexpression of hLRRK2-WT or hLRRK2-I2020T under the DDC-GAL4 promoter causes a decrease in locomotor activity using the *Drosophila* Activity Monitor system (see Figure 3.4D). It was necessary to use the DDC-GAL4 promoter (on the second chromosome) over the TH-GAL4 promoter for screening as both our hLRRK2 constructs and the TH driver are on the third chromosome of the fly which would genetically restricts us from screening the third chromosome candidates. We examined four dopaminergic clusters: protocerebral posterior lateral (PPL) 1, protocerebral posterior medial (PPM) 1/2, PPL2, and PPM3. These are traditionally the main dopaminergic clusters that may mediate motor function in *Drosophila* (Mao and Davis, 2009). Fly heads were dissected and the brains stained with TH antibody and quantified using confocal microscopy. We found that 16 of the 27 candidates screened in this manner modified the loss of TH positive cells observed in the DDC-GAL4; UAS-hLRRK2-I2020T fly (see Table 3.4). Unexpectedly, 15/16 gene disruptions caused suppression of hLRRK2-I2020T induced TH+ cell loss, while only

one (CG31935) gene disruption caused exacerbated death. We did not observe any modification in the PPL2 region in any flies. Strikingly, of these 16 candidates, 6 were in the same direction of modification as the eye phenotype as 10 were the opposite.

Figure 3.4: hLRRK2-I2020T flies show TH+ cell loss and locomotor deficits. Schematic diagram displaying the dopaminergic clusters of the *Drosophila* central nervous system (A). Quantification and representative confocal images of TH+ cell number of 10 day old flies in the PPL1, PPM1/2, PPL2, and PPM3 clusters of DDC-GAL4; UAS-hLRRK2-I2020T (n=11) and DDC-GAL4; + (n=12) flies (B & C). Locomotor activity was analyzed of DDC-GAL4/+ (n=11), DDC-GAL4; UAS-hLRRK2-WT (n=15) and DDC-GAL4; UAS-hLRRK2-I2020T (n=15) aged 10 days with the *Drosophila* Activity Monitor system over 24 hours (D). One-way ANOVA followed by Tukey's least significant difference (LSD) post-test.

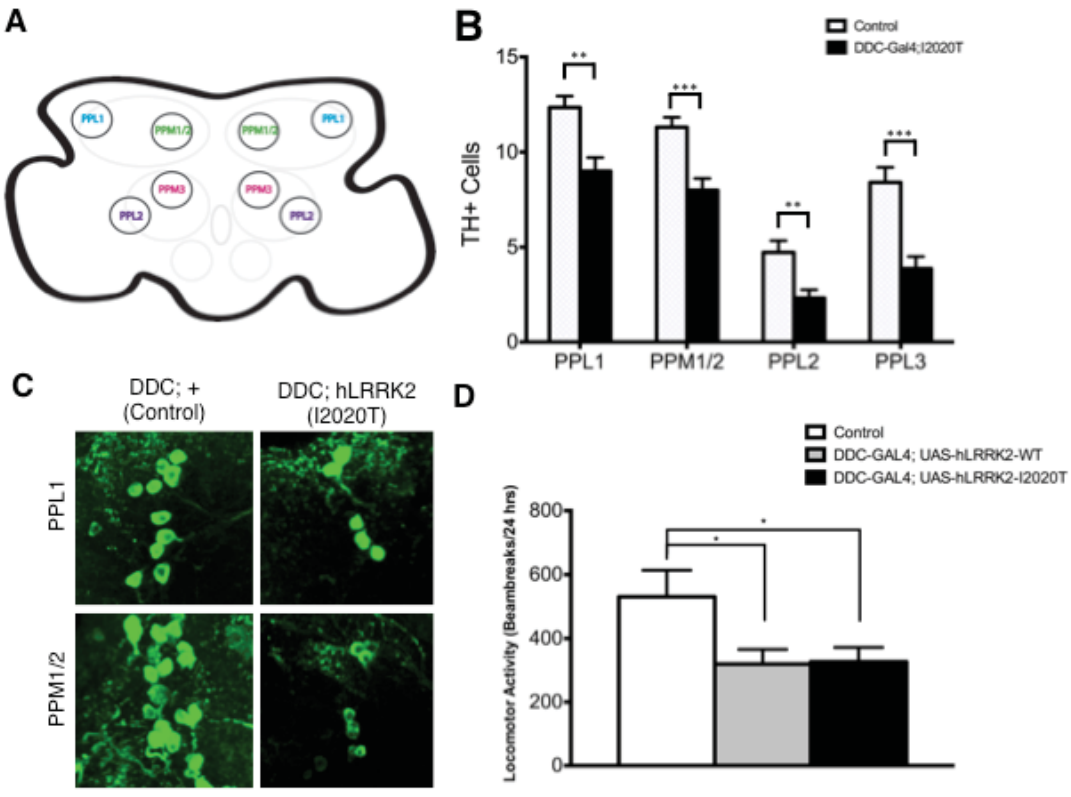
A
PPL1
PPM1/2
PPM1/2
PPL1
PPM3
PPM3
PPL2
PPL2
B
Control
DDC-Gal4;I2020T
TH+ Cells
15
10
5
0
**
***
**
***
PPL1
PPM1/2
PPL2
PPL3
C
DDC; +
(Control)
DDC; hLRRK2
(I2020T)
PPL1
PPM1/2
D
Control
DDC-GAL4; UAS-hLRRK2-WT
DDC-GAL4; UAS-hLRRK2-I2020T
Locomotor Activity (Beambreaks/24 hrs)
800
600
400
200
0
*
*

Table 3.4: Specific gene disruptions that modify loss of TH+ staining in the hLRRK2-I2020T dopaminergic clusters of the *Drosophila* CNS.

Of the 36 interactors found in the eye screen, 27 specific gene disruptions were crossed to the DDC-GAL4;+ and DDC-GAL4; UAS-hLRRK2-I2020T flies with a minimum of 8 flies per group. After dissection and staining, quantification of TH+ cell clusters for PPL1, PPM1/2, PPL2, and PPM3 was performed on experimental and control flies including DDC-GAL4;+ (n=13) and DDC-GAL4; UAS-hLRRK2-I2020T (n=17) flies. Groups had a minimum One-way ANOVA followed by Tukey's least significant difference (LSD) post-test. NS = not significant. (Note: enhancement by deletion of CG31935 under the DDC-GAL4 alone did not cause degeneration).

Type of disruption	Gene	Human Homolog	TH+ Cluster – Direction (significance)		
			PPL1	PPM1/2	PPM3
		Down regulated genes			
Deletion	CG31935	RAB3GAP1	En (****)	NS	NS
dsRNA	Hrs	HGS	Su (**)	Su (***)	Su (**)
Deletion	Rbp9	ELAVL2	NS	NS	NS
dsRNA	SCAR	WAVE1/2/3	NS	NS	NS
dsRNA	CG8888	BDH1	Su (**)	NS	NS
dsRNA	Hsc70-5	HSPA9	NS	NS	NS
dsRNA	convoluted	IGFALS	Su (****)	NS	Su (*)
dsRNA	Mdr50	ABCB1	NS	NS	NS
dsRNA	CG7028	PRPF4B	NS	NS	NS
dsRNA	aly	LIN9	Su (**)	Su (**)	Su (**)
dsRNA	CG32236	PPIA	Su (*)	NS	NS
dsRNA	gef64c	ITSN1	Su (**)	Su (**)	Su (**)
Deletion	rdl	GLRA3	NS	NS	Su (**)
dsRNA	cdk8	CDK8	NS	NS	NS
Deletion	vtd	RAD21	NS	NS	Su (*)
dsRNA	CG1091	ZCCHC6	Su (*)	NS	NS
dsRNA	αTub85E	TUBA1C	Su (*)	NS	NS
dsRNA	Atpα	ATP1A3	Su (***)	Su (*)	Su (*)
Deletion	CG6154	DPEP1	Su (**)	NS	NS
dsRNA	tx	ATOH1	NS	NS	Su (**)
dsRNA	Modulo	RBM39	NS	NS	NS
		Over-expressed genes			
Transgenic Transposon	CG2991	MARCH3	NS	NS	NS
Elevated promoter	CG5846	RFXANK	NS	NS	NS
Elevated promoter	CG13130	UNC13b	NS	NS	NS
Elevated promoter	CG4747	GLYR1	NS	NS	NS
Elevated promoter	cathD	CTSD	Su (****)	Su (***)	Su (*)
Elevated promoter	CG10809	ANKRD54	Su (**)	NS	Su (***)

LRRK2 gene network using STRING v10 analysis:

In order to determine if the wide variety of genetic interactors shared any common molecular pathways we conducted STRING pathway analysis. All candidates that modified hLRRK2-I2020T toxicity in the eye were input into the STRING v10 analysis software to examine if any known connectome would provide a clear picture as to what pathways were elucidated. Allowing for two extra nodes within the network, trimming any unconnected candidates and using a medium confidence level (0.400) we have produced a connectome based on the confidence of the protein associations found in the STRING v10 database (see Figure 3.5). The most connected central node binding most of the gene candidates in the eye was epidermal growth factor receptor (EGFR). We then determined if EGFR disrupted flies could modify hLRRK2-I2020T toxicity in the eye. Down regulation of EGFR by RNAi causes the appearance of black lesions in GMR-GAL4; UAS-hLRRK2-I2020T/EGFR flies at 25°C (see Figure 3.S1). STRING analysis was also conducted for the 16 genes that modified TH+ cell loss of DDC-GAL4; UAS-hLRRK2-I2020T flies as above. This gene network was clustered around ubiquitin C (UBC) (see Figure 3.6).

Figure 3.5: Gene network of eye interactors using the STRING v10 software reveals a central cluster within the EGFR signaling pathway.

The 36 genetic interactors from the eye screen were analyzed with STRING v10 using confidence view. Analysis allowed for two extra nodes within the network with a medium confidence level (0.400). Genes that failed to connect to the central network were removed. Thicker lines represent stronger associations.

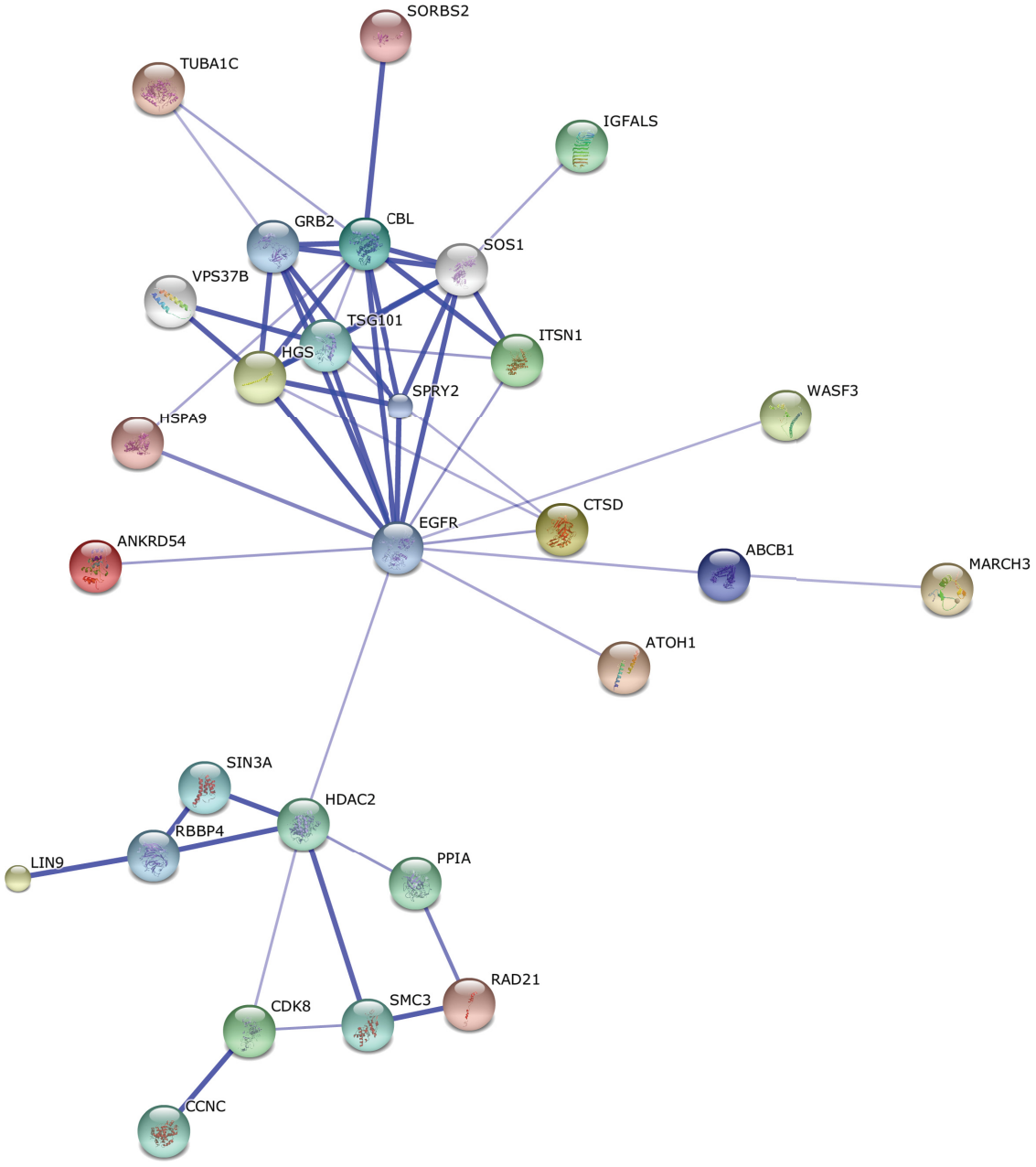
SORBS2
TUBA1C
IGFALS
GRB2
CBL
SOS1
VPS37B
TSG101
ITSN1
HGS
SPRY2
WASF3
HSPA9
CTSD
EGFR
ANKRD54
ABCB1
MARCH3
ATOH1
SIN3A
HDAC2
RBBP4
LIN9
PPIA
RAD21
CDK8
SMC3
CCNC

Figure 3.S1: Down-regulation of *Drosophila* EGFR enhances hLRRK2-I2020T toxicity in the eye.

Down regulation of EGFR by RNAi under the GMR-GAL4 promoter causes the appearance of minimal black lesions. A significant increase in black lesions is apparent in GMR-GAL4; UAS-hLRRK2-I2020T/EGFR flies at 25°C. One-way ANOVA followed by Tukey's least significant difference (LSD) post-test.

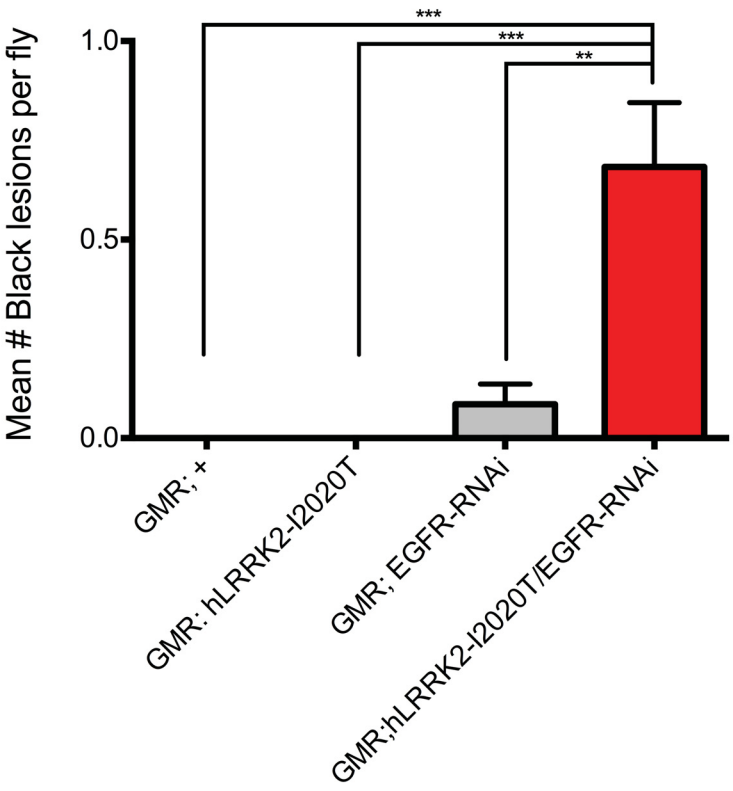
Mean # Black lesions per fly
1.0
0.5
0.0
***
***
**
GMR; +
GMR; hLRRK2-I2020T
GMR; EGFR-RNAi
GMR;hLRRK2-I2020T/EGFR-RNAi

Figure 3.6: Gene network of dopaminergic interactors using the STRING v10 software reveals a central cluster that converges on the ubiquitin signaling pathway. The 16 genetic interactors that modified TH+ cell loss of DDC-GAL4; UAS-hLRRK2-I2020T flies were analyzed with STRING v10 using confidence view. Analysis allowed for 2 extra nodes within the network with a medium confidence level (0.400). Genes that failed to connect to the central network were removed. Thicker lines represent stronger associations.

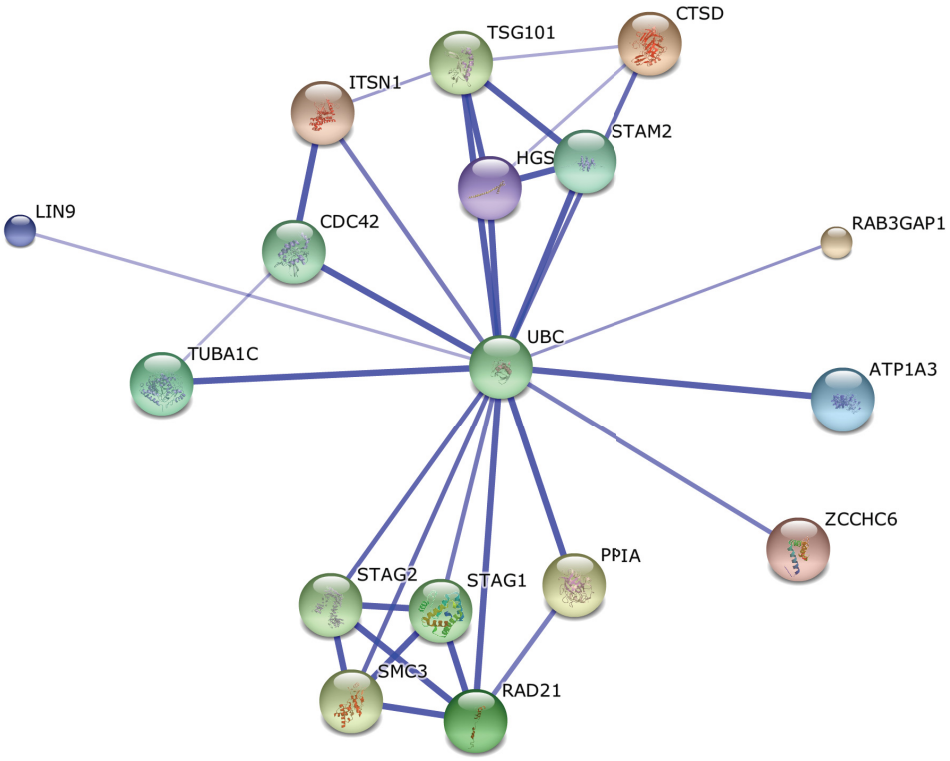
CTSD
TSG101
ITSN1
STAM2
HGS
LIN9
CDC42
RAB3GAP1
UBC
TUBA1C
ATP1A3
ZCCHC6
PPIA
STAG2
STAG1
SMC3
RAD21

Discussion:

In attempts to elucidate LRRK2 genetic interactors and associated pathways, we conducted an unbiased functional genetic screen in *Drosophila*. We utilized a previously established model of LRRK2 induced toxicity in the eye that provided a phenotype that could potentially be both suppressed or exacerbated. Furthermore, we took advantage of lowering LRRK2 expression, removing any damage to the eye, to reveal genetic interactors that could synergistically cause degeneration of the eye when combined with LRRK2 expression. Many of these interactors and their related signaling pathways are associated with LRRK2 in the literature. An interesting candidate is α-tubulin1C (TUBA1C) as LRRK2 has been shown to directly interact with some tubulin family members involved in microtubule dynamics (Law et al., 2014). LRRK2 is associated with various RAB protein family members including RAB3 GTPase's and our screen revealed that down regulation of RAB3GAP1 enhanced both eye toxicity and loss of TH+ neurons (Steger et al., 2016). Hepatocyte Growth Factor-Regulated Tyrosine Kinase Substrate (HGS) and LRRK2 both have potential roles in clathrin-mediated endocytosis (Raiborg et al., 2001; Schreij et al., 2015). Furthermore, LRRK2 has been implicated in synaptic vesicle recycling as has intersectin1 (ITSN1), a protein that interacts with clathrin and other endocytic machinery (Yu et al., 2008; Matta et al., 2012; Cirnaru et al., 2014). LRRK2 has been predicted to have a role in actin dynamics (Meixner et al., 2011). Both WAVE3 and SORBS2 form a complex that controls the actin cytoskeleton (Cestra et al., 2005). Mitochondrial health is implicated in both PD and LRRK2 function (Saha et al., 2009; Mortiboys et al., 2010; Wang et al., 2012). Both mortalin (HSPA9) and 3-Hydroxybutyrate Dehydrogenase (BDH1) are involved in mitochondrial homeostasis and

energy production (Tieu et al., 2003; Kaul et al., 2007). Some of the interactors discovered have been implicated in PD. For instance, the transcript for PRPF4B has been found to be up-regulated in the SNc of PD patients (Cowherd and Lee, 2015). Additionally, polymorphisms in five LRRK2 interactors: CTSD, UNC13b, ATP1A3, HSPA9 and ABCB1 have been associated with risk of developing PD (Schulte et al., 2003; de Carvalho Aguiar et al., 2004; De Mena et al., 2009; Westerlund et al., 2009; Liu et al., 2011a). Overall, these results suggest LRRK2 may interact with other PD risk factors and lends confidence to our screen. Pathway analysis of the LRRK2 genetic interactors converged onto EGFR, which was found to enhance LRRK2-I2020T toxicity upon RNAi mediated down-regulation. Interestingly, LRRK1, although not linked to PD, has been shown to regulate EGFR endosomal trafficking (Hanafusa et al., 2011; Ishikawa et al., 2012; Kedashiro et al., 2015). Recently, LRRK2 has been implicated in EGFR trafficking as well, as PD related LRRK2 mutants have been shown to delay trafficking of EGFR from early endosomes to multi-vesicular bodies, which may be mediated by RAB7 and/or RAB5b (Gómez-Suaga et al., 2014; Yun et al., 2015). The role of the EGFR degradation pathway remains to be examined in context of nigral death.

Surprisingly, we did not reveal any LRRK2 enhancements at 29°C. LRRK2 induced damage at this temperature may be fully saturated under our GMR-GAL4 promoter. Furthermore, screening was performed rapidly with optical microscopy that may have failed to observe any potential ultra-structural changes to the eye.

Some interactors could not be confirmed with LRRK2 WT or other pathogenic mutant expression in the eye. These hLRRK2 transgenic fly lines when originally established showed variable expression, most likely due to their random insertion into the

genome (Venderova et al., 2009). This may explain some of the lack of consistency. Furthermore, while the I2020T mutation may increase the kinase activity of LRRK2, it is still unclear how the two GTPase mutations (R1441C and Y1699C) or the leucine-rich repeat risk allele (I1122V) may affect these genetic pathways.

Unexpectedly, many of the genetic interactors that lead to an enhanced eye phenotype when combined with LRRK2-I2020T revealed suppression phenotypes when examined in the dopaminergic system. However, the expression of hLRRK2 and/or the specific fly gene disruption may result in a different cellular responses depending on cell type. Additionally, STRING analysis for genetic interactors that modified TH+ cell loss converged on ubiquitin C (UBC). Ubiquitin C is the precursor to polyubiquitin C and has a wide variety of roles in the cell, particularly in protein degradation. Changes in the ubiquitin-proteasome system have been observed in PD and PD models (St P McNaught et al., 2003; Olzmann et al., 2007). It is unclear how specific down-regulation of many of these specific genes suppresses LRRK2-I2020T TH+ cell loss.

In summary, we fully saturated an unbiased autosomal screen for LRRK2-I2020T modifiers in both the eye and dopaminergic system of the fly. We noticed a particular difference in both the direction of modification phenotype between the eye and the dopaminergic system. A point that further suggests that LRRK2 may result in different cellular outcomes in the context of cell type. Furthermore, not all LRRK2 mutations interacted with the gene candidates suggesting that not all LRRK2 mutations necessarily work in the same way. This could be particularly true when looking at direct interactions where LRRK2 mutations may affect its repertoire of binding partners. Future studies may

determine if any of these genetic interactors relate to LRRK2 function or pathology in mammals.

Methods:

Drosophila stocks: All flies were maintained on a standard cornmeal/agar medium at ambient RT or at 25°C / 29°C when under experimental conditions. hLRRK2 flies were previously created and characterized in Venderova et al. (2009). The primary deficiency kit, sub-regions lines, all elevated promoter, deletion, transgenic transposon, enhancer trap, gene trap, DDC-GAL4 and some dsRNA lines were obtained from the Bloomington Drosophila Stock Centre (Bloomington, Indiana). GMR-GAL4/BC and w1118 flies were a gift from Dr. Yong Rao (Cafferty et al., 2006) and Dr. Margaret Sonnenfeld (Sun et al., 2006), respectively. All other dsRNA lines were obtained from the Vienna Drosophila Research Centre.

Suppressor/enhancer screen genetics: hLRRK2 flies were kept balanced as GMR-GAL4/Cyo;UAS-hLRRK2/TM2 as our GMR-GAL4 is homozygous lethal. The flies for the TH+ screen were kept as DDC-GAL4/DDC-GAL4; UAS-hLRRK2/TM2. Regardless of screen, these lines are crossed to deficiency or gene disruption lines and w1118 control flies. Importantly, deficiencies and gene disruption lines are also crossed to GMR-GAL4/BC or DDC-GAL4/DDC-GAL4 lines to determine if the they cause a phenotype *sans* hLRRK2. Finally, we always cross GMR-GAL4/BC or DDC-GAL4/DDC-GAL4 to w1118 flies to control for any driver effects.

Phenotypic scoring for the eye screen: All experimental and control flies were rapidly screened for loss of red pigmentation, obvious black lesions and any gross morphological changes to the ommatidia under stereo microscopy at 25°C. Due to the lack of degeneration in hLRRK2 flies at this temperature, scoring was clear among users. The hLRRK2 fly eye at 29°C has a variable phenotype (from simple loss of pigmentation on

half of the eye to loss covering the entirety of the eye and the presence of black lesions). Suppression phenotypes were considered disruption lines that returned the eye to the GMR-GAL4;+ eye at 29°C (some visible surface roughness, minor loss of pigmentation). Our threshold for enhancements at 29°C was high due to the variable LRRK2 phenotype; we did not find any interactors that met this threshold. All interactors found in the screen were confirmed by at least two researchers, blindly. Phenotypic modifications were virtually complete in penetrance. All flies were male.

SEM Imaging: 10 day old heads of male flies were fixed in 2% glutaraldehyde in 0.1M sodium cacodylate buffer (pH 7.3) for 2 hrs and dehydrated in ethanol. The SEM was performed by the Advanced Bioimaging Center, Mount Sinai Hospital, Toronto.

Quantification of TH+ neurons: Male experimental (DDC-GAL4; UAS-hLRRK-I2020T) and control (DDC-GAL4;+) flies were aged to 10 days at 25°C. Briefly, flies were dissected in PBS and fixed in 4% PFA and stained with polyclonal rabbit anti-TH antibody (EMD Millipore AB152) at 1:300 in PBT (0.3% Tween), 5% normal goat serum following standard fly brain protocol (Wu and Luo, 2006). Secondary antibody was donkey anti-rabbit conjugated Alexa 488 (Invitrogen). Whole brains were mounted to slides using the bridge method and confocal images (Zeiss LSM510) were taken (20X objective) in Z-stack to form a 3-D image used for counting the dopaminergic clusters of the fly brain.

Locomotor activity: Male DDC-GAL4; UAS-hLRRK-WT or I2020T and DDC-GAL4;+ flies were aged to 10 days at 25°C and placed in the Drosophila Activity Monitor (DAM) system (TriKinetics). The apparatus has 32 chambers (one for each fly). Flies are able to

walk back and forth within the chamber and have access to food. An infrared beambreak system sums activity every 5 minutes and flies are quantified for a 24 hour period.

Pathway analysis: STRING v10 open access online software was used to determine associated protein networks using confidence view. We input the list of human orthologs of fly genes elucidated in eye and TH+ loss screen. Analysis permitted up to two extra nodes within the network using a medium confidence level (0.400). Genes failing to connect to the network were removed. Thicker blue lines represent stronger associations.

Statistical analysis: The data were analyzed as specified, expressed as means ± standard error of means, and denoted * if $P \leq 0.05$, ** if $P \leq 0.01$, *** if ≤ 0.001 and **** if $p \leq 0.0001$.

Acknowledgements:

We would like to thank undergraduate students that helped maintain fly stocks: Cindy Wei, Amanda Perozzo, Sarah Seang, Francis Lebrun, Yannick Lee and Alaa Fanous. We would like to thank Douglas Holmyard (Mount Sinai Hospital, Toronto) for SEM work. This study was supported by grants from the Michael J Fox Foundation, Canadian Institutes of Health Research, the Parkinson's Society Canada (PSC), the Parkinson's Research Consortium (PRC) in Ottawa, the Network of Centers of Excellence in Neurodegeneration, the Heart and Stroke Foundation of Ontario, and the Neuroscience Brain Canada/Krembil Foundation. PCM was funded by fellowships from PSC and PRC. There is no declared conflict of interest with the contents of this article.

Chapter 4:

LRRK2 regulates phagocytosis via direct phosphorylation of the actin-nucleating complex, WAVE-2.

Submitting to Nature Cell Biology

Kwang Soo Kim*, **Paul C Marcogliese***, Jungwoo Yang, Francis LeBrun, Elizabeth Abdel-Messih, Ghassan Kabbach, Ruth S Slack, Katerina Venderova, Michael G Schlossmacher, David S Park.

*contributed equally

Statement of author contribution:

The following manuscript follows the format for submission to the journal *Nature Cell Biology* to which it will be submitted. This manuscript examines a LRRK2 genetic interactor, SCAR (human WAVE-2), which was identified by Paul Marcogliese from the LRRK2 fly screen described in Chapter 3. Here we show that WAVE-2 protein levels are decreased/increased in LRRK2 null and G2019S myeloid cells which correlates with decreased/increased phagocytic activity, respectively. We provide evidence that LRRK2 and WAVE-2 bind directly and LRRK2 phosphorylates WAVE-2. Furthermore, we show that G2019S immune cells may display increased engulfment of neuronal cells. Lastly, we created a novel PD model in flies by expressing mutant LRRK2 only in fly brain phagocytes that is rescued by SCAR inhibition. Together, this manuscript provides evidence that LRRK2 function in myeloid cells may contribute to PD.

All experiments were designed by Paul Marcogliese, Dr. Kwang Soo Kim and David S Park. Paul Marcogliese conducted the screen work that elucidated SCAR as a LRRK2 interactor. Dr. Kwang Soo Kim performed the *in vitro* phagocytosis assays and biochemistry. Paul Marcogliese performed and analyzed the *in vivo* phagocytosis assays, *Drosophila* characterization, and aided in some of the analysis of the *in vitro* phagocytosis assays. Paul Marcogliese wrote this manuscript with aid from Dr. Kwang Soo Kim in the Methods section.

This work was partly funded by the CIHR and CLINT (Canadian LRRK2 in Inflammation Team) researchers. CLINT Investigators include: Earl Brown, Derrick Gibbings, Shawn Hayley, David Park, Dana C. Philpott, John D. Rioux, Michael Schlossmacher, and Erwin Schurr.

Classification: BIOLOGICAL SCIENCES, Neuroscience

LRRK2 regulates phagocytosis via direct phosphorylation of the actin-nucleating complex, WAVE-2.

Kwang Soo Kim*, **Paul C Marcogliese PC***, Jungwoo Yang, Francis LeBrun, Elizabeth Abdel-Messih, Ghassan Kabbach, Ruth S Slack, Katerina Venderova, Michael G Schlossmacher, David S Park, DS.

*contributed equally

Number of text pages: 17

Number of figures: 9 main, 4 supplemental

Abstract:

Mutations in leucine-rich repeat kinase 2 (LRRK2) are implicated in both familial and sporadic Parkinson's disease (PD). Determining LRRK2's role in dopaminergic cell death has been a challenge to elucidate. However, evidence in the field has been mounting that LRRK2 may be involved in immune cell function. We uncovered the actin-nucleation complex protein SCAR from an unbiased *in vivo* screen for LRRK2 genetic interactors. Due to SCAR's role in immune function, we explored LRRK2's role specifically in *Drosophila* 'microglia'. We ectopically expressed human LRRK2 specifically in *Drosophila* CNS phagocytes (ensheathing cells) which leads to locomotor and lifespan deficits in flies. In mammals, we show both *in vitro* and *in vivo* that LRRK2 G2019S knock-in primary microglia and bone marrow-derived macrophages display increased phagocytic activity that correlates with an increase in WAVE-2 (SCAR), an actin nucleating protein crucial for phagocytosis. Conversely, LRRK2 null myeloid cells display impaired phagocytic activity correlating with a decrease in WAVE-2 protein levels. We also provide evidence that LRRK2 binds WAVE-2 directly and phosphorylates WAVE-2. Finally, we return to flies, modeling locomotor and lifespan deficits in flies expressing G2019S in fly central phagocytes to show that these deficits may be rescued by down-regulation of SCAR. Taken together, our data implicate LRRK2s function in microglial and phagocytic hyper-activity in the pathogenesis of LRRK2-mediated Parkinson's disease.

Introduction:

The pathogenesis underlying the progressive death of midbrain dopamine (DA) neurons in the substantia nigra pars compacta (SNc) in Parkinson's disease (PD) has remained elusive. Autosomal-dominant mutations in leucine rich repeat kinase 2 (LRRK2) are the most commonly linked cause of familial PD and spontaneous alterations in LRRK2 are potentially present in up to 10% of sporadic PD (Correia Guedes et al., 2010). Known pathogenic mutations in LRRK2 reside within its two catalytic domains, a GTPase and a serine/threonine kinase. While LRRK2 has been implicated in a wide variety of cellular processes, the field has yet to find a clear and reproducible mechanism for LRRK2 function, particularly as it relates to PD. In our hands, we have failed to discern a robust role for LRRK2 in neurons in models of oxidative/mitochondrial stress or autophagy (Abdel-Messih et. al., *unpublished*). This has led us to begin examining LRRK2 outside of neurons where it is more heavily expressed. Recent studies have implicated LRRK2 in modulating the neuroinflammatory response. LRRK2 shows relatively high expression in both brain and peripheral immune cells, responds to immune activation and modulates interferon-gamma (IFN- γ) and NF-Kβ pathways (Gardet et al., 2010; Hakimi et al., 2011; Thévenet et al., 2011; Liu et al., 2011b; Moehle et al., 2012). LRRK2 null rats are resistant to dopaminergic cell death when injected with the toll-like receptor (TLR)-4 agonist lipopolysaccharide (LPS) directly into the SNc (Daher et al., 2014). Conversely, G2019S BAC transgenic rats are hypersensitive to LPS induced nigral death (Moehle et al., 2015). Curiously, polymorphisms in LRRK2 are also associated to the immune disorders: Crohn's disease and leprosy (Barrett et al., 2008; Fava et al., 2016).

The field has struggled with observing any robust and reproducible phenotypes in LRRK2 transgenic mice. On the contrary, LRRK2 models in *Drosophila* have shown promise in both recapitulating the disease and elucidating possible relevant LRRK2 function in mammals (Liu et al., 2008; Venderova et al., 2009; Martin et al., 2014). Recently, we found SCAR (orthologous to human WAVE family members) as a potential LRRK2 interactor in an unbiased suppressor/enhancer screen of hLRRK2 induced eye degeneration in flies (Marcogliese et al., *unpublished*). SCAR/WAVE promotes actin nucleation via activation of the actin-related protein-2/3 (ARP2/3) complex. This has been shown to be required for cytoskeletal remodeling for processes such as phagocytosis in both the invertebrate and mammalian systems (Kitamura et al., 2003; Evans et al., 2013).

It has long been known that neuroinflammation may modulate the progression of PD (Hirsch et al., 2012), but the role of microglia may have in the pathogenesis of this disease has largely been ignored. Here we show LRRK2 genetically interacts with SCAR. Furthermore, we establish a model in restricting LRRK2 expression to fly CNS phagocytes that produces both Parkinsonism and survival deficits in flies. In mammals, we demonstrate that LRRK2 reveals itself as a modulator of the phagocytic response via phosphorylation of WAVE-2. Additionally, we show that G2019S microglia exhibit increased engulfment of dopaminergic like cell axons. Finally, we show that Parkinsonism and survival deficits in flies expressing LRRK2 only in CNS phagocytes may be rescued by down-regulation of SCAR.

Results:

LRRK2 genetically interacts with SCAR:

In an unbiased screen to elucidate genetic interactors of LRRK2 in flies, we ectopically expressed UAS-hLRRK2-I2020T in the eye under control of the GMR-GAL4 promoter as previously characterized (Venderova et al., 2009). In this model, hLRRK2 expression in eyes at 25°C fails to produce and visible degeneration, however, in combination with down regulation of SCAR by RNAi, there is enhanced toxicity to hLRRK2 pathogenic compound eyes (see Figure 4.1A&B). In order to determine the consistency of this interaction, we over-expressed SCAR in hLRRK2 flies. hLRRK2 expression in eyes at 29°C produced loss of pigmentation and black lesions in the drosophila eye as previously described (Venderova et al., 2009). Co-expression of UAS-SCAR caused a decrease in black lesions in these flies (see Figure 4.1C).

Figure 4.1: SCAR genetically interacts with LRRK2.

Down-regulation of *Drosophila* SCAR (UAS-SCAR-RNAi) combined with over-expression of hLRRK2 (WT and pathogenic mutants) in the compound eye (GMR-GAL4) at 25°C causes surface roughness, and black spots (white arrows) under optical microscopy and SEM (A) as quantified (B). Conversely, over-expression of UAS-SCAR causes a reduction in black lesions observed in hLRRK2-I2020T flies at 29°C (C). One-way ANOVA followed by Tukey's least significant difference post test.

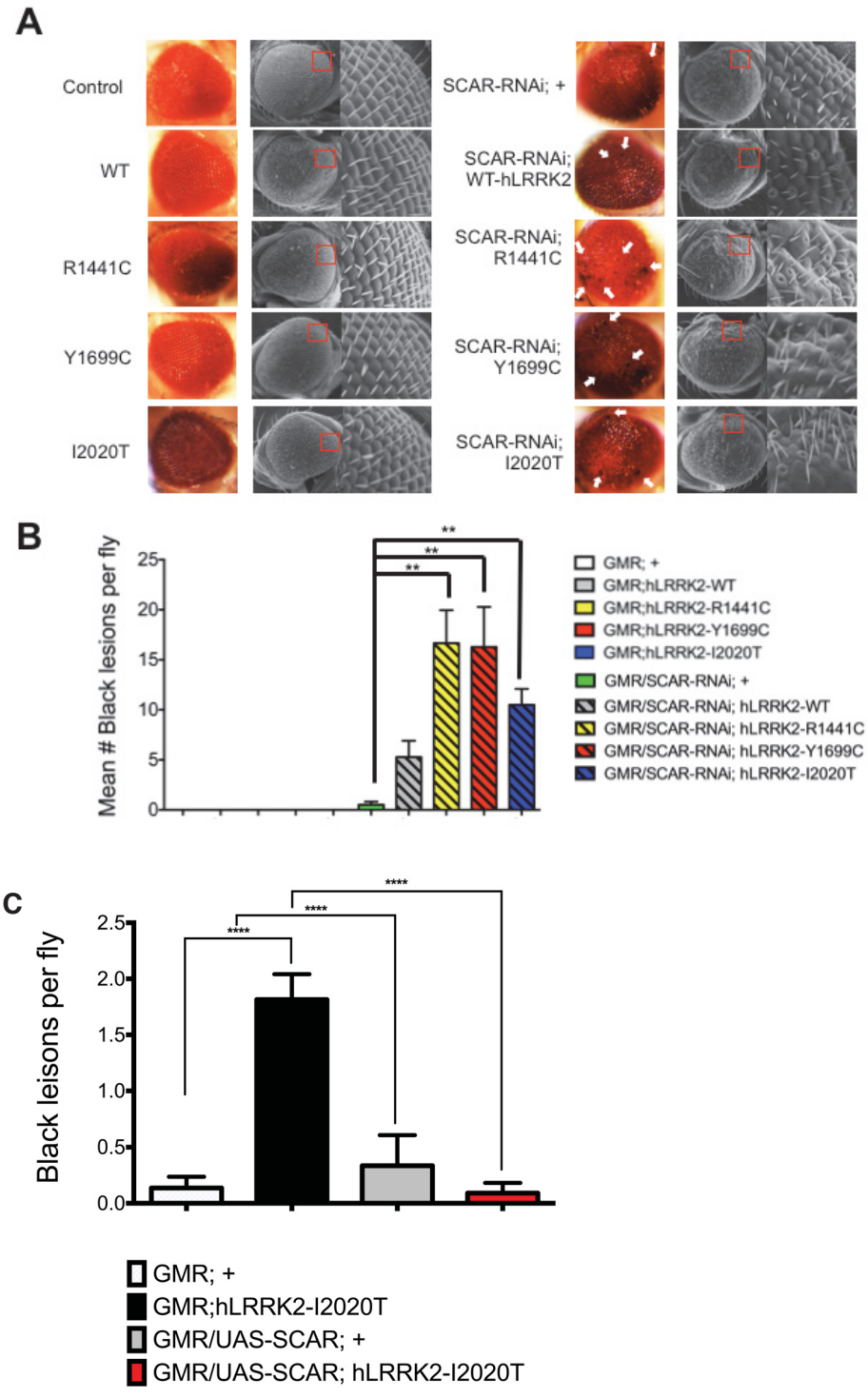
A
Control
WT
R1441C
Y1699C
I2020T
SCAR-RNAi; +
SCAR-RNAi; WT-hLRRK2
SCAR-RNAi; R1441C
SCAR-RNAi; Y1699C
SCAR-RNAi; I2020T
B
Mean # Black lesions per fly
25
20
15
10
5
0
**
**
**
GMR; +
GMR;hLRRK2-WT
GMR;hLRRK2-R1441C
GMR;hLRRK2-Y1699C
GMR;hLRRK2-I2020T
GMR/SCAR-RNAi; +
GMR/SCAR-RNAi; hLRRK2-WT
GMR/SCAR-RNAi; hLRRK2-R1441C
GMR/SCAR-RNAi; hLRRK2-Y1699C
GMR/SCAR-RNAi; hLRRK2-I2020T
C
Black leisons per fly
2.5
2.0
1.5
1.0
0.5
0.0
****
****
****
GMR; +
GMR;hLRRK2-I2020T
GMR/UAS-SCAR; +
GMR/UAS-SCAR; hLRRK2-I2020T

LRRK2 expression in ensheathing cells causes locomotor and survival deficits in flies:

SCAR is known in invertebrates to have a role in immune function, particular as it relates to cell migration and phagocytosis (Evans et al., 2013). In order to test if LRRK2-G2019S expression in immune-like cells could led to cell death, we used the GAL4-UAS system in *Drosophila* to express LRRK2 in ensheathing cells. Ensheathing glia have been established as the primary phagocyte of the *Drosophila* brain responsible for axonal clearance, apoptotic corpse removal and innate defence (Doherty et al., 2009). We expressed hLRRK2 WT or G2019S in ensheathing glia under the mZ0709-GAL4 (MZ-GAL4) promoter. Ectopically expressing WT or G2019S LRRK2 in ensheathing glia results in locomotor deficits in 5 day old flies when compared to control driver flies (see Figure 4.2A). Additionally, flies expressing the I2020T mutation in ensheathing cells have decreased lifespan when compared to mZ0709-GAL4/+ controls (see Figure 4.2B). This interesting phenotype led us to examine SCAR in the mammalian system.

Figure 4.2: LRRK2 expression in CNS phagocytes causes locomotor and lifespan deficits.

Locomotor activity was assessed for 5 day old male flies expressing LRRK WT and G2019S in ensheathing cells by the Drosophila Activity Monitor system for 24 hrs (A). Lifespan was assessed in control and mZ0709-GAL4; UAS-hLRRK2-I2020T flies (B). Flies were assessed for survival deficits were observed daily. All flies were incubated at 25°C. Locomotor assays – one-way ANOVA followed by Tukey's least significant difference. Survival assay – Logrank test.

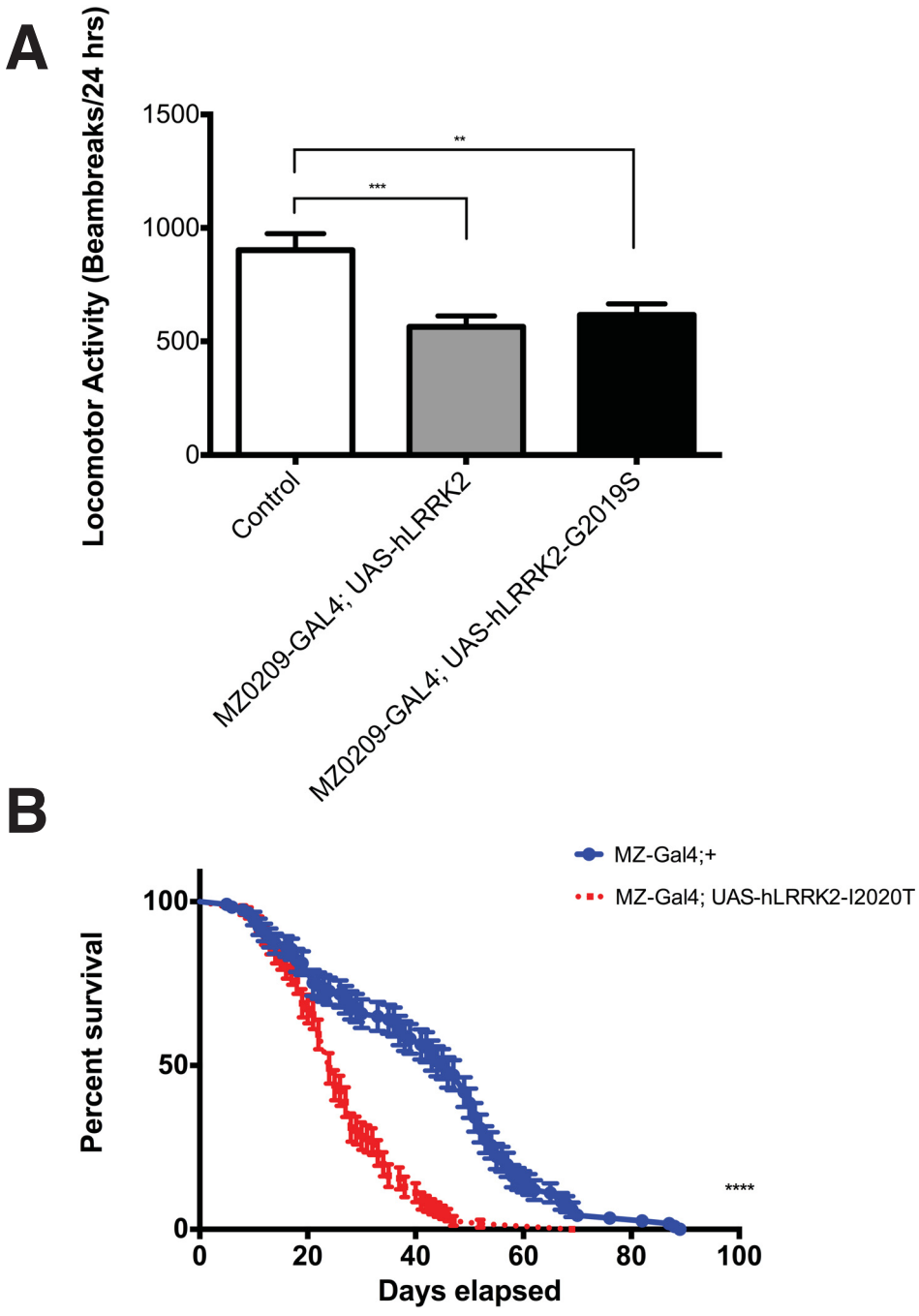
A
Locomotor Activity (Beambreaks/24 hrs)
1500
1000
500
0
**
***
Control
MZ0209-GAL4; UAS-hLRRK2
MZ0209-GAL4; UAS-hLRRK2-G2019S
B
Percent survival
100
50
0
0
20
40
60
80
100
Days elapsed
MZ-Gal4;+
MZ-Gal4; UAS-hLRRK2-I2020T
****

WAVE-2 levels are dependent on LRRK2:

The *Drosophila* SCAR protein is orthologous to the WAVE-1/2/3 family members in humans. The WAVE family members form a complex to activate the ARP2/3 complex to mediate cytoskeletal remodeling (Chen et al., 2010). We first determined if the levels of any WAVE family members were altered in different cell types. In the murine, BV2 microglia like cell line, WAVE-2 levels specifically were decreased after down-regulation of LRRK2 by siRNA (see Figure 4.S1A). The protein levels of WAVE-1 and WAVE-3 remained unchanged, as did the mRNA level of WAVE-2 (see Figure 4.S1B). WAVE-2 levels were unchanged in other cell types including primary astrocytes, cortical neurons, and mouse embryonic fibroblasts (MEFs) (see Figure 4.S1C-E). Due the decrease in WAVE-2 protein level in LRRK2 knock-down (KD) BV-2 cells, we determined if WAVE-2 was altered in other cells of the myeloid lineage. Primary microglia and bone marrow-derived macrophages (BMDMs) from LRRK2 null mice display a significant reduction in WAVE-2 protein when compared to their wildtype (WT) counterparts (see Figure 4.3A&B). Conversely, LRRK2 G2019S endogenous knock-in mice display an increase in WAVE-2 protein in microglia and BMDMs. Furthermore, BMDMs from BAC mice over-expressing human LRRK2 display increased murine WAVE-2 protein (see Figure 4.3B – far right panel).

Figure 4.S1: WAVE-2 is decreased in LRRK2 KD BV2 cells but not LRRK2 null primary astrocytes, cortical neurons nor MEFs.

WAVE family members were probed in lysates of BV2 cells after siRNA mediated knock-down of LRRK2 for protein (A) and mRNA (B). Similarly, WAVE-2 was probed by Western blot in LRRK2 null primary astrocytes (C), primary cortical neurons (D), and MEFs (E). Unpaired student T-test.

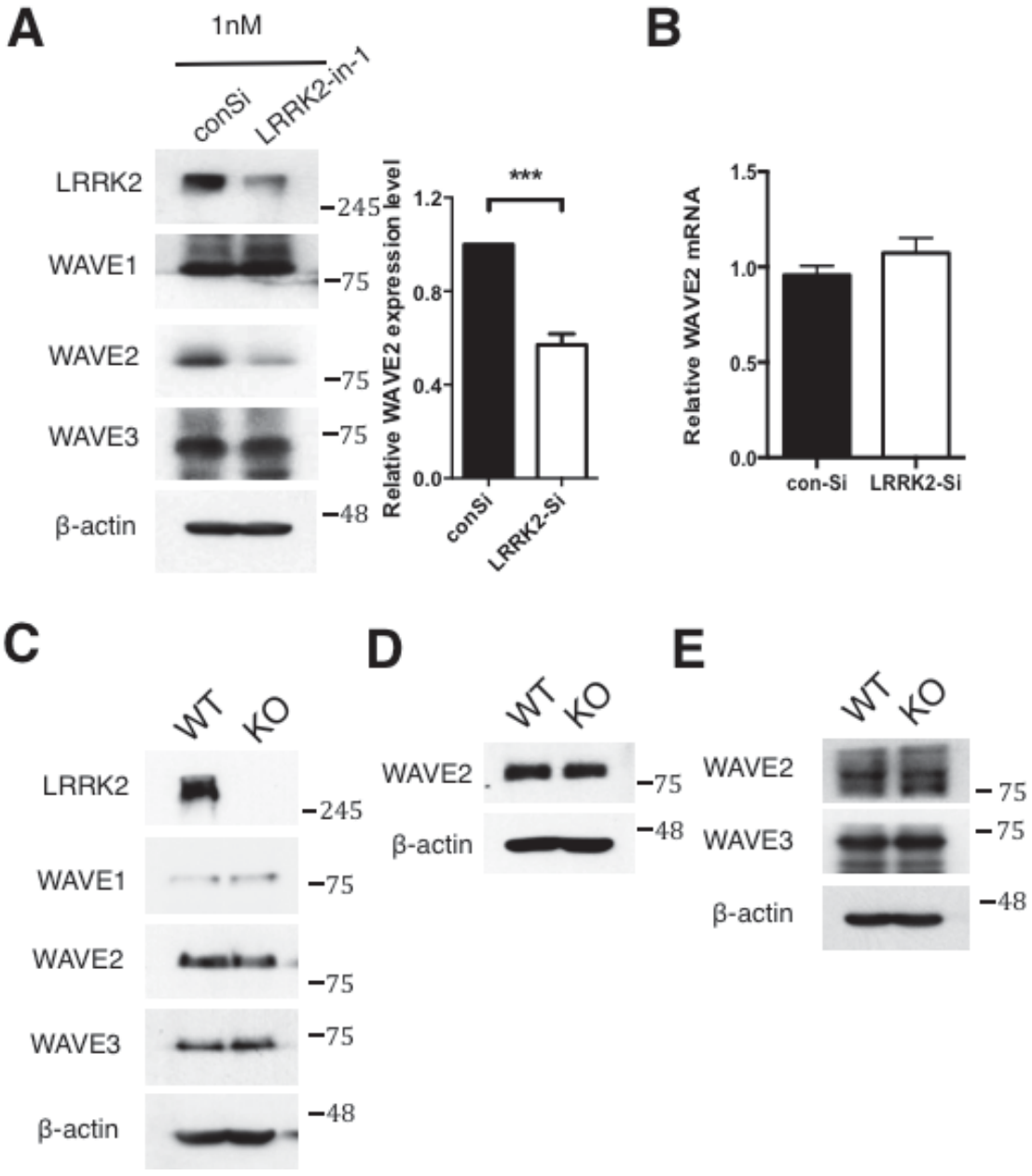
A
1nM
conSi
LRRK2-in-1
LRRK2
WAVE1
WAVE2
WAVE3
β-actin
245
75
75
75
48
***
Relative WAVE2 expression level
1.2
0.8
0.4
0.0
conSi
LRRK2-Si
B
Relative WAVE2 mRNA
1.5
1.0
0.5
0.0
con-Si
LRRK2-Si
C
WT
KO
LRRK2
WAVE1
WAVE2
WAVE3
β-actin
245
75
75
75
48
D
WT
KO
WAVE2
β-actin
75
48
E
WT
KO
WAVE2
WAVE3
β-actin
75
75
48

Figure 4.3: WAVE-2 levels are altered in LRRK2 primary microglia and macrophages.

WAVE-2 protein and mRNA levels were probed in LRRK2 null and G2019S KI primary microglia. Similarly, WAVE-2 protein was probed in LRRK2 null, G2019S KI, or WT-hLRRK2 BAC BMDMs. Unpaired student t-test.

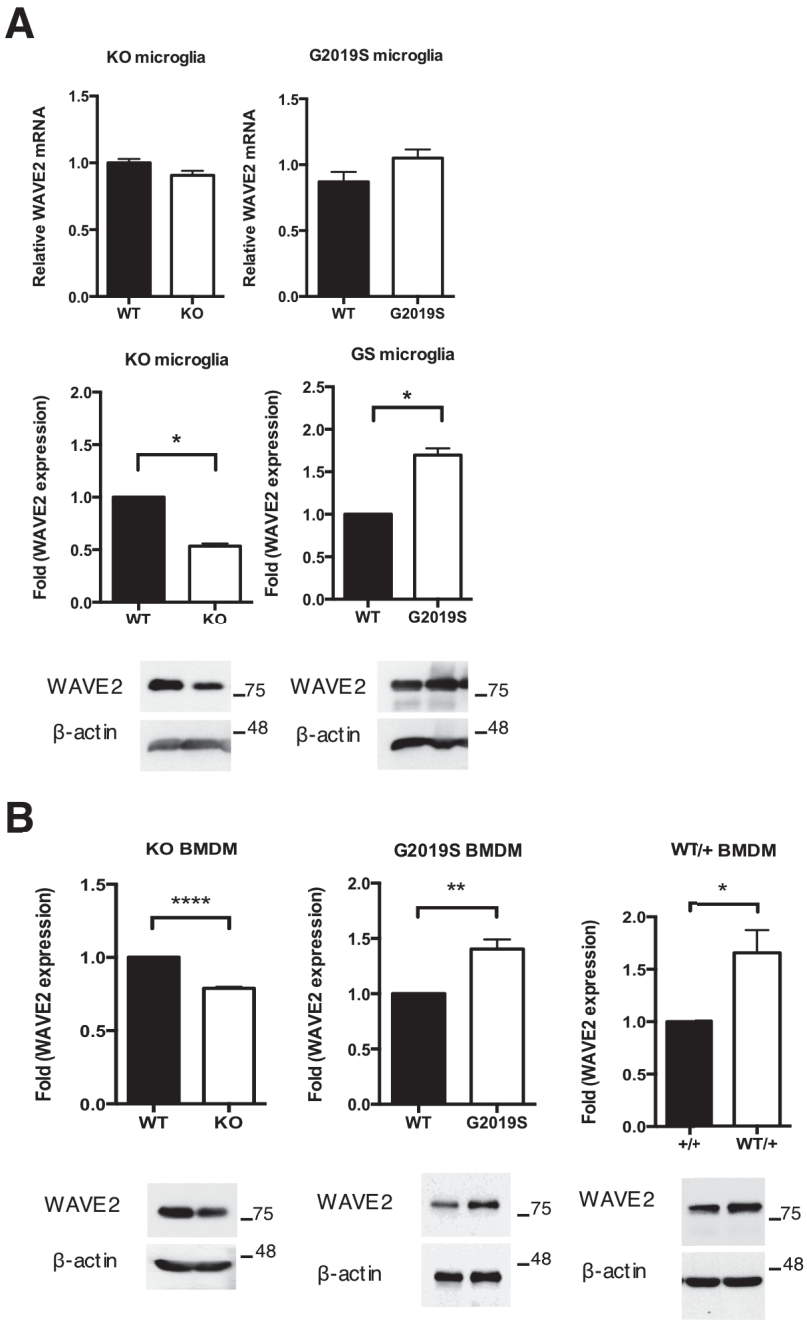
A
KO microglia
G2019S microglia
Relative WAVE2 mRNA
1.5
1.0
0.5
0.0
WT
KO
G2019S
KO microglia
GS microglia
Fold (WAVE2 expression)
2.0
2.5
1.5
*
WAVE2
β-actin
75
48
B
KO BMDM
G2019S BMDM
WT/+ BMDM
****
**
+/+
WT/+

LRRK2 deficiency impairs phagocytic activity in myeloid cells:

Given that a) LRRK2 modulates the levels of WAVE-2, b) WAVE-2 is central in regulating actin dynamics, and c) WAVE-2 is reported to play a critical role in phagocytic activity, we next examined for LRRK2's potential role in phagocytic activity by conducting engulfment assays in primary microglia from LRRK2 null mice. LRRK2 null microglia have impaired uptake of either latex beads or *E. coli* bioparticles both basally and after treatment with various TLR agonists, lipopolysaccharide (LPS), poly(I:C), or zymosan (see Figure 4.4A&B). A similar phagocytic impairment was observed in LRRK2 null primary BMDMs, which was ameliorated by exogenous WAVE-2 expression via transfection (see Figure 4.4C). To extend these findings *in vivo*, we directly injected, pH-sensitive beads into the midbrain, that fluoresce once engulfed and fused to the lysosome as previously characterized (Lucin et al., 2013). There was approximately a 25% reduction in uptake of the beads in LRRK2 null mice when compared their WT littermate controls.

Figure 4.4: Loss of LRRK2 impairs phagocytic engulfment in myeloid cells.

Latex beads were incubated with primary microglia from LRRK2 null mice and were treated with LPS (100ng/mL), poly(I:C) (10μg/mL), or zymozan (50μg/mL) as quantified by confocal microscopy (A). Incubation of *e. coli* bioparticles with LRRK2 null microglia with further stimulation via LPS was also quantified by confocal microscopy (B). WT or KO primary BMDMs transfected with mock or WAVE-2 plasmid were incubated with latex beads and stimulated with LPS (C). Three month old LRRK2 WT and KO mice were injected with pH-sensitive latex beads into the SNc and transcardially perfused 24 hours post injection. Images were obtained by confocal microscopy (D). Two-way ANOVA – Bonferroni (A-C), Student t-test (D).

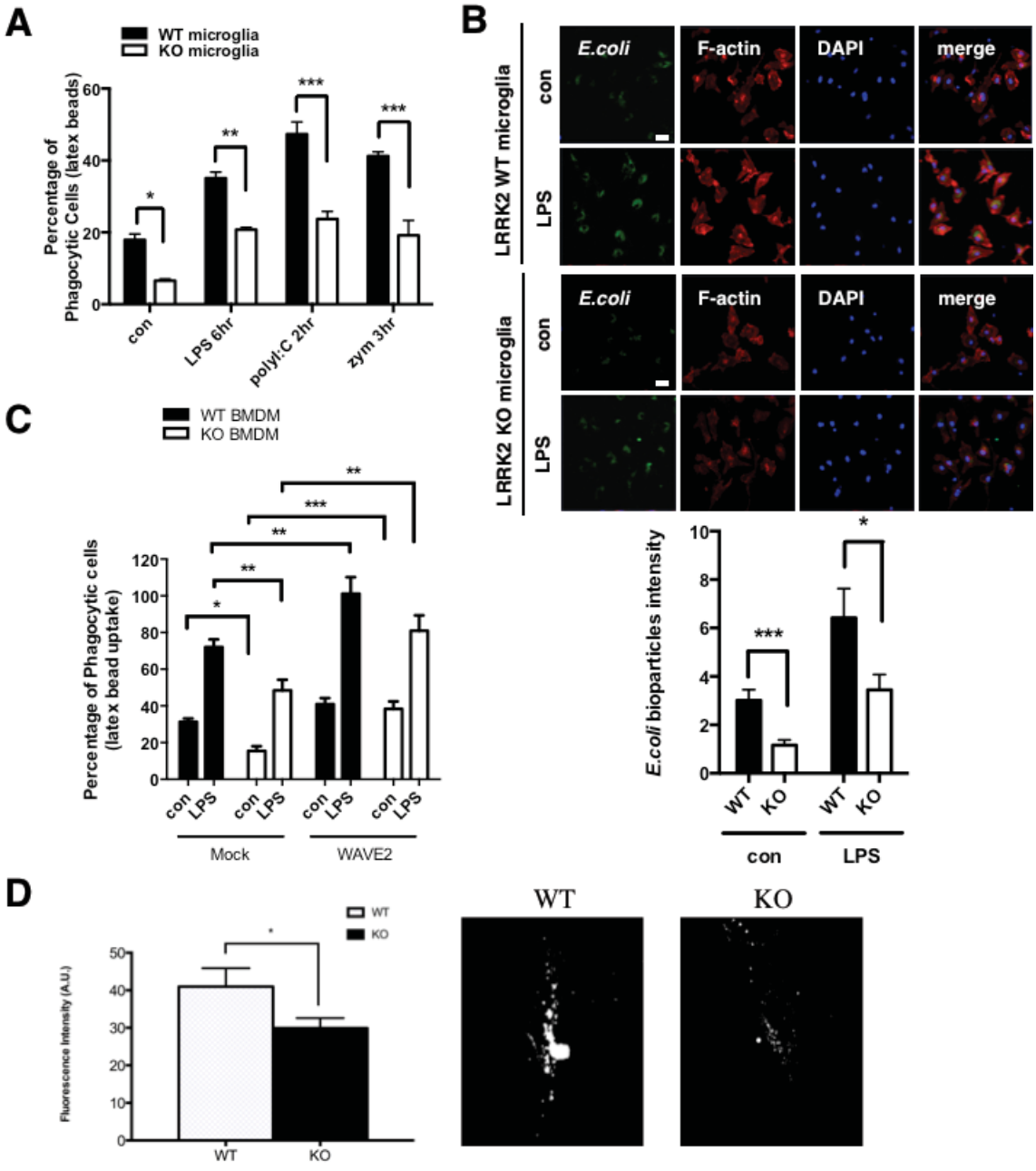
A
WT microglia
KO microglia
Percentage of Phagocytic Cells (latex beads)
con
LPS 6hr
polyI:C 2hr
zym 3hr
B
LRRK2 WT microglia
LRRK2 KO microglia
con
LPS
E.coli
F-actin
DAPI
merge
E.coli bioparticles intensity
WT
KO
con
LPS
C
WT BMDM
KO BMDM
Percentage of Phagocytic cells (latex bead uptake)
Mock
WAVE2
D
WT
KO
Fluorescence Intensity (A.U.)

LRRK2 G2019S increases phagocytic activity of myeloid cells:

In order to determine if PD related LRRK2 mutations could modulate phagocytic activity, we conducted similar bead engulfment assays as we did with our LRRK2 null immune cells utilizing microglia obtained from G2019S KI mice. LRRK2-G2019S KI microglia display increased engulfment of either latex beads or *E. coli* bioparticles basally and after treatment TLR agonists by confocal analysis (see Figure 4.5A&B). We observed that the G2019S mutation caused an increase in engulfment activity consistently in BMDMs by flow cytometry and confocal analysis (see Figure 4.5C-E). Importantly, AV-shRNA mediated reduction in WAVE-2 in G2019S BMDMs returned phagocytosis to WT levels (see Figure 4.5F). Finally an increase in engulfment was observed *in vivo* after direct injection of pH-sensitive beads into the SNc of LRRK2-G2019S mice (see Figure 4.5G). We also wanted to test if exogenous human LRRK2 could modify phagocytosis in macrophages. Consistently, BMDMs derived from WT hLRRK2 BAC mice displayed increased engulfment of latex beads or *E. coli* bioparticles by both flow cytometry and confocal analysis, respectively (see Figure 4.S2A&B). Furthermore, consistent with the gain of function hypothesis of the G2019S kinase mutation, LRRK2 kinase inhibitors were observed to decrease engulfment in G2019S microglia and while having no observable effects on LRRK2 null microglia (see Figure 4.S3).

Figure 4.5: LRRK2 G2019S increases phagocytic activity of myeloid cells.

Latex beads were incubated with primary microglia from LRRK2 G2019S mice and were treated with LPS (100ng/mL), poly(I:C) (10μg/mL), or zymozan (50μg/mL) for the times indicated and as quantified by confocal microscopy (A). Incubation of *E. coli* bioparticles with LRRK2 G2019S microglia was further stimulated with LPS and quantified by confocal microscopy (B). BMDMs from G2019S mice were incubated with latex beads (C-D) or *E. coli* bioparticles (E) and stimulated with LPS and quantified by flow cytometry (C) or confocal analysis (D-E). WT or G2019S primary BMDMs were infected with AV-shWAVE-2 or AV-sh-scramble and incubated with latex beads and stimulated with LPS (F). Three month old LRRK2 WT and G2019S mice were injected with pH-sensitive latex beads into the SNc and transcardially perfused 24 hours post injection. Images were obtained by confocal microscopy (G). Two-way ANOVA – Bonferroni (A-F), Student t-test (G).

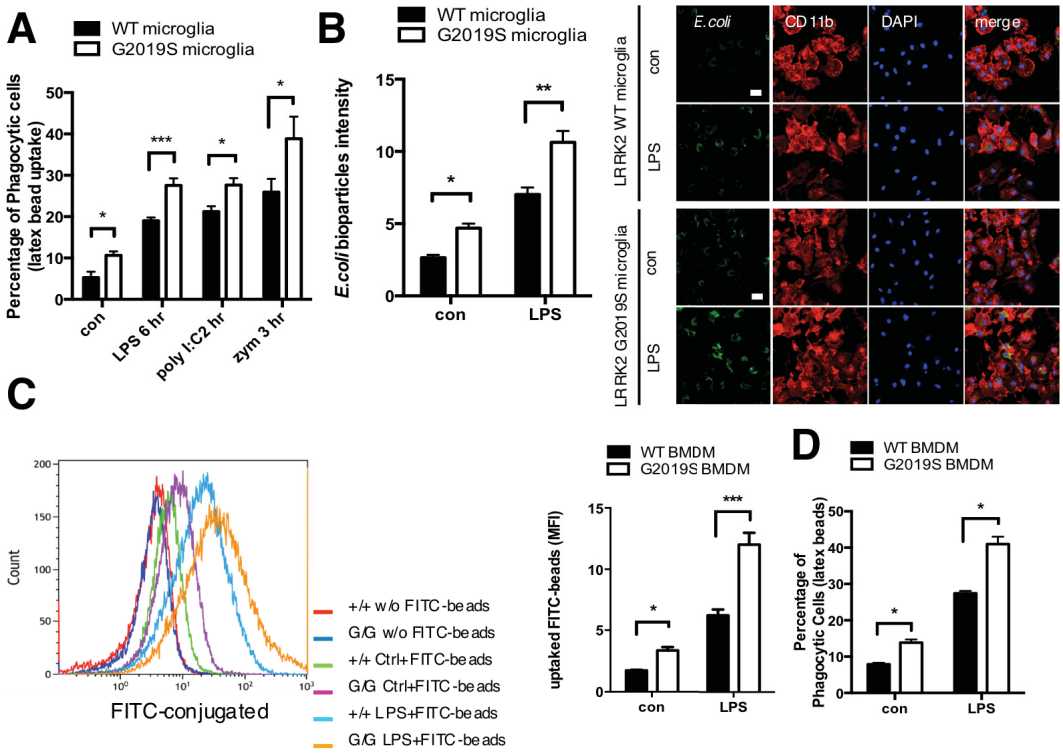
A
WT microglia
G2019S microglia
Percentage of Phagocytic cells (latex bead uptake)
con
LPS 6 hr
poly I:C2 hr
zym 3 hr
B
WT microglia
G2019S microglia
E.coli bioparticles intensity
con
LPS
E.coli
CD 11b
DAPI
merge
LRRK2 WT microglia
LRRK2 G2019S microglia
con
LPS
C
Count
FITC-conjugated
+/+ w/o FITC-beads
G/G w/o FITC-beads
+/+ Ctrl+FITC-beads
G/G Ctrl+FITC-beads
+/+ LPS+FITC-beads
G/G LPS+FITC-beads
WT BMDM
G2019S BMDM
uptaked FITC-beads (MFI)
D
WT BMDM
G2019S BMDM
Percentage of Phagocytic Cells (latex beads)
E
WT BMDM
G2019S BMDM
E.coli bioparticles intensity
F
WT BMDM
G2019S BMDM
Percentage of Phagocytic cells (latex bead uptake)
shCon
shWAVE2
G
WT
G2019S
Fluorescence Intensity (A.U.)

Figure 4.S2: Human LRRK2 over-expression increases phagocytic activity in macrophages.

Latex beads or *E. coli* bioparticles were incubated with primary BMDMs from WT hLRRK2 BAC mice and were treated with LPS (100ng/mL) as quantified by flow cytometry (A) and confocal microscopy (B), respectively. Two-way ANOVA – Bonferroni.

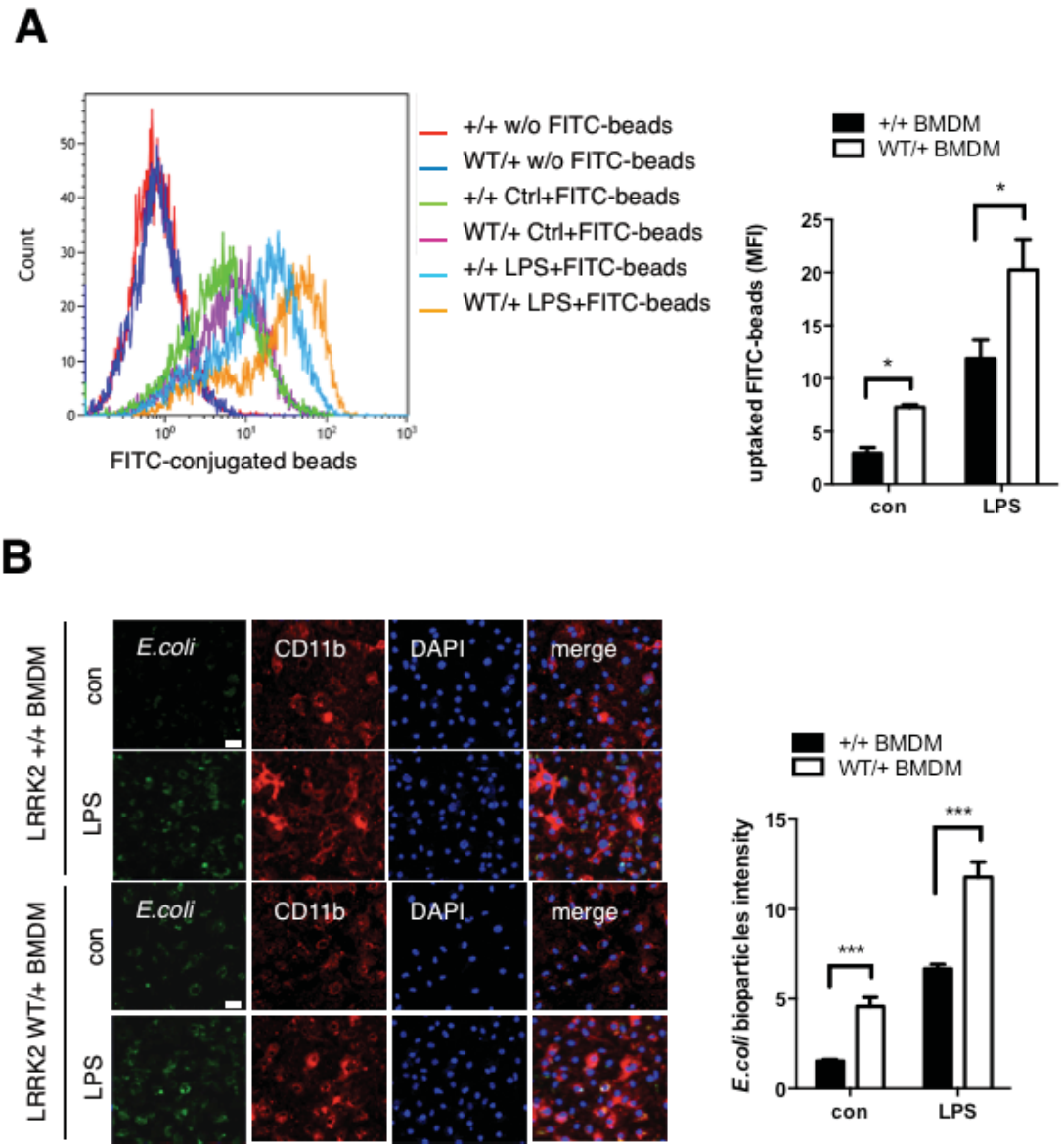
A
Count
FITC-conjugated beads
+/+ w/o FITC-beads
WT/+ w/o FITC-beads
+/+ Ctrl+FITC-beads
WT/+ Ctrl+FITC-beads
+/+ LPS+FITC-beads
WT/+ LPS+FITC-beads
+/+ BMDM
WT/+ BMDM
uptaked FITC-beads (MFI)
con
LPS
B
LRRK2 +/+ BMDM
LRRK2 WT/+ BMDM
con
LPS
E.coli
CD11b
DAPI
merge
+/+ BMDM
WT/+ BMDM
E.coli biopartic les intensity
con
LPS

Figure 4.S3: LRRK2 kinase inhibition decreases engulfment of latex beads in microglia.

Primary microglia derived from LRRK2 G2019S and null mice were incubated with latex beads and treated with various LRRK2 inhibitors (HG-10-102-01, 1μm or GSK 2578215A, 1μm) and stimulated with LPS (100ng/mL) (A&B) and analyzed by confocal microscopy. Two-way ANOVA – Bonferroni.

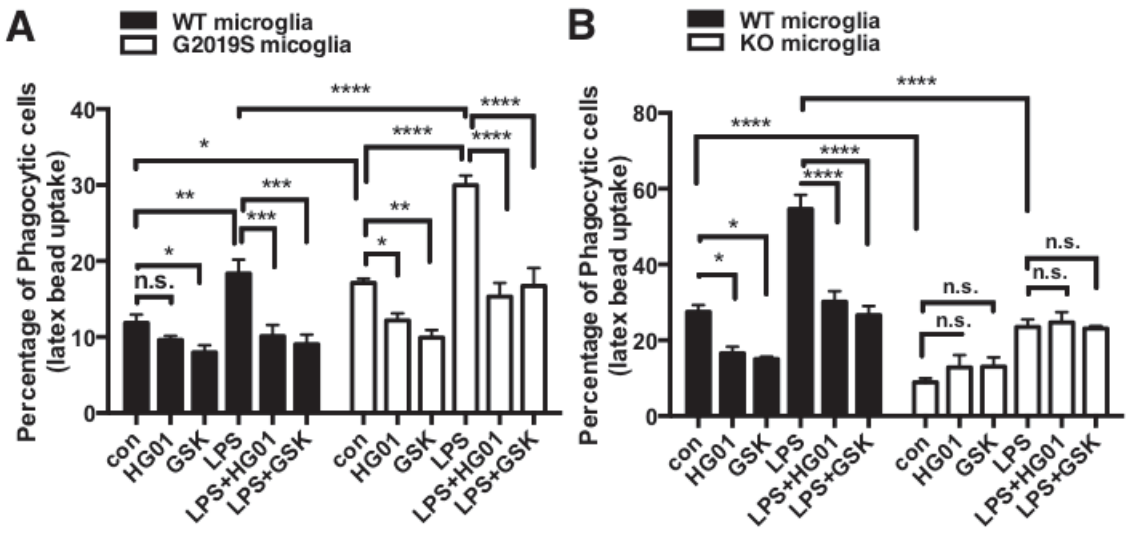
A
WT microglia
G2019S micoglia
Percentage of Phagocytic cells
(latex bead uptake)
0
10
20
30
40
n.s.
*
**
***
****
con
HG01
GSK
LPS
LPS+HG01
LPS+GSK
B
WT microglia
KO microglia
Percentage of Phagocytic cells
(latex bead uptake)
0
20
40
60
80
n.s.
*
****
con
HG01
GSK
LPS
LPS+HG01
LPS+GSK

LRRK2 binds and phosphorylates WAVE-2 directly:

In order to determine the mechanism by which LRRK2 modulates phagocytic activity via WAVE-2, we conducted co-immunoprecipitation (co-ip) studies to determine if LRRK2 and WAVE-2 form a complex. LRRK2 does endogenously form a complex with WAVE-2 that is not detectable in LRRK2 null BMDMs (see Figure 4.6A). This complex binding increases when LRRK2 is pulled down in G2019S BMDMs (see Figure 4.6B). In the context of inflammation, various TLR agonists displayed increased LRRK2 – WAVE-2 complex binding in BV2 cells (see Figure 4.S4). Using recombinant WT and G2019S LRRK2 we co-immunoprecipitated recombinant GST-WAVE-2 *in vitro* to show that LRRK2 and WAVE-2 may bind directly, and that this binding is stronger with G2019S LRRK2 protein (see Figure 4.6C). Intriguingly, multiple recombinant LRRK2 domains were able to bind directly to WAVE-2 including the LRR, COR, kinase, and WD-40 domains (see Figure 4.6D).

To test whether LRRK2 could phosphorylate WAVE-2, we tested recombinant GST-WAVE-2 phosphorylation by *in vitro* kinase assay using fluorescence labeled ATP (see Figure 4.7A). WAVE2 is directly phosphorylated by LRRK2, which is increased by recombinant G2019S and absent in the LRRK2 kinase dead D1994A mutant. To determine what type of residue LRRK2 may be phosphorylating WAVE-2 we probed p-threonine and p-serine antibody after the kinase reaction. Both p-serine and p-threonine (as well as LRRK2 autophosphorylation at Ser1292) are increased with recombinant G2019S, however there is a marked increase in threonine phosphorylation (see Figure 4.7B).

Figure 4.6: LRRK2 forms a complex and binds directly to WAVE-2 *in vitro*. Immunoprecipitated LRRK2 from null and G2019S KI BMDMs forms a complex with WAVE-2 which is increased in the G2019S KI BMDMs (A&B). Recombinant Flag-LRRK2 and GST-WAVE2 bind *in vitro* after GST pull-down, whereas Flag-G2019S displays increased GST-WAVE2 binding (C). Multiple recombinant truncated domains of myc-LRRK2 bind to Flag-WAVE-2 after pull down of Flag (D). Student t-test.

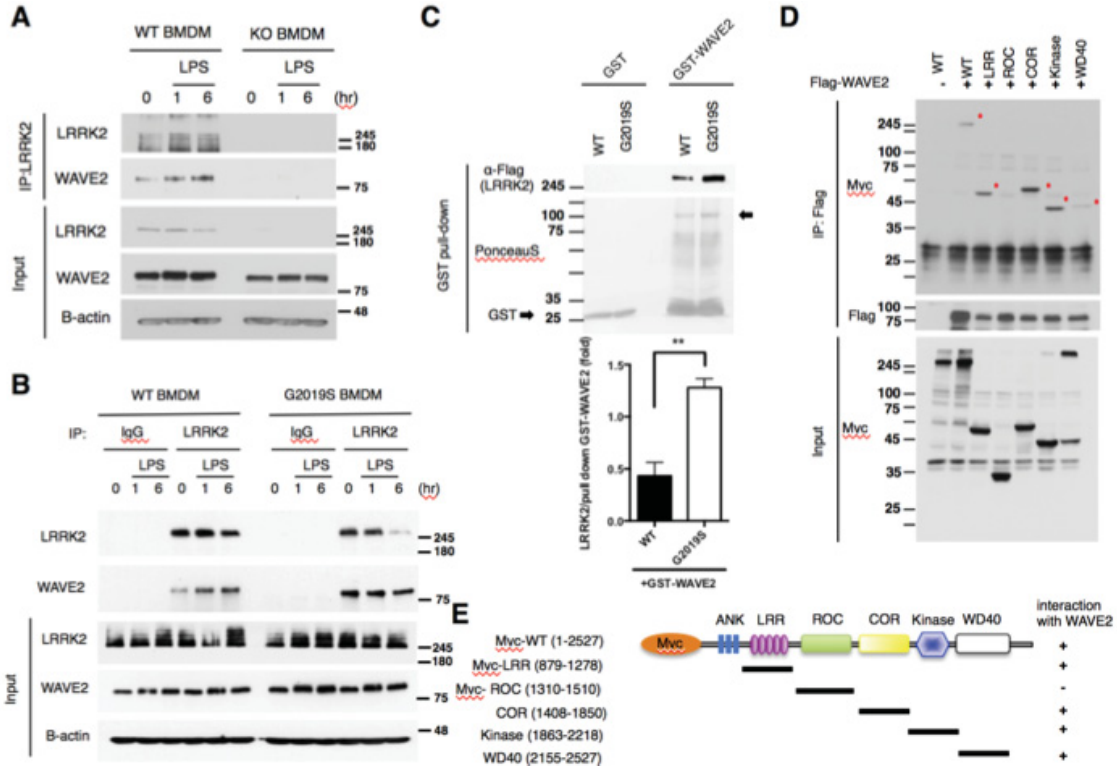
A
WT BMDM
KO BMDM
LPS
0 1 6 0 1 6 (hr)
IP:LRRK2
LRRK2
WAVE2
Input
LRRK2
WAVE2
B-actin
245
180
75
48
B
WT BMDM
G2019S BMDM
IP:
IgG
LRRK2
LPS
0 1 6 0 1 6 0 1 6 0 1 6 (hr)
LRRK2
WAVE2
Input
LRRK2
WAVE2
B-actin
245
180
75
48
C
GST
GST-WAVE2
WT
G2019S
α-Flag (LRRK2)
GST pull-down
PonceauS
GST
245
100
75
35
25
LRRK2/pull down GST-WAVE2 (fold)
1.5
1.0
0.5
0.0
**
+GST-WAVE2
D
Flag-WAVE2
- WT +WT +LRR +ROC +COR +Kinase +WD40
IP: Flag
Myc
Flag
Input
Myc
245
100
75
45
35
25
E
Myc-WT (1-2527)
Myc-LRR (879-1278)
Myc- ROC (1310-1510)
COR (1408-1850)
Kinase (1863-2218)
WD40 (2155-2527)
Myc
ANK
LRR
ROC
COR
Kinase
WD40
interaction with WAVE2
+
+
-
+
+
+

Figure 4.S4: The LRRK2 and WAVE-2 complex is increased with TLR stimulation. LRRK2 was immunoprecipitated in BV2 cells after a TLR agonist treatment time-course with LPS (100ng/mL), poly(I:C) (10μg/mL), or zymozan (50μg/mL).

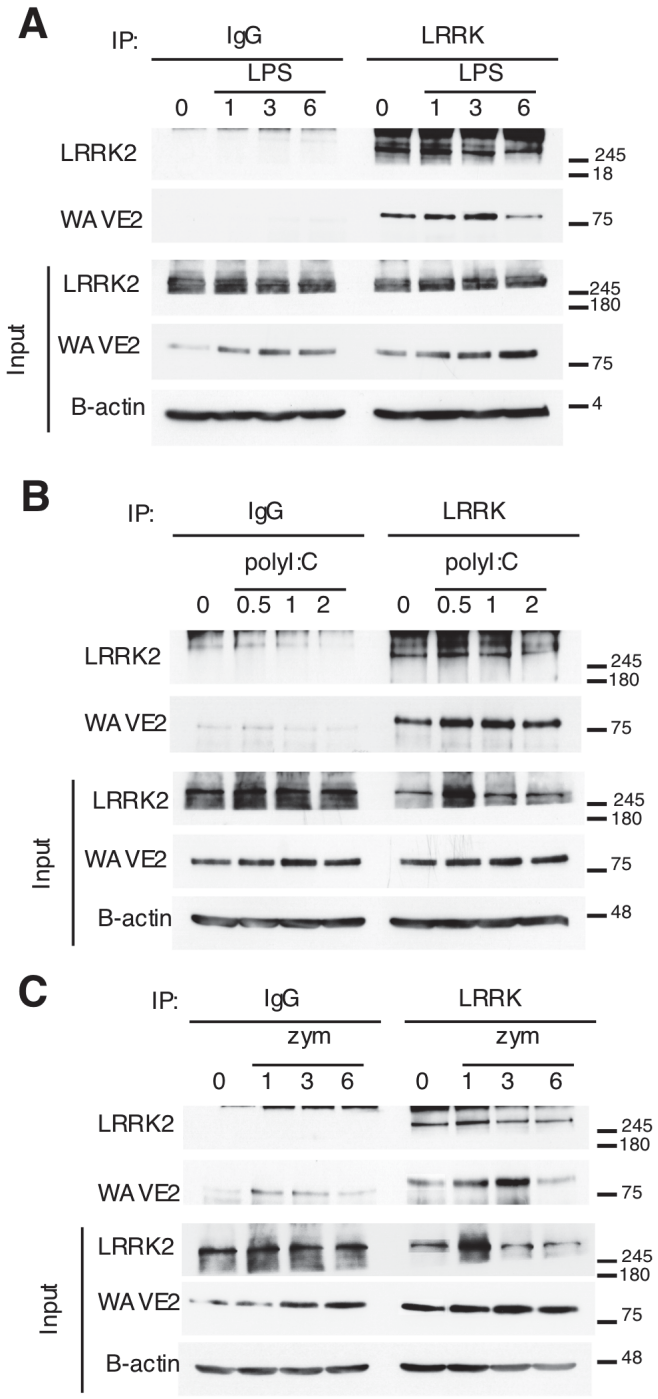
A
IP:
IgG
LRRK
LPS
0 1 3 6
0 1 3 6
LRRK2
WAVE2
Input
LRRK2
WAVE2
B-actin
245
18
75
245
180
75
4
B
IP:
IgG
LRRK
polyI:C
0 0.5 1 2
0 0.5 1 2
LRRK2
WAVE2
Input
LRRK2
WAVE2
B-actin
245
180
75
245
180
75
48
C
IP:
IgG
LRRK
zym
0 1 3 6
0 1 3 6
LRRK2
WAVE2
Input
LRRK2
WAVE2
B-actin
245
180
75
245
180
75
48

Figure 4.7: LRRK2 phosphorylates WAVE-2.

In vitro kinase assays were performed with 30ng of LRRK2 (WT, G2019S, or D1994A) protein and 500ng of GST-WAVE-2 with 10μM ATP - ATTO 590 for 30 min at 30°C (A). This was repeated with Western analysis for p-serine, p-threonine, and LRRK2 auto-phosphorylation (ser1292) (B). One-way ANOVA – Tukey.

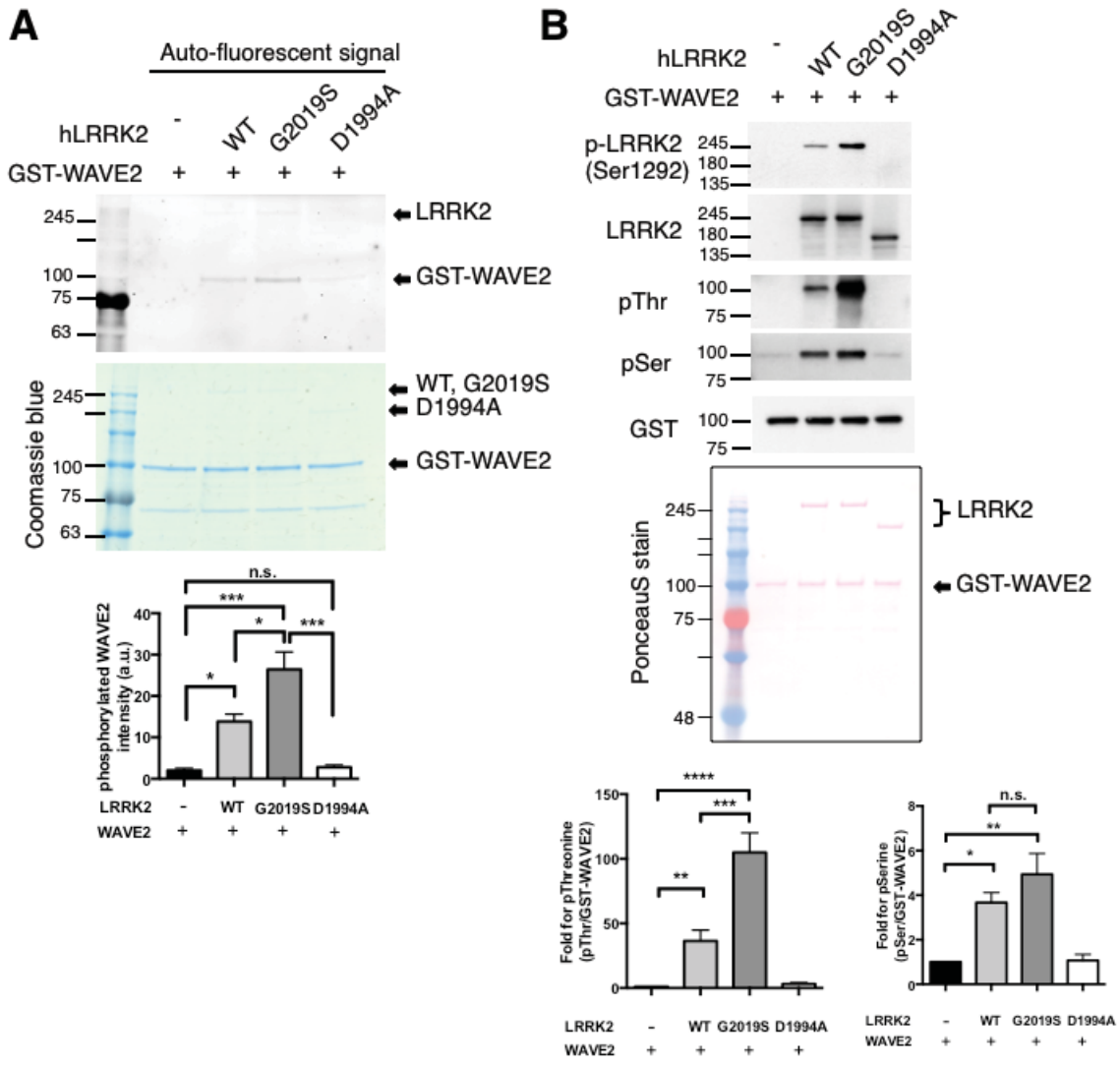
A
Auto-fluorescent signal
hLRRK2
-
WT
G2019S
D1994A
GST-WAVE2
+
+
+
+
245
100
75
63
LRRK2
GST-WAVE2
Coomassie blue
WT, G2019S
D1994A
GST-WAVE2
n.s.
***
*
***
*
phosphorylated WAVE2 intensity (a.u.)
40
30
20
10
0
LRRK2
WAVE2
B
hLRRK2
GST-WAVE2
p-LRRK2 (Ser1292)
LRRK2
pThr
pSer
GST
245
180
135
100
75
PonceauS stain
48
LRRK2
GST-WAVE2
****
***
**
Fold for pThreonine (pThr/GST-WAVE2)
150
100
50
0
n.s.
**
*
Fold for pSerine (pSer/GST-WAVE2)
8
6
4
2
0

LRRK2 G2019S causes increased engulfment of neuronal cells:

In order to test if enhanced phagocytic activity of G2019S microglia could lead to increased dopaminergic cell death, we treated dopaminergic-like differentiated SH-SY5Y cells with WT or G2019S microglia in a co-culture system and examined TAU engulfment in microglia. SH-SY5Y cells treated with G2019S microglia displayed increased TAU staining co-localized with microglia (CD11b), both basally and after LPS stimulation (see Figure 4.8). This suggests that G2019S microglia enhanced phagocytic activity may contribute to increased neuronal cell death.

Figure 4.8: LRRK2 G2019S microglia display increase TAU engulfment of neuronal cells.

Differentiation of SH-SY5Y was confirmed by the presence of TrkB by Western. Differentiated cells ($0.5X10^5$) were treated with primary microglia ($1.5x10^5$) and LPS (100 ng/mL) stimulation for 24 hr. TAU and CD11b co-localization was performed by confocal microscopy. Scale bar-20um. Two-way ANOVA-Bonferroni.

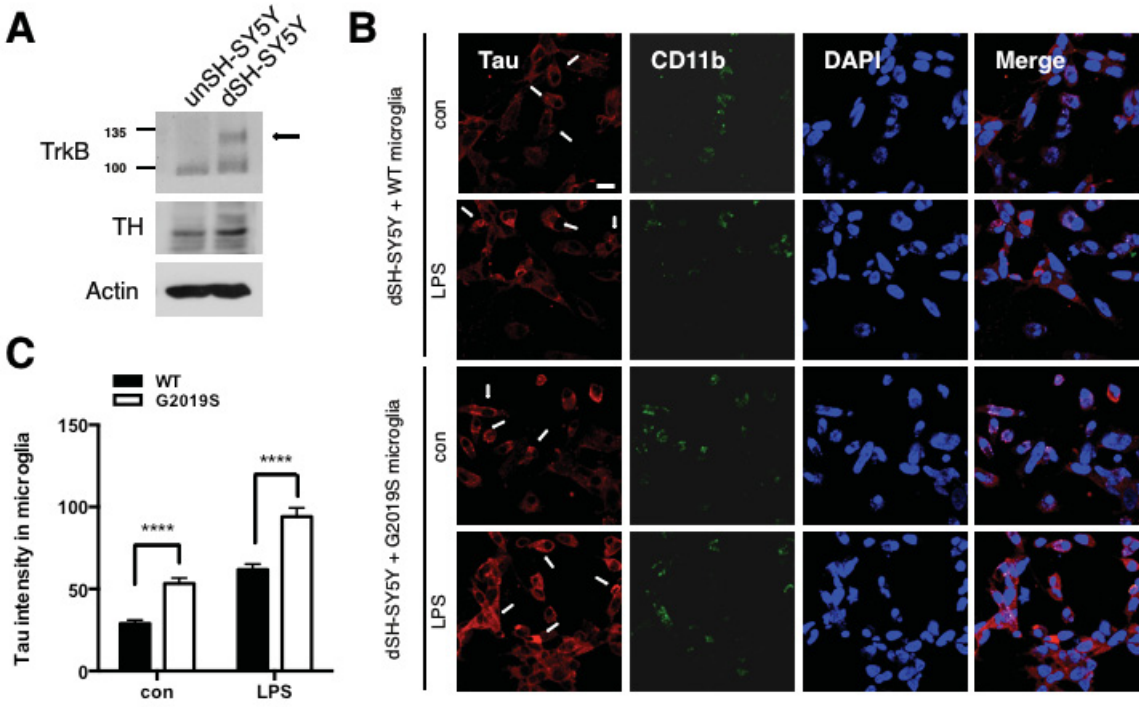
A
unSH-SY5Y
dSH-SY5Y
TrkB
135
100
TH
Actin
B
Tau
CD11b
DAPI
Merge
dSH-SY5Y + WT microglia
con
LPS
dSH-SY5Y + G2019S microglia
con
LPS
C
WT
G2019S
Tau intensity in microglia
150
100
50
0
****
****
con
LPS

Down-regulation of SCAR may rescue Parkinsonism and survival deficits in flies expressing LRRK2 G2019S in Drosophila central phagocytes.

In attempts to provide functional outcomes relevant to PD and the immune system, we returned to the fly model. We wanted to test if down-regulation of SCAR could ameliorate the Parkinsonism and lifespan deficits we had observed in flies expressing G2019S in ensheathing cells. To do this, we established a stable G2019S fly line in order to determine if these locomotor deficits could be rescued by down-regulation of SCAR by RNAi (see Figure 4.9A). Preliminary results indicate that there may be a trend for partial rescue of the locomotor phenotype observed in MZ-GAL4-UAS-hLRRK2-G2019S by SCAR-RNAi (see Figure 4.9B). Finally, the expression of G2019S in ensheathing glia causes a decrease in survival that can by ameliorated by inhibition of SCAR (see Figure 4.9C).

Figure 4.9: Down-regulation of SCAR rescues the Parkinsonism and survival deficits in flies expressing LRRK2 G2019S in CNS phagocytes.

Human LRRK2 protein is detectable in fly head lysate (4 per lane) in MZ-GAL4; UAS-hLRRK2-G2019S and MZ-GAL4/UAS-SCAR-RNAi; UAS-hLRRK2-G2019S flies (A). Locomotor activity was assessed for 3 day old male flies expressing LRRK G2019S and SCAR RNAi in ensheathing cells by the Drosophila Activity Monitor system for 72 hrs (B). The same flies were assessed for survival deficits by lifespan analysis observed daily (C). All flies were incubated at 25°C. Locomotor assays – one-way ANOVA followed by Tukey's least significant difference. Survival assay – Logrank test.

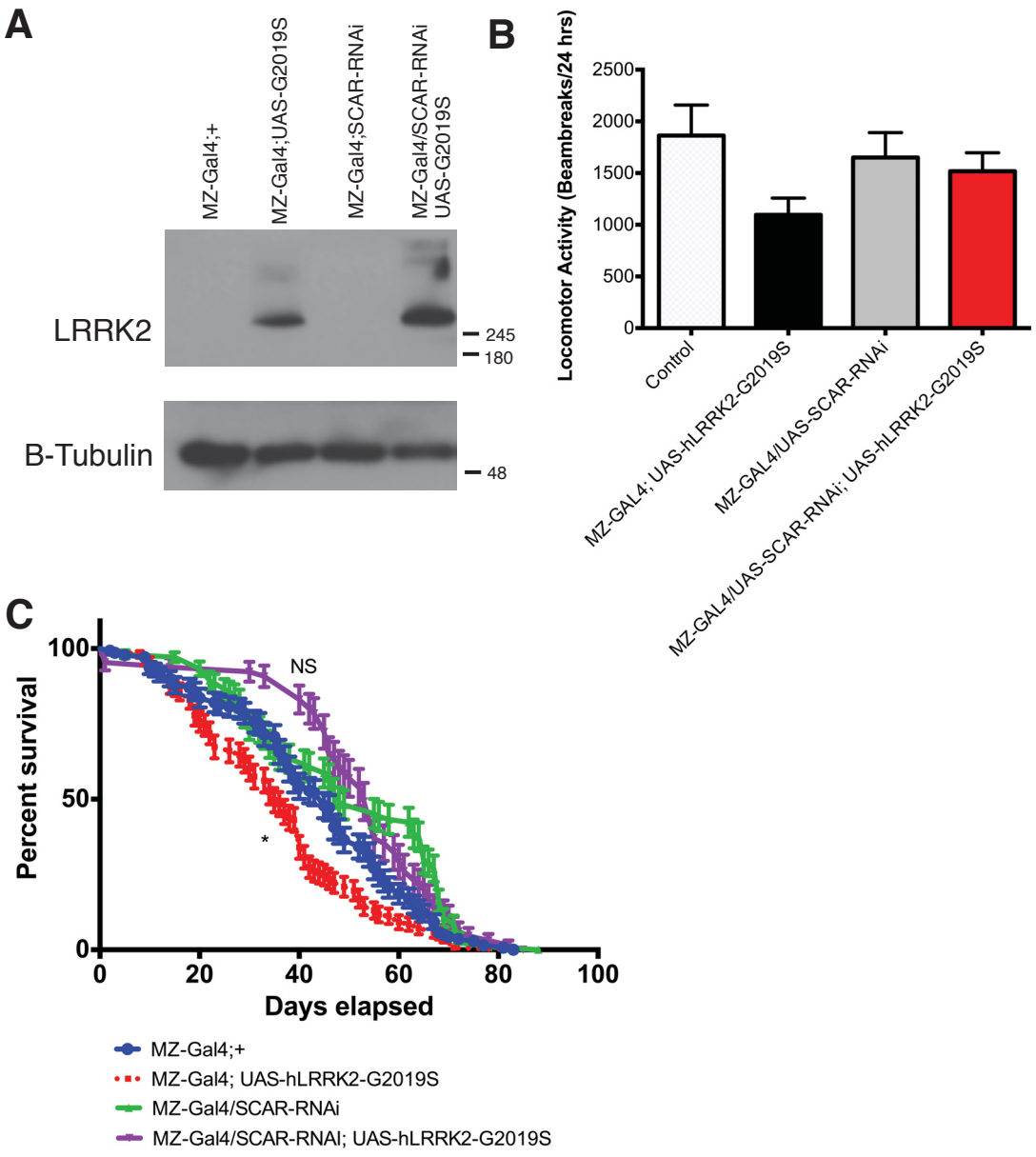
A
MZ-Gal4;+
MZ-Gal4;UAS-G2019S
MZ-Gal4;SCAR-RNAi
MZ-Gal4/SCAR-RNAi UAS-G2019S
LRRK2
245
180
B-Tubulin
48
B
Locomotor Activity (Beambreaks/24 hrs)
2500
2000
1500
1000
500
0
Control
MZ-GAL4; UAS-hLRRK2-G2019S
MZ-GAL4/UAS-SCAR-RNAi
MZ-GAL4/UAS-SCAR-RNAi; UAS-hLRRK2-G2019S
C
Percent survival
100
50
0
NS
*
0
20
40
60
80
100
Days elapsed
MZ-Gal4;+
MZ-Gal4; UAS-hLRRK2-G2019S
MZ-Gal4/SCAR-RNAi
MZ-Gal4/SCAR-RNAI; UAS-hLRRK2-G2019S

Discussion:

This work has attempted to propose that LRRK2 may play a prominent role in modulating the phagocytic response of myeloid cells where the G2019S pathogenic mutation further enhances phagocytic activity. Furthermore, we present indirect evidence that this may result in increased dopaminergic loss. Intriguingly, WAVE-2 appeared to be specifically altered in microglia and BMDMs but not in other cell types tested. This may be in line with the notion that WAVE family members, as well as similar ARP2/3 complex activating protein families such as WASP, WASH, WHAMM and JMY have competed for ARP2/3 complex activation throughout evolution (Rottner et al., 2010). This may be particularly true when comparing non-motile to motile cells such as microglia and macrophages to other cell types (Miller, 2002). Besides phagocytosis, WAVE-2 has been particularly implicated in mediating immune cell migration (Kheir et al., 2005). Microglia from LRRK2-G2019S BAC rats have been shown to be more motile in chemotaxis assays (Moehle et al., 2015). The authors further suggest this increase in migration is dependent on the ARP2/3 complex in which they demonstrate that various ARP components form a complex with LRRK2. On the contrary, another group has opposing results showing that microglia from G2019S-BAC mice on a CX_3CR1^{gfp} heterozygous microglia reporter background have motility deficits (Choi et al., 2015). Regardless of this discrepancy, we opted to use G2019S endogenous KI mice for this study that may be more physiologically relevant for expression of LRRK2 in myeloid cells and limit artefacts.

Our work suggests WAVE-2 is a bona fide substrate of LRRK2 and is supported by evidence that WAVE-2 is a putative LRRK2 kinase substrate by a high-throughput

LRRK2 tandem affinity purification assay (Martin et al., 2014). Future studies should determine what specific residue(s) LRRK2 phosphorylates WAVE-2. Furthermore, phospho-mimetic or deficient WAVE-2 mutants should display an increase or decrease in phagocytic activity, respectively. While WAVE-2 lacks any known consensus motifs for LRRK2 phosphorylation, it contains a significant amount of phosphorylation sites. Furthermore, WAVE-2 is phosphorylated by the kinases: ERK, JNK and CK2, the latter of which has been shown to increase affinity to the ARP2/3 complex (Krause and Gautreau, 2014).

The nature of how LRRK2 mediated phosphorylation of WAVE-2 increases WAVE-2 protein level remains unclear. However, preliminary data in the Park lab suggests that LRRK2 may increase WAVE-2 protein stability by inhibiting the proteasome (data not shown). A similar process has been shown for kinase mediated phosphorylation of the PD related gene, Parkin, which in turn inhibits Parkin's ubiquitination and degradation (Ko et al., 2010). This leads us to a model that the LRRK2-G2019S hyper-kinase promotes WAVE-2 stability via both binding and phosphorylating WAVE-2 preventing its degradation keeping it available and readily in complex to mediate actin restructuring (see Figure 4.10).

Our *in vitro* co-culture model suggested that the G2019S mutation might confer an increase in phagocytic activity that may lead to and increase engulfment of neuronal cells. This should be repeated in WT primary midbrain cultures co-cultured with WT or G2019S microglia. Preliminary primary co-culture data using WT or G2019S BMDM seeded onto WT primary midbrain neurons look promising in that there is enhanced death in the G2019S treated neurons (Data not shown). Also, further studies should determine

Figure 4.10: Model of LRRK2 mediated promotion of WAVE-2 complex stability. LRRK2 kinase activity promotes WAVE-2 stability by inhibition WAVE-2 degradation. This leads to increased WAVE-2 affinity to the ARP2/3 and actin-nucleation. Readily activatable WAVE-2 may then activate the ARP2/3 complex for phagocytic cup formation and engulfment.

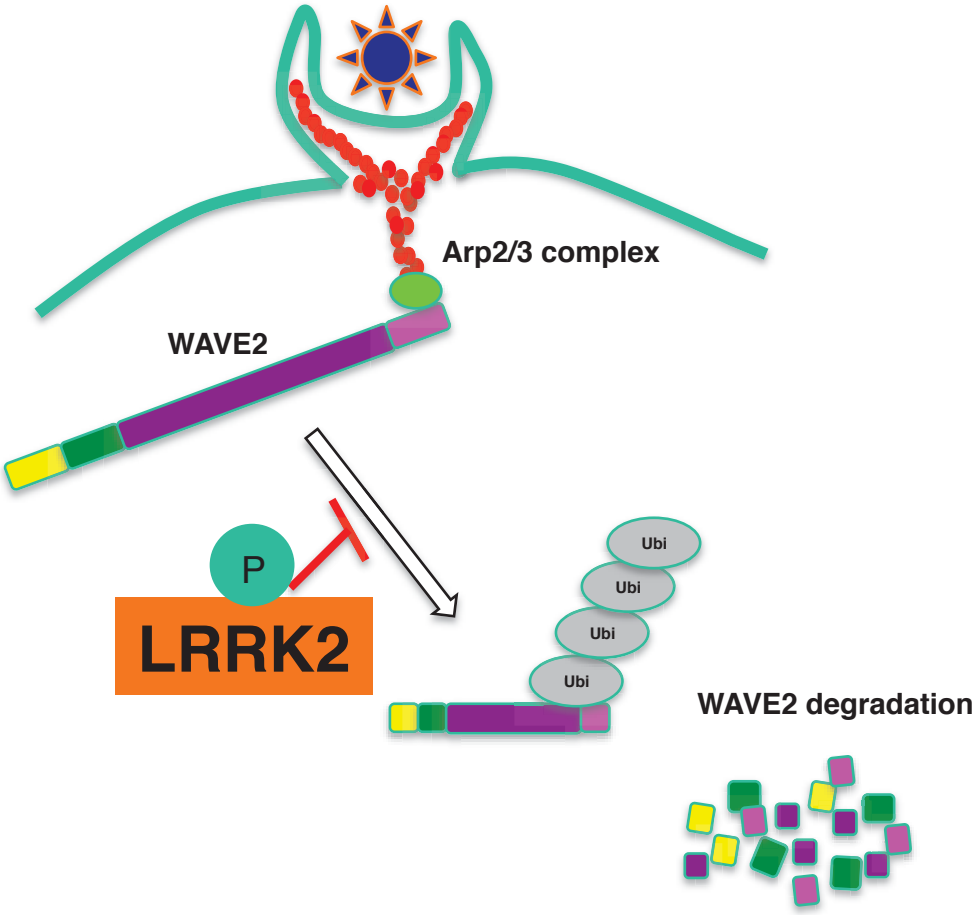
Arp2/3 complex
WAVE2
P
LRRK2
Ubi
Ubi
Ubi
Ubi
WAVE2 degradation

the effect of neurons treated with conditioned media from stimulated microglia to rule out the effects of pro-inflammatory cytokine and chemokine release that may influence neuronal death.

We endeavoured to establish a model of LRRK2 induced Parkinsonism in flies by specifically expressing LRRK2 in fly "microglia like" CNS phagocytes called ensheathing cells. Additional studies should examine the dopaminergic clusters of these flies to confirm whether dopamine cell death ensues and whether down-regulation of SCAR may rescue this loss. Within the context of this study, our work demonstrates that SCAR and WAVE family members have an evolutionary function in immune cells and the more recently evolved LRRK2 has a conserved relationship with *Drosophila* SCAR and murine WAVE-2. It remains to be determined whether WAVE-2 is altered in myeloid cells of humans with PD.

Along with other variants implicated in neurodegeneration, the G2019S mutation has been proposed to have been potentially selected for throughout evolution (Cookson, 2012b). While difficult to test, it may be that enhanced phagocytic activity of G2019S myeloid cells may be beneficial in the periphery while having the potential to lead to increased death of terminally differentiated and susceptible dopamine neurons as humans age. Whether this is true or not, neuroinflammatory signalling in PD, particularly in regards to LRRK2 induced PD, begs further study.

Methods:

LRRK2 animals: LRRK2 null mice were obtained from Dr. Jie Shen and previously characterized (Tong et al., 2010). LRRK2-G2019S KI mice were obtained from Dr. Michael G. Schlossmacher (Novartis) as previously characterized. WT-hLRRK2-BAC mice were obtained from JAX.

Viral Vectors: Custom AV vectors were purchased from lifetech for AdEShuttle-iba1-ZsYellow1-N1:H1-shWAVE2 and AdEShuttle-iba1-ZsYellow1-N1:H1-shControl 1 (Ambion).

Antibodies: Primary antibodies used include the following: α-LRRK2 (ab133474; Abcam, 75-253; Neuromab), α-LRRK2(ser1292), WAVE1 (sc-271506; SantzCruz), WAVE2 (3659; Cell Signaling), WAVE3 (3659; Cell Signaling), anti-phosphothreonine (9386; Cell Signaling), anti-phosphoserine (600-401-261; Rockland), anti-β-actin (A5316; Sigma), TrkB (Cell signaling) , Flag (Sigma), Myc (Roche), *Drosophila* B-Tubulin (DSHB), CD11b (ab-serotech).

Microglia culture: Mixed glia were taken and cultured from cerebral cortices of 1-3 day of mouse pups. Briefly, the cortices were triturated into single cells in MEM with 10% fetal bovine serum (FBS) and 5% horse serum (HS) and were plated into T75 flasks coated poly-D-lysine for 2 weeks. Microglia were detached from the flasks by shaking at 200 rpm for 1 hour and then filtered through 40 μm cell strainer to make pure microglia cultures.

BMDM culture: BMDMs were harvested as previously (Hakimi et al., 2011). Briefly, BMDMs were cultured in RPMI 1640 medium containing 10% FBS, 10% L929

conditioned medium, 1% sodium pyruvate and 1% non-essential amino acid and then maintained at 5% CO_2, 37°C for 7 days.

Western blot and Immunoprecipitation: The cells were lysed in ice-cold RIPA buffer (50mM Tris-HCl, pH7.4, 150mM NaCl, 1% NP-40, 0.25% sodium deoxy-cholate) containing protease inhibitor cocktail. After sonication, the lysates were centrifuged at 12000 rpm for 15min at 4°C, and the supernatant was collected. Proteins were resolved by SDS-PAGE and transferred to a nitrocellulose membrane. For immunoprecipitation, the cells were lysed in ice-cold modified RIPA buffer (50mM Tris-HCl, pH7.4, 300mM NaCl, 1% triton x-100, 0.25% sodium deoxy-cholate) containing protease inhibitors and phosphatase inhibitor cocktails. The lysates were pre-cleared by protein G Sepharose beads for 1 hour at 4°C on an orbital shaker. Equal lysate of each pre-cleared samples were incubated with primary antibody for 12 hours and further for 12 hours with protein G Sepharose and then immune complexes were collected by centrifuge, washed at least three times with cold modified RIPA buffer, and re-suspended in 2x SDS sample buffer. Finally immune complexes were resolved by SDS-PAGE for Western blot analysis.

Latex beads-based *in vitro* and *in vivo* phagocytosis assay: For *in vitro* phagocytosis assay, experimentally-treated cells were exposed to latex beads (Sigma) at a 1:50 ratio (cell/beads) or pHrodo Green *e.coli* bioparticles (Invitrogen) for indicated times. After incubation with latex beads, the cells were washed five times with cold 1X PBS to remove residual non-specific binding of the latex beads to cell surface or plate bottom and fixed with 1% paraformaldehyde (PFA). Each group of fixed cells was analyzed by confocal microscopy. To determine phagocytic activity, we counted ingested latex beads in cell surface and intracellular compartments as performed previously (Koenigsknecht

and Landreth, 2004). Briefly, the number of latex beads per cell was assigned points in such a way that a cell received 1 point for ingesting one bead, 2 points for ingesting two beads, up until a maximum of 6 points for six beads or more ingested per cell. Total number of cells in each group was multiplied by the point value of each group and then those values were added then divided by the total number of cells. For *in vivo* phagocytosis assay, pH-sensitive latex beads were made by coupling 3μm latex beads with CypHer5E mono N-hydroxysuccinimide (NHS) ester (GE Healthcare). CypHer coupled latex beads were diluted in 1 X PBS to a stock concentration of 2 X 10^4 beads/μl. pH-sensitive beads were stereotaxically injected into the substantia nigra pars compacta (SNc) using following coordinates from bregma: -3.1mm anterior, +1.1mm lateral, and a depth of -4.4mm. After 24 hours, mice were transcardially perfused with 4% PFA and then the tissue was analyzed phagocytic activity using a confocal microscope.

Confocal microscopy analysis: Cells were plated on poly-D-lysine coated coverslips for analysis of phagocytosis activity. After incubation with agonists, latex beads or *e.coli* bioparticles for indicated times, the coverslips were washed two or three times with PBS and fixed in 2% PFA for 30 min at room temperature. The fixed cells were permeabilized in PBS containing 0.1% Triton X-100 for 3 min at room temperature and then washed three times with PBS. After blocking with 3% bovine serum albumin (BSA) for 30 min and washing, the preparations were stained indicated antibodies.

Flow cytometry: Flow cytometry was conducted as previously described (Kim et al., 2013). Briefly, BMDMs were dispersed into a single-cell suspension with PBS containing 1 mM EDTA. Cells were fixed with 4% paraformaldehyde for 1 h at 4°C and were blocked by PBS containing 3% BSA for 1 h at 4°C, and then incubated with

primary antibodies for 1 h at 4°C. After washing three times with PBS, the cells were incubated with FITC-conjugated secondary antibody for 1 h at 4°C. After washing, the cells were analyzed using a FACS - BD LSRFortessa (Flow cytometry core University of Ottawa).

GST pull down assay: Recombinant mouse GST-WAVE2 protein and GST alone were mixed with Flag tagged human full length LRRK2 protein and incubated for 4 hours at 4°C. After incubation, glutathione sepharose beads were added into the mixture. The supernatant was removed by centrifugation and the beads were washed three times with binding buffer (0.2% Triton X-100, 50mM Tris-HCl (pH7.5), 100mM NaCl, 5mM EDTA). The bound proteins were eluted by boiling from the beads in SDS sample buffer. The eluted samples were subjected to Western blot using GST and Flag antibody.

Drosophila stocks: All flies were maintained on a standard cornmeal/agar medium at ambient RT or at 25°C when under experimental conditions. hLRRK2 flies were characterized previously (Venderova et al., 2009). UAS-hLRRK-WT and UAS-hLRRK2-G2019S flies were a gift from Dr. Bingwei Lu. mz0709-GAL4 flies were graciously provided by Dr. Marc Freeman. SCAR-RNAi was obtained from the Vienna Drosophila Research Centre. GMR-GAL4/BC and w1118 flies were gifts from Dr. Yong Rao and Dr. Margaret Sonnenfeld, respectively.

SEM imaging: heads of 10 day old male flies were fixed in 2% glutaraldehyde in 0.1M sodium cacodylate buffer (pH 7.3) for 2 hrs then dehydrated in ethanol. SEM was performed by the Advanced Bioimaging Center, Mount Sinai Hospital, Toronto.

Locomotor activity: Flies were aged to 5 days at 25°C and placed in the *Drosophila* Activity Monitor (DAM) system (TriKinetics). The apparatus has 32 chambers (one for

each fly). Flies are able to walk within the chamber with access to food. Activity is summed every 5 minutes and quantified for 24 or 72 hours.

Drosophila Lifespan: Flies were incubated at 25°C. The conditions of the crosses, including the number of parent males and females, were kept the same for all genotypes. The flies from each genotype were collected within 24 hours post-eclosion, divided into sets of 8 and aged. The vials were changed every 4 days. Live and dead flies were recorded every day.

SH-SY5Y – microglia co-culture: Differentiated cells ($0.5X10^5$) were treated with primary microglia ($1.5x10^5$) and LPS (100 ng/mL) stimulation for 24 hr.

In vitro kinase assay: Commercially available (Invitrogen) recombinant LRRK2 (WT, G2019S, or D1994A) (30ng) was incubated with GST-WAVE-2 (500ng) produced and purified from e. coli with 10μM ATP - ATTO 590 for 30 min at 30°C.

Statistical analysis: Data was analyzed as specified, expressed as means ± SEM

* if $P \leq 0.05$, ** if $P \leq 0.01$, *** if ≤ 0.001 and **** if $p \leq 0.0001$.

Acknowledgements:

We would like to thank undergraduate students that helped maintain fly stocks: Cindy Wei and Amanda Perozzo. We would like to thank Douglas Holmyard (Mount Sinai Hospital, Toronto) for SEM pictures. This study was supported by grants from the Michael J Fox Foundation, Canadian Institutes of Health Research, the Parkinson's Society Canada (PSC), the Parkinson's Research Consortium (PRC) in Ottawa, the Network of Centers of Excellence in Neurodegeneration, the Heart and Stroke Foundation of Ontario, and the Neuroscience Brain Canada/Krembil Foundation. PCM was funded by fellowships from PSC and PRC. There is no declared conflict of interest with the contents of this article.

Chapter 5:

General Discussion

5.1 - Summary & Principal Findings:

PD is a complex disease that remains enigmatic despite advances in understanding of some of the genetics underlying this degenerative condition. This dissertation had diverse and ambitious objectives in attempting to 1) produce a better murine model of PD, 2) elucidate LRRK2 genetic interactors from an established *Drosophila* model for improved LRRK2 understanding and 3) investigate the relationship between LRRK2 and SCAR/WAVE-2 in regards to phagocytic activity while establishing an immune related model of Parkinsonism in *Drosophila*.

In a recessive model of PD, we were able to develop the DJ1-C57 null mouse that recapitulates the unilateral onset of the disease as it occurs in humans. This striking feature then proceeds to degenerate in both hemispheres of the nigra in our affected mice. The lack of motor deficits in young mice can be explained by observed up-regulated striatal postsynaptic activity. Our model was also supported by microgliosis in the SNc and additional neuronal loss in the LC. Finally, aged mice displayed mild but significant motor deficits. The impact of developing the first whole germ-line genetic model of PD that displays robust nigral degeneration remains uncertain. The lack of complete penetrance or ability to predict which animal is affected prior to sacrifice and fixation has made the task difficult in using the model as a platform for study. Fortunately, recent DJ-1 null rats have shown robust nigral degeneration, confirming our studies showing that DJ-1 loss may result in SNc degeneration in animals of the Order, *Rodentia* (Dave et al., 2014).

LRRK2 is the most commonly linked PD gene and is involved in the sporadic disease. Therefore LRRK2 is vital for the field to unravel both in its role in the cell and

contribution to the pathogenesis of PD. Our *in vivo* screen in *Drosophila* to reveal functional genetic interactors that modify LRRK2 induced degeneration in the eye and dopaminergic system has already made an impact through our own mammalian studies. We discovered a relationship between LRRK2 and the actin nucleation promoting complex protein, SCAR, which had functional conservation in mammalian cells, specifically of the myeloid lineage. Additionally, our list of interactors also provides the field with other putative pathways for further analysis. Moreover, our list revealed gene candidates that have been implicated in LRRK2 function already or in PD by GWAS studies (as discussed in Chapter 3). Therefore the LRRK2 suppressor / enhancer screen successfully identified LRRK2 pathways we are confident will be relevant to LRRK2 biology and its role in PD pathogenesis.

The relationship between LRRK2 and WAVE-2 found specifically in myeloid cells is consistent with the gain-of-function hypothesis of dominant LRRK2-G2019S mutations. We demonstrate a contrasting effect on WAVE-2 levels between LRRK2 null and G2019S KI animals. Additionally, resulting alterations in WAVE-2 correlates well with observed changes in phagocytic activity in LRRK2 null and G2019S KI mice. We provide *in vitro* evidence that these two proteins, known to be active at membranes, bind, and furthermore that WAVE-2 is a substrate of LRRK2. While a challenge to show directly, we endeavored to deliver evidence that neuronal engulfment is increased in G2019S microglia. In a proof of concept study, we demonstrate that lifespan and locomotor deficits can be produced in flies expressing LRRK2 only in the 'microglia-like' ensheathing cells. Lastly, we show that these lifespan deficits and potentially the locomotor deficits may be rescued by SCAR down-regulation.

5.2 - Future Directions – DJ-1 mice:

Attempts have been made in the lab to further characterize the DJ1-C57 null mice. We have preliminary data in collaboration with the LE Trudeau lab at the University of Montreal that 18 months old DJ-1 null mice have dopamine release deficits (unpublished). Importantly, this was data that averaged all DJ-1 null mice in a cohort with WT littermates regardless of any potential penetrance of the early-onset unilateral degeneration. Future work with these mice will examine if any potential PD therapeutics such as the Ca^{2+} channel blocker, isradipine, may confer neuroprotection to prevent the overall loss of nigral neurons in aged DJ-1 mice. There also remains a question as to why the C57-Bl6 background confers susceptibility in our mice. The C57-Bl6/J sub-strain of mice have been noted to be a more consistent strain for MPTP studies, possibly due to its inherent loss of function truncation in the mitochondrial enzyme nicotinamide nucleotide transhydrogenase (Nnt) (Ronchi et al., 2013). However, we tested our mice, which were the sub-strain C57-Bl6/N, and none of our mice had the Nnt truncation. Future studies will utilize whole exome and genome sequencing to further narrow down candidate genes that contribute to the penetrance of these mice.

5.3 - Future Directions – LRRK2 fly screen:

It is important to note that while we have uncovered some compelling functional interacting candidates for LRRK2, the eye screen may have missed potential genetic interactors for multiple reasons. Firstly, the primary deficiencies leave flies with only one copy of dozens of genes on a chromosome. For some genes, this may not result in any change in protein level in the cell and any potential interaction with LRRK2 may be left unobserved. Secondly, there could be multiple genetic interactions in one deficiency that

causes both suppression and enhancement of LRRK2 induced toxicity. In other words, there could be a potential "cancelling" out of phenotypes, again leaving any modification of the eye phenotype unobserved. Lastly, the deficiency kit cannot be used for genes that are lethal when haploinsufficient. On the other hand, ectopically expressing a large multi-domain protein like LRRK2 in another species may not ensure accurate folding of the protein and thus produce false negative results. We would expect these results to including proteins involved in protein turnover. However, cathepsin D and Hsc-70 were the only genes from our 36 interactors with a known pivotal role in protein quality control. The *Drosophila* field also lacks an understanding of the mechanism underlying loss of retinal pigmentation, bristle disruption or black lesions. A more complete understanding of the causes of the phenotype we examined would aide in understanding LRRK2s role in degeneration and the biological context of the genetic interactors found in the study.

5.4 - Future Directions – LRRK2, WAVE-2 & Phagocytosis:

We observed a striking cell specific change in WAVE-2 depending on the LRRK2 geneotype. Both macrophages and microglia were found to have similar changes in WAVE-2 levels depending on the status of LRRK2. However, we failed to examine other myeloid cells such as B-cells, T-cells, or dendritic cells. In fact, the particular role of infiltrating immune cells may have in our model or in PD remains unclear. There is a common notion that regard microglia as mostly glia that quarantine cells signalling engulfment to infiltrating phagocytes. If this is true, it could be that stochastic mechanisms where CNS infiltration by phagocytes like killer T cells at multiple points during ones lifetime may progressively destroy the SNc.

We demonstrated that WAVE-2 is a substrate of LRRK2. However, we failed to provide the phosphorylation site(s) where LRRK2 acts on WAVE-2. The Park lab has preliminary mass spectrometry data in collaboration with the L Trinkle-Mulcahy lab at the University of Ottawa suggesting that LRRK2 may phosphorylate WAVE-2 at multiple threonines (data not shown). More study is needed, however, once the phosphorylation site(s) are confirmed, studies will determine how the phosphorylation of WAVE-2 stabilizes its protein level and activation of the ARP2/3 complex.

There also still could be a role for LRRK2 in neurons. Much of the work in neurons has implicated LRRK2 in vesicular trafficking (as discussed in Chapter 1). Our LRRK2 genetic interactor SCAR is highly homologous to the WAVE family of proteins, however it also is similar (to a lesser degree) to the WASP and WASH family of proteins. The WASH family is interesting as it is involved in ARP2/3 activation for endocytosis associated with the retromer complex (Duleh and Welch, 2010). LRRK2 has already been implicated in retromer function by studies showing it genetically interacts with VPS35 in and RAB7L1 in flies (MacLeod et al., 2013; Linhart et al., 2014). Future studies may examine the relationship of the WASH complex and LRRK2 in regards to endocytosis and trafficking in neurons.

It is always hoped that by discovering the molecular and cellular pathways that contribute to the pathogenesis of PD, we can uncover new treatments or preventative therapies for this disorder. Recombinant parathyroid hormone (PTH)1-34 (aka teriparatide) is a market available drug used clinically to treat osteoporosis. Interestingly, it has been shown that PTH1-34 is a potent inhibitor of WAVE-2 expression (Uyama et al., 2013). Additionally, PTH1-34 administration has already been shown to promote

recovery using stroke models in mice (Wang et al., 2014b). Future studies could use this therapeutic to test if PTH1-34 decreases WAVE-2 expression in myeloid cells and could be used to curb the hyper-phagocytic activity of LRRK2-G2019S myeloid cells. This can be performed *in vivo* with the injection on pH-sensitive beads (as performed in Chapter 4). Additionally, G2019S over-expressing rats are hypersensitive to nigral injections of LPS (Moehle et al., 2015). PTH1-34 may be used to treat LRRK2-G2019S LPS treated rats as a potential therapeutic to curb DA cell death. To explore this mechanism in more detail, specific down-regulation of WAVE-2 by shRNA constructs should be performed in similar experiments as above. However, if WAVE-2 is indeed a down-stream substrate of LRRK2, then in the context of actin-polymerization, inhibiting WAVE-2 may have broad reaching and potentially negative effects on the cell. Therefore, a concerted and continued effort on developing LRRK2 kinase inhibitors that are specific, safe, and may enter the CNS would also be of interest in this model.

5.5 – DJ-1 vs LRRK2: A common thread?

Mutations in DJ-1 are one of the rarest causes of recessive JO-PD as LRRK2 mutations are the most commonly linked gene to dominant LO-PD and further implicated in iPD. While the field is still waiting for DJ-1 mutant carriers to come to autopsy, the pathology of LRRK2 pathogenic brains is highly heterogeneous. There is also a penetrance difference between DJ-1 and G2019S mutations. While there is an apparent complete penetrance of DJ-1 pathogenic recessive mutations linked to PD, the LRRK2 pathogenic mutations are diverse in penetrance leading some researchers to treat these mutations as strong risk variants as opposed to linked to disease. The question remains: is there one underlying common biological pathway that leads to both familial and sporadic

PD? Based on the evidence discussed in Chapter 1 of this dissertation, it seems there may be multiple cellular and molecular pathways that may lead to the loss of these seemingly vulnerable DA neurons of the SNc. The three recessive genes implicated in early onset PD: Parkin, PINK1, and DJ-1 have lead the majority of researchers to focus on mitochondrial quality control and oxidative stress. On the other hand, the majority of LRRK2 studies are focused on vesicular trafficking. There is potential that these pathways may share an interface in autophagy and lysosomal functioning. However, the difference in age-of-onset and overall lack of dominant Lewy body pathology in recessively-linked brains so far, leaves us to speculate a few ideas. Firstly, given the noted intrinsic vulnerability of SNc neurons, it is easy to see how many pathways that have potential to lead the cell to apoptotic programming could be invovled. It could be imagined that changes in mitochondrial and oxidative stress pathways may lead to robust damage leading to early onset PD. However, minor changes in vesicular trafficking (LRRK2, VPS35, and possibly SNCA) compounded with environmental insults may lead to a slower loss of SNc neurons leading to PD later in life.

There is a common thread that develops from the three studies presented in this dissertation. Upon examination of the potential genetic modifiers of the DJ1-C57 unilateral phenotype, variants in SIRPB1 segregate with the affected DJ1-C57 null mice. Both humans and mice have at least three highly similar SIRP genes. Interestingly, SIRPB1 protein is down-regulated in the SNc of PD patients (Licker et al., 2014). SIRPα in both humans and mice is implicated in phagocytosis (Gaikwad et al., 2009). SIRPα resides on the membrane of myeloid cells that binds to CD47 expressed on other cells, including neurons, leading to inhibition of neuronal phagocytosis. The failure of SIRPα –

CD47 binding will promote phagocytic engulfment (Matozaki et al., 2009). Taken together, the double mutation of SIRPB1 in affected DJ1-C57 null mice may cause a disruption of CD47 binding and promote engulfment of neurons. To support this, DJ-1 deficient microglia have been shown to have increased phagocytic activity, display hypersensitivity to dopamine, and produce increased pro-inflammatory cytokines (Trudler et al., 2013). Therefore, DJ-1 null mice may be at increased susceptibility to neuronal engulfment by microglia and variants in the SIRPB1 gene may exacerbate this by preventing CD47 mediated inhibition during neuronal-microglia crosstalk. The idea of microglia-mediated neuronal engulfment in neurodegenerative diseases is not new. Evidence has been demonstrated of microglia engulfing live neurons (Neher et al., 2011; Neniskyte et al., 2011; Fricker et al., 2012a; 2012b; Neher et al., 2013; Neniskyte and Brown, 2013). This has led to the term 'phagoptosis' to describe cell death caused by phagocytosis of live cells (Brown and Neher, 2014). A key concept to this may be that neurons may encounter sub-toxic insults that may initiate apoptotic programming. Signalling to microglia then follows to initiate corpse removal. However, sub-lethal insults to neurons may dissipate and apoptotic programming may be reversed. But, over-active microglia may initiate neuronal engulfment prior to these “don’t eat me signals” from the neuron (Brown and Neher, 2014). Experimentally, this could be tested by making use of SIRPα null mice that are prone to infection (Li et al., 2012). DJ-1 null mice could be crossed to SIRPα null mice to potentially exacerbate neural engulfment due to a lack of CD47-SIRPα binding. Another method to possibly avoid compensatory mechanisms during development, could be to use already variant mice (determined by sequencing) from the Park laboratory or using gene editing techniques like the CRISPR-

Cas9 to reproduce the candidate mutations in SIRPB1 as described (Rousseaux et al., 2012). We would hypothesize that the loss of DJ-1, which is suggested to increase microglia phagocytic activity, could cause a consistent loss of SNc neurons if SIRPα or SIRPB1 is ablated or mutated, respectively. This could also be performed in other genetic mouse models of PD, like the LRRK2-G2019S KI mice. Importantly, polymorphisms in both SIRPα and SIRPB1 may be implicated in sporadic PD as searchable on the PDgene.org database ($p<0.05$). The over-arching cellular pathway implicated in this dissertation implicates neuroinflammation, and more specifically phagocytosis, via over-active cytoskeletal restructuring in LRRK2-G2019S cells, or possibly lack of 'don't eat me signals' from neurons to microglia in DJ-1 null mice through variants in SIRPB1.

A major gap in this dissertation is that it implores analysis of release of neuroinflammatory-related neurotoxins from myeloid cells. The challenge to this lies in that phagocytic activity potentiates the release of pro-inflammatory cytokines and chemokines, which may further enhance phagocytic activity (García-García and Rosales, 2006). LRRK2 has been implicated in altered signalling of pro-inflammatory cytokines as discussed in Chapter 1. DJ-1 null astrocytes have been shown to release increased iNOS, COX2, and IL-6 after treatment with the TLR-4 agonist, LPS. To test if, neurotoxins released from microglia may be, at least partially, responsible for increased cell death in G2019S neuronal cells, primary co-cultures may be performed with midbrain mesencephalic cultures and primary microglia. The genotype of the neurons may remain WT as the genotype of the microglia may be either WT or G2019S. Furthermore, the microglia may be stimulated with LPS and added to the neurons directly, or the conditioned media may be added. These *in vitro* co-cultures may provide evidence as to

the contribution microglia have directly or through the release of pro-inflammatory cytokines, chemokines and iNOS. This could also be true for DJ-1 mice and co-cultures could be performed in a similar manner. However, both WAVE-2 and SIRPα seem to be directly involved in the mechanics of phagocytosis, and therefore demand further study in regard to cytoskeletal dynamics and neuron-microglia "do/don't eat me signals".

5.6 – Concluding remarks:

The hypothesis that neuroinflammatory mechanisms may underlie the cause of neurodegenerative disorders like PD remains a peripheral but consistent idea in the field. This is true especially now given LRRK2s association to Crohn's disease and leprosy. Also, it has long been thought that the CNS lacks its own lymphatic system, however there was a recent landmark study that discovered that the human brain may indeed have its own lymphatic system (Louveau et al., 2015). This finding needs to be reproduced, but if true, is another reason why neuroinflammation may play a more prominent role in neurodegeneration than previously thought. On the other hand, even if the immune system lacks a vital role in the pathogenesis of PD, evidence seems clear that the activation of microglia may exacerbate cell loss in the basal ganglia. In fact, preliminary work with B MacVicar at the University of British Columbia indicates that the microglia of the basal ganglia are in a more active state intrinsically than microglia in the cortex or hippocampus. The determination of their role in PD is expected to provide new avenues for understanding and therapeutics for this debilitating disease.

Appendix A: References

Aarsland D, Andersen K, Larsen JP, Lolk A, Kragh-Sørensen P (2003) Prevalence and characteristics of dementia in Parkinson disease: an 8-year prospective study. Arch Neurol 60:387–392.

Aarsland D, Andersen K, Larsen JP, Lolk A, Nielsen H, Kragh-Sørensen P (2001) Risk of dementia in Parkinson's disease: a community-based, prospective study. Neurology 56:730–736.

Aasly JO, Shi M, Sossi V, Stewart T, Johansen KK, Wszolek ZK, Uitti RJ, Hasegawa K, Yokoyama T, Zabetian CP, Kim HM, Leverenz JB, Ginghina C, Armaly J, Edwards KL, Snapinn KW, Stoessl AJ, Zhang J (2012) Cerebrospinal fluid amyloid β and tau in LRRK2 mutation carriers. Neurology 78:55–61.

Abbas N et al. (1999) A wide variety of mutations in the parkin gene are responsible for autosomal recessive parkinsonism in Europe. French Parkinson“s Disease Genetics Study Group and the European Consortium on Genetic Susceptibility in Parkinson”s Disease. Hum Mol Genet 8:567–574.

Adams RN, Murrill E, McCreery R, Blank L, Karolczak M (1972) 6-Hydroxydopamine, a new oxidation mechanism. Eur J Pharmacol 17:287–292.

Adams-Carr KL, Bestwick JP, Shribman S, Lees A, Schrag A, Noyce AJ (2015) Constipation preceding Parkinson's disease: a systematic review and meta-analysis. J Neurol Neurosurg Psychiatr:jnnp–2015–311680.

Alam ZI, Daniel SE, Lees AJ, Marsden DC, Jenner P, Halliwell B (1997) A generalised increase in protein carbonyls in the brain in Parkinson's but not incidental Lewy body disease. J Neurochem 69:1326–1329.

Alegre-Abarrategui J, Christian H, Lufino MMP, Mutihac R, Venda LL, Ansorge O, Wade-Martins R (2009) LRRK2 regulates autophagic activity and localizes to specific membrane microdomains in a novel human genomic reporter cellular model. Hum Mol Genet 18:4022–4034.

Aleyasin H, Rousseaux MWC, Marcogliese PC, Hewitt SJ, Irrcher I, Joselin AP, Parsanejad M, Kim RH, Rizzu P, Callaghan SM, Slack RS, Mak TW, Park DS (2010) DJ-1 protects the nigrostriatal axis from the neurotoxin MPTP by modulation of the AKT pathway. Proc Natl Acad Sci USA 107:3186–3191.

Ambermoon P, Carter A, Hall WD, Dissanayaka NNW, O'Sullivan JD (2011) Impulse control disorders in patients with Parkinson's disease receiving dopamine replacement therapy: evidence and implications for the addictions field. Addiction 106:283–293.

Andres-Mateos E, Mejias R, Sasaki M, Li X, Lin BM, Biskup S, Zhang L, Banerjee R, Thomas B, Yang L, Liu G, Beal MF, Huso DL, Dawson TM, Dawson VL (2009) Unexpected lack of hypersensitivity in LRRK2 knock-out mice to MPTP (1-methyl-4-phenyl-1,2,3,6-tetrahydropyridine). J Neurosci 29:15846–15850.

Andres-Mateos E, Perier C, Zhang L, Blanchard-Fillion B, Greco TM, Thomas B, Ko HS, Sasaki M, Ischiropoulos H, Przedborski S, Dawson TM, Dawson VL (2007) DJ-1 gene deletion reveals that DJ-1 is an atypical peroxiredoxin-like peroxidase. Proc Natl Acad Sci USA 104:14807–14812.

Anichtchik OV, Kaslin J, Peitsaro N, Scheinin M, Panula P (2004) Neurochemical and behavioural changes in zebrafish Danio rerio after systemic administration of 6-hydroxydopamine and 1-methyl-4-phenyl-1,2,3,6-tetrahydropyridine. J Neurochem

88:443–453.

Arena G, Valente EM. Mitochondria in Parkinson's. The Functions, Disease-Related Dysfunctions, and Therapeutic Targeting of Neuronal Mitochondria. 2015 Sep 21:339.

Ashley AK, Hinds AI, Hanneman WH, Tjalkens RB, Legare ME (2016) DJ-1 mutation decreases astroglial release of inflammatory mediators. Neurotoxicology 52:198–203.

Bailey RM, Covy JP, Melrose HL, Rousseau L, Watkinson R, Knight J, Miles S, Farrer MJ, Dickson DW, Giasson BI, Lewis J (2013) LRRK2 phosphorylates novel tau epitopes and promotes tauopathy. Acta Neuropathol 126:809–827.

Barbeau A, Roy M, Bernier G, Campanella G, Paris S (1987) Ecogenetics of Parkinson's disease: prevalence and environmental aspects in rural areas. Can J Neurol Sci 14:36–41.

Bardien S, Lesage S, Brice A, Carr J (2011) Genetic characteristics of leucine-rich repeat kinase 2 (LRRK2) associated Parkinson's disease. Parkinsonism Relat Disord 17:501–508.

Barrett JC et al. (2008) Genome-wide association defines more than 30 distinct susceptibility loci for Crohn's disease. Nat Genet 40:955–962.

Beckman KB, Ames BN (1998) The free radical theory of aging matures. Physiol Rev 78:547–581.

Bedford L, Hay D, Devoy A, Paine S, Powe DG, Seth R, Gray T, Topham I, Fone K, Rezvani N, Mee M, Soane T, Layfield R, Sheppard PW, Ebendal T, Usoskin D, Lowe J, Mayer RJ (2008) Depletion of 26S proteasomes in mouse brain neurons

causes neurodegeneration and Lewy-like inclusions resembling human pale bodies. J Neurosci 28:8189–8198.

Belluzzi E, Gonnelli A, Cirnaru M-D, Marte A, Plotegher N, Russo I, Civiero L, Cogo S, Carrion MP, Franchin C, Arrigoni G, Beltramini M, Bubacco L, Onofri F, Piccoli G, Greggio E (2016) LRRK2 phosphorylates pre-synaptic N-ethylmaleimide sensitive fusion (NSF) protein enhancing its ATPase activity and SNARE complex disassembling rate. Mol Neurodegener 11:1.

Benabid AL, Chabardès S, Seigneuret E (2005) Deep-brain stimulation in Parkinson's disease: long-term efficacy and safety - What happened this year? Curr Opin Neurol 18:623–630.

Bender A, Krishnan KJ, Morris CM, Taylor GA, Reeve AK, Perry RH, Jaros E, Hersheson JS, Betts J, Klopstock T, Taylor RW, Turnbull DM (2006) High levels of mitochondrial DNA deletions in substantia nigra neurons in aging and Parkinson disease. Nat Genet 38:515–517.

Berger Z, Smith KA, LaVoie MJ (2010) Membrane localization of LRRK2 is associated with increased formation of the highly active LRRK2 dimer and changes in its phosphorylation. Biochemistry 49:5511–5523.

Bing GY, Lu X, Zheng NY, Jin L, Floyd RA, Kim HC. Microglia mediated dopaminergic cell death in the substantia nigra: A new animal model for Parkinson's disease. InFree Radical Biology and Medicine 1998 Jan 1 (Vol. 25, pp. S44-S44). THE BOULEVARD, LANGFORD LANE, KIDLINGTON, OXFORD OX5 1GB, ENGLAND: PERGAMON-ELSEVIER SCIENCE LTD.

Biskup S, Moore DJ, Celsi F, Higashi S, West AB, Andrabi SA, Kurkinen K, Yu S-W,

Savitt JM, Waldvogel HJ, Faull RLM, Emson PC, Torp R, Ottersen OP, Dawson TM, Dawson VL (2006) Localization of LRRK2 to membranous and vesicular structures in mammalian brain. Ann Neurol 60:557–569.

Bjørnarå KA, Dietrichs E, Toft M (2015) Longitudinal assessment of probable rapid eye movement sleep behaviour disorder in Parkinson's disease. Eur J Neurol 22:1242–1244.

Blesa J, Trigo-Damas I, Quiroga-Varela A, Jackson-Lewis VR (2015) Oxidative stress and Parkinson's disease. Frontiers in Neuroanatomy 9:91.

Blonder LX, Slevin JT (2011) Emotional dysfunction in Parkinson's disease. Behav Neurol 24:201–217.

Boeve BF et al. (2007) Pathophysiology of REM sleep behaviour disorder and relevance to neurodegenerative disease. Brain 130:2770–2788.

Bonifacino JS, Hurley JH (2008) Retromer. Curr Opin Cell Biol 20:427–436.

Bonifati V, Rizzu P, Squitieri F, Krieger E, Vanacore N, van Swieten JC, Brice A, van Duijn CM, Oostra B, Meco G, Heutink P (2003) DJ-1(PARK7), a novel gene for autosomal recessive, early onset parkinsonism. Neurol Sci 24:159–160.

Bonini NM, Giasson BI (2005) Snaring the Function of α-Synuclein. Cell 123:359–361.

Bové J, Prou D, Perier C, Przedborski S (2005) Toxin-induced models of Parkinson's disease. Neurotherapeutics 2:484–494.

Braak H, Del Tredici K, Bratzke H, Hamm-Clement J, Sandmann-Keil D, Rüb U (2002) Staging of the intracerebral inclusion body pathology associated with idiopathic Parkinson's disease (preclinical and clinical stages). J Neurol 249 Suppl 3:III–1–5.

Braak H, Del Tredici K, Rüb U, de Vos RAI, Jansen Steur ENH, Braak E (2003a)

Staging of brain pathology related to sporadic Parkinson's disease. Neurobiol Aging 24:197–211.

Braak H, Rüb U, Gai WP, Del Tredici K (2003b) Idiopathic Parkinson's disease: possible routes by which vulnerable neuronal types may be subject to neuroinvasion by an unknown pathogen. J Neural Transm 110:517–536.

Brain C (2007) The burden of neurological diseases, disorders and injuries in Canada. Canadian Institute for Health Information

Brand MD, Affourtit C, Esteves TC, Green K, Lambert AJ, Miwa S, Pakay JL, Parker N (2004) Mitochondrial superoxide: production, biological effects, and activation of uncoupling proteins. Free Radic Biol Med 37:755–767.

Braungart E, Gerlach M, Riederer P, Baumeister R, Hoener MC (2004) Caenorhabditis elegans MPP+ model of Parkinson's disease for high-throughput drug screenings. Neurodegener Dis 1:175–183.

Bravo-San Pedro JM, Niso-Santano M, Gómez-Sánchez R, Pizarro-Estrella E, Aiastui-Pujana A, Gorostidi A, Climent V, Lopez de Maturana R, Sanchez-Pernaute R, Lopez de Munain A, Fuentes JM, González-Polo RA (2013) The LRRK2 G2019S mutant exacerbates basal autophagy through activation of the MEK/ERK pathway. Cell Mol Life Sci 70:121–136.

Bretaud S, Allen C, Ingham PW, Bandmann O (2007) p53-dependent neuronal cell death in a DJ-1-deficient zebrafish model of Parkinson's disease. J Neurochem 100:1626–1635.

Bretaud S, Lee S, Guo S (2004) Sensitivity of zebrafish to environmental toxins implicated in Parkinson's disease. Neurotoxicol Teratol 26:857–864.

Brown GC, Neher JJ (2014) Microglial phagocytosis of live neurons. Nat Rev Neurosci 15:209–216.

Brundin P, Barker RA, Parmar M (2010) Neural grafting in Parkinson's disease. In: Recent Advances in Parkinson'S Disease - Translational and Clinical Research, pp 265–294 Progress in Brain Research. Elsevier.

Cafferty P, Yu L, Long H, Rao Y (2006) Semaphorin-1a functions as a guidance receptor in the Drosophila visual system. J Neurosci 26:3999–4003.

Canet-Avilés RM, Wilson MA, Miller DW, Ahmad R, McLendon C, Bandyopadhyay S, Baptista MJ, Ringe D, Petsko GA, Cookson MR (2004) The Parkinson's disease protein DJ-1 is neuroprotective due to cysteine-sulfinic acid-driven mitochondrial localization. Proc Natl Acad Sci USA 101:9103–9108.

Cang C, Aranda K, Seo Y-J, Gasnier B, Ren D (2015) TMEM175 Is an Organelle K+ Channel Regulating Lysosomal Function. Cell 162:1101–1112.

Cappellano G, Carecchio M, Fleetwood T, Magistrelli L, Cantello R, Dianzani U, Comi C (2013) Immunity and inflammation in neurodegenerative diseases. Am J Neurodegener Dis 2:89–107.

Castano A, Herrera AJ, Cano J, Machado A (1998) Lipopolysaccharide Intranigral Injection Induces Inflammatory Reaction and Damage in Nigrostriatal Dopaminergic System. J Neurochem 70:1584–1592.

Cestra G, Toomre D, Chang S, De Camilli P (2005) The Abl/Arg substrate ArgBP2/nArgBP2 coordinates the function of multiple regulatory mechanisms converging on the actin cytoskeleton. Proc Natl Acad Sci USA 102:1731–1736.

Chandran JS, Lin X, Zapata A, Höke A, Shimoji M, Moore SO, Galloway MP, Laird FM,

Wong PC, Price DL, Bailey KR, Crawley JN, Shippenberg T, Cai H (2008) Progressive behavioral deficits in DJ-1-deficient mice are associated with normal nigrostriatal function. Neurobiol Dis 29:505–514.

Chartier-Harlin M-C et al. (2011) Translation Initiator EIF4G1 Mutations in Familial Parkinson Disease. The American Journal of Human Genetics 89:398–406.

Chartier-Harlin M-C, Kachergus J, Roumier C, Mouroux V, Douay X, Lincoln S, Levecque C, Larvor L, Andrieux J, Hulihan M, Waucquier N, Defebvre L, Amouyel P, Farrer M, Destée A (2004) α-synuclein locus duplication as a cause of familial Parkinson's disease. The Lancet 364:1167–1169.

Chaudhuri KR, Naidu Y (2008) Early Parkinson's disease and non-motor issues. J Neurol 255 Suppl 5:33–38.

Chen C-Y, Weng Y-H, Chien K-Y, Lin K-J, Yeh T-H, Cheng Y-P, Lu C-S, Wang H-L (2012) (G2019S) LRRK2 activates MKK4-JNK pathway and causes degeneration of SN dopaminergic neurons in a transgenic mouse model of PD. Cell Death Differ 19:1623–1633.

Chen, L, Cagniard B, Mathews T, Jones S, Koh HC, Ding Y, Carvey PM, Ling Z, Kang UJ, Zhuang X (2005) Age-dependent motor deficits and dopaminergic dysfunction in DJ-1 null mice. J Biol Chem 280:21418-21426.

Chen P, Chakraborty S, Mukhopadhyay S, Lee E, Paoliello MMB, Bowman AB, Aschner M (2015) Manganese homeostasis in the nervous system. J Neurochem 134:601–610.

Chen Z, Borek D, Padrick SB, Gomez TS, Metlagel Z, Ismail AM, Umetani J, Billadeau DD, Otwinowski Z, Rosen MK (2010) Structure and control of the actin regulatory WAVE complex. Nature 468:533–538.

Cherra SJ, Steer E, Gusdon AM, Kiselyov K, Chu CT (2013) Mutant LRRK2 elicits calcium imbalance and depletion of dendritic mitochondria in neurons. Am J Pathol 182:474–484.

Choi I, Kim B, Byun J-W, Baik SH, Huh YH, Kim J-H, Mook-Jung I, Song WK, Shin J-H, Seo H, Suh YH, Jou I, Park SM, Kang HC, Joe E-H (2015) LRRK2 G2019S mutation attenuates microglial motility by inhibiting focal adhesion kinase. Nat Commun 6:8255.

Choi J, Sullards MC, Olzmann JA, Rees HD, Weintraub ST, Bostwick DE, Gearing M, Levey AI, Chin L-S, Li L (2006) Oxidative damage of DJ-1 is linked to sporadic Parkinson and Alzheimer diseases. J Biol Chem 281:10816–10824.

Chuang C-L, Lu Y-N, Wang H-C, Chang H-Y (2014) Genetic dissection reveals that Akt is the critical kinase downstream of LRRK2 to phosphorylate and inhibit FOXO1, and promotes neuron survival. Hum Mol Genet 23:ddu281–ddu5658.

Cirnaru MD, Marte A, Belluzzi E, Russo I, Gabrielli M, Longo F, Arcuri L, Murru L, Bubacco L, Matteoli M, Fedele E, Sala C, Passafaro M, Morari M, Greggio E, Onofri F, Piccoli G (2014) LRRK2 kinase activity regulates synaptic vesicle trafficking and neurotransmitter release through modulation of LRRK2 macro-molecular complex. Front Mol Neurosci 7:49.

Clark LN, Afridi S, Mejia Santana H, Harris J, Louis ED, Cote LJ, Andrews H, Singleton A, Wavrant De-Vrieze F, Hardy J, Mayeux R, Fahn S, Waters C, Ford B, Frucht S, Ottman R, Marder K (2004) Analysis of an early-onset Parkinson's disease cohort for DJ-1 mutations. Mov Disord 19:796–800.

Clark LN, Wang Y, Karlins E, Saito L, Mejia-Santana H, Harris J, Louis ED, Cote LJ,

Andrews H, Fahn S, Waters C, Ford B, Frucht S, Ottman R, Marder K (2006) Frequency of LRRK2 mutations in early- and late-onset Parkinson disease. Neurology 67:1786–1791.

Cleeter MW, Cooper JM, Schapira AH (1992) Irreversible inhibition of mitochondrial complex I by 1-methyl-4-phenylpyridinium: evidence for free radical involvement. J Neurochem 58:786–789.

Coelln von R, Thomas B, Savitt JM, Lim K-L, Sasaki M, Hess EJ, Dawson VL, Dawson TM (2004) Loss of locus coeruleus neurons and reduced startle in parkin null mice. Proc Natl Acad Sci USA 101:10744–10749.

Cook C, Stetler C, Petrucelli L (2012) Disruption of protein quality control in Parkinson's disease. Cold Spring Harb Perspect Med 2:a009423–a009423.

Cookson MR (2010) The role of leucine-rich repeat kinase 2 (LRRK2) in Parkinson's disease. Nat Rev Neurosci 11:791–797.

Cookson MR (2012a) Cellular effects of LRRK2 mutations. Biochem Soc Trans 40:1070–1073.

Cookson MR (2012b) Evolution of Neurodegeneration. Current Biology 22:R753–R761.

Cooper Ja, Sagar Hj, Jordan N, Harvey Ns, Sullivan Ev (1991) Cognitive impairment in early, untreated Parkinson's disease and its relationship to motor disability. Brain 114:2095–2122.

Cooper O et al. (2012) Pharmacological rescue of mitochondrial deficits in iPSC-derived neural cells from patients with familial Parkinson's disease. Sci Transl Med 4:141ra90–141ra90.

Correia Guedes L, Ferreira JJ, Rosa MM, Coelho M, Bonifati V, Sampaio C (2010)

Worldwide frequency of G2019S LRRK2 mutation in Parkinson's disease: a systematic review. Parkinsonism Relat Disord 16:237–242.

Coulom H, Birman S (2004) Chronic exposure to rotenone models sporadic Parkinson's disease in Drosophila melanogaster. J Neurosci 24:10993–10998.

Cowherd M, Lee I (2015) Transcriptional Regulators are Upregulated in the Substantia Nigra of Parkinson's Disease Patients.

Credle JJ, Forcelli PA, Delannoy M, Oaks AW, Permaul E, Berry DL, Duka V, Wills J, Sidhu A (2015) α-Synuclein-mediated inhibition of ATF6 processing into COPII vesicles disrupts UPR signaling in Parkinson's disease. Neurobiol Dis 76:112–125.

Crocker SJ, Lamba WR, Smith PD, Callaghan SM, Slack RS, Anisman H, Park DS (2001) c-Jun mediates axotomy-induced dopamine neuron death in vivo. Proc Natl Acad Sci USA 98:13385–13390.

Crofts HS, Dalley JW, Collins P, Van Denderen JC, Everitt BJ, Robbins TW, Roberts AC (2001) Differential effects of 6-OHDA lesions of the frontal cortex and caudate nucleus on the ability to acquire an attentional set. Cereb Cortex 11:1015–1026.

Członkowska A, Kohutnicka M, Kurkowska-Jastrzębska I, Członkowski A (1996) Microglial Reaction in MPTP (1-methyl-4-phenyl-1,2,3,6-tetrahydropyridine) Induced Parkinson's Disease Mice Model. Neurodegeneration 5:137–143.

Daher JPL, Volpicelli-Daley LA, Blackburn JP, Moehle MS, West AB (2014) Abrogation of α-synuclein-mediated dopaminergic neurodegeneration in LRRK2-deficient rats. Proc Natl Acad Sci USA 111:9289–9294.

Dave KD et al. (2014) Phenotypic characterization of recessive gene knockout rat models of Parkinson's disease. Neurobiol Dis 70:190–203.

Dawson TM, Ko HS, Dawson VL (2010) Genetic animal models of Parkinson's disease. Neuron 66:646–661.

Dächsel JC, Nishioka K, Vilariño-Güell C, Lincoln SJ, Soto-Ortolaza AI, Kachergus J, Hinkle KM, Heckman MG, Jasinska-Myga B, Taylor JP, Dickson DW, Gibson RA, Hentati F, Ross OA, Farrer MJ (2010) Heterodimerization of Lrrk1-Lrrk2: Implications for LRRK2-associated Parkinson disease. Mech Ageing Dev 131:210–214.

de Carvalho Aguiar P, Sweadner KJ, Penniston JT, Zaremba J, Liu L, Caton M, Linazasoro G, Borg M, Tijssen MAJ, Bressman SB, Dobyns WB, Brashear A, Ozelius LJ (2004) Mutations in the Na+/K+-ATPase α3 Gene ATP1A3 Are Associated with Rapid-Onset Dystonia Parkinsonism. Neuron 43:169–175.

de Lau LM, Breteler MM (2006) Epidemiology of Parkinson's disease. The Lancet Neurology 5:525–535.

De Mena L, Coto E, Sánchez-Ferrero E, Ribacoba R, Guisasola LM, Salvador C, Blazquez M, Alvarez V (2009) Mutational screening of the mortalin gene (HSPA9) in Parkinson's disease. J Neural Transm 116:1289–1293.

Deleersnijder A, Gerard M, Debyser Z, Baekelandt V (2013) The remarkable conformational plasticity of alpha-synuclein: blessing or curse? Trends Mol Med 19:368–377.

Deng H, Dodson MW, Huang H, Guo M. The Parkinson's disease genes pink1 and parkin promote mitochondrial fission and/or inhibit fusion in Drosophila. Proceedings of the National Academy of Sciences. 2008 Sep 23;105(38):14503-8.

Dexter DT, Carter CJ, Wells FR, Javoy-Agid F, Agid Y, Lees A, Jenner P, Marsden CD

(1989) Basal lipid peroxidation in substantia nigra is increased in Parkinson's disease. J Neurochem 52:381–389.

Dickson DW (2012) Parkinson's disease and parkinsonism: neuropathology. Cold Spring Harb Perspect Med 2:a009258–a009258.

Dodson MW, Leung LK, Lone M, Lizzio MA, Guo M (2014) Novel ethyl methanesulfonate (EMS)-induced null alleles of the Drosophila homolog of LRRK2 reveal a crucial role in endolysosomal functions and autophagy in vivo. Dis Model Mech 7:1351–1363.

Dodson MW, Zhang T, Jiang C, Chen S, Guo M (2012) Roles of the Drosophila LRRK2 homolog in Rab7-dependent lysosomal positioning. Hum Mol Genet 21:1350–1363.

Doherty J, Logan MA, Taşdemir OE, Freeman MR (2009) Ensheathing glia function as phagocytes in the adult Drosophila brain. J Neurosci 29:4768–4781.

Doherty KM, Hardy J (2013) Parkin disease and the Lewy body conundrum. Mov Disord 28:702–704.

Doty RL, Deems DA, Stellar S (1988) Olfactory dysfunction in parkinsonism: a general deficit unrelated to neurologic signs, disease stage, or disease duration. Neurology 38:1237–1244.

Doucet JP, Nakabeppu Y, Bedard PJ, Hope BT, Nestler EJ, Jasmin BJ, Chen JS, Ladarola MJ, St Jean M, Wigle N, Blanchet P, Grondin R, Robertson GS (1996) Chronic Alterations in Dopaminergic Neurotransmission Produce a Persistent Elevation of ΔFosB-like Protein(s) in both the Rodent and Primate Striatum. European Journal of Neuroscience 8:365–381.

Duleh SN, Welch MD (2010) WASH and the Arp2/3 complex regulate endosome shape

and trafficking. Cytoskeleton (Hoboken) 67:193–206.

Edvardson S, Cinnamon Y, Ta-Shma A, Shaag A, Yim Y-I, Zenvirt S, Jalas C, Lesage S, Brice A, Taraboulos A, Kaestner KH, Greene LE, Elpeleg O (2012) A Deleterious Mutation in DNAJC6 Encoding the Neuronal-Specific Clathrin-Uncoating Co-Chaperone Auxilin, Is Associated with Juvenile Parkinsonism Wider C, ed. PLoS ONE 7:e36458.

Edwards L, Quigley EM, Hofman R, Pfeiffer RF (1993) Gastrointestinal symptoms in Parkinson disease: 18-month follow-up study. Mov Disord 8:83–86.

Ekstrand MI, Terzioglu M, Galter D, Zhu S, Hofstetter C, Lindqvist E, Thams S, Bergstrand A, Hansson FS, Trifunovic A, Hoffer B, Cullheim S, Mohammed AH, Olson L, Larsson N-G (2007) Progressive parkinsonism in mice with respiratory-chain-deficient dopamine neurons. Proc Natl Acad Sci USA 104:1325–1330.

Esposito G, Ana Clara F, Verstreken P (2012) Synaptic vesicle trafficking and Parkinson's disease Ferrús A, ed. Developmental Neurobiology 72:134–144.

Evans AH, Lees AJ (2004) Dopamine dysregulation syndrome in Parkinson's disease. Curr Opin Neurol 17:393–398.

Evans IR, Ghai PA, Urbančič V, Tan KL, Wood W. SCAR/WAVE-mediated processing of engulfed apoptotic corpses is essential for effective macrophage migration in Drosophila. Cell Death & Differentiation. 2013 May 1;20(5):709-20.

Farrer MJ, Stone JT, Lin C-H, Dächsel JC, Hulihan MM, Haugarvoll K, Ross OA, Wu R-M (2007) Lrrk2 G2385R is an ancestral risk factor for Parkinson's disease in Asia. Parkinsonism Relat Disord 13:89–92.

Fava VM, Manry J, Cobat A, Orlova M, Van Thuc N, Ba NN, Thai VH, Abel L, Alcaïs

A, Schurr E, Canadian Lrrk2 in Inflammation Team (CLINT) (2016) A Missense LRRK2 Variant Is a Risk Factor for Excessive Inflammatory Responses in Leprosy. Johnson C, ed. PLoS Negl Trop Dis 10:e0004412.

Feany MB, Bender WW (2000) A Drosophila model of Parkinson's disease. Nature 404:394–398.

Fehling C (1966) Treatment of Parkinson's syndrome with L-dopa. A double blind study. Acta Neurol Scand 42:367–372.

Ferreira JJ, Guedes LC, Rosa MM, Coelho M, van Doeselaar M, Schweiger D, Di Fonzo A, Oostra BA, Sampaio C, Bonifati V (2007) High prevalence of LRRK2 mutations in familial and sporadic Parkinson's disease in Portugal. Mov Disord 22:1194–1201.

Findley LJ (2007) The economic impact of Parkinson's disease. Parkinsonism Relat Disord 13:S8–S12.

Fioravanti E, Durá MA, Lascoux D, Micossi E, Franzetti B, McSweeney S (2008) Structure of the stress response protein DR1199 from Deinococcus radiodurans: a member of the DJ-1 superfamily. Biochemistry 47:11581–11589.

Flinn L, Mortiboys H, Volkmann K, Köster RW, Ingham PW, Bandmann O (2009) Complex I deficiency and dopaminergic neuronal cell loss in parkin-deficient zebrafish (Danio rerio). Brain 132:awp108–awp1623.

Forno LS, Alvord EC (1974) Depigmentation in the nerve cells of the substantia nigra and locus ceruleus in Parkinsonism. Adv Neurol 5:195–202.

Frank-Cannon TC, Tran T, Ruhn KA, Martinez TN, Hong J, Marvin M, Hartley M, Treviño I, O'Brien DE, Casey B, Goldberg MS, Tansey MG (2008) Parkin deficiency increases vulnerability to inflammation-related nigral degeneration. J Neurosci

28:10825–10834.

Fricker M, Neher JJ, Zhao J-W, Théry C, Tolkovsky AM, Brown GC (2012a) MFG-E8 mediates primary phagocytosis of viable neurons during neuroinflammation. J Neurosci 32:2657–2666.

Fricker M, Oliva-Martín MJ, Brown GC (2012b) Primary phagocytosis of viable neurons by microglia activated with LPS or Aβ is dependent on calreticulin/LRP phagocytic signalling. J Neuroinflammation 9:196.

Funayama M, Hasegawa K, Kowa H, Saito M, Tsuji S, Obata F (2002) A new locus for Parkinson's disease (PARK8) maps to chromosome 12p11.2-q13.1. Ann Neurol 51:296–301.

Funayama M, Hasegawa K, Ohta E, Kawashima N, Komiyama M, Kowa H, Tsuji S, Obata F (2005) An LRRK2 mutation as a cause for the parkinsonism in the original PARK8 family. Ann Neurol 57:918–921.

Funayama M, Li Y, Tomiyama H, Yoshino H, Imamichi Y, Yamamoto M, Murata M, Toda T, Mizuno Y, Hattori N (2007) Leucine-rich repeat kinase 2 G2385R variant is a risk factor for Parkinson disease in Asian population. Neuroreport 18:273–275.

Gaikwad S, Larionov S, Wang Y, Dannenberg H, Matozaki T, Monsonego A, Thal DR, Neumann H (2009) Signal regulatory protein-beta1: a microglial modulator of phagocytosis in Alzheimer's disease. Am J Pathol 175:2528–2539.

Gao X, Chen H, Schwarzschild MA, Ascherio A (2011) Use of ibuprofen and risk of Parkinson disease. Neurology 76:863–869.

Garcia-Miralles M, Coomaraswamy J, Häbig K, Herzig MC, Funk N, Gillardon F, Maisel M, Jucker M, Gasser T, Galter D, Biskup S (2015) No Dopamine Cell Loss or

Changes in Cytoskeleton Function in Transgenic Mice Expressing Physiological Levels of Wild Type or G2019S Mutant LRRK2 and in Human Fibroblasts Lewis P, ed. PLoS ONE 10:e0118947.

García-García E, Rosales C (2006) Adding Complexity to Phagocytic Signaling: Phagocytosis-Associated Cell Responses and Phagocytic Efficiency. In: Molecular Mechanisms of Phagocytosis, pp 58–71 Medical Intelligence Unit. Boston, MA: Springer US.

Gardet A, Benita Y, Li C, Sands BE, Ballester I, Stevens C, Korzenik JR, Rioux JD, Daly MJ, Xavier RJ, Podolsky DK (2010) LRRK2 is involved in the IFN-gamma response and host response to pathogens. J Immunol 185:5577–5585.

German DC, Liang CL, Manaye KF, Lane K, Sonsalla PK (2000) Pharmacological inactivation of the vesicular monoamine transporter can enhance 1-methyl-4-phenyl-1,2,3,6-tetrahydropyridine-induced neurodegeneration of midbrain dopaminergic neurons, but not locus coeruleus noradrenergic neurons. Neuroscience 101:1063–1069.

Gibrat C, Saint Pierre M, Bousquet M, Lévesque D, Rouillard C, Cicchetti F (2009) Differences between subacute and chronic MPTP mice models: investigation of dopaminergic neuronal degeneration and α-synuclein inclusions. J Neurochem 109:1469–1482.

Giesert F, Hofmann A, Bürger A, Zerle J, Kloos K, Hafen U, Ernst L, Zhang J, Vogt-Weisenhorn DM, Wurst W (2013) Expression analysis of Lrrk1, Lrrk2 and Lrrk2 splice variants in mice. PLoS ONE 8:e63778.

Gilsbach BK, Kortholt A (2014) Structural biology of the LRRK2 GTPase and kinase

domains: implications for regulation. Front Mol Neurosci 7:32.

Ginhoux F, Prinz M (2015) Origin of microglia: current concepts and past controversies. Cold Spring Harb Perspect Biol 7:a020537.

Gjerstad MD, Wentzel-Larsen T, Aarsland D, Larsen JP (2007) Insomnia in Parkinson's disease: frequency and progression over time. J Neurol Neurosurg Psychiatr 78:476–479.

Goetz CG (2011) The History of Parkinson's Disease: Early Clinical Descriptions and Neurological Therapies. Cold Spring Harb Perspect Med 1:a008862–a008862.

Goldberg MS, Pisani A, Haburcak M, Vortherms TA, Kitada T, Costa C, Tong Y, Martella G, Tscherter A, Martins A, Bernardi G, Roth BL, Pothos EN, Calabresi P, Shen J (2005) Nigrostriatal Dopaminergic Deficits and Hypokinesia Caused by Inactivation of the Familial Parkinsonism-Linked Gene DJ-1. Neuron 45:489–496.

Gonzalez-Reyes LE, Verbitsky M, Blesa J, Jackson-Lewis V, Paredes D, Tillack K, Phani S, Kramer ER, Przedborski S, Kottmann AH (2012) Sonic Hedgehog Maintains Cellular and Neurochemical Homeostasis in the Adult Nigrostriatal Circuit. Neuron 75:306–319.

Goodwin VA, Richards SH, Taylor RS, Taylor AH, Campbell JL (2008) The effectiveness of exercise interventions for people with Parkinson's disease: a systematic review and meta-analysis. Mov Disord 23:631–640.

Gómez-Suaga P, Rivero-Ríos P, Fdez E, Blanca Ramírez M, Ferrer I, Aiastui A, Lopez de Munain A, Hilfiker S (2014) LRRK2 delays degradative receptor trafficking by impeding late endosomal budding through decreasing Rab7 activity. Hum Mol Genet 23:6779–6796.

Graybiel AM (2000) The basal ganglia. Curr Biol 10:R509–R511.

Greenwood CE, Tatton WG, Seniuk NA, Biddle FG (1991) Increased dopamine synthesis in aging substantia nigra neurons. Neurobiol Aging 12:557–565.

Haehner A, Hummel T, Reichmann H (2011) Olfactory loss in Parkinson's disease. Parkinsons Dis 2011:450939–6.

Hague S, Rogaeva E, Hernandez D, Gulick C, Singleton A, Hanson M, Johnson J, Weiser R, Gallardo M, Ravina B, Gwinn-Hardy K, Crawley A, St George-Hyslop PH, Lang AE, Heutink P, Bonifati V, Hardy J, Singleton A (2003) Early-onset Parkinson's disease caused by a compound heterozygous DJ-1 mutation. Ann Neurol 54:271–274.

Hakimi M, Selvanantham T, Swinton E, Padmore RF, Tong Y, Kabbach G, Venderova K, Girardin SE, Bulman DE, Scherzer CR, LaVoie MJ, Gris D, Park DS, Angel JB, Shen J, Philpott DJ, Schlossmacher MG (2011) Parkinson's disease-linked LRRK2 is expressed in circulating and tissue immune cells and upregulated following recognition of microbial structures. J Neural Transm 118:795–808.

Halliday GM, Blumbergs PC, Cotton RG, Blessing WW, Geffen LB (1990) Loss of brainstem serotonin- and substance P-containing neurons in Parkinson's disease. Brain Res 510:104–107.

Hanafusa H, Ishikawa K, Kedashiro S, Saigo T, Iemura S-I, Natsume T, Komada M, Shibuya H, Nara A, Matsumoto K (2011) Leucine-rich repeat kinase LRRK1 regulates endosomal trafficking of the EGF receptor. Nat Commun 2:158.

Hauser DN, Hastings TG (2013) Mitochondrial dysfunction and oxidative stress in Parkinson's disease and monogenic parkinsonism. Neurobiol Dis 51:35–42.

Hayashi A, Ohnishi H, Okazawa H, Nakazawa S, Ikeda H, Motegi S-I, Aoki N, Kimura S, Mikuni M, Matozaki T (2004) Positive regulation of phagocytosis by SIRPbeta and its signaling mechanism in macrophages. J Biol Chem 279:29450–29460.

Häbig K, Gellhaar S, Heim B, Djuric V, Giesert F, Wurst W, Walter C, Hentrich T, Riess O, Bonin M (2013) LRRK2 guides the actin cytoskeleton at growth cones together with ARHGEF7 and Tropomyosin 4. Biochim Biophys Acta 1832:2352–2367.

Henchcliffe C, Beal MF (2008) Mitochondrial biology and oxidative stress in Parkinson disease pathogenesis. Nat Clin Pract Neurol 4:600–609.

Heutink P (2006) PINK-1 and DJ-1--new genes for autosomal recessive Parkinson's disease. J Neural Transm Suppl:215–219.

Hindle S, Afsari F, Stark M, Middleton CA, Evans GJO, Sweeney ST, Elliott CJH (2013) Dopaminergic expression of the Parkinsonian gene LRRK2-G2019S leads to non-autonomous visual neurodegeneration, accelerated by increased neural demands for energy. Hum Mol Genet 22:2129–2140.

Hinkle KM, Yue M, Behrouz B, Dächsel JC, Lincoln SJ, Bowles EE, Beevers JE, Dugger B, Winner B, Prots I, Kent CB, Nishioka K, Lin W-L, Dickson DW, Janus CJ, Farrer MJ, Melrose HL (2012) LRRK2 knockout mice have an intact dopaminergic system but display alterations in exploratory and motor co-ordination behaviors. Mol Neurodegener 7:25.

Hirsch EC, Vyas S, Hunot S (2012) Neuroinflammation in Parkinson's disease. Parkinsonism Relat Disord 18:S210–S212.

Ho CC-Y, Rideout HJ, Ribe E, Troy CM, Dauer WT (2009) The Parkinson disease protein leucine-rich repeat kinase 2 transduces death signals via Fas-associated

protein with death domain and caspase-8 in a cellular model of neurodegeneration. J Neurosci 29:1011–1016.

Hockey LN, Kilpatrick BS, Eden ER, Lin-Moshier Y, Brailoiu GC, Brailoiu E, Futter CE, Schapira AH, Marchant JS, Patel S (2015) Dysregulation of lysosomal morphology by pathogenic LRRK2 is corrected by TPC2 inhibition. J Cell Sci 128:232–238.

Hoehn MM, Yahr MD (1967) Parkinsonism: onset, progression and mortality. Neurology 17:427–442.

Hoozemans JJM, van Haastert ES, Eikelenboom P, de Vos RAI, Rozemuller JM, Scheper W (2007) Activation of the unfolded protein response in Parkinson's disease. Biochem Biophys Res Commun 354:707–711.

Hughes AJ, Daniel SE, Ben-Shlomo Y, Lees AJ (2002) The accuracy of diagnosis of parkinsonian syndromes in a specialist movement disorder service. Brain 125:861–870.

Hulihan MM, Ishihara-Paul L, Kachergus J, Warren L, Amouri R, Elango R, Prinjha RK, Upmanyu R, Kefi M, Zouari M, Sassi SB, Yahmed SB, Euch-Fayeche El G, Matthews PM, Middleton LT, Gibson RA, Hentati F, Farrer MJ (2008) LRRK2 Gly2019Ser penetrance in Arab-Berber patients from Tunisia: a case-control genetic study. Lancet Neurol 7:591–594.

Huse DM, Schulman K, Orsini L, Castelli Haley J, Kennedy S, Lenhart G (2005) Burden of illness in Parkinson's disease. Mov Disord 20:1449–1454.

Hwang WY, Fu Y, Reyon D, Maeder ML, Tsai SQ, Sander JD, Peterson RT, Yeh J-RJ, Joung JK (2013) Efficient genome editing in zebrafish using a CRISPR-Cas system.

Nat Biotechnol 31:227–229.

Iaccarino C, Crosio C, Vitale C, Sanna G, Carri MT, Barone P (2007) Apoptotic mechanisms in mutant LRRK2-mediated cell death. Hum Mol Genet 16:1319–1326.

Imai Y, Gehrke S, Wang H-Q, Takahashi R, Hasegawa K, Oota E, Lu B (2008) Phosphorylation of 4E-BP by LRRK2 affects the maintenance of dopaminergic neurons in Drosophila. EMBO J 27:2432–2443.

Imai Y, Kobayashi Y, Inoshita T, Meng H, Arano T, Uemura K, Asano T, Yoshimi K, Zhang C-L, Matsumoto G, Ohtsuka T, Kageyama R, Kiyonari H, Shioi G, Nukina N, Hattori N, Takahashi R (2015) The Parkinson's Disease-Associated Protein Kinase LRRK2 Modulates Notch Signaling through the Endosomal Pathway. Lim K-L, ed. PLoS Genet 11:e1005503.

Imai Y, Soda M, Takahashi R (2000) Parkin suppresses unfolded protein stress-induced cell death through its E3 ubiquitin-protein ligase activity. J Biol Chem 275:35661–35664.

Irrcher I et al. (2010) Loss of the Parkinson's disease-linked gene DJ-1 perturbs mitochondrial dynamics. Hum Mol Genet 19:3734–3746.

Ishikawa K, Nara A, Matsumoto K, Hanafusa H (2012) EGFR-dependent phosphorylation of leucine-rich repeat kinase LRRK1 is important for proper endosomal trafficking of EGFR. Mol Biol Cell 23:1294–1306.

Ishikawa S, Taira T, Niki T, Takahashi-Niki K, Maita C, Maita H, Ariga H, Iguchi-Ariga SMM (2009) Oxidative status of DJ-1-dependent activation of dopamine synthesis through interaction of tyrosine hydroxylase and 4-dihydroxy-L-phenylalanine (L-DOPA) decarboxylase with DJ-1. J Biol Chem 284:28832–28844.

Jankovic J (2008) Parkinson's disease: clinical features and diagnosis. J Neurol Neurosurg Psychiatr 79:368–376.

Jaramillo-Gómez J, Niño A, Arboleda H, Arboleda G (2015) Overexpression of DJ-1 protects against C2-ceramide-induced neuronal death through activation of the PI3K/AKT pathway and inhibition of autophagy. Neurosci Lett 603:71–76.

Jeong H-K, Jou I, Joe E-H (2010) Systemic LPS administration induces brain inflammation but not dopaminergic neuronal death in the substantia nigra. Exp Mol Med 42:823–832.

Joselin AP, Hewitt SJ, Callaghan SM, Kim RH, Chung Y-H, Mak TW, Shen J, Slack RS, Park DS (2012) ROS-dependent regulation of Parkin and DJ-1 localization during oxidative stress in neurons. Hum Mol Genet 21:4888–4903.

Kachergus J, Mata IF, Hulihan M, Taylor JP, Lincoln S, Aasly J, Gibson JM, Ross OA, Lynch T, Wiley J, Payami H, Nutt J, Maraganore DM, Czyzewski K, Styczynska M, Wszolek ZK, Farrer MJ, Toft M (2005) Identification of a novel LRRK2 mutation linked to autosomal dominant parkinsonism: evidence of a common founder across European populations. Am J Hum Genet 76:672–680.

Kanao T, Venderova K, Park DS, Unterman T, Lu B, Imai Y (2010) Activation of FoxO by LRRK2 induces expression of proapoptotic proteins and alters survival of postmitotic dopaminergic neuron in Drosophila. Hum Mol Genet 19:3747–3758.

Kaul SC, Deocaris CC, Wadhwa R (2007) Three faces of mortalin: A housekeeper, guardian and killer. Experimental Gerontology 42:263–274.

Kedashiro S, Pastuhov SI, Nishioka T, Watanabe T, Kaibuchi K, Matsumoto K, Hanafusa H (2015) LRRK1-phosphorylated CLIP-170 regulates EGFR trafficking by recruiting

p150Glued to microtubule plus ends. J Cell Sci 128:385–396.

Kheir WA, Gevrey J-C, Yamaguchi H, Isaac B, Cox D (2005) A WAVE2-Abi1 complex mediates CSF-1-induced F-actin-rich membrane protrusions and migration in macrophages. J Cell Sci 118:5369–5379.

Kim B, Yang M-S, Choi D, Kim J-H, Kim H-S, Seol W, Choi S, Jou I, Kim E-Y, Joe E-H (2012) Impaired inflammatory responses in murine Lrrk2-knockdown brain microglia. PLoS ONE 7:e34693.

Kim KS, Kim JS, Park J-Y, Suh YH, Jou I, Joe E-H, Park SM (2013) DJ-1 associates with lipid rafts by palmitoylation and regulates lipid rafts-dependent endocytosis in astrocytes. Hum Mol Genet 22:4805–4817.

Kim RH, Smith PD, Aleyasin H, Hayley S, Mount MP, Pownall S, Wakeham A, You-Ten AJ, Kalia SK, Horne P, Westaway D, Lozano AM, Anisman H, Park DS, Mak TW (2005) Hypersensitivity of DJ-1-deficient mice to 1-methyl-4-phenyl-1,2,3,6-tetrahydropyrindine (MPTP) and oxidative stress. Proc Natl Acad Sci USA 102:5215–5220.

Kim WG, Mohney RP, Wilson B (2000) Regional difference in susceptibility to lipopolysaccharide-induced neurotoxicity in the rat brain: role of microglia. The Journal of ….

Kirik D, Rosenblad C, Burger C, Lundberg C, Johansen TE, Muzyczka N, Mandel RJ, Björklund A (2002) Parkinson-like neurodegeneration induced by targeted overexpression of alpha-synuclein in the nigrostriatal system. J Neurosci 22:2780–2791.

Kitada T, Asakawa S, Hattori N, Matsumine H, Yamamura Y, Minoshima S, Yokochi M,

Mizuno Y, Shimizu N (1998) Mutations in the parkin gene cause autosomal recessive juvenile parkinsonism. Nature 392:605–608.

Kitada T, Tomlinson JJ, Ao HS, Grimes DA, Schlossmacher MG (2012) Considerations regarding the etiology and future treatment of autosomal recessive versus idiopathic Parkinson disease. Curr Treat Options Neurol 14:230–240.

Kitada T, Tong Y, Gautier CA, Shen J (2009) Absence of nigral degeneration in aged parkin/DJ-1/PINK1 triple knockout mice. J Neurochem 111:696–702.

Kitamura Y, Shibagaki K, Takata K, Tsuchiya D, Taniguchi T, Gebicke-Haerter PJ, Miki H, Takenawa T, Shimohama S (2003) Involvement of Wiskott-Aldrich syndrome protein family verprolin-homologous protein (WAVE) and Rac1 in the phagocytosis of amyloid-beta(1-42) in rat microglia. J Pharmacol Sci 92:115–123.

Klein C, Westenberger A (2012) Genetics of Parkinson's disease. Cold Spring Harb Perspect Med 2:a008888–a008888.

Ko HS, Lee Y, Shin J-H, Karuppagounder SS, Gadad BS, Koleske AJ, Pletnikova O, Troncoso JC, Dawson VL, Dawson TM (2010) Phosphorylation by the c-Abl protein tyrosine kinase inhibits parkin's ubiquitination and protective function. Proc Natl Acad Sci USA 107:16691–16696.

Koenigsknecht J, Landreth G (2004) Microglial phagocytosis of fibrillar beta-amyloid through a beta1 integrin-dependent mechanism. J Neurosci 24:9838–9846.

Kordower JH, Chu Y, Hauser RA, Freeman TB, Olanow CW (2008) Lewy body-like pathology in long-term embryonic nigral transplants in Parkinson's disease. Nat Med 14:504–506.

Korolchuk VI, Schütz MM, Gómez-Llorente C, Rocha J, Lansu NR, Collins SM, Wairkar

YP, Robinson IM, O'Kane CJ (2007) Drosophila Vps35 function is necessary for normal endocytic trafficking and actin cytoskeleton organisation. J Cell Sci 120:4367–4376.

Korvatska O, Strand NS, Berndt JD, Strovas T, Chen DH, Leverenz JB, Kiianitsa K, Mata IF, Karakoc E, Greenup JL, Bonkowski E. Altered splicing of ATP6AP2 causes X-linked parkinsonism with spasticity (XPDS). Human molecular genetics. 2013 Aug 15;22(16):3259-68.

Krause M, Gautreau A (2014) Steering cell migration: lamellipodium dynamics and the regulation of directional persistence. Nat Rev Mol Cell Biol 15:577–590.

Krebiehl G, Ruckerbauer S, Burbulla LF, Kieper N, Maurer B, Waak J, Wolburg H, Gizatullina Z, Gellerich FN, Woitalla D, Riess O, Kahle PJ, Proikas-Cezanne T, Kruger R (2010) Reduced Basal Autophagy and Impaired Mitochondrial Dynamics Due to Loss of Parkinson's Disease-Associated Protein DJ-1 Petrucelli L, ed. PLoS ONE 5:e9367.

Kumar A, Greggio E, Beilina A, Kaganovich A, Chan D, Taymans J-M, Wolozin B, Cookson MR (2010) The Parkinson's disease associated LRRK2 exhibits weaker in vitro phosphorylation of 4E-BP compared to autophosphorylation. PLoS ONE 5:e8730.

Kuzuhara S, Mori H, Izumiyama N, Yoshimura M, Ihara Y (1988) Lewy bodies are ubiquitinated. A light and electron microscopic immunocytochemical study. Acta Neuropathol 75:345–353.

Lakso M, Vartiainen S, Moilanen A-M, Sirviö J, Thomas JH, Nass R, Blakely RD, Wong G (2003) Dopaminergic neuronal loss and motor deficits in Caenorhabditis elegans

overexpressing human alpha-synuclein. J Neurochem 86:165–172.

Lang AE, Lozano AM (1998) Parkinson's disease. First of two parts. N Engl J Med 339:1044–1053.

Langston JW, Ballard P, Tetrud JW, Irwin I (1983) Chronic Parkinsonism in humans due to a product of meperidine-analog synthesis. Science 219:979–980.

Langston JW, Forno LS, Tetrud J, Reeves AG, Kaplan JA, Karluk D. Evidence of active nerve cell degeneration in the substantia nigra of humans years after 1-methyl-4-phenyl-1, 2, 3, 6-tetrahydropyridine exposure. Annals of neurology. 1999 Oct 1;46(4):598-605.

Lauterbach EC, Freeman A, Vogel RL (2003) Correlates of generalized anxiety and panic attacks in dystonia and Parkinson disease. Cogn Behav Neurol 16:225–233.

Law BMH, Spain VA, Leinster VHL, Chia R, Beilina A, Cho HJ, Taymans J-M, Urban MK, Sancho RM, Ramírez MB, Biskup S, Baekelandt V, Cai H, Cookson MR, Berwick DC, Harvey K (2014) A direct interaction between leucine-rich repeat kinase 2 and specific β-tubulin isoforms regulates tubulin acetylation. J Biol Chem 289:895–908.

Lee BD, Shin J-H, VanKampen J, Petrucelli L, West AB, Ko HS, Lee Y-I, Maguire-Zeiss KA, Bowers WJ, Federoff HJ, Dawson VL, Dawson TM (2010) Inhibitors of leucine-rich repeat kinase-2 protect against models of Parkinson's disease. Nat Med 16:998–1000.

Lee D-W, Wu X, Eisenberg E, Greene LE (2006) Recruitment dynamics of GAK and auxilin to clathrin-coated pits during endocytosis. J Cell Sci 119:3502–3512.

Lee J-W, Tapias V, Di Maio R, Greenamyre JT, Cannon JR (2015) Behavioral,

neurochemical, and pathologic alterations in bacterial artificial chromosome transgenic G2019S leucine-rich repeated kinase 2 rats. Neurobiol Aging 36:505–518.

Lee Y, Dawson VL, Dawson TM (2012) Animal models of Parkinson's disease: vertebrate genetics. Cold Spring Harb Perspect Med 2.

Lesage S, Leutenegger AL, Ibanez P, Janin S, Lohmann E, Dürr A, Brice A, French Parkinson's Disease Genetics Study Group. LRRK2 haplotype analyses in European and North African families with Parkinson disease: a common founder for the G2019S mutation dating from the 13th century. The American Journal of Human Genetics. 2005 Aug 31;77(2):330-2.

Li HM, Niki T, Taira T, Iguchi-Ariga SMM, Ariga H (2005) Association of DJ-1 with chaperones and enhanced association and colocalization with mitochondrial Hsp70 by oxidative stress. Free Radic Res 39:1091–1099.

Li L-X, Atif SM, Schmiel SE, Lee S-J, McSorley SJ (2012) Increased susceptibility to Salmonella infection in signal regulatory protein α-deficient mice. J Immunol 189:2537–2544.

Li N, Ragheb K, Lawler G, Sturgis J, Rajwa B, Melendez JA, Robinson JP (2003) Mitochondrial complex I inhibitor rotenone induces apoptosis through enhancing mitochondrial reactive oxygen species production. J Biol Chem 278:8516–8525.

Li X, Patel JC, Wang J, Avshalumov MV, Nicholson C, Buxbaum JD, Elder GA, Rice ME, Yue Z (2010) Enhanced striatal dopamine transmission and motor performance with LRRK2 overexpression in mice is eliminated by familial Parkinson's disease mutation G2019S. J Neurosci 30:1788–1797.

Li Y, Liu W, Oo TF, Wang L, Tang Y, Jackson-Lewis V, Zhou C, Geghman K,

Bogdanov M, Przedborski S, Beal MF, Burke RE, Li C (2009) Mutant LRRK2(R1441G) BAC transgenic mice recapitulate cardinal features of Parkinson's disease. Nat Neurosci 12:826–828.

Licker V, Turck N, Kövari E, Burkhardt K, Côte M, Surini Demiri M, Lobrinus JA, Sanchez JC, Burkhard PR (2014) Proteomic analysis of human substantia nigra identifies novel candidates involved in Parkinson's disease pathogenesis. Proteomics 14:784–794.

Lill CM et al. (2012) Comprehensive research synopsis and systematic meta-analyses in Parkinson's disease genetics: The PDGene database. PLoS Genet 8:e1002548.

Lill CM, Hansen J, Olsen JH, Binder H, Ritz B, Bertram L (2015) Impact of Parkinson's disease risk loci on age at onset. Mov Disord 30:847–850.

Lin C-H, Tsai P-I, Wu R-M, Chien C-T (2010) LRRK2 G2019S mutation induces dendrite degeneration through mislocalization and phosphorylation of tau by recruiting autoactivated GSK3ß. J Neurosci 30:13138–13149.

Lin MT, Beal MF (2006) Mitochondrial dysfunction and oxidative stress in neurodegenerative diseases. Nature 443:787–795.

Linhart R, Wong SA, Cao J, Tran M, Huynh A, Ardrey C, Park JM, Hsu C, Taha S, Peterson R, Shea S. Vacuolar protein sorting 35 (Vps35) rescues locomotor deficits and shortened lifespan in Drosophila expressing a Parkinson's disease mutant of Leucine-rich repeat kinase 2 (LRRK2). Mol Neurodegener. 2014 Jun 11;9:23.

Liu G-H et al. (2012) Progressive degeneration of human neural stem cells caused by pathogenic LRRK2. Nature 491:603–607.

Liu M, Bing G (2011) Lipopolysaccharide Animal Models for Parkinson's Disease.

Parkinsons Dis 2011:1–7.

Liu X, Cheng R, Verbitsky M, Kisselev S, Browne A, Mejia-Sanatana H, Louis ED, Cote LJ, Andrews H, Waters C, Ford B, Frucht S, Fahn S, Marder K, Clark LN, Lee JH (2011a) Genome-wide association study identifies candidate genes for Parkinson's disease in an Ashkenazi Jewish population. BMC Med Genet 12:104.

Liu Z, Lee J, Krummey S, Lu W, Cai H, Lenardo MJ (2011b) The kinase LRRK2 is a regulator of the transcription factor NFAT that modulates the severity of inflammatory bowel disease. Nat Immunol 12:1063–1070.

Liu Z, Wang X, Yu Y, Li X, Wang T, Jiang H, Ren Q, Jiao Y, Sawa A, Moran T, Ross CA, Montell C, Smith WW (2008) A Drosophila model for LRRK2-linked parkinsonism. Proc Natl Acad Sci USA 105:2693–2698.

Louveau A, Smirnov I, Keyes TJ, Eccles JD, Rouhani SJ, Peske JD, Derecki NC, Castle D, Mandell JW, Lee KS, Harris TH, Kipnis J (2015) Structural and functional features of central nervous system lymphatic vessels. Nature 523:337–341.

Lucin KM, O'Brien CE, Bieri G, Czirr E, Mosher KI, Abbey RJ, Mastroeni DF, Rogers J, Spencer B, Masliah E, Wyss-Coray T (2013) Microglial beclin 1 regulates retromer trafficking and phagocytosis and is impaired in Alzheimer's disease. Neuron 79:873–886.

Luk KC, Kehm V, Carroll J, Bin Zhang, O'Brien P, Trojanowski JQ, Lee VM-Y (2012) Pathological α-Synuclein Transmission Initiates Parkinson-like Neurodegeneration in Nontransgenic Mice. Science 338:949–953.

Lücking CB et al. (2000) Association between Early-Onset Parkinson's Disease and Mutations in the ParkinGene. N Engl J Med 342:1560–1567.

Ma K-H, Huang W-S, Chen C-H, Lin S-Z, Wey S-P, Ting G, Wang S-D, Liu H-W, Liu J-C (2002) Dual SPECT of dopamine system using [99mTc]TRODAT-1 and [123I]IBZM in normal and 6-OHDA-lesioned formosan rock monkeys. Nuclear Medicine and Biology 29:561–567.

MacLeod D, Dowman J, Hammond R, Leete T, Inoue K, Abeliovich A (2006) The familial Parkinsonism gene LRRK2 regulates neurite process morphology. Neuron 52:587–593.

MacLeod DA, Rhinn H, Kuwahara T, Zolin A, Di Paolo G, McCabe BD, MacCabe BD, Marder KS, Honig LS, Clark LN, Small SA, Abeliovich A (2013) RAB7L1 interacts with LRRK2 to modify intraneuronal protein sorting and Parkinson's disease risk. Neuron 77:425–439.

Maekawa T, Mori S, Sasaki Y, Miyajima T, Azuma S, Ohta E, Obata F (2012) The I2020T Leucine-rich repeat kinase 2 transgenic mouse exhibits impaired locomotive ability accompanied by dopaminergic neuron abnormalities. Mol Neurodegener 7:15.

Mandel RJ, Randall PK (1985) Quantification of lesion-induced dopaminergic supersensitivity using the rotational model in the house. Brain Res 330:358–363.

Mann VM, Cooper JM, Daniel SE, Srai K, Jenner P, Marsden CD, Schapira AH (1994) Complex I, iron, and ferritin in Parkinson's disease substantia nigra. Ann Neurol 36:876–881.

Manning-Boğ AB, Caudle WM, Perez XA, Reaney SH, Paletzki R, Isla MZ, Chou VP, McCormack AL, Miller GW, Langston JW, Gerfen CR, DiMonte DA (2007) Increased vulnerability of nigrostriatal terminals in DJ-1-deficient mice is mediated by the dopamine transporter. Neurobiol Dis 27:141–150.

Manzoni C, Mamais A, Dihanich S, Abeti R, Soutar MPM, Plun-Favreau H, Giunti P, Tooze SA, Bandopadhyay R, Lewis PA (2013) Inhibition of LRRK2 kinase activity stimulates macroautophagy. Biochim Biophys Acta 1833:2900–2910.

Mao Z, Davis RL. Eight different types of dopaminergic neurons innervate the Drosophila mushroom body neuropil: anatomical and physiological heterogeneity. Frontiers in neural circuits. 2009 Jul 1;3:5.

Marcinek P, Jha AN, Shinde V, Sundaramoorthy A, Rajkumar R, Suryadevara NC, Neela SK, van Tong H, Balachander V, Valluri VL, Thangaraj K, Velavan TP (2013) LRRK2 and RIPK2 variants in the NOD 2-mediated signaling pathway are associated with susceptibility to Mycobacterium leprae in Indian populations. PLoS ONE 8:e73103.

Marconi R, Landi A, Valzania F (2008) Subthalamic nucleus stimulation in Parkinson's disease. Neurol Sci 29 Suppl 5:S389–S391.

Marín I, van Egmond WN, van Haastert PJM (2008) The Roco protein family: a functional perspective. FASEB J 22:3103–3110.

Marker DF, Puccini JM, Mockus TE, Barbieri J, Lu S-M, Gelbard HA (2012) LRRK2 kinase inhibition prevents pathological microglial phagocytosis in response to HIV-1 Tat protein. J Neuroinflammation 9:261.

Marks WJ et al. (2010) Gene delivery of AAV2-neurturin for Parkinson's disease: a double-blind, randomised, controlled trial. Lancet Neurol 9:1164–1172.

Martin I, Kim JW, Lee BD, Kang HC, Xu J-C, Jia H, Stankowski J, Kim M-S, Zhong J, Kumar M, Andrabi SA, Xiong Y, Dickson DW, Wszolek ZK, Pandey A, Dawson TM, Dawson VL (2014) Ribosomal Protein s15 Phosphorylation Mediates LRRK2

Neurodegeneration in Parkinson's Disease. Cell 157:472–485.

Mata IF, Wedemeyer WJ, Farrer MJ, Taylor JP, Gallo KA (2006) LRRK2 in Parkinson's disease: protein domains and functional insights. Trends Neurosci 29:286–293.

Matozaki T, Murata Y, Okazawa H, Ohnishi H (2009) Functions and molecular mechanisms of the CD47-SIRPalpha signalling pathway. Trends Cell Biol 19:72–80.

Matta S et al. (2012) LRRK2 controls an EndoA phosphorylation cycle in synaptic endocytosis. Neuron 75:1008–1021.

McGeer PL, Itagaki S, Boyes BE, McGeer EG (1988) Reactive microglia are positive for HLA-DR in the substantia nigra of Parkinson"s and Alzheimer"s disease brains. Neurology 38:1285–1285.

Meixner A, Boldt K, Van Troys M, Askenazi M, Gloeckner CJ, Bauer M, Marto JA, Ampe C, Kinkl N, Ueffing M (2011) A QUICK screen for Lrrk2 interaction partners--leucine-rich repeat kinase 2 is involved in actin cytoskeleton dynamics. Mol Cell Proteomics 10:M110.001172.

Melrose HL et al. (2010) Impaired dopaminergic neurotransmission and microtubule-associated protein tau alterations in human LRRK2 transgenic mice. Neurobiol Dis 40:503–517.

Menzies FM, Yenisetti SC, Min K-T (2005) Roles of Drosophila DJ-1 in Survival of Dopaminergic Neurons and Oxidative Stress. Current Biology 15:1578–1582.

Mercuri NB, Bernardi G (2005) The 'magic' of L-dopa: why is it the gold standard Parkinson's disease therapy? Trends Pharmacol Sci 26:341–344.

Migheli R, Del Giudice MG, Spissu Y, Sanna G, Xiong Y, Dawson TM, Dawson VL, Galioto M, Rocchitta G, Biosa A, Serra PA, Carri MT, Crosio C, Iaccarino C (2013)

LRRK2 affects vesicle trafficking, neurotransmitter extracellular level and membrane receptor localization. PLoS ONE 8:e77198.

Miller DW, Ahmad R, Hague S, Baptista MJ, Canet-Aviles R, McLendon C, Carter DM, Zhu P-P, Stadler J, Chandran J, Klinefelter GR, Blackstone C, Cookson MR (2003) L166P mutant DJ-1, causative for recessive Parkinson's disease, is degraded through the ubiquitin-proteasome system. J Biol Chem 278:36588–36595.

Miller KG (2002) Extending the Arp2/3 complex and its regulation beyond the leading edge. J Cell Biol 156:591–593.

Mitsui J et al. (2013) Mutations in COQ2 in familial and sporadic multiple-system atrophy the multiple-system atrophy research collaboration. N Engl J Med 369:233–244.

Mitsumoto A, Nakagawa Y, Takeuchi A, Okawa K, Iwamatsu A, Takanezawa Y (2009) Oxidized forms of peroxiredoxins and DJ-1 on two-dimensional gels increased in response to sublethal levels of paraquat. Free Radic Res 35:301–310.

Mizuno Y, Ohta S, Tanaka M, Takamiya S, Suzuki K, Sato T, Oya H, Ozawa T, Kagawa Y (1989) Deficiencies in complex I subunits of the respiratory chain in Parkinson's disease. Biochem Biophys Res Commun 163:1450–1455.

Mizuno Y, Sone N, Saitoh T (1987) Effects of 1-methyl-4-phenyl-1,2,3,6-tetrahydropyridine and 1-methyl-4-phenylpyridinium ion on activities of the enzymes in the electron transport system in mouse brain. J Neurochem 48:1787–1793.

Moehle MS, Daher JPL, Hull TD, Boddu R, Abdelmotilib HA, Mobley J, Kannarkat GT, Tansey MG, West AB (2015) The G2019S LRRK2 mutation increases myeloid cell chemotactic responses and enhances LRRK2 binding to actin-regulatory proteins.

Hum Mol Genet:ddv157.

Moehle MS, Webber PJ, Tse T, Sukar N, Standaert DG, DeSilva TM, Cowell RM, West AB (2012) LRRK2 inhibition attenuates microglial inflammatory responses. J Neurosci 32:1602–1611.

Moretto A, Colosio C (2013) The role of pesticide exposure in the genesis of Parkinson's disease: epidemiological studies and experimental data. Toxicology 307:24–34.

Mortiboys H, Johansen KK, Aasly JO, Bandmann O (2010) Mitochondrial impairment in patients with Parkinson disease with the G2019S mutation in LRRK2. Neurology 75:2017–2020.

Mortiboys H, Thomas KJ, Koopman WJH, Klaffke S, Abou-Sleiman P, Olpin S, Wood NW, Willems PHGM, Smeitink JAM, Cookson MR, Bandmann O (2008) Mitochondrial function and morphology are impaired in parkin-mutant fibroblasts. Ann Neurol 64:555–565.

Mount MP, Lira A, Grimes D, Smith PD, Faucher S, Slack R, Anisman H, Hayley S, Park DS (2007) Involvement of interferon-gamma in microglial-mediated loss of dopaminergic neurons. J Neurosci 27:3328–3337.

Mouret J (1975) Differences in sleep in patients with Parkinson's disease. Electroencephalogr Clin Neurophysiol 38:653–657.

Mullin S, Schapira A (2015) The genetics of Parkinson's disease. Br Med Bull 114:39–52.

Munsie LN, Milnerwood AJ, Seibler P, Beccano-Kelly DA, Tatarnikov I, Khinda J, Volta M, Kadgien C, Cao LP, Tapia L, Klein C, Farrer MJ (2015) Retromer-dependent neurotransmitter receptor trafficking to synapses is altered by the Parkinson's disease

VPS35 mutation p.D620N. Hum Mol Genet 24:1691–1703.

Muñoz P, Huenchuguala S, Paris I, Segura-Aguilar J (2012) Dopamine oxidation and autophagy. Parkinsons Dis 2012:920953–13.

Nagatsu T, Sawada M (2005) Inflammatory Process in Parkinson's Disease: Role for Cytokines. Curr Pharm Des 11:999–1016.

Nass R, Miller DM, Blakely RD (2001) C. elegans: a novel pharmacogenetic model to study Parkinson's disease. Parkinsonism Relat Disord 7:185–191.

Neher JJ, Emmrich JV, Fricker M, Mander PK, Théry C, Brown GC (2013) Phagocytosis executes delayed neuronal death after focal brain ischemia. Proc Natl Acad Sci USA 110:E4098–E4107.

Neher JJ, Neniskyte U, Zhao J-W, Bal-Price A, Tolkovsky AM, Brown GC (2011) Inhibition of microglial phagocytosis is sufficient to prevent inflammatory neuronal death. J Immunol 186:4973–4983.

Neniskyte U, Brown GC (2013) Lactadherin/MFG-E8 is essential for microglia-mediated neuronal loss and phagoptosis induced by amyloid β. J Neurochem 126:312–317.

Neniskyte U, Neher JJ, Brown GC (2011) Neuronal death induced by nanomolar amyloid β is mediated by primary phagocytosis of neurons by microglia. J Biol Chem 286:39904–39913.

Ng C-H, Guan MSH, Koh C, Ouyang X, Yu F, Tan E-K, O'Neill SP, Zhang X, Chung J, Lim K-L (2012) AMP kinase activation mitigates dopaminergic dysfunction and mitochondrial abnormalities in Drosophila models of Parkinson's disease. J Neurosci 32:14311–14317.

Ng C-H, Mok SZS, Koh C, Ouyang X, Fivaz ML, Tan E-K, Dawson VL, Dawson TM,

Yu F, Lim K-L (2009) Parkin protects against LRRK2 G2019S mutant-induced dopaminergic neurodegeneration in Drosophila. J Neurosci 29:11257–11262.

Nichols WC, Pankratz N, Hernandez D, Paisán-Ruiz C, Jain S, Halter CA, Michaels VE, Reed T, Rudolph A, Shults CW, Singleton A, Foroud T, Parkinson Study Group - PROGENI Investigators (2005) Genetic screening for a single common LRRK2 mutation in familial Parkinson's disease. Lancet 365:410–412.

Niu J, Yu M, Wang C, Xu Z (2012) Leucine-rich repeat kinase 2 disturbs mitochondrial dynamics via Dynamin-like protein. J Neurochem 122:650–658.

OBERG KE (1961) The site of the action of rotenone in the respiratory chain. Exp Cell Res 24:163–164.

Olzmann JA, Li L, Chudaev MV, Chen J, Perez FA, Palmiter RD, Chin L-S (2007) Parkin-mediated K63-linked polyubiquitination targets misfolded DJ-1 to aggresomes via binding to HDAC6. J Cell Biol 178:1025–1038.

Orenstein SJ, Kuo S-H, Tasset I, Arias E, Koga H, Fernandez-Carasa I, Cortes E, Honig LS, Dauer W, Consiglio A, Raya A, Sulzer D, Cuervo AM (2013) Interplay of LRRK2 with chaperone-mediated autophagy. Nat Neurosci 16:394–406.

Ouchi Y, Yoshikawa E, Sekine Y, Futatsubashi M, Kanno T, Ogusu T, Torizuka T (2005) Microglial activation and dopamine terminal loss in early Parkinson's disease. Ann Neurol 57:168–175.

Ozelius LJ, Senthil G, Saunders-Pullman R, Ohmann E, Deligtisch A, Tagliati M, Hunt AL, Klein C, Henick B, Hailpern SM, Lipton RB, Soto-Valencia J, Risch N, Bressman SB (2006) LRRK2 G2019S as a cause of Parkinson's disease in Ashkenazi Jews. N Engl J Med 354:424–425.

Pacelli C, Giguère N, Bourque M-J, Lévesque M, Slack RS, Trudeau L-É (2015) Elevated Mitochondrial Bioenergetics and Axonal Arborization Size Are Key Contributors to the Vulnerability of Dopamine Neurons. Curr Biol 25:2349–2360.

Pahwa R, Lyons KE, Roller WC (2003) Handbook of Parkinson's.

Paisán-Ruiz C (2009) LRRK2 gene variation and its contribution to Parkinson disease. Hum Mutat 30:1153–1160.

Paisán-Ruiz C et al. (2004) Cloning of the gene containing mutations that cause PARK8-linked Parkinson's disease. Neuron 44:595–600.

Paisán-Ruiz C, Bhatia KP, Li A, Hernandez D, Davis M, Wood NW, Hardy J, Houlden H, Singleton A, Schneider SA (2009) Characterization of PLA2G6 as a locus for dystonia-parkinsonism. Ann Neurol 65:19–23.

Papapetropoulos S, Singer C, Ross OA, Toft M, Johnson JL, Farrer MJ, Mash DC (2006) Clinical heterogeneity of the LRRK2 G2019S mutation. Arch Neurol 63:1242–1246.

Papkovskaia TD, Chau K-Y, Inesta-Vaquera F, Papkovsky DB, Healy DG, Nishio K, Staddon J, Duchen MR, Hardy J, Schapira AHV, Cooper JM (2012) G2019S leucine-rich repeat kinase 2 causes uncoupling protein-mediated mitochondrial depolarization. Hum Mol Genet 21:4201–4213.

Park J, Kim SY, Cha G-H, Lee SB, Kim S, Chung J (2005) Drosophila DJ-1 mutants show oxidative stress-sensitive locomotive dysfunction. Gene 361:133–139.

Park J, Lee SB, Lee S, Kim Y, Song S, Kim S, Bae E, Kim J, Shong M, Kim JM, Chung J (2006) Mitochondrial dysfunction in Drosophila PINK1 mutants is complemented by parkin. Nature 441:1157–1161.

Parkinson J (1817) Parkinson: The shaking palsy - Google Scholar. Sherwood.

Parkinson Study Group PRECEPT Investigators (2007) Mixed lineage kinase inhibitor CEP-1347 fails to delay disability in early Parkinson disease. Neurology 69:1480–1490.

Perl DP (2011) Neuropathologic Involvement of the Dopaminergic Neuronal Systems in Parkinson's Disease. Oxford, UK: Blackwell Publishing Ltd.

Pérez-Otaño I, Mandelzys A, Morgan JI (1998) MPTP-Parkinsonism is accompanied by persistent expression of a Δ-FosB-like protein in dopaminergic pathways. Molecular Brain Research 53:41–52.

Pham TT, Giesert F, Röthig A, Floss T, Kallnik M, Weindl K, Hölter SM, Ahting U, Prokisch H, Becker L, Klopstock T, Hrabé de Angelis M, Beyer K, Görner K, Kahle PJ, Vogt Weisenhorn DM, Wurst W (2010) DJ-1-deficient mice show less TH-positive neurons in the ventral tegmental area and exhibit non-motoric behavioural impairments. Genes Brain Behav 9:305–317.

Piccoli G et al. (2014) Leucine-rich repeat kinase 2 binds to neuronal vesicles through protein interactions mediated by its C-terminal WD40 domain. Mol Cell Biol 34:2147–2161.

Piccoli G, Condliffe SB, Bauer M, Giesert F, Boldt K, De Astis S, Meixner A, Sarioglu H, Vogt-Weisenhorn DM, Wurst W, Gloeckner CJ, Matteoli M, Sala C, Ueffing M (2011) LRRK2 controls synaptic vesicle storage and mobilization within the recycling pool. J Neurosci 31:2225–2237.

Plowey ED, Cherra SJ, Liu Y-J, Chu CT (2008) Role of autophagy in G2019S-LRRK2-associated neurite shortening in differentiated SH-SY5Y cells. J Neurochem 105:1048–1056.

Polymeropoulos MH et al. (1997) Mutation in the α-Synuclein Gene Identified in Families with Parkinson's Disease. Science 276:2045–2047.

Polymeropoulos MH, Higgins JJ, Golbe LI, Johnson WG, Ide SE, Di Iorio G, Sanges G, Stenroos ES, Pho LT, Schaffer AA, Lazzarini AM, Nussbaum RL, Duvoisin RC (1996) Mapping of a gene for Parkinson's disease to chromosome 4q21-q23. Science 274:1197–1199.

Postuma RB, Gagnon JF, Montplaisir J (2010) Clinical prediction of Parkinson's disease: planning for the age of neuroprotection. J Neurol Neurosurg Psychiatr 81:1008–1013.

Poulopoulos M, Cortes E, Vonsattel J-PG, Fahn S, Waters C, Cote LJ, Moskowitz C, Honig LS, Clark LN, Marder KS, Alcalay RN (2012) Clinical and pathological characteristics of LRRK2 G2019S patients with PD. J Mol Neurosci 47:139–143.

Pritzel M, Huston JP, Sarter M (1983) Behavioral and neuronal reorganization after unilateral substantia nigra lesions: Evidence for increased interhemispheric nigrostriatal projections. Neuroscience 9:879–888.

Przedborski S, Vila M (2003) The 1-methyl-4-phenyl-1,2,3,6-tetrahydropyridine mouse model: a tool to explore the pathogenesis of Parkinson's disease. Ann N Y Acad Sci 991:189–198.

Purisai MG, McCormack AL, Cumine S, Li J, Isla MZ, Di Monte DA (2007) Microglial activation as a priming event leading to paraquat-induced dopaminergic cell degeneration. Neurobiol Dis 25:392–400.

Qin L, Wu X, Block ML, Liu Y, Breese GR, Hong J-S, Knapp DJ, Crews FT (2007) Systemic LPS causes chronic neuroinflammation and progressive neurodegeneration. Glia 55:453–462.

Qu D, Hage A, Don-Carolis K, Huang E, Joselin A, Safarpour F, Marcogliese PC, Rousseaux MWC, Hewitt SJ, Huang T, Im D-S, Callaghan S, Dewar-Darch D, Figeys D, Slack RS, Park DS (2015) BAG2 Gene-mediated Regulation of PINK1 Protein Is Critical for Mitochondrial Translocation of PARKIN and Neuronal Survival. J Biol Chem 290:30441–30452.

Quadri M et al. (2013) Mutation in the SYNJ1 Gene Associated with Autosomal Recessive, Early-Onset Parkinsonism. Hum Mutat 34:1208–1215.

Raiborg C, Bache KG, Mehlum A, Stang E, Stenmark H (2001) Hrs recruits clathrin to early endosomes. EMBO J 20:5008–5021.

Ramirez A, Heimbach A, Gründemann J, Stiller B, Hampshire D, Cid LP, Goebel I, Mubaidin AF, Wriekat A-L, Roeper J, Al-Din A, Hillmer AM, Karsak M, Liss B, Woods CG, Behrens MI, Kubisch C (2006) Hereditary parkinsonism with dementia is caused by mutations in ATP13A2, encoding a lysosomal type 5 P-type ATPase. Nat Genet 38:1184–1191.

Ramonet D et al. (2011) Dopaminergic neuronal loss, reduced neurite complexity and autophagic abnormalities in transgenic mice expressing G2019S mutant LRRK2. PLoS ONE 6:e18568.

Ramsey CP, Tsika E, Ischiropoulos H, Giasson BI (2010) DJ-1 deficient mice demonstrate similar vulnerability to pathogenic Ala53Thr human alpha-syn toxicity. Hum Mol Genet 19:1425–1437.

Reijnders JSAM, Ehrt U, Weber WEJ, Aarsland D, Leentjens AFG (2008) A systematic review of prevalence studies of depression in Parkinson's disease. Mov Disord 23:183–9–quiz313.

Ren G, Xin S, Li S, Zhong H, Lin S (2011) Disruption of LRRK2 does not cause specific loss of dopaminergic neurons in zebrafish. PLoS ONE 6:e20630.

Rhodes SL, Sinsheimer JS, Bordelon Y, Bronstein JM, Ritz B (2011) Replication of GWAS Associations for GAK and MAPT in Parkinson's Disease. Ann Hum Genet 75:195–200.

Rivero-Ríos P, Gómez-Suaga P, Fernández B, Madero-Pérez J, Schwab AJ, Ebert AD, Hilfiker S (2015) Alterations in late endocytic trafficking related to the pathobiology of LRRK2-linked Parkinson's disease. Biochem Soc Trans 43:390–395.

Ronchi JA, Figueira TR, Ravagnani FG, Oliveira HCF, Vercesi AE, Castilho RF (2013) A spontaneous mutation in the nicotinamide nucleotide transhydrogenase gene of C57BL/6J mice results in mitochondrial redox abnormalities. Free Radic Biol Med 63:446–456.

Rosen GD, La Porte NT, Diechtiareff B, Pung CJ, Nissanov J, Gustafson C, Bertrand L, Gefen S, Fan Y, Tretiak OJ, Manly KF, Park MR, Williams AG, Connolly MT, Capra JA, Williams RW (2003) Informatics center for mouse genomics. Neuroinform 1:327–342.

Ross OA, Spanaki C, Griffith A, Lin C-H, Kachergus J, Haugarvoll K, Latsoudis H, Plaitakis A, Ferreira JJ, Sampaio C, Bonifati V, Wu R-M, Zabetian CP, Farrer MJ (2009) Haplotype analysis of Lrrk2 R1441H carriers with parkinsonism. Parkinsonism Relat Disord 15:466–467.

Rottner K, Hänisch J, Campellone KG (2010) WASH, WHAMM and JMY: regulation of Arp2/3 complex and beyond. Trends Cell Biol 20:650–661.

Rousseaux MWC, Marcogliese PC, Qu D, Hewitt SJ, Seang S, Kim RH, Slack RS,

Schlossmacher MG, Lagace DC, Mak TW, Park DS (2012) Progressive dopaminergic cell loss with unilateral-to-bilateral progression in a genetic model of Parkinson disease. Proc Natl Acad Sci USA 109:15918–15923.

Russo I, Berti G, Plotegher N, Bernardo G, Filograna R, Bubacco L, Greggio E (2015) Leucine-rich repeat kinase 2 positively regulates inflammation and down-regulates NF-κB p50 signaling in cultured microglia cells. J Neuroinflammation 12:230.

Ryu EJ, Harding HP, Angelastro JM, Vitolo OV, Ron D, Greene LA (2002) Endoplasmic reticulum stress and the unfolded protein response in cellular models of Parkinson's disease. J Neurosci 22:10690–10698.

Saha S, Guillily MD, Ferree A, Lanceta J, Chan D, Ghosh J, Hsu CH, Segal L, Raghavan K, Matsumoto K, Hisamoto N, Kuwahara T, Iwatsubo T, Moore L, Goldstein L, Cookson M, Wolozin B (2009) LRRK2 modulates vulnerability to mitochondrial dysfunction in Caenorhabditis elegans. J Neurosci 29:9210–9218.

Saha S, Liu-Yesucevitz L, Wolozin B (2014) Regulation of Autophagy by LRRK2 in Caenorhabditis elegans. Neurodegener Dis 13:110–113.

Samaranch L, Lorenzo-Betancor O, Arbelo JM, Ferrer I, Lorenzo E, Irigoyen J, Pastor MA, Marrero C, Isla C, Herrera-Henriquez J, Pastor P (2010) PINK1-linked parkinsonism is associated with Lewy body pathology. Brain 133:1128–1142.

Sanchez G, Varaschin RK, Büeler H, Marcogliese PC, Park DS, Trudeau L-É (2014) Unaltered Striatal Dopamine Release Levels in Young Parkin Knockout, Pink1 Knockout, DJ-1 Knockout and LRRK2 R1441G Transgenic Mice Cookson MR, ed. PLoS ONE 9:e94826.

Sang T-K, Chang H-Y, Lawless GM, Ratnaparkhi A, Mee L, Ackerson LC, Maidment

NT, Krantz DE, Jackson GR (2007) A Drosophila model of mutant human parkin-induced toxicity demonstrates selective loss of dopaminergic neurons and dependence on cellular dopamine. J Neurosci 27:981–992.

Sauer H, Oertel WH (1994) Progressive degeneration of nigrostriatal dopamine neurons following intrastriatal terminal lesions with 6-hydroxydopamine: A combined retrograde tracing and immunocytochemical study in the rat. Neuroscience 59:401–415.

Sánchez-Danés A, Richaud-Patin Y, Carballo-Carbajal I, Jiménez-Delgado S, Caig C, Mora S, Di Guglielmo C, Ezquerra M, Patel B, Giralt A, Canals JM, Memo M, Alberch J, López-Barneo J, Vila M, Cuervo AM, Tolosa E, Consiglio A, Raya A (2012) Disease-specific phenotypes in dopamine neurons from human iPS-based models of genetic and sporadic Parkinson's disease. EMBO Mol Med 4:380–395.

Scarffe LA, Stevens DA, Dawson VL, Dawson TM (2014) Parkin and PINK1: much more than mitophagy. Trends Neurosci 37:315–324.

Scatton B, Javoy-Agid F, Rouquier L, Dubois B, Agid Y (1983) Reduction of cortical dopamine, noradrenaline, serotonin and their metabolites in Parkinson's disease. Brain Res 275:321–328.

Schapansky J, Nardozzi JD, Felizia F, LaVoie MJ (2014) Membrane recruitment of endogenous LRRK2 precedes its potent regulation of autophagy. Hum Mol Genet 23:4201–4214.

Schapira AH, Cooper JM, Dexter D, Clark JB, Jenner P, Marsden CD (1990) Mitochondrial complex I deficiency in Parkinson's disease. J Neurochem 54:823–827.

Schapira AH, Cooper JM, Dexter D, Jenner P, Clark JB, Marsden CD (1989) Mitochondrial complex I deficiency in Parkinson's disease. Lancet 1:1269.

Schreij AMA, Chaineau M, Ruan W, Lin S, Barker PA, Fon EA, McPherson PS (2015) LRRK2 localizes to endosomes and interacts with clathrin-light chains to limit Rac1 activation. EMBO Rep 16:79–86.

Schulte T, Böhringer S, Schöls L, Müller T, Fischer C, Riess O, Przuntek H, Berger K, Epplen JT, Krüger R (2003) Modulation of disease risk according to a cathepsin D / apolipoprotein E genotype in Parkinson's disease. J Neural Transm 110:749–755.

Sheng D, Qu D, Kwok KHH, Ng SS, Lim AYM, Aw SS, Lee CWH, Sung WK, Tan E-K, Lufkin T, Jesuthasan S, Sinnakaruppan M, Liu J (2010) Deletion of the WD40 domain of LRRK2 in Zebrafish causes Parkinsonism-like loss of neurons and locomotive defect. PLoS Genet 6:e1000914.

Sherer TB, Betarbet R, Kim J-H, Greenamyre JT (2003) Selective microglial activation in the rat rotenone model of Parkinson's disease. Neurosci Lett 341:87–90.

Shimura H, Hattori N, Kubo SI, Mizuno Y, Asakawa S, Minoshima S, Shimizu N, Iwai K, Chiba T, Tanaka K, Suzuki T (2000) Familial Parkinson disease gene product, parkin, is a ubiquitin-protein ligase. Nat Genet 25:302–305.

Shin N, Jeong H, Kwon J, Heo HY, Kwon JJ, Yun HJ, Kim C-H, Han BS, Tong Y, Shen J, Hatano T, Hattori N, Kim KS, Chang S, Seol W (2008) LRRK2 regulates synaptic vesicle endocytosis. Exp Cell Res 314:2055–2065.

Shinbo Y, Niki T, Taira T, Ooe H, Takahashi-Niki K, Maita C, Seino C, Iguchi-Ariga SMM, Ariga H (2006) Proper SUMO-1 conjugation is essential to DJ-1 to exert its full activities. Cell Death Differ 13:96–108.

Shojaee S, Sina F, Banihosseini SS, Kazemi MH, Kalhor R, Shahidi G-A, Fakhrai-Rad H, Ronaghi M, Elahi E (2008) Genome-wide Linkage Analysis of a Parkinsonian-Pyramidal Syndrome Pedigree by 500 K SNP Arrays. The American Journal of Human Genetics 82:1375–1384.

Shulman LM (2007) Gender differences in Parkinson's disease. Gender Medicine 4:8–18.

Singleton AB et al. (2003) α-Synuclein Locus Triplication Causes Parkinson's Disease. Science 302:841–841.

Skipper L, Li Y, Bonnard C, Pavanni R, Yih Y, Chua E, Sung WK, Tan L, Wong M-C, Tan E-K, Liu J (2005) Comprehensive evaluation of common genetic variation within LRRK2 reveals evidence for association with sporadic Parkinson's disease. Hum Mol Genet 14:3549–3556.

Smith WW, Jiang H, Pei Z, Tanaka Y, Morita H, Sawa A, Dawson VL, Dawson TM, Ross CA (2005) Endoplasmic reticulum stress and mitochondrial cell death pathways mediate A53T mutant alpha-synuclein-induced toxicity. Hum Mol Genet 14:3801–3811.

Snow BJ, Rolfe FL, Lockhart MM, Frampton CM, O'Sullivan JD, Fung V, Smith RAJ, Murphy MP, Taylor KM, Protect Study Group (2010) A double-blind, placebo-controlled study to assess the mitochondria-targeted antioxidant MitoQ as a disease-modifying therapy in Parkinson's disease. Mov Disord 25:1670–1674.

Song DD, Haber SN (2000) Striatal responses to partial dopaminergic lesion: evidence for compensatory sprouting. J Neurosci 20:5102–5114.

Spillantini MG, Schmidt ML, Lee VM, Trojanowski JQ, Jakes R, Goedert M (1997) Alpha-synuclein in Lewy bodies. Nature 388:839–840.

Sriram K, Pai KS, Boyd MR, Ravindranath V (1997) Evidence for generation of oxidative stress in brain by MPTP: in vitro and in vivo studies in mice. Brain Res 749:44–52.

St P McNaught K, Belizaire R, Isacson O, Jenner P, Olanow CW (2003) Altered Proteasomal Function in Sporadic Parkinson's Disease. Exp Neurol 179:38–46.

Stafa K, Tsika E, Moser R, Musso A, Glauser L, Jones A, Biskup S, Xiong Y, Bandopadhyay R, Dawson VL, Dawson TM, Moore DJ (2013) Functional interaction of Parkinson's disease-associated LRRK2 with members of the dynamin GTPase superfamily. Hum Mol Genet.

Steger M, Tonelli F, Ito G, Davies P, Trost M, Vetter M, Wachter S, Lorentzen E, Duddy G, Wilson S, Baptista MA, Fiske BK, Fell MJ, Morrow JA, Reith AD, Alessi DR, Mann M (2016) Phosphoproteomics reveals that Parkinson's disease kinase LRRK2 regulates a subset of Rab GTPases. eLife Sciences 5:e12813.

Stein MB, Heuser IJ, Juncos JL, Uhde TW (1990) Anxiety disorders in patients with Parkinson's disease. Am J Psychiatry 147:217–220.

Stocchi F, Barbato L, Nordera G, Berardelli A, Ruggieri S (1998) Sleep disorders in Parkinson's disease. J Neurol 245 Suppl 1:S15–S18.

Stocchi F, Jenner P, Obeso JA (2010) When do levodopa motor fluctuations first appear in Parkinson's disease? Eur Neurol 63:257–266.

Su X, Maguire-Zeiss KA, Giuliano R, Prifti L, Venkatesh K, Federoff HJ (2008) Synuclein activates microglia in a model of Parkinson's disease. Neurobiol Aging 29:1690–1701.

Sun X, Morozova T, Sonnenfeld M (2006) Glial and Neuronal Functions of the

Drosophila Homolog of the Human SWI/SNF Gene ATR-X (DATR-X) and the jing Zinc-Finger Gene Specify the Lateral Positioning of Longitudinal Glia and Axons. Genetics 173:1397–1415.

Surmeier DJ, Guzman JN, Sanchez-Padilla J (2010) Calcium, cellular aging, and selective neuronal vulnerability in Parkinson's disease. Cell Calcium 47:175–182.

Surmeier DJ, Guzman JN, Sanchez-Padilla J, Schumacker PT (2011) The role of calcium and mitochondrial oxidant stress in the loss of substantia nigra pars compacta dopaminergic neurons in Parkinson's disease. Neuroscience 198:221–231.

Tagliaferro P, Kareva T, Oo TF, Yarygina O, Kholodilov N, Burke RE (2015) An early axonopathy in a hLRRK2(R1441G) transgenic model of Parkinson disease. Neurobiol Dis 82:359–371.

Taira T, Saito Y, Niki T, Iguchi-Ariga SMM, Takahashi K, Ariga H (2004) DJ-1 has a role in antioxidative stress to prevent cell death. EMBO Rep 5:213–218.

Takahashi K, Taira T, Niki T, Seino C, Iguchi-Ariga SM, Ariga H (2001) DJ-1 positively regulates the androgen receptor by impairing the binding of PIASx alpha to the receptor. J Biol Chem 276:37556–37563.

Takeuchi H, Mizuno T, Zhang G, Wang J, Kawanokuchi J, Kuno R, Suzumura A (2005) Neuritic beading induced by activated microglia is an early feature of neuronal dysfunction toward neuronal death by inhibition of mitochondrial respiration and axonal transport. J Biol Chem 280:10444–10454.

Tan E-K (2006) Identification of a common genetic risk variant (LRRK2 Gly2385Arg) in Parkinson's disease. Ann Acad Med Singap 35:840–842.

Tang FL, Erion JR, Tian Y, Liu W, Yin DM, Ye J, Tang B, Mei L, Xiong WC. VPS35 in

Dopamine Neurons Is Required for Endosome-to-Golgi Retrieval of Lamp2a, a Receptor of Chaperone-Mediated Autophagy That Is Critical for α-Synuclein Degradation and Prevention of Pathogenesis of Parkinson's Disease. The Journal of Neuroscience. 2015 Jul 22;35(29):10613-28.

Tanner CM, Ottman R, Goldman SM, Ellenberg J, Chan P, Mayeux R, Langston JW (1999) Parkinson disease in twins: an etiologic study. JAMA 281:341–346.

Tanti GK, Pandey S, Goswami SK (2015) SG2NA enhances cancer cell survival by stabilizing DJ-1 and thus activating Akt. Biochem Biophys Res Commun 463:524–531.

Tayebi N, Callahan M, Madike V, Stubblefield BK, Orvisky E, Krasnewich D, Fillano JJ, Sidransky E (2001) Gaucher Disease and Parkinsonism: A Phenotypic and Genotypic Characterization. Mol Genet Metab 73:313–321.

Teismann P, Tieu K, Choi D-K, Wu D-C, Naini A, Hunot S, Vila M, Jackson-Lewis V, Przedborski S (2003) Cyclooxygenase-2 is instrumental in Parkinson's disease neurodegeneration. Proc Natl Acad Sci USA 100:5473–5478.

Tekumalla PK, Calon F, Rahman Z, Birdi S, Rajput AH, Hornykiewicz O, Di Paolo T, Bédard PJ, Nestler EJ (2001) Elevated levels of ΔFosB and RGS9 in striatum in Parkinson's disease. Biological Psychiatry 50:813–816.

Thévenet J, Pescini Gobert R, Hooft van Huijsduijnen R, Wiessner C, Sagot YJ (2011) Regulation of LRRK2 expression points to a functional role in human monocyte maturation. PLoS ONE 6:e21519.

Tieu K, Perier C, Caspersen C, Teismann P, Wu D-C, Yan S-D, Naini A, Vila M, Jackson-Lewis V, Ramasamy R, Przedborski S (2003) D-β-Hydroxybutyrate rescues

mitochondrial respiration and mitigates features of Parkinson disease. J Clin Invest 112:892–901.

Tong Y, Giaime E, Yamaguchi H, Ichimura T, Liu Y, Si H, Cai H, Bonventre JV, Shen J (2012) Loss of leucine-rich repeat kinase 2 causes age-dependent bi-phasic alterations of the autophagy pathway. Mol Neurodegener 7:2.

Tong Y, Pisani A, Martella G, Karouani M, Yamaguchi H, Pothos EN, Shen J (2009) R1441C mutation in LRRK2 impairs dopaminergic neurotransmission in mice. Proc Natl Acad Sci USA 106:14622–14627.

Tong Y, Yamaguchi H, Giaime E, Boyle S, Kopan R, Kelleher RJ, Shen J (2010) Loss of leucine-rich repeat kinase 2 causes impairment of protein degradation pathways, accumulation of alpha-synuclein, and apoptotic cell death in aged mice. Proc Natl Acad Sci USA 107:9879–9884.

Trancikova A, Mamais A, Webber PJ, Stafa K, Tsika E, Glauser L, West AB, Bandopadhyay R, Moore DJ (2012) Phosphorylation of 4E-BP1 in the mammalian brain is not altered by LRRK2 expression or pathogenic mutations. PLoS ONE 7:e47784.

Trudler D, Weinreb O, Mandel SA, Youdim MB, Frenkel D. DJ-1 deficiency triggers microglia sensitivity to dopamine toward a pro-inflammatory phenotype that is attenuated by rasagiline. Journal of neurochemistry. 2014 May 1;129(3):434-47.

Tsika E, Kannan M, Foo CS-Y, Dikeman D, Glauser L, Gellhaar S, Galter D, Knott GW, Dawson TM, Dawson VL, Moore DJ (2014) Conditional expression of Parkinson's disease-related R1441C LRRK2 in midbrain dopaminergic neurons of mice causes nuclear abnormalities without neurodegeneration. Neurobiol Dis 71:345–358.

Uyama M, Kawanami M, Tamura M (2013) Wasf2: a novel target of intermittent parathyroid hormone administration. Int J Mol Med 31:1243–1247.

Valente EM et al. (2004) Hereditary early-onset Parkinson's disease caused by mutations in PINK1. Science 304:1158–1160.

van der Brug MP, Blackinton J, Chandran J, Hao L-Y, Lal A, Mazan-Mamczarz K, Martindale J, Xie C, Ahmad R, Thomas KJ, Beilina A, Gibbs JR, Ding J, Myers AJ, Zhan M, Cai H, Bonini NM, Gorospe M, Cookson MR (2008) RNA binding activity of the recessive parkinsonism protein DJ-1 supports involvement in multiple cellular pathways. Proc Natl Acad Sci USA 105:10244–10249.

Ved R, Saha S, Westlund B, Perier C, Burnam L, Sluder A, Hoener M, Rodrigues CMP, Alfonso A, Steer C, Liu L, Przedborski S, Wolozin B (2005) Similar patterns of mitochondrial vulnerability and rescue induced by genetic modification of alpha-synuclein, parkin, and DJ-1 in Caenorhabditis elegans. J Biol Chem 280:42655–42668.

Venderova K, Kabbach G, Abdel-Messih E, Zhang Y, Parks RJ, Imai Y, Gehrke S, Ngsee J, LaVoie MJ, Slack RS, Rao Y, Zhang Z, Lu B, Haque ME, Park DS (2009) Leucine-Rich Repeat Kinase 2 interacts with Parkin, DJ-1 and PINK-1 in a Drosophila melanogaster model of Parkinson's disease. Hum Mol Genet 18:4390–4404.

Verstraeten A, Theuns J, Van Broeckhoven C (2015) Progress in unraveling the genetic etiology of Parkinson disease in a genomic era. Trends Genet 31:140–149.

Vilariño-Güell C et al. (2011) VPS35 mutations in Parkinson disease. Am J Hum Genet 89:162–167.

Vilariño-Güell C et al. (2014) DNAJC13 mutations in Parkinson disease. Hum Mol Genet 23:1794–1801.

Visanji NP, Brooks PL, Hazrati L-N, Lang AE (2013) The prion hypothesis in Parkinson's disease: Braak to the future. Acta Neuropathologica Communications 2013 1:1 1:1.

Vives-Bauza C, Zhou C, Huang Y, Cui M, de Vries RL, Kim J, May J, Tocilescu MA, Liu W, Ko HS, Magrané J. PINK1-dependent recruitment of Parkin to mitochondria in mitophagy. Proceedings of the National Academy of Sciences. 2010 Jan 5;107(1):378-83.

Vogiatzi T, Xilouri M, Vekrellis K, Stefanis L (2008) Wild type alpha-synuclein is degraded by chaperone-mediated autophagy and macroautophagy in neuronal cells. J Biol Chem 283:23542–23556.

Volpicelli-Daley LA, Luk KC, Lee VM-Y (2014) Addition of exogenous α-synuclein preformed fibrils to primary neuronal cultures to seed recruitment of endogenous α-synuclein to Lewy body and Lewy neurite–like aggregates. Nature Protocols 9:2135–2146.

Volta M, Cataldi S, Beccano-Kelly D, Munsie L, Tatarnikov I, Chou P, Bergeron S, Mitchell E, Lim R, Khinda J, Lloret A, Bennett CF, Paradiso C, Morari M, Farrer MJ, Milnerwood AJ (2015) Chronic and acute LRRK2 silencing has no long-term behavioral effects, whereas wild-type and mutant LRRK2 overexpression induce motor and cognitive deficits and altered regulation of dopamine release. Parkinsonism Relat Disord 21:1156–1163.

Waak J, Weber SS, Waldenmaier A, Görner K, Alunni-Fabbroni M, Schell H, Vogt-

Weisenhorn D, Pham T-T, Reumers V, Baekelandt V, Wurst W, Kahle PJ (2009) Regulation of astrocyte inflammatory responses by the Parkinson's disease-associated gene DJ-1. FASEB J 23:2478–2489.

Waldmeier P, Bozyczko-Coyne D, Williams M, Vaught JL (2006) Recent clinical failures in Parkinson's disease with apoptosis inhibitors underline the need for a paradigm shift in drug discovery for neurodegenerative diseases. Biochem Pharmacol 72:1197–1206.

Wang H-S, Toh J, Ho P, Tio M, Zhao Y, Tan E-K (2014a) In vivo evidence of pathogenicity of VPS35 mutations in the Drosophila. Mol Brain 7:1.

Wang L, Xie C, Greggio E, Parisiadou L, Shim H, Sun L, Chandran J, Lin X, Lai C, Yang W-J, Moore DJ, Dawson TM, Dawson VL, Chiosis G, Cookson MR, Cai H (2008) The chaperone activity of heat shock protein 90 is critical for maintaining the stability of leucine-rich repeat kinase 2. J Neurosci 28:3384–3391.

Wang L-L, Chen D, Lee J, Gu X, Alaaeddine G, Li J, Wei L, Yu SP (2014b) Mobilization of endogenous bone marrow derived endothelial progenitor cells and therapeutic potential of parathyroid hormone after ischemic stroke in mice. Xiao Q, ed. PLoS ONE 9:e87284.

Wang X, Yan MH, Fujioka H, Liu J, Wilson-Delfosse A, Chen SG, Perry G, Casadesus G, Zhu X (2012) LRRK2 regulates mitochondrial dynamics and function through direct interaction with DLP1. Hum Mol Genet 21:1931–1944.

Ward RJ, Zucca FA, Duyn JH, Crichton RR, Zecca L (2014) The role of iron in brain ageing and neurodegenerative disorders. Lancet Neurol 13:1045–1060.

Waschbüsch D, Michels H, Strassheim S, Ossendorf E, Kessler D, Gloeckner CJ,

Barnekow A (2014) LRRK2 transport is regulated by its novel interacting partner Rab32. Chu CT, ed. PLoS ONE 9:e111632.

Wenger Y, Buzgariu W, Reiter S, Galliot B. Injury-induced immune responses in Hydra. InSeminars in immunology 2014 Aug 31 (Vol. 26, No. 4, pp. 277-294). Academic Press.

West AB, Cowell RM, Daher JPL, Moehle MS, Hinkle KM, Melrose HL, Standaert DG, Volpicelli-Daley LA (2014) Differential LRRK2 expression in the cortex, striatum, and substantia nigra in transgenic and nontransgenic rodents. J Comp Neurol 522:2465–2480.

West AB, Moore DJ, Choi C, Andrabi SA, Li X, Dikeman D, Biskup S, Zhang Z, Lim K-L, Dawson VL, Dawson TM (2007) Parkinson's disease-associated mutations in LRRK2 link enhanced GTP-binding and kinase activities to neuronal toxicity. Hum Mol Genet 16:223–232.

Westerlund M, Belin AC, Anvret A, Håkansson A, Nissbrandt H, Lind C, Sydow O, Olson L, Galter D (2009) Association of a polymorphism in the ABCB1 gene with Parkinson's disease. Parkinsonism Relat Disord 15:422–424.

Whitton PS (2007) Inflammation as a causative factor in the aetiology of Parkinson's disease. British Journal of Pharmacology 150:963–976.

Wilson MA, Collins JL, Hod Y, Ringe D, Petsko GA (2003) The 1.1-A resolution crystal structure of DJ-1, the protein mutated in autosomal recessive early onset Parkinson's disease. Proc Natl Acad Sci USA 100:9256–9261.

Winslow AR, Chen C-W, Corrochano S, Acevedo-Arozena A, Gordon DE, Peden AA, Lichtenberg M, Menzies FM, Ravikumar B, Imarisio S, Brown S, O'Kane CJ,

Rubinsztein DC (2010) α-Synuclein impairs macroautophagy: implications for Parkinson's disease. J Cell Biol 190:1023–1037.

Wirdefeldt K, Adami H-O, Cole P, Trichopoulos D, Mandel J (2011) Epidemiology and etiology of Parkinson's disease: a review of the evidence. Eur J Epidemiol 26:1–58.

Wong SL, Gilmour H, Ramage-Morin PL (2014) Parkinson's disease: Prevalence, diagnosis and impact. Health reports.

Wu DC, Jackson-Lewis V, Vila M, Tieu K, Teismann P, Vadseth C, Choi D-K, Ischiropoulos H, Przedborski S (2002) Blockade of microglial activation is neuroprotective in the 1-methyl-4-phenyl-1,2,3,6-tetrahydropyridine mouse model of Parkinson disease. J Neurosci 22:1763–1771.

Wu JS, Luo L (2006) A protocol for dissecting Drosophila melanogaster brains for live imaging or immunostaining. Nature Protocols 1:2110–2115.

Xi Y, Ryan J, Noble S, Yu M, Yilbas AE, Ekker M (2010) Impaired dopaminergic neuron development and locomotor function in zebrafish with loss of pink1 function. European Journal of Neuroscience 31:623–633.

Yang Y, Gehrke S, Haque ME, Imai Y, Kosek J, Yang L, Beal MF, Nishimura I, Wakamatsu K, Ito S, Takahashi R, Lu B (2005) Inactivation of Drosophila DJ-1 leads to impairments of oxidative stress response and phosphatidylinositol 3-kinase/Akt signaling. Proc Natl Acad Sci USA 102:13670–13675.

Yao C, Johnson WM, Gao Y, Wang W, Zhang J, Deak M, Alessi DR, Zhu X, Mieyal JJ, Roder H, Wilson-Delfosse AL, Chen SG (2013) Kinase inhibitors arrest neurodegeneration in cell and C. elegans models of LRRK2 toxicity. Hum Mol Genet 22:328–344.

Ye J, Jiang Z, Chen X, Liu M, Li J, Liu N (2016) Electron transport chain inhibitors induce microglia activation through enhancing mitochondrial reactive oxygen species production. Exp Cell Res 340:315–326.

Youdim MB, Ben-Shachar D, Riederer P (1989) Is Parkinson's disease a progressive siderosis of substantia nigra resulting in iron and melanin induced neurodegeneration? Acta Neurol Scand, Supplc 126:47–54.

Yu Y, Chu P-Y, Bowser DN, Keating DJ, Dubach D, Harper I, Tkalcevic J, Finkelstein DI, Pritchard MA (2008) Mice deficient for the chromosome 21 ortholog Itsn1 exhibit vesicle-trafficking abnormalities. Hum Mol Genet 17:3281–3290.

Yuan Y, Cao P, Smith MA, Kramp K, Huang Y, Hisamoto N, Matsumoto K, Hatzoglou M, Jin H, Feng Z (2011) Dysregulated LRRK2 signaling in response to endoplasmic reticulum stress leads to dopaminergic neuron degeneration in C. elegans. PLoS ONE 6:e22354.

Yue M et al. (2015) Progressive dopaminergic alterations and mitochondrial abnormalities in LRRK2 G2019S knock-in mice. Neurobiol Dis 78:172–195.

Yun HJ, Kim H, Ga I, Oh H, Ho D-H, Kim J, Seo H, Son I, Seol W (2015) An early endosome regulator, Rab5b, is an LRRK2 kinase substrate. J Biochem 157:485–495.

Yun HJ, Park J, Ho D-H, Kim H, Kim C-H, Oh H, Ga I, Seo H, Chang S, Son I, Seol W (2013) LRRK2 phosphorylates Snapin and inhibits interaction of Snapin with SNAP-25. Exp Mol Med 45:e36.

Zarow C, Lyness SA, Mortimer JA, Chui HC (2003) Neuronal loss is greater in the locus coeruleus than nucleus basalis and substantia nigra in Alzheimer and Parkinson diseases. Arch Neurol 60:337–341.

Zhang J, Perry G, Smith MA, Robertson D, Olson SJ, Graham DG, Montine TJ (1999) Parkinson's disease is associated with oxidative damage to cytoplasmic DNA and RNA in substantia nigra neurons. Am J Pathol 154:1423–1429.

Zhu Z-M, Li Z-R, Huang Y, Yu H-H, Huang X-S, Yan Y-F, Shao J-H, Chen H-P (2014) DJ-1 is involved in the peritoneal metastasis of gastric cancer through activation of the Akt signaling pathway. Oncol Rep 31:1489–1497.

Zimprich A et al. (2004) Mutations in LRRK2 cause autosomal-dominant parkinsonism with pleomorphic pathology. Neuron 44:601–607.

Zimprich A et al. (2011) A mutation in VPS35, encoding a subunit of the retromer complex, causes late-onset Parkinson disease. Am J Hum Genet 89:168–175.

Zweig RM, Cardillo JE, Cohen M, Giere S, Hedreen JC (1993) The locus ceruleus and dementia in Parkinson's disease. Neurology 43:986–991.

Appendix B: Appended Publications with Permissions

PNAS -- Rights and Permissions

Beginning with articles submitted in Volume 106 (2009) the author(s) retains copyright to individual articles, and the National Academy of Sciences of the United States of America retains an exclusive license to publish these articles and holds copyright to the collective work. Volumes 90–105 (1993–2008) copyright © by the National Academy of Sciences. Volumes 1–89 (1915–1992), the author(s) retains copyright to individual articles, and the National Academy of Sciences holds copyright to the collective work.

The PNAS listing on the Sherpa RoMEO publisher copyright policies & self-archiving detail pages can be found here.

Requests for Permission to Reprint

Requests for permission should be made in writing. For the fastest response time, please send your request via email to PNASPermissions@nas.edu. If necessary, requests may be faxed to 202-334-2739 or mailed to:

PNAS Permissions Editor
500 Fifth Street, NW
NAS 340
Washington, DC 20001 USA

Anyone may, without requesting permission, use original figures or tables published in PNAS for noncommercial and educational use (i.e., in a review article, in a book that is not for sale) provided that the original source and the applicable copyright notice are cited.

For permission to reprint material in volumes 1–89 (1915–1992), requests should be addressed to the original authors, who hold the copyright. The full journal reference must be cited.

For permission to reprint material in volumes 90–present (1993–present), requests must be sent via email, fax, or mail and include the following information about the original material:

1. Your full name, affiliation, and title
2. Your complete mailing address, phone number, fax number, and email address
3. PNAS volume number, issue number, and issue date
4. PNAS article title
5. PNAS authors' names
6. Page numbers of items to be reprinted
7. Figure/table number or portion of text to be reprinted

Also include the following information about the intended use of the material:

1. Title of work in which PNAS material will appear
2. Authors/editors of work
3. Publisher of work
4. Retail price of work
5. Number of copies of work to be produced
6. Intended audience
7. Whether work is for nonprofit or commercial use

PNAS authors need not obtain permission for the following cases: (1) to use their original figures or tables in their future works; (2) to make copies of their papers for their own personal use, including classroom use, or for the personal use of colleagues, provided those copies are not for sale and are not distributed in a systematic way; (3) to include their papers as part of their dissertations; or (4) to use all or part of their articles in printed compilations of their own works. Citation of the original source must be included and copies must include the applicable copyright notice of the original report.

Authors whose work will be reused should be notified. PNAS cannot supply original artwork. Use of PNAS material must not imply any endorsement by PNAS or the National Academy of Sciences. The full journal reference must be cited and, for articles published in Volumes 90–105 (1993–2008), "Copyright (copyright year) National Academy of Sciences, USA."

Requests for Permission to Photocopy

For permission to photocopy beyond that permitted by Section 107 or 108 of the US Copyright Law, contact:

Copyright Clearance Center
222 Rosewood Drive
Danvers, MA 01923 USA
Phone: 1-978-750-8400
Fax: 1-978-750-4770
Email: info@copyright.com

Authorization to photocopy items for the internal or personal use of specific clients is granted by The National Academy of Sciences provided that the proper fee is paid directly to CCC.

[12/14]

Corrections

PHYSICS

Correction for "Quantitative field theory of the glass transition," by Silvio Franz, Hugo Jacquin, Giorgio Parisi, Pierfrancesco Urbani, and Francesco Zamponi, which appeared in issue 46, November 13, 2012, of *Proc Natl Acad Sci USA* (109: 18725–18730; first published October 29, 2012; 10.1073/pnas.1216578109).

On page 18727, right column, Eq. **12** should instead appear as

$$\Gamma[\{\phi_{ab}\}] = \frac{1}{2}\int \frac{\mathrm{d}p}{(2\pi)^D}\left(\sum_{a\neq b}(\mu\sqrt{\epsilon}+\sigma p^2)|\phi_{ab}(p)|^2 + m_2\sum_a\Big|\sum_b \phi_{ab}(p)\Big|^2 + m_3\Big|\sum_{a\neq b}\phi_{ab}(p)\Big|^2\right) + \frac{w_1}{6}\int\sum_{a\neq b\neq c\neq a}\frac{\mathrm{d}p\mathrm{d}p'}{(2\pi)^{2D}}\phi_{ab}(p)\phi_{bc}(p')\phi_{ca}(-p-p') + \frac{w_2}{6}\int\sum_{a\neq b}\frac{\mathrm{d}p\mathrm{d}p'}{(2\pi)^{2D}}\phi_{ab}(p)\phi_{ab}(p')\phi_{ab}(-p-p'), \quad [12]$$

On page 18728, right column, Eq. **21** should instead appear as

$$\lambda = \frac{1}{2}\frac{\frac{1}{\rho^4}\int \mathrm{d}x\frac{k_0^3(x)}{g^2(x)}}{\frac{1}{\rho^3}\int\frac{\mathrm{d}q}{(2\pi)^D}k_0^3(q)[1-\rho\Delta c(q)]^3} \quad [21]$$

The authors note that Tables 1 and 2 appeared incorrectly. The corrected tables appear below.

Table 1. Numerical values of the coefficients of the effective action and the physical quantities from the HNC approximation

System	T	ρ_d	$-w_1$	$-w_2$	m_2	m_3	σ	μ	λ	ξ_0	G_0	Gi
SS-6	1	6.691	$3.88\cdot10^{-6}$	$1.35\cdot10^{-6}$	-0.000925	0.000110	0.000195	0.000525	0.348	0.601	224	0.0267
SS-9	1	2.912	0.0000772	0.0000272	-0.00539	0.000633	0.00163	0.00543	0.353	0.548	34.3	0.0125
SS-12	1	2.057	0.000275	0.0000973	-0.0116	0.00132	0.00378	0.0152	0.354	0.498	14.2	0.0118
LJ	0.7	1.407	0.00106	0.000376	-0.0258	0.00290	0.00989	0.0414	0.355	0.489	6.00	0.00833
HarmS	10^{-3}	1.336	0.00129	0.000465	-0.0336	0.00343	0.00772	0.0779	0.359	0.315	2.82	0.0434
HarmS	10^{-4}	1.196	0.00165	0.000622	-0.0403	0.00386	0.00819	0.109	0.378	0.274	1.69	0.0632
HarmS	10^{-5}	1.170	0.00174	0.000663	-0.0416	0.00395	0.00845	0.109	0.382	0.278	1.66	0.0635
HS	0	1.169	0.00174	0.000664	-0.0418	0.00397	0.00847	0.108	0.381	0.280	1.67	0.0639

For each potential, lengths are given in units of r_0 and energies in units of ε, with $k_B = 1$. Data at fixed temperature, using density as a control parameter with $\epsilon = \rho_d - \rho$.

Table 2. Same as Table 1, but here the data are at fixed density, using temperature as a control parameter with $\epsilon = T_d - T$

System	ρ	T_d	$-w_1$	$-w_2$	m_2	m_3	σ	μ	λ	ξ_0	G_0	Gi
LJ	1.2	0.336	0.00186	0.000663	-0.0361	0.00403	0.0147	0.0572	0.356	0.507	4.56	0.00730
LJ	1.27	0.438	0.00153	0.000541	-0.0321	0.00370	0.0128	0.0447	0.353	0.536	5.74	0.00771
LJ	1.4	0.684	0.00108	0.000383	-0.0260	0.00293	0.0100	0.0292	0.355	0.586	8.52	0.00825
WCA	1.2	0.325	0.00195	0.000686	-0.0389	0.00426	0.0133	0.0607	0.351	0.467	4.37	0.0134
WCA	1.4	0.692	0.00111	0.000388	-0.0270	0.00301	0.00966	0.0291	0.350	0.576	8.67	0.0106

www.pnas.org/cgi/doi/10.1073/pnas.1309463110

CHEMISTRY, BIOPHYSICS AND COMPUTATIONAL BIOLOGY

Correction for "Probing the relative orientation of molecules bound to DNA through controlled interference using second-harmonic generation," by Benjamin Doughty, Yi Rao, Samuel W. Kazer, Sheldon J. J. Kwok, Nicholas J. Turro, and Kenneth B. Eisenthal, which appeared in issue 15, April 9, 2013, of *Proc Natl Acad Sci USA* (110:5756–5758; first published March 25, 2013; 10.1073/pnas.1302554110).

The authors note that the following statement should be added to the Acknowledgments: "We also acknowledge funding from the Chemical Sciences, Geosciences and Bioscience Division, Office of Basic Energy Sciences, Office of Science of the US Department of Energy."

www.pnas.org/cgi/doi/10.1073/pnas.1310422110

IN THIS ISSUE

Correction for "In This Issue," which appeared in issue 21, May 21, 2013, of *Proc Natl Acad Sci USA* (110:8315–8316; 10.1073/iti2113110).

The authors note that within "Measuring telomeres in single cells" on page 8316 the writing credit "C.R." should instead appear as "C.B." The online version has been corrected.

www.pnas.org/cgi/doi/10.1073/pnas.1310833110

NEUROSCIENCE

Correction for "Progressive dopaminergic cell loss with unilateral-to-bilateral progression in a genetic model of Parkinson disease," by Maxime W. C. Rousseaux, Paul C. Marcogliese, Dianbo Qu, Sarah J. Hewitt, Sarah Seang, Raymond H. Kim, Ruth S. Slack, Michael G. Schlossmacher, Diane C. Lagace, Tak W. Mak, and David S. Park, which appeared in issue 39, September 25, 2012, of *Proc Natl Acad Sci USA* (109:15918–15923; first published September 10, 2012; 10.1073/pnas.1205102109).

The authors note that the incorrect term appeared for the mice background that they used. All instances of "C57BL/6J" should instead appear as "C57BL/6." The locations were:

On page 15918, left column, line 4 within the Abstract
On page 15918, right column, first full paragraph, line 5
On page 15922, left column, second full paragraph, line 2

These errors do not affect the conclusions of the article.

www.pnas.org/cgi/doi/10.1073/pnas.1310560110

Progressive dopaminergic cell loss with unilateral-to-bilateral progression in a genetic model of Parkinson disease

Maxime W. C. Rousseaux[a], Paul C. Marcogliese[a], Dianbo Qu[a], Sarah J. Hewitt[a], Sarah Seang[a], Raymond H. Kim[b], Ruth S. Slack[a], Michael G. Schlossmacher[c,d], Diane C. Lagace[a], Tak W. Mak[b], and David S. Park[a,e,1]

[a]Department of Cellular and Molecular Medicine, University of Ottawa, Ottawa, ON, Canada, K1H 8M5; [b]Campbell Family Institute for Breast Cancer Research, Department of Medical Biophysics, University of Toronto, Toronto, ON, Canada, M5G 2C1; [c]Division of Neurology, Department of Medicine, Ottawa Hospital, Ottawa, ON, Canada, K1H 8M5; [d]Division of Neuroscience, Ottawa Hospital Research Institute, Ottawa, ON, Canada, K1H 8M5; and [e]Department of Cogno-Mechatronics Engineering, Pusan National University, Geumjeong-gu, Busan 609-735, South Korea

Edited by Thomas C. Südhof, Stanford University School of Medicine, Stanford, CA, and approved August 10, 2012 (received for review March 26, 2012)

DJ-1 mutations cause autosomal recessive early-onset Parkinson disease (PD). We report a model of PD pathology: the DJ1-C57 mouse. A subset of DJ-1–nullizygous mice, when fully backcrossed to a C57BL/6J background, display dramatic early-onset unilateral loss of dopaminergic (DA) neurons in their *substantia nigra pars compacta*, progressing to bilateral degeneration of the nigrostriatal axis with aging. In addition, these mice exhibit age-dependent bilateral degeneration at the *locus ceruleus* nucleus and display mild motor behavior deficits at aged time points. These findings effectively recapitulate the early stages of PD. Therefore, the DJ1-C57 mouse provides a tool to study the preclinical aspects of neurodegeneration. Importantly, by exome sequencing, we identify candidate modifying genes that segregate with the phenotype, providing potentially critical clues into how certain genes may influence the penetrance of DJ-1–related degeneration in mice.

animal model | PARK7 | neuritic beading | neuronal death | neuroinflammation

Parkinson disease (PD) is a progressive neurodegenerative disorder with complex symptomology and etiology affecting an ever-increasing number of individuals. Although multifactorial in nature, increasing insight has been gained with regard to the pathogenesis of PD through investigation of genes linked to the disease. Because monogenic forms of PD can be modeled in a laboratory, numerous animal models have been created to recapitulate the disease. For instance, loss-of-function mutations in the *DJ-1* (*PARK7*) gene cause early-onset autosomal recessive PD (1, 2). Patients harboring *DJ-1* mutations exhibit certain key characteristics principally in early-onset PD and may lack certain neuropathological attributes present in sporadic PD cases such as Lewy bodies (LBs) (3). However, generation of DJ-1–nullizygous mice (DJ-$1^{-/-}$) on mixed background by various laboratories, including our own, failed to detect any basal levels of neurodegeneration even in aged mice (4–11) (see Table S1). Similarly, a number of PD-related, genetically manipulated mice have been created in attempts to recapitulate the disease process, whereas little or none has shown clear or robust neurodegeneration specific to the *substantia nigra pars compacta* (SNc) (reviewed in ref. 12). Therefore, the creation of murine PD models that demonstrate significant dopaminergic (DA) loss remains an acute need in the field. The need for an early-onset model of PD is made more pressing given that no postmortem analyses of human DJ-1 mutant-carrying patients have been reported. This is particularly critical if we are to understand how specific signaling pathways govern DA loss in monogenic forms of early-onset human PD. Presently, most mechanistic studies of DA loss rely on acute toxin models of Parkinsonism. However, the relevance of such studies to the human condition remains uncertain, because acute neurotoxins are rarely the culprit in the majority of PD cases. This potential discrepancy is highlighted by a number of failed clinical trials that have heavily relied on toxin models as preclinical evidence for efficacy (13–16). A more representative model of DA loss that uses known factors in human PD is likely vital to develop better therapeutic outcomes.

Results

In the course of our studies examining the effects of environmental perturbations in DJ-$1^{-/-}$ mice, we continued to examine the long-term effects of DJ-1 deficiency on DA neuron loss. Importantly, this was accomplished in animals completely backcrossed onto a C57BL/6J background (14× backcrossed, DJ-$1^{-/-}$; herein, referred to as DJ1-C57). Intriguingly, unilateral SNc degeneration in a subset of these DJ1-C57 knockout mice is observed as early as 2 mo of age (Fig. 1*A*, Fig. S1, and Table S2). This phenotype is not observed in animals younger than 2 mo ($n = 8$; Fig. S1), thus indicating that this defect is unlikely to be developmental in origin. Moreover, this phenotype is not observed in any of the wild-type (WT) mice examined ($n = 71$). In addition, the ventral tegmental area (VTA) of these mice is mostly spared (Fig. 1*D*). This latter finding is particularly interesting given the observation that in postmortem brains from PD patients, VTA neurons remain relatively protected compared with their nigral counterparts (17).

To objectively assess this phenotype, mice in this study are classified as either "affected" (unilateral phenotype: having a greater than 40% unilateral reduction of DA cells in the SNc compared with the other side) or "unaffected" (no unilateral phenotype: having similar bilateral DA cell numbers). No clear side or sex specificity is observed (right, 53%; female, 67%, respectively). Thus, to maintain consistency, "side A" is the term given for the side of the brain with the least number of neurons, regardless of the genotype (side B being the side with more DA neurons). When quantified, affected DJ1-C57 mice exhibit a dramatic reduction of neurons in their SNc, as visualized by tyrosine hydroxylase (TH) and cresyl violet (CV) staining (Fig. 1*B* and *C* and see Fig. 3*A*). Upon closer magnification of the SNc, the affected DJ1-C57 mice exhibit TH-positive fiber

Author contributions: M.W.C.R. and D.S.P. designed research; M.W.C.R., P.C.M., D.Q., S.J.H., and S.S. performed research; R.H.K., R.S.S., M.G.S., D.C.L., and T.W.M. contributed new reagents/analytic tools; M.W.C.R. and P.C.M. analyzed data; and M.W.C.R. and D.S.P. wrote the paper.

The authors declare no conflict of interest.

This article is a PNAS Direct Submission.

Freely available online through the PNAS open access option.

Data deposition: The sequences reported in this paper have been deposited in the Mouse Genome Informatics (MGI) database, ftp://ftp.informatics.jax.org/pub/datasets/index.html.

[1]To whom correspondence should be addressed. E-mail: dpark@uottawa.ca.

This article contains supporting information online at www.pnas.org/lookup/suppl/doi:10.1073/pnas.1205102109/-/DCSupplemental.

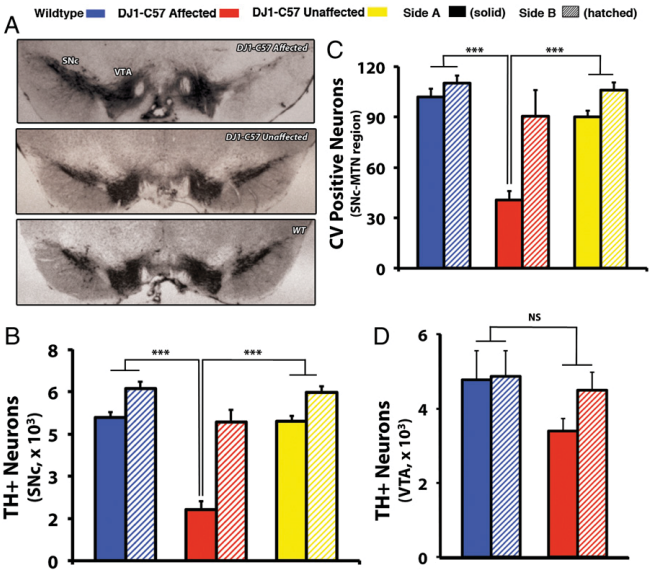

Fig. 1. Young affected DJ1-C57 mice exhibit selective unilateral degeneration in their SNc. (*A*) Representative midbrain sections of DJ1-C57 affected (*Top*), DJ1-C57 Unaffected (*Middle*), and WT (*Bottom*) mice depicting TH staining in the SNc and VTA. (*B* and *C*) Quantification of *A* by stereology of total number of TH-positive cells in the SNc (*B*) and of CV-stained cells at the level of the MTN in the SNc (*C*). (*D*) Quantification of TH-positive neurons in the VTA of WT and DJ-1 affected mice. Note that WT, DJ1-C57 affected and DJ1-C57 unaffected are represented by blue, red, and yellow bars, respectively. Side A is depicted as solid shading and side B as hatched shading. NS, not significant ($P > 0.05$); ***$P < 0.001$; ANOVA, followed by Tukey's LSD post hoc tests. Data are represented as means (n = 7–80 per group) ± SEM.

staining but with clear neuronal process disruption. When quantified, the remaining fibers at the level of the SNc in the affected DJ1-C57 mice display an elevated number of shortened processes with obvious neuritic beading (Fig. 2*A*) compared with unaffected DJ1-C57 or control mice. Consistent with this finding, an increase in CD11b-positive microglia is noted in young, affected animals (Fig. 3*B*), whereas no clear increase in astrocytosis on the affected side is observed (Fig. S2).

To assess whether this histopathological phenotype corresponds with a functional outcome, we subjected animals to behavioral testing. However, DJ1-C57 affected mice do not exhibit a clear decrease in gross motor function at 2, 6, or 12 mo of age (Fig. S3 *A*–*C*) or any differences in drug-induced rotational behavior (Fig. S3*D*). The lack of behavioral differences may be accounted for by two observations. First, examination of the striatal DA terminals revealed no clear loss in striatal fibers in young animals (Fig. 2*B*). This finding raised the possibility that sprouting of neurites within the nigrostriatal pathway may be compensatory in young mice. This is of marked interest because we note significant sprouting of dysmorphic neurites (as seen in Fig. 2*A*) in the SNc, which may be compensating for the loss of cell bodies as reported previously (18, 19). Second, an increase in the striatal postsynaptic marker ΔFBJ murine osteosarcoma viral oncogene homolog B (ΔFosB) is observed in affected DJ1-C57 mice (Fig. 2*C*). PD patients have been shown to have up-regulated ΔFosB in their caudate/putamen (20). Moreover, ΔFosB has been shown previously to be up-regulated in toxin models of neurodegeneration such as 1-methyl-4-phenyl-1,2,3,6-tetrahydropyrindine (MPTP) and 6-hydroxydopamine (6-OHDA) as a compensatory response to a loss of DA innervation (21, 22).

With aging of DJ-1–deficient animals, an increase in the prevalence of the DJ1-C57 affected unilateral phenotype was observed over time, peaking at 12 mo of age (42.9% penetrance, Fig. 4*A* and Table S2). When only affected unilateral DJ1-C57 animals are considered, there was a clear loss in total number of SNc DA neurons even at early time points (Fig. S4). However, if all (affected and unaffected) DJ-1–deficient animals were evaluated together, the total number of DA neurons was not significantly reduced until later aging stages (15 mo). At this time, the unilateral phenotype dissipated and a more bilateral phenotype of nerve cell loss was observed (Fig. 4 *A* and *B* and Table S2). Interestingly, these aged mice, unlike at the earlier times, exhibited a decrease in DA-synthesizing TH-positive striatal terminals (Fig. 4*C*). Upon evaluation of any neuritic beading in these aged animals, we noted that although process length itself did not further change between young and aged DJ1-C57 mice (Fig. S5 *A* and *B*), aged DJ1-C57 mice exhibited a decreased number of sprouting processes in the SNc region (Fig. S5*C*). Moreover, long-term behavior testing revealed a mild motor defect in the aged (14–16 mo) DJ1-C57 mice when examined by both the grid test (Fig. 4*E*) and the pole test (males; Fig. 4*F*).

The neuropathology of PD encompasses degeneration not only of the SNc but also of other nuclei in the brainstem including the *locus ceruleus* (LC) (23). Therefore, LC of DJ1-C57 mice were examined for TH-immunoreactive cell bodies. A significant reduction in TH-positive cells of the LC was observed in aged DJ1-C57 mice compared with WT controls (Fig. 4*D*). Furthermore, because α-synuclein aberrant processing is a hallmark of idiopathic PD, we examined whether our DJ1-C57 mice exhibited altered expression or localization of the protein. No visible changes were noted in the expression of endogenous α-synuclein between DJ1-C57 mice and littermate controls (Fig. S6 *A* and *B*). In addition, upon examination of leucine-rich repeat kinase 2 (LRRK2) expression (another autosomal dominant PD-linked protein), we did not note any significant changes in expression or localization of the protein (Fig. S6*B*).

Finally, to elucidate potential mechanism(s) through which this selective neurodegeneration occurs in a subset of these DJ1-C57 mice, we performed whole-exome sequencing on affected (n = 3) and unaffected (n = 3) DJ-1-C57 mice as an approach to identify candidate modifiers (Fig. 5*A*). After filtering for coding regions and for variants found in all three affected but none of the three unaffected mice, only five candidates in coding regions were

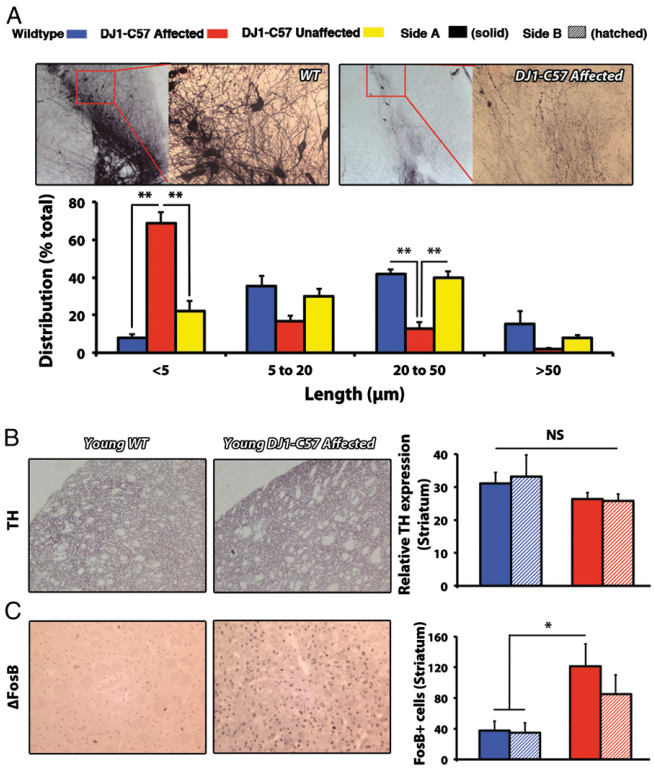

Fig. 2. Widespread process disruption and aberrant striatal innervation in young affected DJ1-C57 mice. (*A*) Fiber sprouting in WT (*Upper Left*) and DJ1-C57 affected animals (*Upper Right*). Distribution of quantified uninterrupted process (TH^+) length in a single vision plain (in microns) is presented (*Lower*). (*B*) Representative sections of striatum stained for ΔFosB in young WT (*Left*) and DJ1-C57 affected (*Center*) mice. (*Right*) Quantification of ΔFosB-positive puncta in the striatum. (*C*) Representative sections of the striatum stained for TH as in *B*. Quantification of striatal TH density is shown (*Right*). WT, DJ1-C57 affected, and DJ1-C57 unaffected are represented by blue, red, and yellow bars, respectively. Side A is depicted as solid shading and side B as hatched shading. NS, not significant ($P > 0.05$); $*P < 0.05$; $**P < 0.01$; ANOVA, followed by Tukey's LSD post hoc tests. Data are represented as means ($n = 3$–11 per group) ± SEM.

identified as potential modifiers of the phenotype [signal regulatory protein β (Sirbp)1A, 2610203C20Rik, zinc finger, SWIM domain containing 6 (Zswim6), kinesin family member (Kif) C5b, and SWI5-dependent recombination repair 1 (Sfr1); Fig. 5*B*]. Moreover, because exome sequencing also covers flanking intronic sequences, an additional 23 candidates were identified in noncoding regions (Table S3), although none of these were in known intron–exon splice sites. Together, these results suggest the segregation of several genomic loci with the phenotype.

Discussion

In our DJ1-C57 mice, we have uncovered an early PD-type phenotype that progressed with age and showed incomplete penetrance. In backcrossing and extensively interbreeding DJ-1–null mice, we obtained a subset of DJ1-C57 mice that exhibited robust unilateral nigral degeneration as early as 8 wk of age: a finding potentially consistent with the early-onset pathogenicity of DJ-1 loss in human carriers of DJ-1 mutations (1). This cell loss was accompanied with compensatory sprouting and the appearance of dysmorphic and beading neurites, as well as microgliosis, a result congruent with the notion that microglia may induce neuritic beading during neuronal dysfunction (24). Furthermore, findings of compensatory sprouting upon cell loss, dysmorphic neurites, and an increase in proinflammatory responses are all present in postmortem samples from PD patients (25–30). Therefore, given the early age of onset of degeneration in these mice, our findings are of particular significance and may correlate with features of autosomal recessive PD. This loss-of-function phenotype has not yet been modeled successfully in rodents, with the possible exception of a partial reduction in LC neurons in one *parkin*$^{-/-}$ mouse model (31).

We also noted that although DJ-1 loss–mediated neurodegeneration will invariably lead to PD in humans, this might not be as dramatic in mice with a relatively short lifespan of ∼24 mo. However, early pathological changes associated with this genetic form of PD are nonetheless observed. Thus, much like preclinical PD, where no clear clinicopathological correlate may be apparent until over 80% of the nigral cell population has been lost, a compensatory mechanism such as neuritic sprouting or postsynaptic sensitization may account for the lack of motor defects in these young animals. Furthermore, the relevance of this model is made even more apparent as the DJ1-C57 mice

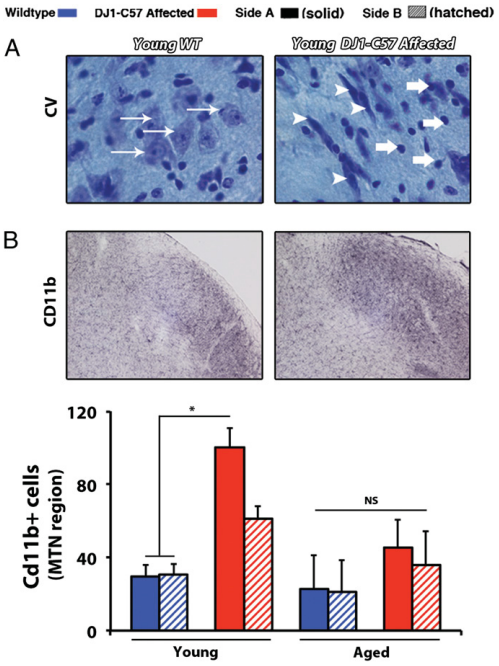

Fig. 3. Focal microgliosis in young affected DJ1-C57 mice. (*A*) Representative midbrain sections stained for CV in young WT and DJ1-C57 affected mice (1000× magnification). Thin arrows denote typical morphology of DA neurons of the SNc; thick arrows denote shrunken, dead nuclei; and arrowheads denote appearance of cells with altered morphology. (*B*) CD11b staining in the midbrain of young WT (*Left*) and DJ1-C57 affected (*Right*) mice was quantified and represented as the number of Cd11b-positive cells in the MTN region of the SNc. WT and DJ1-C57 affected are represented by blue and red bars, respectively. Side A is depicted as solid shading and side B as hatched shading. NS, not significant ($P > 0.05$); *$P < 0.05$; ANOVA, followed by Tukey's LSD post hoc tests. Data are represented as means (n = 3–9 per group) ± SEM.

age. Aged DJ1-C57 mice progressed to bilateral degeneration of their SNc, as well as of their nigrostriatal projections to the forebrain. Thus, this preclinical phenotype likely first occurs at 2 mo and progresses over the course of the following 10–12 mo. In addition, at this older stage, these mice exhibited cell loss at the level of the LC, a pathological characteristic of the human condition. Finally, aged mice beyond 12 mo start to show basal behavioral deficits. Therefore, our DJ1-C57 mouse model presents a potentially important role in filling the gap in our understanding of early-onset preclinical PD in humans.

The reason behind the observed phenotype remains unknown. To begin to explore this issue, we performed whole-exome sequencing to identify potential genes that may contain polymorphisms in affected but not unaffected mice. Surprisingly, the list of genes that met these criteria was limited to five candidates with exon-containing changes. One potential modifier gene candidate, *Sirbp1a*, was particularly interesting given the increase in microglial activation observed in the affected DJ1-C57 mice. SIRBP1A has been associated with a role in promoting phagocytosis in macrophages and monocytes (32). It is possible that disruption of this function may result in aberrant microglial activity. Future studies will seek to elucidate the putative relationship between DJ-1 and SIRBP1A, as well as with other coding modifiers. These exon candidates, although intriguing, are not the only factors that may account for the degenerative phenotype. Other possibilities include intron changes, particularly at loci-flanking

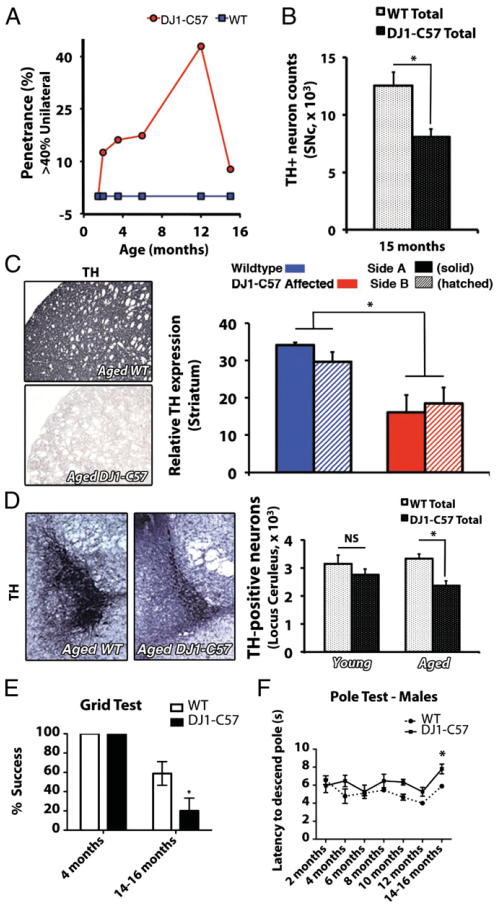

Fig. 4. Aged DJ1-C57 mice exhibit bilateral DA and noradrenergic denervation in the brainstem. (*A*) Penetrance of unilateral phenotype over time. Penetrant threshold: greater than 40% loss of DA neurons on one side (side A) vs. the other (side B). (*B*) Total stereological counts of DA neurons in the SNc of WT and DJ1-C57 aged (15-mo) animals. (*C*) Representative striatal sections of aged (12–15 mo) WT (*Upper Left*) and DJ1-C57 (*Lower Left*) mice stained for TH. Quantification of TH expression in the striatum relative to the *corpus callosum* was performed in young and aged animals (*Right*). (*D*) Representative micrographs of LC sections in the pons stained for TH for either aged WT (*Left*) or aged DJ1-C57 (*Center*). Quantification of TH-positive neurons for both young and aged animals is shown (*Right*). (*E*) The grip test evaluated the capacity of the mouse to stay on an inverted metal grid for 60 s. (*F*) The pole test evaluated the latency of mice to descend a gauze-wrapped pole (in seconds). NS, not significant ($P > 0.05$); *$P < 0.05$; ANOVA, followed by Tukey's LSD post hoc tests. Data are represented as means (n = 3–13 per group) ± SEM.

NEUROSCIENCE

A

Genomic DNA isolation from affected/unaffected DJ1-C57 → Targeted Exome Capture (Agilent SureSelect^{XT}) → Illumina HiSeq2000 Paired end sequencing (2x100bp) → Alignment (C57Bl/6J genome) → Variant Calling (Genome Analysis Toolkit) → Identify Putative Mutations: Segregation by group

B

Gene name	Gene description	Position	Chromosome	Mutation type	Codon	Effect	Amino Acid	Function	Presence	
									Affected (/3)	Unaffected (/3)
Sirpb1a	signal-regulatory protein beta 1A	15,417,016	3	SNP	tCc/tTc	Missense Mutation	S84F	Phagocytosis	3	0
Sirpb1a	signal-regulatory protein beta 1A	15,417,020	3	SNP	Cat/Tat	Missense Mutation	H83Y	Phagocytosis	3	0
2610203C20Rik	RIKEN cDNA 2610203C20 gene	41,389,287	9	SNP	Acc/Ccc	Missense Mutation	T59P	Unknown	3	0
2610203C20Rik	RIKEN cDNA 2610203C20 gene	41,389,294	9	SNP	cAc/cCc	Missense Mutation	H61P	Unknown	3	0
Zswim6	zinc finger, SWIM domain containing 6	108,679,774	13	SNP	gCg/gGg	Missense Mutation	A157G	Unknown	3	0
Kifc5b	kinesin family member C5B	27,061,155	17	SNP	Gtc/Atc	Missense Mutation	V319I	Chromosomal segregation	3	0
Sfr1	SWI5 dependent recombination repair 1	47,807,383	19	SNP	Ccc/Acc	Missense Mutation	P93T	DNA recombination	3	0

Fig. 5. List of exonic variants unique to affected DJ1-C57 mice. (*A*) Schematic workflow of exome sequencing to determine candidate mutations in affected DJ1-C57 mice (vs. unaffected littermate controls). (*B*) Table of variants present in all three examined affected animals and no unaffected littermates. See *Experimental Procedures* for selection criteria.

exons. In this regard, we observed that 23 intronic modifiers segregated with the phenotype. The specific role of these polymorphisms/indels remains unclear, because they do not correspond to splice donor/acceptor sites. Finally, it is possible that a combination of all of these factors may contribute to the phenotype. Therefore, more careful analyses must be performed to examine among these possibilities. What is important, however, is that our studies demonstrate that a defined group of polymorphisms can segregate with our phenotype. How these factors regulate DA loss in DJ-1–deficient mice will require further analyses.

Collectively, we present a murine model that reproduces a clinically detectable phenotype owing to the modification of a PD-related gene. Affected DJ1-C57 mice display: (*i*) unilateral DA cell loss with a predilection for the SNc versus VTA as early as 2 mo of age; (*ii*) development of aberrant neuritic processes with ensuing microgliosis in the SNc and increased ΔFosB staining in the striatum at a young age; and (*iii*) progression to bilateral degeneration of the nigrostriatal axis and of the LC at an older age (model; Fig. 6), which are associated with mild motoric changes. This progression to a bilateral phenotype is of particular interest to us given the typical unilateral-to-bilateral progression of the disease in humans (33). Interestingly, no significant changes were noted in α-synuclein or LRRK2 expression, suggesting a disease process independent of Lewy body generation. These results strongly suggest that this murine model of early parkinsonism mimics autosomal recessive early-onset PD pathology, rather than that of sporadic PD (3). It, thus, provides a tool to elucidate the cascade of pathogenic changes that occurs in autosomal recessive, early-onset PD, as well as a platform to explore neuroprotective interventions in the future.

Experimental Procedures

DJ1-C57 Mouse Creation. DJ-1$^{-/-}$ mice were generated as described previously (9). Mice were subsequently backcrossed 14 times onto a pure C57BL/6J background (Charles River) to obtain DJ1-C57 mice. Animals were then interbred extensively for colony maintenance and experimentation. Animals were kept at 25 °C on a light (12 h)/dark (12 h) cycle with ad libitum access to standard rodent laboratory chow and water. Animal care was carried out in accordance with the guidelines of the Canadian Council and Care of Animals in Research and the Canadian Institutes of Health Research and was approved by the University of Ottawa Animal Care Veterinary Services.

Histology. After being perfused transcardially, mouse brains were fixed in 4% paraformaldehyde and cryoprotected as described elsewhere (34). Midbrain sections containing the SNc (40 μm), pontine sections containing LC (40 μμ), and striatal (14 μm) sections were immunostained via avidin–biotin complex staining as described previously (26).

DA Cell Survival Quantification. DA neuron survival in the SNc was blindly assessed by stereology using Stereo Investigator as described previously (26). Striatal TH quantification was performed at 200×. For each picture, five samples of striatum and one sample of corpus callosum were used for densitometric analysis. Relative intensity of immunodetection was calculated using ImageJ v.1.41o (National Institutes of Health). For each sample, three slices of striatum were used to calculate the mean striatal density.

Neuritic Beading Measurement. Neuritic beading was measured using ImageJ. Briefly, average length of uninterrupted process in a visually focused plane

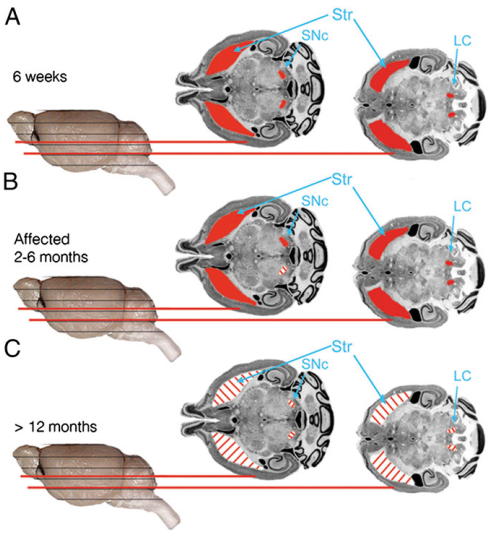

Fig. 6. DJ1-C57 preclinical model of DA neurodegeneration. (*A*) Altered representative micrographs reproduced with permission from the Mouse Brain Library [www.mbl.org; Rosen et al. (36)] depicting healthy (red) SNc, striatum, and LC in 6-wk-old DJ1-C57 mice or all WT groups examined. (*B*) Affected DJ1-C57 mice demonstrate unilateral DA cell loss in the SNc but not in the LC. (*C*) Aged DJ1-C57 mice exhibit widespread degeneration in their nigrostriatal tract, as well as their LC.

was measured as 20 measurements/section and measuring three sections per animal. Raw data were then binned into five categories of length and represented as percentage distribution.

ΔFosB and CD11b Measurement. Striatal (ΔFosB) and midbrain [cluster of differentiation (CD)11b] sections were stained, and three pictures were taken per animal, per side. Puncta in a given visual field were assessed blindly using ImageJ v1.41o.

Locus Ceruleus Neuron Quantification. Noradrenergic cell survival in the LC was measured by counting four representative sections and projecting their counts to a total value as described previously (35).

CV Quantification. CV staining and quantification were performed as described previously (26). Briefly, cell viability in the medial terminal nucleus (MTN) region of the midbrain was assessed as per the nuclear integrity of the cells present.

Antibodies Used. CD11b (1:200; AbD Serotec), FosB (1:250; Santa Cruz Biotechnologies), glial fibrillary acidic protein (GFAP) (1:1,000; Cell Signaling), DJ-1 (1:50,000; Abcam), α-synuclein (1:1,000; BD Transduction), LRRK2 (1:50,000; Epitomics), and TH (1:10,000; Immunostar or 1:2,000; Chemicon) were used for either avidin–biotin complex (ABC) visualization by 3,3′-diaminobenzidine (DAB) or via fluorophore-conjugated secondary antibody.

Motor Behavior Testing. The grid test was carried out by placing DJ1-C57 affected, unaffected, and WT mice on a metal grid (0.5-cm spacing between metal wires) and then turning the grid over for 60 s. If a mouse could hold on for the entire 60 s, it was scored as "success," whereas if it fell before the set time, it was scored as a "fail." The pole test was used to measure the latency to descent an 18-inch pole wrapped in gauze.

Exome Sequencing. Genomic DNA (6 μg) was isolated from ear samples of affected/unaffected mice using the DNeasy Blood and Tissue kit (Qiagen). Samples underwent targeted exome capture using the Agilent SureSelectXT Mouse All Exon kit and subsequently underwent next-generation sequencing via an Illumina HiSeq 2000 sequencer. Raw data were aligned to the mouse genome, and variants were called using the Broad Institute GATK (Genome Analysis ToolKit).

Statistical Analysis. Data throughout the paper are expressed as averages ± SEM for a given sample size (*n*). Statistical analysis for histological and behavioral data were performed by means of either a paired *t* test or one-way ANOVA, followed by Tukey's least significant difference (LSD) post hoc test, as indicated in *SI Text* and the figure legends.

ACKNOWLEDGMENTS. We thank the University of Ottawa Faculty of Medicine Behavior Core Facility for use of their equipment; Daniele Merico (Centre for Applied Genomics, Hospital for Sick Children) for assistance with bioinformatics analysis of the exome data; and Linda Jui, Mirela Hasu, Steve M. Callaghan, Carmen Estey, Elizabeth Abdel-Messih, and Hossein Aleyasin for technical assistance and scientific input. This work was supported by grants from Parkinson Society Canada; the Canadian Institutes of Health Research; the Centres of Excellence in Neurodegeneration (COEN); the Heart and Stroke Foundation of Ontario (HSFO); the Neuroscience Canada/Krembil Foundation; the Parkinson's Disease Foundation; The Michael J. Fox Foundation for Parkinson's Research; the Parkinson Research Consortium (PRC); the Canadian Stroke Network; the Heart and Stroke Foundation of Canada (HSFC) for Stroke Recovery; and the World Class University Program through the National Research Foundation of Korea, funded by Ministry of Education, Science, and Technology, South Korea Grant R31-2008-000-20004-0 (to D.S.P.). D.S.P. is a recipient of the HSFO Career Investigator Award. M.W.C.R. is a recipient of the HSFC Focus on Stroke Award, as well as the Canadian Institutes of Health Research (CIHR) Training Program in Neurodegenerative Lipidomics Supplement Scholarship. P.C.M. is a recipient of The PRC Toth Family Fellowship in Parkinson's Research.

1. Bonifati V, et al. (2003) Mutations in the DJ-1 gene associated with autosomal recessive early-onset parkinsonism. *Science* 299:256–259.
2. Hague S, et al. (2003) Early-onset Parkinson's disease caused by a compound heterozygous DJ-1 mutation. *Ann Neurol* 54:271–274.
3. Kitada T, Tomlinson JJ, Ao HS, Grimes DA, Schlossmacher MG (2012) Considerations regarding the etiology and future treatment of autosomal recessive versus idiopathic Parkinson disease. *Curr Treat Options Neurol* 14:230–240.
4. Ramsey CP, Tsika E, Ischiropoulos H, Giasson BI (2010) DJ-1 deficient mice demonstrate similar vulnerability to pathogenic Ala53Thr human alpha-syn toxicity. *Hum Mol Genet* 19:1425–1437.
5. Andres-Mateos E, et al. (2007) DJ-1 gene deletion reveals that DJ-1 is an atypical peroxiredoxin-like peroxidase. *Proc Natl Acad Sci USA* 104:14807–14812.
6. Chandran JS, et al. (2008) Progressive behavioral deficits in DJ-1-deficient mice are associated with normal nigrostriatal function. *Neurobiol Dis* 29:505–514.
7. Chen L, et al. (2005) Age-dependent motor deficits and dopaminergic dysfunction in DJ-1 null mice. *J Biol Chem* 280:21418–21426.
8. Goldberg MS, et al. (2005) Nigrostriatal dopaminergic deficits and hypokinesia caused by inactivation of the familial Parkinsonism-linked gene DJ-1. *Neuron* 45:489–496.
9. Kim RH, et al. (2005) Hypersensitivity of DJ-1-deficient mice to 1-methyl-4-phenyl-1,2,3,6-tetrahydropyrindine (MPTP) and oxidative stress. *Proc Natl Acad Sci USA* 102:5215–5220.
10. Manning-Boğ AB, et al. (2007) Increased vulnerability of nigrostriatal terminals in DJ-1-deficient mice is mediated by the dopamine transporter. *Neurobiol Dis* 27:141–150.
11. Pham TT, et al. (2010) DJ-1-deficient mice show less TH-positive neurons in the ventral tegmental area and exhibit non-motoric behavioural impairments. *Genes Brain Behav* 9:305–317.
12. Dawson TM, Ko HS, Dawson VL (2010) Genetic animal models of Parkinson's disease. *Neuron* 66:646–661.
13. Parkinson Study Group PRECEPT Investigators (2007) Mixed lineage kinase inhibitor CEP-1347 fails to delay disability in early Parkinson disease. *Neurology* 69:1480–1490.
14. Waldmeier P, Bozyczko-Coyne D, Williams M, Vaught JL (2006) Recent clinical failures in Parkinson's disease with apoptosis inhibitors underline the need for a paradigm shift in drug discovery for neurodegenerative diseases. *Biochem Pharmacol* 72:1197–1206.
15. Snow BJ, et al.; Protect Study Group (2010) A double-blind, placebo-controlled study to assess the mitochondria-targeted antioxidant MitoQ as a disease-modifying therapy in Parkinson's disease. *Mov Disord* 25:1670–1674.
16. Marks WJ, Jr., et al. (2010) Gene delivery of AAV2-neurturin for Parkinson's disease: A double-blind, randomised, controlled trial. *Lancet Neurol* 9:1164–1172.
17. Perl DP (2011) *Neuropathologic Involvement of the Dopaminergic Neuronal Systems in Parkinson's Disease* (Blackwell, Oxford), Chap 2, pp 8–10.
18. Song DD, Haber SN (2000) Striatal responses to partial dopaminergic lesion: Evidence for compensatory sprouting. *J Neurosci* 20:5102–5114.
19. Pritzel M, Huston JP, Sarter M (1983) Behavioral and neuronal reorganization after unilateral substantia nigra lesions: Evidence for increased interhemispheric nigrostriatal projections. *Neuroscience* 9:879–888.
20. Tekumalla PK, et al. (2001) Elevated levels of DeltaFosB and RGS9 in striatum in Parkinson's disease. *Biol Psychiatry* 50:813–816.
21. Doucet JP, et al. (1996) Chronic alterations in dopaminergic neurotransmission produce a persistent elevation of deltaFosB-like protein(s) in both the rodent and primate striatum. *Eur J Neurosci* 8:365–381.
22. Pérez-Otaño I, Mandelzys A, Morgan JI (1998) MPTP-Parkinsonism is accompanied by persistent expression of a delta-FosB-like protein in dopaminergic pathways. *Brain Res Mol Brain Res* 53:41–52.
23. Forno LS, Alvord EC, Jr. (1974) Depigmentation in the nerve cells of the substantia nigra and locus ceruleus in Parkinsonism. *Adv Neurol* 5:195–202.
24. Takeuchi H, et al. (2005) Neuritic beading induced by activated microglia is an early feature of neuronal dysfunction toward neuronal death by inhibition of mitochondrial respiration and axonal transport. *J Biol Chem* 280:10444–10454.
25. Greenwood CE, Tatton WG, Seniuk NA, Biddle FG (1991) Increased dopamine synthesis in aging substantia nigra neurons. *Neurobiol Aging* 12:557–565.
26. Mount MP, et al. (2007) Involvement of interferon-gamma in microglial-mediated loss of dopaminergic neurons. *J Neurosci* 27:3328–3337.
27. Ouchi Y, et al. (2005) Microglial activation and dopamine terminal loss in early Parkinson's disease. *Ann Neurol* 57:168–175.
28. McGeer PL, Itagaki S, Boyes BE, McGeer EG (1988) Reactive microglia are positive for HLA-DR in the substantia nigra of Parkinson's and Alzheimer's disease brains. *Neurology* 38:1285–1291.
29. Whitton PS (2007) Inflammation as a causative factor in the aetiology of Parkinson's disease. *Br J Pharmacol* 150:963–976.
30. Nagatsu T, Sawada M (2005) Inflammatory process in Parkinson's disease: Role for cytokines. *Curr Pharm Des* 11:999–1016.
31. Von Coelln R, et al. (2004) Loss of locus coeruleus neurons and reduced startle in parkin null mice. *Proc Natl Acad Sci USA* 101:10744–10749.
32. Hayashi A, et al. (2004) Positive regulation of phagocytosis by SIRPbeta and its signaling mechanism in macrophages. *J Biol Chem* 279:29450–29460.
33. Pahwa RLK, Koller WC (2003) *Handbook of Parkinson's Disease* (CRC, Boca Raton, FL), 3rd Ed, 597 pp.
34. Crocker SJ, et al. (2001) c-Jun mediates axotomy-induced dopamine neuron death in vivo. *Proc Natl Acad Sci USA* 98:13385–13390.
35. German DC, Liang CL, Manaye KF, Lane K, Sonsalla PK (2000) Pharmacological inactivation of the vesicular monoamine transporter can enhance 1-methyl-4-phenyl-1,2,3,6-tetrahydropyridine-induced neurodegeneration of midbrain dopaminergic neurons, but not locus coeruleus noradrenergic neurons. *Neuroscience* 101:1063–1069.
36. Rosen GD, et al. (2003) Informatics center for mouse genomics: The dissection of complex traits of the nervous system. *Neuroinformatics* 1:327–342.

Supporting Information

Rousseaux et al. 10.1073/pnas.1205102109

SI Experimental Procedures

Additional Motor Behavior. In all behavior tests except for the pole test, mice were habituated to the testing room with white noise for an hour before testing. In the open field test (OFT), mice were placed in the corner of a novel (~45-cm^3) box, and video was analyzed for 10 min. Total distance moved was measured in centimeters. In the rotorod test, mice were placed on an accelerating rotorod, and latency to fall of the rod was measured in seconds. In the beam break test, mice were subjected to a novel cage for 24 h, and total activity (beam breaks) was recorded. All video data were obtained and analyzed with the Noldus Ethnovision 8.0 software. Data analysis was carried out in age-matched littermates for 2, 6, and 12 mo. Amphetamine- and apomorphine-induced rotational behavior was performed in an open field environment (see open field test). Briefly, animals received an i.p. injection of amphetamine (2 mg/kg) or an s.c. injection of apomorphine (2 mg/kg) and were placed in the open field 5 min following the injection. Rotations [clockwise (CW) or counterclockwise (CCW)] were measured, and analysis was carried out post hoc using side A as the presumed affected side to compute net rotations.

Relative Density of Fibers in the SNc. Density of fibers in the SNc was performed using ImageJ. Briefly, pictures originally taken for the beading experiments were taken (at 40×) and subjected to the following processing. Background was reduced by selecting "subtract background" with a rolling ball radius of 15 pixels. Images were then converted into binary format, after which the area occupied by black within the field was measured as an indirect measurement of fiber density in the region of the SNc.

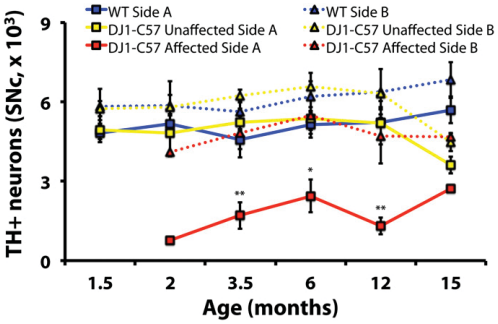

Fig. S1. Unilateral DA cell loss in the SNc of a subset of DJ1-C57 mice as early as 2 mo of age. Stereological counts of TH-positive neurons in midbrain sections from WT and DJ1-C57 mice were performed at various time points. No mice were qualified as affected according to the >40% unilateral criteria in 6-wk-old mice. Each data point represents mean ± SEM (n = 1–37 per data point). $^{**}P < 0.01$ by ANOVA, followed by Tukey's LSD post hoc test.

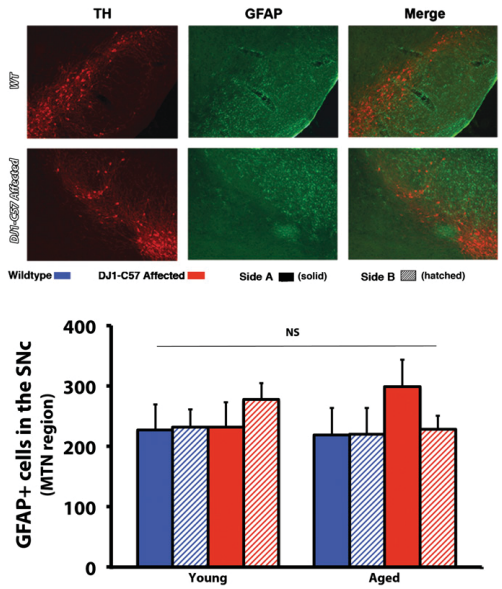

Fig. S2. No visible astrocytic aggregation in affected DJ1-C57 midbrain. (*Upper*) Midbrain sections from young WT ($n = 6$) and DJ1-C57 affected ($n = 6$) (*Left*) or aged WT ($n = 4$) and DJ1-C57 mice ($n = 4$) (*Right*) were costained for GFAP and TH. (*Lower*) GFAP-positive puncta in the SNc (MTN region) were quantified in three representative sections. NS denotes a nonsignificant difference by means of ANOVA.

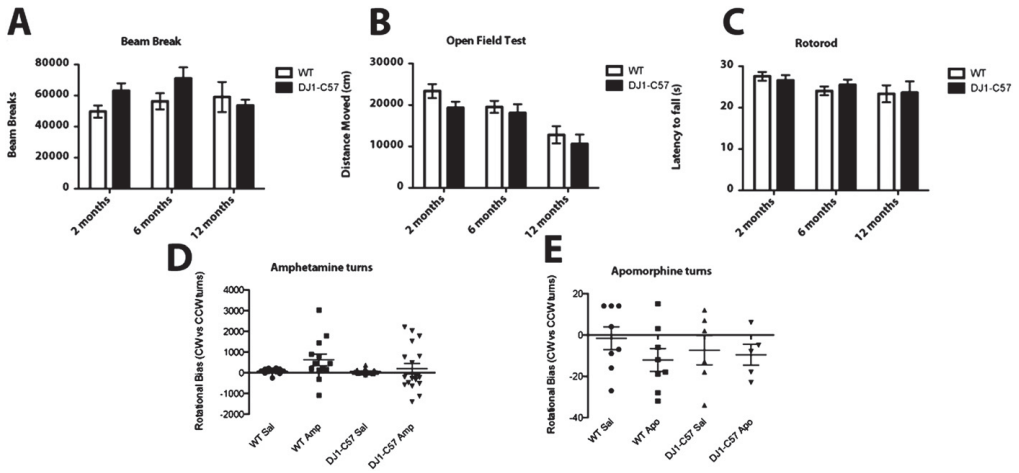

Fig. S3. No visible motor behavior defects in young DJ1-C57 mice. (*A–C*) Littermate DJ1-C57 mice ($n = 15$) and WT ($n = 12$) controls were subjected to motor behavioral testing at 2, 6, and 12 mo. No significant differences were observed in either beam break (*A*), open field test (*B*), or rotorod (*C*). (*D* and *E*) Amphetamine- and apomorphine-induced rotational behavior was also performed at 6 mo. No significant differences in turn number or directionality was observed. Bars represent means ± SEM.

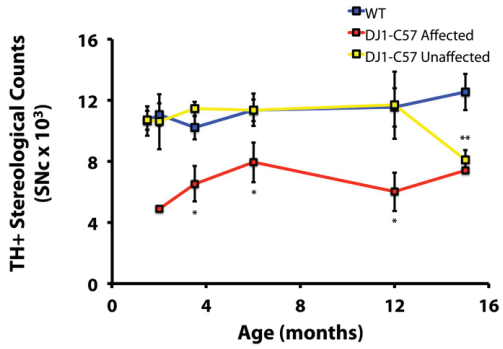

Fig. S4. Bilateral DA cell loss in the SNc of aged DJ1-C57 mice. Stereological counts of TH-positive neurons in midbrain sections from WT and DJ1-C57 mice were performed at various time points. Each data point represents mean ± SEM (n = 1–37 per data point). *P < 0.05; **P < 0.01 by ANOVA, followed by Tukey's LSD post hoc test.

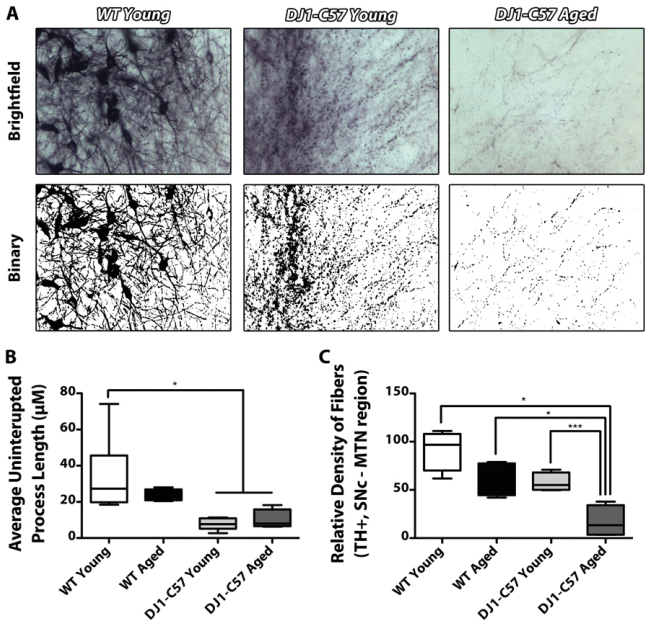

Fig. S5. DJ1-C57 affected mice exhibit neuritic beading in the SNc throughout their lifespan but show a marked decrease in fiber density with age. (*A*) Representative pictures of affected DJ1-C57 mice vs. WT animals. (*B*) Quantification of uninterrupted process length as in Fig. 2*A*. (*C*) Quantification of relative fiber density in the SNc. Each box represents mean ± SEM (n = 4–11 per data point). *P < 0.05; ***P < 0.001 by ANOVA, followed by Tukey's LSD post hoc test.

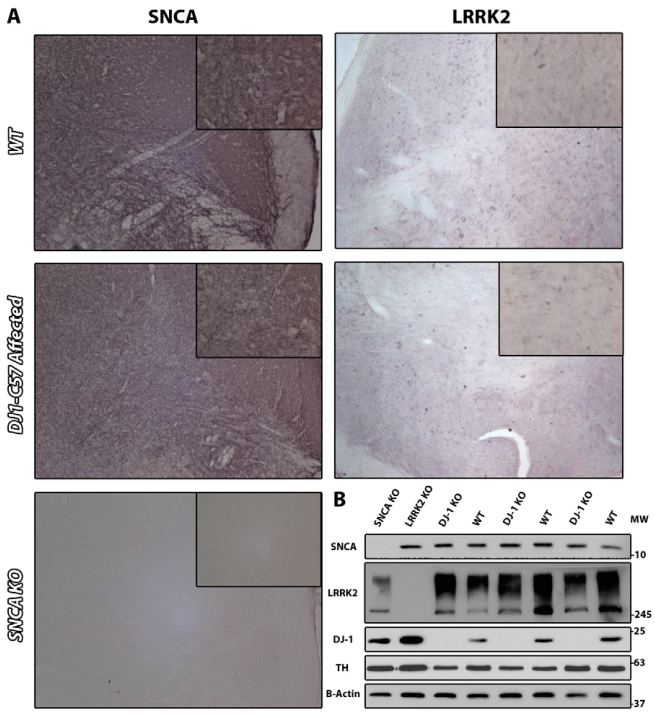

Fig. S6. DJ1-C57 affected mice do not show visible alterations in α-synuclein expression. (*A*) Representative midbrain sections stained for α-synuclein and LRRK2 at the level of the MTN. SNCA KO denotes α-synuclein–null animal tissue. (*B*) Changes in α-synuclein and LRRK2 expression were also determined by Western blot. Striatal punches were taken from SNCA KO, LRRK2 KO, DJ-1 KO, and WT animals to assess expression of α-synuclein and LRRK2, as well as confirm loss of DJ-1, in the brain.

Table S1. Comparison of previously generated DJ-1$^{-/-}$ mice

Gene disruption	Background	Backcross no. (to C57BL/6)	Phenotype	Refs.
ΔExon 2–3	C57BL/6 mixed	1	No gross behavioral or histological phenotype	Andres-Mateos et al. (1)
ΔExon 2	129/Sv/C57BL/6 mixed	1	Mild decrease in motor performance	Chandran et al. (2)
ΔExon 1–5 + promoter	129/C57BL/6 mixed	1	Mild decrease in motor performance; increase in striatal DA and its metabolites	Chen et al. (3)
ΔExon 2	B6/129	1	Mild decrease in motor performance; reduced DA overflow/increased DA reuptake; reduced response to DA	Goldberg et al. (4)
ΔExon 3–5	129/Ola /C57BL/6 mixed	1 (6 for 2 mo MPTP)	No gross unstimulated behavioral or histological phenotype	Kim et al. (5)
Gene trap between exon 6–7	B6/129	1	Subtle locomotor deficit	Manning-Boğ et al. (6)
Gene trap between exon 6–7	129P2/OlaHsd/C57BL/6 mixed	1	Mild decrease of TH^{+} cells in the VTA; mild cognitive impairment	Pham et al. (7)
Gene trap between exon 6–7	129P2/OlaHsd/C57BL/6 mixed	1	No gross behavioral or histological phenotype	Ramsey et al. (8)

A comprehensive search of the literature is presented in this table to note the gross differences between the generation of these knockout animals. Specifically, we note that the number of backcrossings (at least published) remain very low for other DJ-1$^{-/-}$ mice. MPTP, 1-methyl-4-phenyl-1,2,3,6-tetrahydropyrindine. "6 for 2 mo" means six backcrosses for the MPTP study.

1. Andres-Mateos E, et al. (2007) DJ-1 gene deletion reveals that DJ-1 is an atypical peroxiredoxin-like peroxidase. *Proc Natl Acad Sci USA* 104:14807–14812.
2. Chandran JS, et al. (2008) Progressive behavioral deficits in DJ-1-deficient mice are associated with normal nigrostriatal function. *Neurobiol Dis* 29:505–514.
3. Chen L, et al. (2005) Age-dependent motor deficits and dopaminergic dysfunction in DJ-1 null mice. *J Biol Chem* 280:21418–21426.
4. Goldberg MS, et al. (2005) Nigrostriatal dopaminergic deficits and hypokinesia caused by inactivation of the familial Parkinsonism-linked gene DJ-1. *Neuron* 45:489–496.
5. Kim RH, et al. (2005) Hypersensitivity of DJ-1-deficient mice to 1-methyl-4-phenyl-1,2,3,6-tetrahydropyrindine (MPTP) and oxidative stress. *Proc Natl Acad Sci USA* 102:5215–5220.
6. Manning-Boğ AB, et al. (2007) Increased vulnerability of nigrostriatal terminals in DJ-1-deficient mice is mediated by the dopamine transporter. *Neurobiol Dis* 27:141–150.
7. Pham TT, et al. (2010) DJ-1-deficient mice show less TH-positive neurons in the ventral tegmental area and exhibit non-motoric behavioural impairments. *Genes Brain Behav* 9:305–317.
8. Ramsey CP, Tsika E, Ischiropoulos H, Giasson BI (2010) DJ-1 deficient mice demonstrate similar vulnerability to pathogenic Ala53Thr human alpha-syn toxicity. *Hum Mol Genet* 19: 1425–1437.

Table S2. Penetrance of affected phenotype over time in DJ1-C57 and WT mice

Genotype	Age (mo)	Sample size (*n*)	Unilateral phenotype	Penetrance (%)
WT	1.5	5	No	0
	2	9	No	0
	3.5	19	No	0
	6	16	No	0
	12	10	No	0
	15	12	No	0
Total WT	—	71	No	0
DJ1-C57	1.5	8	No	0
	2	8	Yes	12.5
	3.5	37	Yes	16.2
	6	23	Yes	17.4
	12	7	Yes	42.9
	15	13	Yes	7.7
Total DJ1-C57	—	96	Yes	15.6

Penetrance was measured as an animal possessing a greater than 40% loss of neurons on one side of the SNc (side A) vs. the other side (side B). Samples were gathered at 1.5, 2, 3.5, 6, 12, and 15 mo. Sample sizes (*n*) for each group varied from 5 to 37. Only DJ1-C57 animals exhibited the phenotype that begins at 2 mo of age ($n = 15$ penetrant DJ1-C57 vs. $n = 0$ penetrant WT). Dashes represent not applicable.

Table S3. Noncoding putative modifiers that segregate with the DJ1-C57 phenotype

Gene name	Gene description	Position	Chromosome	Mutation type	Location	Genotype	Function	Presence	
								Affected (of 3)	Unaffected (of 3)
Pigt	Phosphatidylinositol glycan anchor biosynthesis, class T	164,332,071	2	Indel	Intron	Het	GPI transfer to proteins	3	0
Sox2	SRY-box containing gene 2	34,549,323	3	SNP	UTR 5′	Het	Transcription factor	3	0
Ptgr1	Prostaglandin reductase 1	58,994,758	4	Indel	Intron	Het	Metabolic inactivation of leukotriene B4	3	0
Gm13150	Predicted gene 13150	146,356,934	4	SNP	Intron	Het	Unknown	3	0
Sri	Sorcin	8,062,470	5	Indel	Intron	Het	Modulates calcium homeostasis by directly binding to it	3	0
RP24-449D6.1	—	15,032,507	5	SNP	Intron	Het	Unknown	3	0
Plxnd1	Plexin D1	115,920,073	6	SNP	Intron	Het	Semaphorin signaling	3	0
Supt5h	Suppressor of Ty 5 homolog (*Saccharomyces cerevisiae*)	29,116,278	7	Indel	Intron	Het	Homolog of "foggy," a zebrafish gene that shows DA degeneration when knocked out; regulates transcriptional elongation	3	0
Myh14	Myosin heavy chain 7B, cardiac muscle β	51,894,551	7	SNP	Intron	Het	Cardiac and skeletal muscle contraction	3	0
Trim30a	Tripartite motif–containing 30A	111,578,560	7	Indel	Intron	Het	Negatively regulates NLRP3 inflammasome activation and reduces ROS formation	3	0
Nucb2	Nucleobindin 2	123,671,348	7	SNP	Intron	Het	Calcium-binding EF-hand protein	3	0
Gm10348	—	20,020,424	8	SNP	Upstream	Het	Unknown	3	0
Thy1	Thymus cell antigen 1θ	43,855,093	9	SNP	Intron	Het	Glycoprotein involved in cell–cell interactions in thymocytes and neurons	3	0
Snora62	Small nucleolar RNA, H/ACA box 62	120,044,385	9	SNP	Downstream	Het	Processing rRNA precursors	3	0
Dgka	Diacylglycerol kinase α	128,160,214	10	SNP	Intron	Het	Phospholipid and TAG synthesis; regulates RAS and RHO	3	0
Kcnip1	Kv channel–interacting protein 1	33,545,464	11	Indel	Intron	Het	Synaptic transmission regulation	3	0
Fam33a	Family with sequence similarity 33, member A	86,929,722	11	SNP	Intron	Het	Chromosomal segregation	3	0
Tecpr2	Tectonin β–propeller repeat containing 2	112,136,799	12	Indel	Intron	Hom	Unknown	3	0
Slc34a1	Solute carrier family 34 (sodium phosphate), member 1	55,504,541	13	Indel	Intron	Het	Sodium-phosphate cotransporter (renal)	3	0
Atp8a2	ATPase, aminophospholipid transporter–like, class I, type 8A, member 2	60,392,606	14	Indel	Intron	Het	Drive uphill transport of ions across membranes	3	0
1110020G09Rik	RIKEN cDNA 1110020G09 gene	9,001,555	15	SNP	Intron	Het	Unknown	3	0
Pdpk1	3-Phosphoinositide–dependent protein kinase 1	24,244,255	17	SNP	Intron	Het	Phosphorylates AKT at Thr308	3	0
Tcte1	t-complex–associated testis expressed 1	45,676,562	17	SNP	Intron	Het	Testes-specific of unclear function	3	0

The table shows variants present in all examined affected animals ($n = 3$) and no unaffected littermates ($n = 3$) as in Fig. 5. See *Experimental Procedures* for selection criteria. AKT, serine/threonine kinase; Het, heterozygous; Hom, homozygous; Kv channel, voltage-gated potassium channel; NLRP3, NLR family, pyrin domain–containing 3; ROS, reactive oxygen species; SRY, sex-determining region Y; TAG, triacylglycerol. Dash represents not defined.

DJ-1 protects the nigrostriatal axis from the neurotoxin MPTP by modulation of the AKT pathway

Hossein Aleyasin[a,1], Maxime W. C. Rousseaux[a,1], Paul C. Marcogliese[a], Sarah J. Hewitt[a], Isabella Irrcher[a], Alvin P. Joselin[a], Mohammad Parsanejad[a], Raymond H. Kim[b], Patrizia Rizzu[c], Steve M. Callaghan[a], Ruth S. Slack[a], Tak W. Mak[b,2], and David S. Park[a,d,2]

[a]Department of Cellular and Molecular Medicine, University of Ottawa, Ottawa, ON K1H 8M5, Canada; [b]Campbell Family Institute for Breast Cancer Research, Toronto, ON M5G 2C1, Canada; [c]Section Medical Genomics, Department of Clinical Genetics, Vrije Universiteit University Medical Center, Van der Boechorststraat 7, 1081 BT, Amsterdam, The Netherlands; and [d]Department of Cogno-Mechatronics Engineering, Pusan National University, Geumjeong GU, Busan 609 735 South Korea

Contributed by Tak Wah Mak, December 24, 2009 (sent for review December 15, 2009)

Loss-of-function DJ-1 (PARK7) mutations have been linked with a familial form of early onset Parkinson disease. Numerous studies have supported the role of DJ-1 in neuronal survival and function. Our initial studies using DJ-1-deficient neurons indicated that DJ-1 specifically protects the neurons against the damage induced by oxidative injury in multiple neuronal types and degenerative experimental paradigms, both in vitro and in vivo. However, the manner by which oxidative stress-induced death is ameliorated by DJ-1 is not completely clear. We now present data that show the involvement of DJ-1 in modulation of AKT, a major neuronal pro-survival pathway induced upon oxidative stress. We provide evidence that DJ-1 promotes AKT phosphorylation in response to oxidative stress induced by H_2O_2 in vitro and in vivo following 1-methyl-4-phenyl-1,2,3,6-tetrahydropyridine (MPTP) treatment. Moreover, we show that DJ-1 is necessary for normal AKT-mediated protective effects, which can be bypassed by expression of a constitutively active form of AKT. Taken together, these data suggest that DJ-1 is crucial for full activation of AKT upon oxidative injury, which serves as one explanation for the protective effects of DJ-1.

neurodegeneration | Parkinson disease | reactive oxygen species

Individuals with homozygous loss-of-function mutations of DJ-1 (PARK7) have been clinically characterized with familial early onset Parkinson disease (PD) (1, 2). Although the physiological role of DJ-1 is not completely understood, several lines of evidence indicate a protective role for DJ-1 in multiple models of neuronal and nonneuronal oxidative stress-induced cell death (3–7). For example, we have previously shown that genetic ablation of DJ-1 in mice hypersensitizes dopamine neurons to the toxic effects induced by the mitochondrial toxin, 1-methyl-4-phenyl-1,2,3,6-tetrahydropyridine (MPTP). This sensitivity was reversed by the induction of virally delivered human DJ-1 (8). These observations are in line with data by other groups showing sensitivity of dopaminergic neurons in DJ-1–deficient *Drosophila* models, as well as increased susceptibility to oxidative stress in vitro (9–11). To further support the importance of DJ-1 in managing oxidative stress, we provided evidence showing that DJ-1 protects the brain against ischemic injury that models clinical stroke. Moreover, our data indicated a direct correlation between DJ-1 neuroprotective activity and the reduced levels of oxidized DNA nucleotide species, 8-oxo guanine, a marker of oxidative damage (12).

Despite the fact that the neuroprotective role of DJ-1 has been consistently shown in multiple models of neurodegeneration, the exact mechanism of the neuroprotective function has not been fully elucidated. A direct antioxidant property of DJ-1 as a reactive oxygen species (ROS) scavenger has been proposed as a mechanism to overcome oxidative stress (7, 13). In fact, recombinant human DJ-1 confers some ROS scavenging activity; however, this activity is much weaker than any known peroxidase, thus not fully explaining its neuroprotective function (10, 13). Several alternative mechanisms to account for the neuroprotective function of DJ-1 have been suggested. For example, via its putative role in transcription regulation (14), DJ-1 up-regulates the expression of other antioxidant genes, such as glutathione synthase, during oxidative stress (15). Interestingly, it has also been reported that DJ-1 enhances the activity of the transcription factor Nrf2, a master regulator of antioxidant genes (16, 17). Alternatively, DJ-1 has also been shown to modulate key signaling pathways (3, 10). One signaling pathway implicated with DJ-1 function and relevant to the present work is AKT (10, 18).

AKT is a member of a larger class of serine/threonine kinases called AGC [protein kinase A (AMP protein kinase), PKG (GMP protein kinase), and PKC]. AKT has an N-terminus pleckstrin homology domain that mediates the interaction of AKT with a plasma membrane phospholipid, phophatidylinositol 3,4,5-triphosphate (PIP3). Extensive studies have shown that recruitment of AKT to the plasma membrane, and its association with PIP3, is crucial for its activation (19, 20). Phosphatase and tensin homolog deleted on chromosome 10 (PTEN) is particularly known for its action to convert PIP3 to phosphatidylinositol-4, 5- biphosphate (PIP2). This function of PTEN directly antagonizes PI3K to eventually down-regulate AKT (21, 22). Several lines of evidence indicated that the AKT signaling pathway responds to oxidative stress (23) and exerts a neuroprotective function (24, 25). Moreover, a large number of studies in vitro have illustrated that pharmacological compounds that protect cells against oxidative stress exert their neuroprotective effects through activation of the AKT pathway (26–30).

Early studies described DJ-1 as a negative regulator of PTEN using a *Drosophila* genetic screen (31). Evidence to confirm this negative regulation was demonstrated via down-regulation of DJ-1 using small interfering RNA, which resulted in the inhibition of endogenous AKT phosphorylation in cancer cell lines as well as in the *Drosophila* brain (10, 31, 32). Furthermore, loss of DJ-1 has been shown to reduce AKT activation in response to hypoxia in murine embryonic fibroblasts (MEFs) (33). However, the relevance of this pathway has yet to be shown in the context of neurons either in vitro or in vivo. Evidence to support a role for DJ-1 in the regulation of the AKT pathway would be particularly important when one considers the genetic linkage of DJ-1 to familial PD. Presently, we provide direct evidence, both in vitro and in vivo, that DJ-1 exerts an important role in the regulation of the AKT pathway in response to oxidative stress and neuronal protection. In

Author contributions: H.A., M.W.C.R., R.H.K., R.S.S., T.W.M., and D.S.P. designed research; H.A., M.W.C.R., P.C.M., S.J.H., I.I., A.P.J., and M.P. performed research; R.H.K., P.R., S.C., R.S.S., and T.W.M. contributed new reagents/analytic tools; H.A., M.W.C.R., P.C.M., S.J.H., A.P.J., M.P., and D.S.P. analyzed data; and H.A., M.W.C.R., I.I., and D.S.P. wrote the paper.

The authors declare no conflict of interest.

Freely available online through the PNAS open access option.

[1]H.A. and M.W.C.R. contributed equally to this work.

[2]To whom correspondence should be addressed. E-mail: dpark@uottawa.ca or tmak@uhnresearch.ca.

This article contains supporting information online at www.pnas.org/cgi/content/full/0914876107/DCSupplemental.

addition, based on our results, we propose a mechanism suggesting that DJ-1 acts as an upstream regulator of AKT through membrane recruitment to confer neuroprotection.

Results

Phosphorylation of AKT in Response to Oxidative Stress Is Reduced in the Absence of DJ-1 in Vitro and in Vivo. To examine the role of DJ-1 on AKT signaling, we first determined whether lack of DJ-1 affects AKT phosphorylation following hydrogen peroxide (H_2O_2) treatment. To test this, neurons harvested from DJ-$1^{-/-}$ or DJ-$1^{+/+}$ embryos were treated with 100-μM H_2O_2 for indicated time points. As demonstrated in Fig. 1*A*, phosphorylation of AKT peaked in wild-type neurons at 15 min, whereas in the knockout there was a reduction in AKT phosphorylation. Quantification of three independent experiments revealed a significant reduction in p-AKT 15 min following treatment (3.67 ± 0.17 in DJ-$1^{+/+}$ vs. 1.49 ± 0.76 in DJ-$1^{-/-}$), as demonstrated in Fig. 1*B*. To further support this observation and to examine this response in a more clinically relevant model of PD, we examined AKT phosphorylation in dopaminergic neurons of the *substantia nigra* (SNc) in response to MPTP treatment. As indicated in Fig. 1*C*, and quantified in Fig. 1*D*, AKT phosphorylation in response to MPTP was reduced in the SNc cells of DJ-$1^{-/-}$ compared to wild-type controls (1.19 ± 0.10 vs. 1.52 ± 0.14, respectively). There was no significant increase in AKT phosphorylation when comparing saline and MPTP treated DJ-$1^{-/-}$ animals (1.00 ± 0.2 vs. 1.19 ± 0.10, respectively). To further confirm these results, we also examined AKT phosphorylation in response to H_2O_2 in human lymphoblasts from human PD patients harboring DJ-1 mutations. As demonstrated in Fig. 1*E*, AKT response was significantly attenuated in L166P mutated cells compared to the controls.

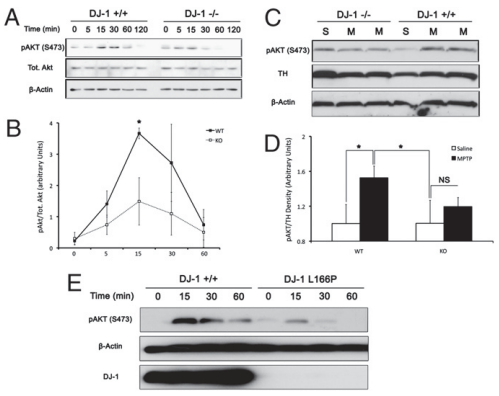

Fig. 1. AKT activation is suppressed in the absence of DJ-1. (*A*) Cortical neurons from DJ-$1^{+/+}$ and DJ-$1^{-/-}$ embryos were harvested, plated, and treated with H_2O_2 (100 μM) in a time-dependent fashion. Extracts were probed for pAKT (S473), total AKT, and β-actin by Western blot. (*B*) Quantification of *A* from three independent experiments. Values are presented as mean optical density relative to total AKT. (*C*) Eight- to 10-week-old C57Bl6 mice of WT and DJ-1 knockout genotype were treated with two 30-mg/kg doses of MPTP (M), or saline (S), given 24 h apart. Three hours following the second injection, mice brains were quickly dissected for SNc and samples were processed for Western blot analysis. (*D*) Quantification of *C*. $n = 3$–6 per group. (*E*) Immortalized lymphoblasts derived from patients with the DJ-1 L166P mutation or healthy control lymphoblasts were treated with H_2O_2 in a time dependant manner. Analysis of cell lysates was carried out by Western blot. Blot presented is representative of two independent experiments. Data are presented as mean ± SEM.

DJ-1 Is Necessary for AKT-Mediated Neuroprotective Function in Vitro and in Vivo. We next evaluated the functional role of DJ-1 in the protective effects of AKT following oxidative stress. First, we examined the role of AKT in protecting neurons against oxidative stress induced by H_2O_2 in vitro. Neurons, transfected with HA-tagged wild-type AKT along with GFP expression vectors as a marker of transfection (or GFP/empty vector transfection as control) were treated with H_2O_2, 24 h after transfection, and survival was assessed as described in *Materials and Methods* (Fig. 2*A*). As shown in Fig. 2*B*, induction of exogenous wild-type AKT confers protection in DJ-$1^{+/+}$ neuronal cells in response to H_2O_2. Next, DJ-$1^{-/-}$ cortical neurons were tested to examine whether induction of wild-type AKT could provide similar protection in DJ-1-deficient cells. Surprisingly, induction of exogenous AKT failed to protect DJ-$1^{-/-}$ neurons against H_2O_2-induced death (Fig. 2*C*). To confirm these observations, we cultured neurons harvested from DJ-$1^{-/-}$ and DJ-$1^{+/+}$ litters at the same time. Three days after plating, the cells were transiently transfected with wild-type AKT together with or without a DJ-1

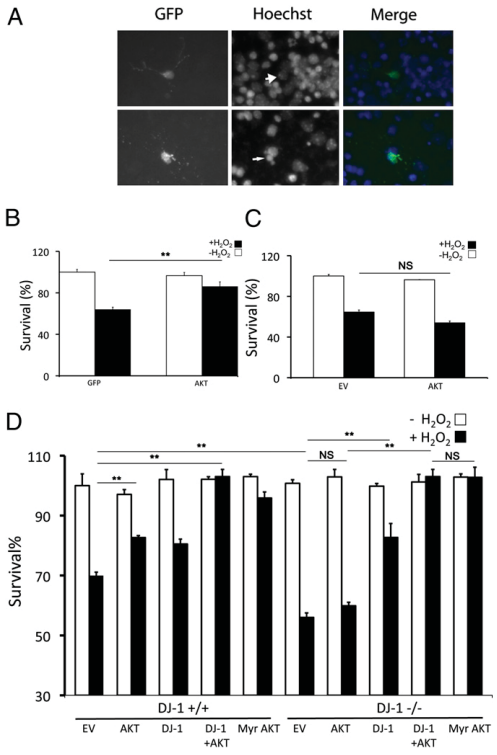

Fig. 2. AKT requires DJ-1 to exert its neuroprotective function in vitro. (*A*) Representative pictures of alive (*Upper*, large arrowhead) and dead (*Lower*, thin arrowhead) neurons. Neuronal survival was measured by identifying GFP-positive cells and determining their nuclear integrity by Hoechst stain. (*B–D*) Cortical neurons from either DJ-$1^{+/+}$ or DJ-$1^{-/-}$ embryos were harvested, plated, and transfected with empty vector (EV), AKT, DJ-1, or Myr AKT. Cells were treated with H_2O_2 (30 μM) or vehicle control ($-H_2O_2$) for 3 h. Quantification was assessed as in *A*. Data are presented as mean ± SEM. **, $P < 0.01$; NS, no significant difference.

expression vector, DJ-1 only, or myristoylated AKT, a membrane-anchored constitutively active form of AKT (34). After treatment with H_2O_2, cell survival was assessed. The results of this experiment clearly verified our findings in Fig. 2*C*, indicating the protective role of wildtype AKT expressed in DJ-$1^{+/+}$ neurons but not in DJ-$1^{-/-}$ cells (82.65 ± 0.65% DJ-$1^{+/+}$ vs. 59.88 ± 1.18% DJ-$1^{-/-}$) (Fig. 2*D*). Interestingly, myristoylated AKT significantly protects neurons against oxidative damage induced by H_2O_2 regardless of DJ-1 genotype (95.85 ± 2.02% DJ-$1^{+/+}$ vs. 102.77 ± 3.38% DJ-$1^{-/-}$).

Suppression of AKT Abolishes the Neuroprotective Function of DJ-1 in Vitro and in Vivo. The observations that DJ-1 deficiency reduces AKT activation and that wild-type AKT requires DJ-1 to effectively protect neurons against oxidative stress suggests DJ-1 acts as an upstream activator of AKT. We next determined whether DJ-1 exerts its neuroprotective effects, at least partially, through the AKT pathway. To examine this, we first used a conventional pharmacological inhibitor of AKT, LY294002 (LY) (35). Because the basal activity of AKT is essential for the long-term health of cultured neurons, we determined the optimal dose of inhibitor that suppressed AKT with minimal toxicity to the cultured neurons (Fig. 3*A*). We next infected cultured cortical neurons with adenoviral vectors expressing GFP only or DJ-1 and GFP on separate promoters at the time of plating. Thirty-six hours after plating, we pretreated the cells with 10-μM LY or vehicle for 30 min before application of H_2O_2 or vehicle for 3 h. Cells were then assessed for survival. As shown in Fig. 3*B*, the neuroprotective activity of DJ-1 is significantly reduced upon suppression of AKT phosphorylation by LY (52.78 ± 0.20% vs. 40.55 ± 0.55%, respectively). We also used a more specific molecular strategy to validate our results by transiently transfecting a phosphorylation mutant, dominant-negative form (DN-AKT) of AKT (AAA-AKT) into cortical neurons. In this mutant, all phosphorylation sites of AKT have been mutated to alanine; therefore, this artificial mutant of AKT is incapable of being phosphorylated and displays dominant-negative properties toward endogenous AKT (21). As shown in Fig. 3*C*, the results of this experiment confirmed that suppression of AKT diminished the neuroprotective function of DJ-1 (84.46 ± 2.90% without DN-AKT vs. 59.26 ± 2.01% with DN-AKT).

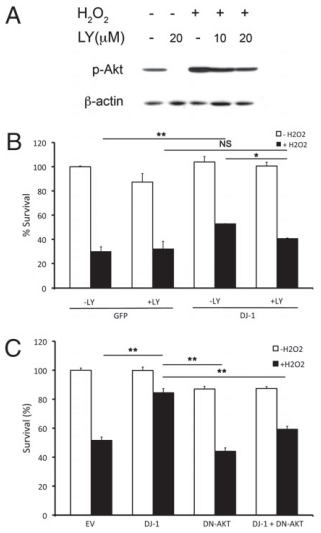

Fig. 3. DJ-1 requires AKT activation to promote cellular survival in vitro. (*A*) Cortical neurons were treated for either 10 or 20 μM of LY with and without H_2O_2 (100 μM, 15 min) to determine the effective dose of LY. (*B*) Cortical neurons were infected with either GFP or DJ-1 with GFP. Cells were then pretreated with LY followed by H_2O_2 treatment for survival assessment. (*C*) Cortical neurons were cotransfected with GFP and empty vector (EV), DJ-1, DN-AKT, or a DJ-1/DN-AKT combination followed by H2O2 treatment. Survival was assessed as in *B*. Data are presented as mean ± SEM. *, $P < 0.05$; **, $P < 0.01$; NS, no significant difference.

DJ-1 Is Necessary for AKT-Mediated Neuroprotection in Vivo Following MPTP Treatment. In vitro experiments indicated that DJ-1 is necessary for AKT activation and is neuroprotective in response to H_2O_2. To confirm these results and to test this hypothesis in a more clinically relevant paradigm, we examined whether induction of wild-type AKT can protect nigrostriatal neurons against the dopaminergic specific neurotoxin MPTP in vivo. To achieve this, we injected adenoviral vectors harboring HA-tagged wild-type AKT or myristoylated AKT into the striatum of DJ-$1^{+/+}$ and DJ-$1^{-/-}$ age-matched mice. β-gal expressing adenoviruses

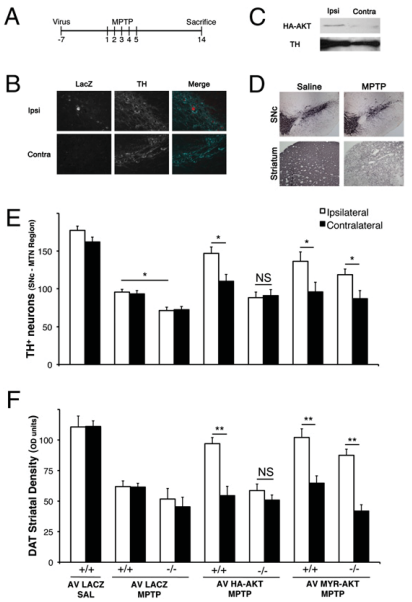

Fig. 4. AKT requires DJ-1 to exert its neuroprotective function in an in vivo model of PD. (*A*) Schematic representation of treatment course. Mice were injected ipsilaterally in the striatum with adenovirus (LacZ, HA-AKT, Myr-AKT) 7 d before commencement of MPTP injections. MPTP was injected for 5 consecutive days and brains were collected 14 days following the first MPTP injection. (*B*) Confirmation of virus expression was performed by immunohistochemistry. Dual labeling of both TH and protein of interest in the SNc. (*C*) HA expression was tested in the SNc by Western blot analysis. (*D*) Representative pictures of both striatum and SNc of mice treated with MPTP or saline. SNc and striatum were stained for TH and DAT, respectively. (*E*) Quantification of TH-immunoreactive neurons was performed at the MTN region of the SNc where virus expression was highest. "Ipsi" denotes the side of the brain ipsilateral to the virus injection, whereas "contra" denotes the contralateral side. (*F*) Quantification of DAT-positive fibers normalized to cortex (DAT-negative). Data are presented as mean ± SEM. *, $P < 0.05$; **, $P < 0.01$; NS, no significant difference.

were used as control. As shown in Fig. 4 *B* and *C*, the virus localizes specifically to the ipsilateral side in dopamine neurons. One week after virus injection, we performed a subchronic MPTP treatment paradigm as indicated in Fig. 4*A*. Two weeks after the initial MPTP injection, animals in all groups were sacrificed and prepared for histological analysis. We first assessed survival by counting the number TH+ neurons of SNc at the level of the medial terminal nucleus (MTN) (Fig. 4*E*). Consistent with our in vitro observations, DJ-$1^{+/+}$ animals that received wild-type HA-tagged AKT and were subjected to MPTP treatments showed larger number of surviving TH+ neurons in the ipsilateral side of virus injection, compared to the contralateral side (146.9 ± 8.5 vs. 109.9 ± 9.2, respectively). Meanwhile, there was no significant difference between ipsi- and contralateral sides of the SNc in the knockout animals that received HA-AKT. (88.2 ± 7.4 vs. 90.9 ± 8.0, respectively). To verify whether the loss of TH immunoreactivity was in fact a result of the death of dopaminergic neurons and not loss of expression, we stained for cresyl violet and assessed neuronal survival in the MTN region of the SNc. Similarly, a substantial rescue was observed in the wild-type mice (62.8 ± 1.9% vs. 50.7 ± 3.0%, ipsilateral vs. contralateral), whereas no protective effect was observed when injecting HA-AKT in the DJ-$1^{-/-}$ mice (48.9 ± 3.0% vs. 51.9 ± 4.0% ipsilateral vs. contralateral) (Fig. S1). To further substantiate the SNc neuronal survival results, we examined whether prophylactic administration of virus could rescue dopaminergic terminals in the striatum of the animals subjected to MPTP injection in each group using expression of dopamine transporter (DAT) as a marker of dopaminergic terminals. Consistent with SNc results, higher densities, and thus greater survival of dopaminergic terminals, were observed following MPTP treatment in the striatum of virus-injected sides compared to the contralateral sides in the AKT-expressing group (97.0 ± 5.0 vs. 54.5 ± 7.6 for HA-AKT, respectively) (Fig. 4*F*). Such protection was not observed in DJ-$1^{-/-}$ animals, which signifies that the AKT-mediated neuroprotection is dependent upon the presence of DJ-1. In line with our observations in vitro and in vivo, myristoylated AKT (Myr-AKT) provides protection to both DJ-$1^{-/-}$ and DJ-$1^{+/+}$ animals (87.5 ± 5.0 ipsilateral vs. 41.9 ± 5.2 contralateral, and 102.0 ± 7.1 ipsilateral vs. 64.7 ± 6.0 contralateral, respectively). All viruses were also injected without MPTP treatment to note effects of virus toxicity. No significant death of SNc neurons was attributed to viral vectors.

DJ-1 Modulates AKT Translocation to Membranous Fractions. Our results in vitro and in vivo demonstrated specifically that myristoylated rather than a wild-type form of AKT promotes protection in DJ-$1^{-/-}$ neurons. We therefore tested whether DJ-1 was affecting AKT translocation to membranous compartments following oxidative stress. This was done by determining the subcellular localization of AKT following H_2O_2 treatment in DJ-$1^{+/+}$ and DJ-$1^{-/-}$ neurons and MEFs. As shown in Fig. 5*A*, the H_2O_2-induced AKT localization to the membrane fraction is greatly decreased in the DJ-$1^{-/-}$ compared with the DJ-$1^{+/+}$ MEFs. Quantification revealed AKT translocation to the membrane fraction following treatment that was 4-fold greater in the DJ-$1^{+/+}$ than in DJ-$1^{-/-}$ cells (2.94 ± 1.14 vs. 0.78 ± 0.30, respectively). Similarly, in DJ-$1^{-/-}$ neurons, no AKT translocation was observed following H_2O_2 (0.58 ± 0.10-fold increase), whereas DJ-$1^{+/+}$ neurons showed an AKT translocation 5 min post-treatment (1.55 ± 0.37 fold increase) No significant differences were observed in levels of total AKT in the cytoplasmic fraction.

Discussion

DJ-1 was first discovered as a weak oncogene with an unclear mechanism of action (36). Since then, putative roles for DJ-1 have been proposed, which include functions in transcriptional regulation either via binding to and modulating an androgen receptor inhibitor, PIASx-alpha (37), as well as RNA–protein

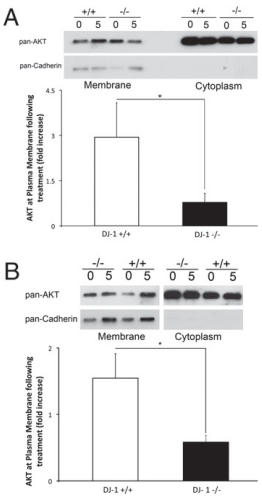

Fig. 5. AKT requires DJ-1 to localize to membranous fractions following oxidative insult. (*A*) DJ-$1^{+/+}$ and DJ-$1^{-/-}$ MEFs were treated with 500 μM of H_2O_2 for 5 min or with media control. Western blot analysis by probing pan-AKT and pan-Cadherin as membranous fraction control. Quantification of membranous fractions was performed in the lower panel by calculating relative AKT density normalized to Cadherin levels and normalizing treatment group to control. Data are representative of $n = 4$ experiments. (*B*) DJ-$1^{+/+}$ and DJ-$1^{-/-}$ cortical neurons were subjected to 100 μM of H_2O_2 for 5 min or media control. Quantification was performed as in *A*. Data are presented as mean ± SEM. *, $P < 0.05$.

interactions (38). The DJ-1 protein also displayed some homology to the proteins of the ThiJ/PfpI family of bacterial proteases (39, 40), suggesting a putative chaperone function. Interestingly, DJ-1 was also noted to display an isoelectric pH shift upon induction of oxidative stress, potentially placing DJ-1 within the oxidative stress-response pathway. Despite these important implications, its physiological relevance was not entirely clear until its genetic linkage to PD. To this end, several themes regarding DJ-1 have now emerged that link this protein to neurodegeneration, PD, and oxidative stress. These themes include, but are not limited to the following: (*i*) DJ-1 protects neurons against oxidative stress (4, 9, 11, 41–44); (*ii*) Loss of DJ-1 on its own does not lead to dopamine neuron death, at least in mice, but DJ-1-deficient animals are sensitized to environmental stress and exhibit impaired dopamine signaling (45–48); and (*iii*) DJ-1 modulates signaling pathways critical to cell survival such as PTEN and AKT, at least in select nonneuronal contexts (31).

In the present study, we more carefully characterized the necessity of DJ-1 for activation of the AKT pathway in response to oxidative injury, particularly in neurons. We first demonstrated that the absence of DJ-1 significantly attenuates AKT phosphorylation in vitro and in vivo, as well as in human lymphoblasts derived from PD patients harboring pathogenic DJ-1 mutations. Importantly, even though AKT phosphorylation is not completely abolished by loss of DJ-1, we also demonstrated that the significant attenuation in AKT signaling brought about by DJ-1 deficiency resulted in enhanced cell death both in vitro and in vivo. These data not only highlighted an important functional role for DJ-1 in AKT-mediated cell survival, but also indicated that the AKT pathway is integral to the mechanism of protection conferred by DJ-1 and suggested that DJ-1 could be an upstream regulator of AKT.

In light of our findings above, together with the knowledge that AKT is considered to be part of the survival pathway, we sought to further investigate the nature of the DJ-1/AKT relationship. We first demonstrated that overexpression of AKT alone protects cultured neurons exposed to oxidative stress in vitro as well as dopamine neurons exposed to MPTP in vivo. Furthermore, inhibition of the PI3K/Akt pathway significantly reduces the protection that is conferred by DJ-1. Importantly, we also demonstrated that wild-type AKT required DJ-1 to exert its protective effect as DJ-1 deficiency abrogated the effect of AKT on cell survival. Interestingly, the protective effects of AKT in a DJ-1-deficient background can be bypassed using myristoylated AKT, its membrane-anchored constitutively active form. This latter observation is consistent with reports that membrane-bound AKT is sufficient to provide protection following MPP^+ treatment both in vitro (49) as well as 6-OHDA treatment in vivo (50). Because AKT recruitment to the membrane is a prior event to its phosphorylation and activation (51, 52), these results, in addition to the cell fractionation experiments presented in our study, suggested that DJ-1 permits AKT translocation to the membrane fractions.

Our study therefore proposes a working model in which DJ-1 acts upstream of AKT, thereby facilitating its activation following neuronal injury via oxidative stress. We propose that DJ-1 may be involved in fine-tuning the response of neurons to ROS and modulation of signaling pathways that mediate survival. In this regard, it will be critical in future studies to address the possible mechanisms underlying the ROS-mediated, DJ-1-dependent activation of AKT. One might consider the possibility that DJ-1 regulates AKT by modulating its recruitment to the membrane in a ROS-dependent manner. It is noteworthy that the AKT response to H_2O_2 can be altered depending on antioxidant protein activity within the cell (53–55). Thus, further studies in models that permit well-controlled ROS levels are needed to address these questions. However, other possibilities exist. For example, a recent study has suggested that DJ-1 interacts with PTEN to permit AKT activation, although this needs to be further investigated in more physiologically relevant models (56). Additionally, DJ-1 may interact with other PI3K pathway kinases, such as mTOR and PDK, to permit AKT phosphorylation. Finally, while DJ-1 plays a significant role in facilitating AKT phosphorylation, other factors may also each play a role (21, 57, 58). Thus, additional studies should be performed to investigate the nature of the DJ-1/AKT interdependence.

Finally, it is interesting to note that even though it is clear that DJ-1 is linked to familial PD, there is a report of an epidemiological association with certain haplotype of AKT1 and a reduced risk of PD (59). This observation provides further strength to the notion that the DJ-1/AKT signaling axis may be important in regulating dopaminergic function or death. Elucidation of these mechanisms may provide an eventual basis for neuroprotective therapies.

Materials and Methods

Cell culture, Western blot analysis, and in vivo stereotaxic injections and MPTP administration were performed as previously described (60). All procedures involving animals were approved by the University of Ottawa Animal Care Committee and were maintained in strict accordance with the Guidelines for the Use and Treatment of Animals put forth by the Animal Care Council of Canada and endorsed by the Canadian Institutes of Health Research. For additional in vivo and in vitro procedures, see *SI Materials and Methods.*

Subcellular Fractionation. Membrane fractions were obtained similarly for MEFs and DIV 6 cortical neurons using differential centrifugation. Briefly, cells were harvested in cold PBS and centrifuged at 1,200 × *g* for 3 min. The cell pellet was resuspended in 200 μL of hypo-osmolar buffer [50 mM Tris-HCl, pH 7.4; 50 mM NaCl; protease inhibitor complex (Roche)] and homogenized for 30 s. Samples were centrifuged at 20,000 × *g*, at 4 °C for 20 min. Supernatants (cellular debris) were transferred to 1.5-mL ultracentrifuge tubes (Beckman) and centrifuged at 100,000 × *g*, at 4 °C for 3 h. The pellets (microsomal enriched) were resuspended in RIPA buffer (150 mM NaCl; 1% Nonidet P-40; 0.5% deoxycholic acid; 0.1% SDS; 50 mM Tris-HCl, pH 8.0) and sonicated briefly for subsequent Western blot analysis. Supernatants from final spin were used as a cytoplasmic control.

Statistical Analysis. Statistical significance was either determined by Student's *t*-test or one-way ANOVA followed by Tukey's post hoc test. All data are presented as mean ± SEM. Significance at $P < 0.05$ (*) and $P < 0.01$ (**), and NS denotes no significant difference.

ACKNOWLEDGMENTS. This work was supported by grants from Canadian Institutes of Health Research, Heart and Stroke Foundation of Ontario, the Canadian Stroke Network, The Centre for Stroke Recovery, Parkinson Society Canada, and Parkinson's Disease Foundation (to D.S.P), Heart and Stroke Foundation of Canada (to H.A.), Heart and Stroke Foundation of Ontario (to M.W.C.R.), Canadian Institutes of Health Research (to I.I.), and the Parkinson Society Canada (to S.J.H.), and the World Class University program through the National Research Foundation of Korea (Grant R31-2008-000-20004-0). Adenoviral constructs were provided by Dr. J. Albrecht at the Hennepin County Medical Center (Minneapolis, MN).

1. Bonifati V, et al. (2003) Mutations in the DJ-1 gene associated with autosomal recessive early-onset parkinsonism. *Science* 299:256–259.
2. Abou-Sleiman PM, Healy DG, Quinn N, Lees AJ, Wood NW (2003) The role of pathogenic DJ-1 mutations in Parkinson's disease. *Ann Neurol* 54:283–286.
3. Gu L, et al. (2009) Involvement of ERK1/2 signaling pathway in DJ-1-induced neuroprotection against oxidative stress. *Biochem Biophys Res Commun* 383:469–474.
4. Inden M, et al. (2006) PARK7 DJ-1 protects against degeneration of nigral dopaminergic neurons in Parkinson's disease rat model. *Neurobiol Dis* 24:144–158.
5. Lev N, et al. (2009) DJ-1 protects against dopamine toxicity. *J Neural Transm* 116: 151–160.
6. Canet-Avilés RM, et al. (2004) The Parkinson's disease protein DJ-1 is neuroprotective due to cysteine-sulfinic acid-driven mitochondrial localization. *Proc Natl Acad Sci USA* 101:9103–9108.
7. Taira T, et al. (2004) DJ-1 has a role in antioxidative stress to prevent cell death. *EMBO Rep* 5:213–218.
8. Kim RH, et al. (2005) Hypersensitivity of DJ-1-deficient mice to 1-methyl-4-phenyl-1,2,3,6-tetrahydropyrindine (MPTP) and oxidative stress. *Proc Natl Acad Sci USA* 102:5215–5220.
9. Lavara-Culebras E, Paricio N (2007) *Drosophila* DJ-1 mutants are sensitive to oxidative stress and show reduced lifespan and motor deficits. *Gene* 400:158–165.
10. Yang Y, et al. (2005) Inactivation of *Drosophila* DJ-1 leads to impairments of oxidative stress response and phosphatidylinositol 3-kinase/Akt signaling. *Proc Natl Acad Sci USA* 102:13670–13675.
11. Martinat C, et al. (2004) Sensitivity to oxidative stress in DJ-1-deficient dopamine neurons: an ES- derived cell model of primary Parkinsonism. *PLoS Biol* 2:e327.
12. Aleyasin H, et al. (2007) The Parkinson's disease gene DJ-1 is also a key regulator of stroke-induced damage. *Proc Natl Acad Sci USA* 104:18748–18753.
13. Andres-Mateos E, et al. (2007) DJ-1 gene deletion reveals that DJ-1 is an atypical peroxiredoxin-like peroxidase. *Proc Natl Acad Sci USA* 104:14807–14812.
14. Xu J, et al. (2005) The Parkinson's disease-associated DJ-1 protein is a transcriptional co-activator that protects against neuronal apoptosis. *Hum Mol Genet* 14:1231–1241.
15. Zhou W, Freed CR (2005) DJ-1 up-regulates glutathione synthesis during oxidative stress and inhibits A53T alpha-synuclein toxicity. *J Biol Chem* 280:43150–43158.
16. Malhotra D, et al. (2008) Decline in NRF2-regulated antioxidants in chronic obstructive pulmonary disease lungs due to loss of its positive regulator, DJ-1. *Am J Respir Crit Care Med* 178:592–604.
17. Clements CM, McNally RS, Conti BJ, Mak TW, Ting JP (2006) DJ-1, a cancer- and Parkinson's disease-associated protein, stabilizes the antioxidant transcriptional master regulator Nrf2. *Proc Natl Acad Sci USA* 103:15091–15096.
18. van der Brug MP, et al. (2008) RNA binding activity of the recessive Parkinsonism protein DJ-1 supports involvement in multiple cellular pathways. *Proc Natl Acad Sci USA* 105:10244–10249.
19. Klippel A, Kavanaugh WM, Pot D, Williams LT (1997) A specific product of phosphatidylinositol 3-kinase directly activates the protein kinase Akt through its pleckstrin homology domain. *Mol Cell Biol* 17:338–344.
20. Kohn AD, Takeuchi F, Roth RA (1996) Akt, a pleckstrin homology domain containing kinase, is activated primarily by phosphorylation. *J Biol Chem* 271:21920–21926.
21. Stambolic V, et al. (1998) Negative regulation of PKB/Akt-dependent cell survival by the tumor suppressor PTEN. *Cell* 95:29–39.
22. Sun H, et al. (1999) PTEN modulates cell cycle progression and cell survival by regulating phosphatidylinositol 3,4,5,-trisphosphate and Akt/protein kinase B signaling pathway. *Proc Natl Acad Sci USA* 96:6199–6204.
23. Crossthwaite AJ, Hasan S, Williams RJ (2002) Hydrogen peroxide-mediated phosphorylation of ERK1/2, Akt/PKB and JNK in cortical neurones: dependence on Ca(2+) and PI3-kinase. *J Neurochem* 80:24–35.
24. Sun X, et al. (2009) Insulin/PI3K signaling protects dentate neurons from oxygen-glucose deprivation in organotypic slice cultures. *J Neurochem*112:377–388.

25. Lee HJ, Kim MK, Kim HJ, Kim SU (2009) Human neural stem cells genetically modified to overexpress Akt1 provide neuroprotection and functional improvement in mouse stroke model. *PLoS One* 4:e5586.
26. Li Z, Hu Y, Zhu Q, Zhu J (2008) Neurotrophin-3 reduces apoptosis induced by 6-OHDA in PC12 cells through Akt signaling pathway. *Int J Dev Neurosci* 26:635–640.
27. Dudek H, et al. (1997) Regulation of neuronal survival by the serine-threonine protein kinase Akt. *Science* 275:661–665.
28. Malagelada C, Jin ZH, Greene LA (2008) RTP801 is induced in Parkinson's disease and mediates neuron death by inhibiting Akt phosphorylation/activation. *J Neurosci* 28: 14363–14371.
29. Heo SR, Han AM, Kwon YK, Joung I (2009) p62 protects SH-SY5Y neuroblastoma cells against H2O2-induced injury through the PDK1/Akt pathway. *Neurosci Lett* 450: 45–50.
30. Liu JH, Yin F, Guo LX, Deng XH, Hu YH (2009) Neuroprotection of geniposide against hydrogen peroxide induced PC12 cells injury: involvement of PI3 kinase signal pathway. *Acta Pharmacol Sin* 30:159–165.
31. Kim RH, et al. (2005) DJ-1, a novel regulator of the tumor suppressor PTEN. *Cancer Cell* 7:263–273.
32. Sitaram RT, et al. (2009) The PTEN regulator DJ-1 is associated with hTERT expression in clear cell renal cell carcinoma. *Int J Cancer* 125:783–790.
33. Vasseur S, et al. (2009) DJ-1/PARK7 is an important mediator of hypoxia-induced cellular responses. *Proc Natl Acad Sci USA* 106:1111–1116.
34. Meier R, Alessi DR, Cron P, Andjelković M, Hemmings BA (1997) Mitogenic activation, phosphorylation, and nuclear translocation of protein kinase Bbeta. *J Biol Chem* 272: 30491–30497.
35. Taylor JM, et al. (2004) Akt phosphorylation and NFkappaB activation are counterregulated under conditions of oxidative stress. *Exp Cell Res* 300:463–475.
36. Nagakubo D, et al. (1997) DJ-1, a novel oncogene which transforms mouse NIH3T3 cells in cooperation with ras. *Biochem Biophys Res Commun* 231:509–513.
37. Takahashi K, et al. (2001) DJ-1 positively regulates the androgen receptor by impairing the binding of PIASx alpha to the receptor. *J Biol Chem* 276:37556–37563.
38. Hod Y, Pentyala SN, Whyard TC, El-Maghrabi MR (1999) Identification and characterization of a novel protein that regulates RNA-protein interaction. *J Cell Biochem* 72:435–444.
39. Mitsumoto A, et al. (2001) Oxidized forms of peroxiredoxins and DJ-1 on two-dimensional gels increased in response to sublethal levels of paraquat. *Free Radic Res* 35:301–310.
40. Wilson MA, St Amour CV, Collins JL, Ringe D, Petsko GA (2004) The 1.8-A resolution crystal structure of YDR533Cp from *Saccharomyces cerevisiae*: a member of the DJ-1/ThiJ/PfpI superfamily. *Proc Natl Acad Sci USA* 101:1531–1536.
41. Liu M, et al. (2008) Parkin regulates Eg5 expression by Hsp70 ubiquitination-dependent inactivation of c-Jun NH2-terminal kinase. *J Biol Chem* 283:35783–35788.
42. Paterna JC, Leng A, Weber E, Feldon J, Büeler H (2007) DJ-1 and Parkin modulate dopamine-dependent behavior and inhibit MPTP-induced nigral dopamine neuron loss in mice. *Mol Ther* 15:698–704.
43. Meulener M, et al. (2005) *Drosophila* DJ-1 mutants are selectively sensitive to environmental toxins associated with Parkinson's disease. *Curr Biol* 15:1572–1577.
44. Yokota T, et al. (2003) Down regulation of DJ-1 enhances cell death by oxidative stress, ER stress, and proteasome inhibition. *Biochem Biophys Res Commun* 312: 1342–1348.
45. Yamaguchi H, Shen J (2007) Absence of dopaminergic neuronal degeneration and oxidative damage in aged DJ-1-deficient mice. *Mol Neurodegener* 2:10.
46. Pisani A, et al. (2006) Enhanced sensitivity of DJ-1-deficient dopaminergic neurons to energy metabolism impairment: role of Na+/K+ ATPase. *Neurobiol Dis* 23:54–60.
47. Park J, et al. (2005) *Drosophila* DJ-1 mutants show oxidative stress-sensitive locomotive dysfunction. *Gene* 361:133–139.
48. Goldberg MS, et al. (2005) Nigrostriatal dopaminergic deficits and hypokinesia caused by inactivation of the familial Parkinsonism-linked gene DJ-1. *Neuron* 45:489–496.
49. Salinas M, Martín D, Alvarez A, Cuadrado A (2001) Akt1/PKBalpha protects PC12 cells against the parkinsonism-inducing neurotoxin 1-methyl-4-phenylpyridinium and reduces the levels of oxygen-free radicals. *Mol Cell Neurosci* 17:67–77.
50. Ries V, et al. (2006) Oncoprotein Akt/PKB induces trophic effects in murine models of Parkinson's disease. *Proc Natl Acad Sci USA* 103:18757–18762.
51. James SR, et al. (1996) Specific binding of the Akt-1 protein kinase to phosphatidylinositol 3,4,5-trisphosphate without subsequent activation. *Biochem J* 315:709–713.
52. Franke TF, Kaplan DR, Cantley LC, Toker A (1997) Direct regulation of the Akt proto-oncogene product by phosphatidylinositol-3,4-bisphosphate. *Science* 275:665–668.
53. Taylor JM, Ali U, Iannello RC, Hertzog P, Crack PJ (2005) Diminished Akt phosphorylation in neurons lacking glutathione peroxidase-1 (Gpx1) leads to increased susceptibility to oxidative stress-induced cell death. *J Neurochem* 92: 283–293.
54. Endo H, Nito C, Kamada H, Yu F, Chan PH (2007) Reduction in oxidative stress by superoxide dismutase overexpression attenuates acute brain injury after subarachnoid hemorrhage via activation of Akt/glycogen synthase kinase-3beta survival signaling. *J Cereb Blood Flow Metab* 27:975–982.
55. Handy DE, et al. (2009) Glutathione peroxidase-1 regulates mitochondrial function to modulate redox-dependent cellular responses. *J Biol Chem* 284:11913–11921.
56. Kim YC, Kitaura H, Taira T, Iguchi-Ariga SM, Ariga H (2009) Oxidation of DJ-1-dependent cell transformation through direct binding of DJ-1 to PTEN. *Int J Oncol* 35: 1331–1341.
57. Alessi DR, et al. (1997) Characterization of a 3-phosphoinositide-dependent protein kinase which phosphorylates and activates protein kinase Balpha. *Curr Biol* 7: 261–269.
58. Sarbassov DD, Guertin DA, Ali SM, Sabatini DM (2005) Phosphorylation and regulation of Akt/PKB by the rictor-mTOR complex. *Science* 307:1098–1101.
59. Xiromerisiou G, et al. (2008) Association between AKT1 gene and Parkinson's disease: a protective haplotype. *Neurosci Lett* 436:232–234.
60. Qu D, et al. (2007) Role of Cdk5-mediated phosphorylation of Prx2 in MPTP toxicity and Parkinson's disease. *Neuron* 55:37–52.

Supporting Information

Aleyasin et al. 10.1073/pnas.0914876107

SI Materials and Methods

Cell Culture. Embryonic cortical neurons were harvested from wild type or DJ-1 null littermate embryos as described (1). For survival experiments, at 4 days in vitro (DIV), cotransfection of target plasmids (gene of interest + GFP as a marker of transfected cells) was performed using Lipofectamine 2000 transfection reagent (Invitrogen). The following day, cells were treated with 30 μM H_2O_2 for 3 h. Neurons were fixed with 4% PFA/Picric acid in PBS and survival was assessed by evaluating the nuclear integrity of GFP-positive cells. Alternatively, viral vectors were introduced at time of plating (multiplicity of infection = 60) and left to express for 36 h before being subjected to treatment. In biochemical experiments, at 2 DIV, cells were treated with 100 μM H_2O_2 for various times and cells were harvested for Western blot analysis. Murine embryonic fibroblasts were harvested at the same time as cortical neurons as previously described (2). Cell transformation and immortalization was achieved by transducing a SV40 construct as adapted from Smith et al. (3). Antibodies used for analysis were pAKT (Ser-473, CST), total AKT (CST), β-actin (Sigma), pan-Cadherin (Abcam), DJ-1 (SCBT), HA (CST) and β-galactosidase (Promega).

In Vivo Adenoviral Gene Delivery and MPTP Administration. As described previously, recombinant adenoviruses that are injected into the striatum retrogradely translocate and express on the ipsilateral SNc at the level of the medial terminal nucleus (4). Brain samples from all experimental groups were harvested and analyzed by Western blot and immunohistochemistry to confirm virus expression. Samples were probed for markers of the virus of interest. Ipsilateral sides were compared to their contralateral counterparts. Seven days postvirus injection, mice underwent a subchronic 1-methyl-4-phenyl-1,2,3,6-tetrahydropyridine (MPTP) regimen. For biochemistry, 3 h following the second MPTP injection, brains were quickly removed and SNc were dissected and flash-frozen.

Immunohistochemistry and Assessment of Neuronal Loss in Vivo. After being perfused transcardially, mice brains were fixed and cryoprotected as previously described (5). Midbrain sections containing the SNc and striatal sections were immunostained as previously described (6). At least three sections per brain were chosen at the level of the medial terminal nucleus and TH-positive neurons were counted on sides both ipsilateral and contralateral to the virus injection. Striatal dopamine transporter quantification was performed at 200×. For each picture, 20 samples of striatum and 3 samples of cortex were used for analysis. Relative intensity was measured using National Insitutes of Health ImageJ. Three pictures per animal were used to calculate the average striatal density.

1. Xiang H, et al. (1996) Evidence for p53-mediated modulation of neuronal viability. *J Neurosci* 16:6753–6765.
2. Camarasa M, Brison D, Kimber SJ, Handyside AH (2009) Naturally immortalised mouse embryonic fibroblast lines support human embryonic stem cell growth. *Cloning Stem Cells* 11:453–462.
3. Smith RW, Morganroth J, Mora PT (1970) SV40 virus-induced tumour specific transplantation antigen in cultured mouse cells. *J Nature* 227:141–145.
4. Crocker SJ, et al. (2003) Inhibition of calpains prevents neuronal and behavioral deficits in an MPTP mouse model of Parkinson's disease. *J Neurosci* 23: 4081–4091.
5. Crocker SJ, et al. (2001) c-Jun mediates axotomy-induced dopamine neuron death in vivo. *Proc Natl Acad Sci USA* 98:13385–13390.
6. Mount MP, et al. (2007) Involvement of interferon-gamma in microglial-mediated loss of dopaminergic neurons. *J Neurosci* 27:3328–3337.

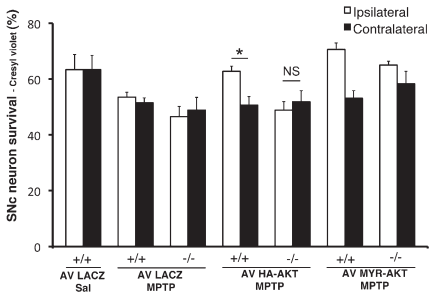

Fig. S1. Cresyl violet staining was performed at the level of the medial terminal nucleus region of the SNc where virus expression was highest. Round nuclei with visible nucleoli were considered alive; shrunken and fragmented nuclei were quantified as dead. Survival was assessed as the ratio of alive over total number of cresyl violet-stained cells. "Ipsi" denotes the side of the brain ipsilateral to the virus injection, whereas "contra" denotes the contralateral side. *, $P < 0.05$; NS, no significant difference.

Content License

The following policy applies to all of PLOS journals, unless otherwise noted.

PLOS applies the Creative Commons Attribution (CC BY) license to works we publish. This license was developed to facilitate open access – namely, free immediate access to, and unrestricted reuse of, original works of all types.

Under this license, authors agree to make articles legally available for reuse, without permission or fees, for virtually any purpose. Anyone may copy, distribute or reuse these articles, as long as the author and original source are properly cited.

Using PLOS Content

No permission is required from the authors or the publishers to reuse or repurpose PLOS content provided the original article is cited. In most cases, appropriate attribution can be provided by simply citing the original article.

Example citation:

Kaltenbach LS et al. (2007) Huntingtin Interacting Proteins Are Genetic Modifiers of Neurodegeneration. *PLOS Genet* 3(5): e82. doi:10.1371/journal.pgen.0030082.

If the item you plan to reuse is not part of a published article (e.g., a featured issue image), then indicate the originator of the work, and the volume, issue, and date of the journal in which the item appeared.

For any reuse or redistribution of a work, you must also make clear the license terms under which the work was published.

Figures, Tables, and Images

Figures, tables, and images are published under the Creative Commons Attribution (CC BY) license.

Data

If any relevant accompanying data is submitted to repositories with stated licensing policies, the policies should not be more restrictive than CC BY.

Submitting Copyrighted or Proprietary Content

Do not submit any figures, photos, tables, or other works that have been previously copyrighted or that contain proprietary data unless you have and can supply written permission from the copyright holder to use that content. This includes:

- maps and satellite images
- slogans and logos
- social media content.

OPEN ACCESS Freely available online

PLOS ONE

Unaltered Striatal Dopamine Release Levels in Young *Parkin* Knockout, *Pink1* Knockout, *DJ-1* Knockout and LRRK2 R1441G Transgenic Mice

Gonzalo Sanchez[1], Rafael K. Varaschin[1], Hansruedi Büeler[2], Paul C. Marcogliese[3], David S. Park[3], Louis-Eric Trudeau[1]*

1 Departments of pharmacology and neurosciences, Central Nervous System Research Group, Faculty of Medicine, Université de Montréal, Montreal, Canada, **2** School of Life Sciences and Technology, Harbin Institute of Technology, Harbin, China, **3** Department of cellular and molecular medicine, Faculty of Medicine, University of Ottawa, Ottawa, Canada

Abstract

Parkinson's disease (PD) is one of the most prevalent neurodegenerative brain diseases; it is accompanied by extensive loss of dopamine (DA) neurons of the substantia nigra that project to the putamen, leading to impaired motor functions. Several genes have been associated with hereditary forms of the disease and transgenic mice have been developed by a number of groups to produce animal models of PD and to explore the basic functions of these genes. Surprisingly, most of the various mouse lines generated such as *Parkin* KO, *Pink1* KO, *DJ-1* KO and *LRRK2* transgenic have been reported to lack degeneration of nigral DA neuron, one of the hallmarks of PD. However, modest impairments of motor behavior have been reported, suggesting the possibility that the models recapitulate at least some of the early stages of PD, including early dysfunction of DA axon terminals. To further evaluate this possibility, here we provide for the first time a systematic comparison of DA release in four different mouse lines, examined at a young age range, prior to potential age-dependent compensations. Using fast scan cyclic voltammetry in striatal sections prepared from young, 6–8 weeks old mice, we examined sub-second DA overflow evoked by single pulses and action potential trains. Unexpectedly, none of the models displayed any dysfunction of DA overflow or reuptake. These results, compatible with the lack of DA neuron loss in these models, suggest that molecular dysfunctions caused by the absence or mutation of these individual genes are not sufficient to perturb the function and survival of mouse DA neurons.

Citation: Sanchez G, Varaschin RK, Büeler H, Marcogliese PC, Park DS, et al. (2014) Unaltered Striatal Dopamine Release Levels in Young *Parkin* Knockout, *Pink1* Knockout, *DJ-1* Knockout and LRRK2 R1441G Transgenic Mice. PLoS ONE 9(4): e94826. doi:10.1371/journal.pone.0094826

Editor: Mark R. Cookson, National Institutes of Health, United States of America

Received November 24, 2013; **Accepted** March 19, 2014; **Published** April 14, 2014

Funding: This work was funded by a Rapid Response award from the Michael J. Fox Foundation for Parkinson's Research to L.-E.T. as well as by a grant to L.-E.T. and D.S.P. from the Brain Canada Foundation and the Krembil Foundation. R.K.V. was supported by a Science without Borders fellowship from the Conselho Nacional de Pesquisa e Desenvolvimento (CNPq), Brazil. The funders had no role in study design, data collection and analysis, decision to publish, or preparation of the manuscript.

Competing Interests: The authors have declared that no competing interests exist.

* E-mail: louis-eric.trudeau@umontreal.ca

Introduction

The main symptoms of Parkinson's disease (PD) including tremor, rigidity and slowness of movements are due in part to the degeneration of dopamine (DA) neurons of the substantia nigra *pars compacta* (SNc) and the associated loss of dopaminergic inputs to the striatum, leading to perturbation of basal ganglia circuits [1]. Although multiple populations of neurons appear to be perturbed at different stages of the disease, DA neurons of the SNc are thought to be particularly vulnerable to environmental and genetic insults, which are believed to interact to cause PD [2]. Both sporadic and familial forms of PD are age-related and thought to implicate cellular dysfunctions including perturbed mitochondrial quality control, impaired reactive oxygen species scavenging and protein aggregation, leading to impaired axonal function and DA release, eventually leading to cell death [3–8].

Several transgenic mouse lines have been generated to study the role of PD-related genes in motor behavior, neuronal survival and function and DA release. Knock out approaches have been widely used for autosomal recessive alleles including *parkin*, *DJ-1* and *Pink1* [9–15], while knockin, knockout and BAC driven overexpression strategies have been used to evaluate the implication of potential gain of function mutant alleles of genes such as *LRRK2* [16], *parkin* [17] or alpha-synuclein [18,19]. A number of molecular perturbations have been shown to result from these gene defects including fragmented and dysfunctional mitochondria [6,7,15,20–22], altered mitophagy [23–27] and altered reactive oxygen species and calcium handling [28–30]. However, studies evaluating the structural integrity of the nigrostriatal DA system in most of these genetically-modified mice failed to identify significant loss of DA neurons or DAergic markers [9,11,16,18,31–34], although increased sensitivity to the neurotoxic effects of MPTP have been reported [10,35–37]. Finally, a number of authors reported mild alterations in locomotor function in Parkin KO, DJ-1 KO, Pink1 KO and LRRK2 transgenic mice [9,31,33,34,38]. Interestingly, a recently described DJ-1 KO mouse backcrossed on a C57/BL6 background showed unilateral loss of DA neurons at 2 months in a subset of animals, suggesting that the penetrance of some of the gene defects examined previously can vary depending on some unknown modifying genes

[39]. Although no major loss of DA neurons occurs in most PD genetic models, if mitochondrial dysfunctions also occur in DA neurons in these mice, this could perturb ATP supply and calcium handling in axon terminals and lead to perturbed DA release, especially since DAergic axon terminals are suspected of having particularly high energy requirements [40] and because of the purported heightened vulnerability of axonal mitochondria [41]. A similar hypothesis has been raised in Alzheimers' disease mouse models, in which synaptic dysfunction in hippocampus has been shown to precede plaque formation and cell loss by many months in some models [42]. A number of studies have thus been performed to study DA release in mouse genetic PD models using electrochemical techniques such as amperometry, fast scan cyclic voltammetry (FSCV) and microdialysis coupled to HPLC. Although only a limited number of studies have been performed, most of them using amperometry, these studies have provided support for the existence of mild impairments in activity-dependent DA overflow in the striatum, attributed either to impaired DA release or increased reuptake: while decreased DA overflow has been reported to occur in Parkin KO mice [12,14], PINK1 KO mice [11] and LRRK2-G2019S [16] or LRRK2-R1441G [34] transgenic mice, evidence for increased DA reuptake has been reported in DJ-1 KO mice [33]. Of note, in most of these studies DA release was triggered by single pulses (or spontaneous firing) and only one has evaluated DA release in response to more energetically-demanding pulse trains [14] (but see Platt et al., for a recent evaluation of DA overflow by pulse trains in A53T alpha-synuclein transgenic mice [43]. Furthermore, in most of these studies, mice were examined at ages of 3 months and older. In this context, it is interesting to note that Oyama and colleagues reported reduced in vivo DA overflow evoked by 50 Hz stimulation trains in 3 and 6 months old male Parkin KO mice, but not in 9 or 12 months old mice [14], arguing for the existence of age-dependent compensations. It would thus be important to conduct a comparative reevaluation of activity-dependent DA overflow in multiple genetic models at ages below 3 months.

In the present study, we used FSCV to provide a comparative evaluation of DA overflow evoked by single pulses, paired pulses and pulse trains in striatal slices prepared from 6–8 weeks-old male transgenic mice, comparing Parkin KO, DJ-1 KO, Pink1 KO and LRRK2 R1441G transgenic mice. Our results fail to detect any significant changes in DA overflow parameters in these mice.

Materials and Methods

Animals

All procedures were approved by the animal ethics committee (CDEA) of the Université de Montréal (protocol number 12–161). All efforts were made to minimize animal suffering. Parkin KO mice (WT n = 11; KO n = 14) were a kind gift of Dr. Alexis Brice [44]. DJ-1 KO mice (WT n = 9; KO n = 10) were a kind gift of Dr. Tak Mak [10]. Pink1 KO mice (WT n = 6; KO n = 6) were described in our previous work [15]. LRRK2 (R1441G) transgenic mice (WT n = 10; KO n = 10) were purchased from The Jackson Laboratory (stock # 009604) [34]. Animals were housed with water and food *ad libitum* and a light cycle of 12/12 (lights on at 6:00 AM).

Brain slice preparation and solutions

Six to eight weeks old male mice were anesthetized with halothane and promptly decapitated. Their brain was quickly removed after gentle opening of the skull and placed in ice-cold artificial cerebrospinal fluid (ACSF) (in mM): 125 NaCl, 26 $NaHCO_3$, 2.5 KCl, 2.4 $CaCl_2$, 1.3 $MgSO_4$, 0.3 KH_2PO_4 and 10 D-Glucose; adjusted to 300 mOsm/kg and saturated with 95% O_2–5% CO_2). 300 µm thick coronal brain slices containing the most rostral portion of the striatum (as defined by Bregma coordinates: from 1.42 to 0.14 mm [45] were prepared with a VT1000S vibratome (Leica Microsystems Inc., Nussloch, Germany) in ice-cold ACSF, and then kept in ACSF at room temperature in a custom-made submerged recovery chamber for at least 1 hour. Slices were transferred to a custom-made submerged recording chamber superfused with ACSF (approximately 1 ml/min, gravity driven) and maintained at 32°C with a TC-324B single channel heater controller (Warner Instrument Inc., Hamden, CT, USA). WT and transgenic littermates were alternatively euthanized in each experiment to account for the different time elapsed between slice preparation and FSCV recordings. The number of experimental observations ("n") refers to the number of slices. One or two slices per animal were used.

All drugs and chemicals were obtained from Sigma-Aldrich Canada (Oakville, ON). A stock solution of nomifensine was prepared in H_2O (3 mM) and stored at 4°C; it was directly diluted into circulating ACSF during the experiment and 5 minutes later electrical stimulation resumed.

Electrochemical recordings

Action potential-induced DA overflow transients were evoked by electrical stimulation with a bipolar electrode (Plastics One, Roanoke, VA) and detected by FSCV using a carbon-fiber electrode placed into the dorsal striatum, approximately 100 µm below the surface. Carbon-fiber electrodes were fabricated as previously described [46]. Briefly, carbon fibers (Cytec Industries Inc., NJ, USA) approximately 5 µm in diameter were aspirated into ethanol-cleaned glass capillaries (1.2 mm 60.68 mm, 4 inches long; A-M Systems, WA, USA). The glass capillaries were then shaped using a P-2000 micropipette puller (Sutter Instruments, Novato, USA), dipped into 90°C epoxy for 30 s (Epo-Tek 301, Epoxy Technology, MASS, USA) and cleaned in hot acetone for 3 s. The electrodes were heated at 100°C for 12 h and 150°C for 5 days. Before and after usage, electrodes were cleaned with isopropyl alcohol to promote greater sensitivity. Carbon fibers were cut using a scalpel blade under direct visualization to obtain maximal basal currents in ACSF between 100 and 180 nA. Electrodes were finally selected for their sensitivity to DA using in vitro calibration with 1 µM DA in ACSF. The potential of the carbon fiber electrode was scanned at a rate of 300 V/s according to a 10 ms triangular voltage waveform (−400 to 1000 mV vs Ag/AgCl reference) with a 100 ms sampling interval using an Axopatch 200B amplifier (Molecular Devices, Sunnyvale, CA). Data were acquired using a DigiData 1440A analog to digital board converter (Molecular Devices) connected to a computer running Clampex 10 (Molecular Devices). Stimulation (1 ms long monophasic pulses of 400 µA) was generated by a S-900 stimulator (Dagan Corporation, Minneapolis, MN) every 2 min to evoke DA release (single pulse, 100 Hz double pulse or 10 Hz 20 pulses train). FSCV was done with the same electrode for at least one pair of slices corresponding to each genotype during the same day of experiment. Recordings in which peak DA overflow showed run-down greater than 20% between the first and the fifth response to single stimulation were considered unstable and not used for further analyses and a new slice was tested.

Rejection frequencies did not differ between WT and Tg groups in any of the 4 different colonies (Parkin WT 2 out of 13 and KO 4 out of 22; DJ-1 all slices reached criterion; Pink1 WT 1 out of 13; LRRK2 WT 2 out of 13 and OE 1 out of 14).

To estimate the rate of DA re-uptake, a single exponential model was fitted to the single pulse evoked DA transients from the peak to the end of the signal [47]; the down stroke of the transient is known to represent the clearance of DA by concurrent reuptake and diffusion. The model had a good fit to the data (goodness of fit medians with 25 and 75% percentiles: 0.9726 (0.8230–0.9867).

Statistical analysis

Statistical comparisons were carried out with Prism 5 (GraphPad software); significance level was set at 0.05. All data samples were tested for normal distribution to choose between parametric versus non parametric statistics and to represent population parameters either as mean ± standard error (SEM) or as median with 25% percentile range; figure legends state the specific test employed in each case.

Results

FSCV was used to record electrically-evoked DA overflow in the dorso-lateral aspect of the striatum in brain slices prepared from 6–8 weeks old KO and matched WT littermate animals. Single pulses, double pulses (two pulses separated by a 10 ms interval) and train stimulation (20 pulses at 10 Hz) were used to trigger DA overflow under conditions of increasing energy demands. DA overflow was also evoked in the same slices under conditions of DA transporter (DAT) blockade (5 μM nomifensine) so as to evaluate changes in DA release that may be masked by DA reuptake and to detect possible changes in DAT function.

6–8 week old mice carrying a deletion of the *parkin* gene were first examined [44]. Single pulses and double pulses were first administered in an alternating fashion every 2 min for a total period of 20 min. After 20 min, train stimulation was administered for an additional 10 min period. All slices were subsequently exposed to nomifensine (5 μM) in the presence of which the complete protocol was carried out a second time. In order to validate our experimental design we first compared maximal DA overflow produced in striatal slice from WT mice by the different stimuli employed. The heat-map in figure 1A depicts the color coded voltammetric current as a function of applied potential and time. Figure 1B shows a DA transient evoked by single pulse stimulation and the fit of the exponential model to estimate DA clearance. A background-subtracted cyclic voltammogram confirms that the detected analyte is DA.

The concentration of DA at the peak of the transients elicited by single pulse stimulation was statistically different from that evoked by double pulses (Fig. 1C). The first single pulse stimulation in WT animals evoked an average DA peak of 0.41±0.28 μM (median ±25% percentile range) (Fig. 1D, left upper panel). The first double pulses stimulation evoked a DA peak of 0.52±0.30 μM (median ±25% percentile range), which was significantly increased in comparison to the single pulse response (n = 11 two tailed Wilcoxon matched pairs test p = 0.0010). Comparing the last single pulse (0.47±0.28 μM, median ±25% percentile range) to the first train stimulation (0.58±0.31 μM, median ±25% percentile range), also yielded a significant difference in peak amplitude (p = 0.0020 n = 11 two-tailed Wilcoxon matched pairs test. Fig 1D, right upper panel).

In the presence of the DA transporter blocker nomifensine, the first single pulse response (0.73±0.54 μM, median ±25% percentile range) was significantly different from the first double pulse response (0.87±0.28 μM, median ±25% percentile range) (two-tailed Wilcoxon matched pairs test p = 0.0010; n = 11. Fig 1D, left lower panel). Likewise, the last single pulse response (0.69±0.48 μM) was statistically different from the first train response (1.51±1.09 μM) (medians ±25% percentile range; two-tailed Wilcoxon matched pairs test p = 0.0010; n = 11. Fig 1D, right lower panel p = 0.0010; n = 11), indicating that the different stimuli were mobilizing different amounts of neurotransmitter vesicles from the releasable pool in axon terminals.

Comparing slices obtained from *parkin* KO and WT littermate controls, a two way repeated measures ANOVA comparing the peaks of DA transients normalized to the first evoked response provided no evidence for any difference between genotypes (n = 11 WT and n = 18 KO; p = 0.5478) (Fig. 2B). An analysis of non-normalized peak DA levels detected in response to single pulses confirmed a lack of difference between genotypes (0.45±0.28 μM n = 11 WT, 0.72±0.45 μM n = 18 KO medians ±25% percentile range; p = 0.2909 two-tailed Mann Whitney test; Fig. 2A, left), compatible with the absence of any impairment in activity-dependent DA release. The half-life of DA overflow responses evoked by single pulses was also not different between genotypes (0.38±0.05 s for WT and 0.48±0.07 s for KO, means ± SEM; student t test P value = 0.3109) (Fig. 2A, right), suggesting that DAT function was not altered.

6–8 week old mice carrying a deletion of the DJ-1 gene (Kim et al., 2005) were next examined using the same stimulation protocol (Fig. 3). A two way repeated measures ANOVA comparing WT and KO data sets collected in the absence or in the presence of nomifensine provided no evidence for any difference between genotypes (n = 10 WT and n = 12 KO; p = 0.9679). An analysis of raw peak DA levels detected in response to single pulses confirmed a lack of difference between genotypes (WT median: 0.72 μM; 25% percentile: 0.49; KO median 0.60 μM; 25% percentile: 0.41; p = 0.2225 Mann Whitney two-tailed test; Fig. 3A, left). The half-life of DA overflow responses evoked by single pulses was also not different between genotypes (WT mean of 0.43±0.04 s; KO 0.42±0.04 s; student t test P value = 0.8562; Fig. 3A, right).

6-8 week old mice carrying a deletion of the Pink1 gene (Akundi et al., 2011) were also examined (Fig. 4). A two way repeated measures ANOVA comparing WT and KO data sets collected in the absence or in the presence of nomifensine provided no evidence for any difference between genotypes (n = 12; p>0.05). An analysis of raw peak DA levels detected in response to single pulses confirmed a lack of difference between genotypes (0.386±0.066 μM and 0.387±0.073 μM, mean ± SEM of WT and KO respectively; n = 12; p>0.05; Fig. 4A, 4B). The half-life of DA overflow responses evoked by single pulses was also not different between genotypes (0.34±0.04 s and 0.37±0.04 s mean ± SEM of WT and KO respectively; n = 12; p>0.05; Fig. 4A).

Finally, 6–8 week old transgenic mice carrying a mutated version of the LRRK2 gene (R1441G) [34] were examined with the same protocol. A two way repeated measures ANOVA comparing WT and homozygous LRRK2 transgenic data sets collected in the absence or in the presence of nomifensine provided no evidence for any difference between genotypes (p = 0.4337; Fig. 5). An analysis of non-normalized DA levels detected in response to single pulses confirmed a lack of difference between genotypes (WT n = 11: 0.84±0.10 μM, mean ± SEM, Tg n = 13: 0.75±0.11 μM, mean ± SEM; two-tailed student t test p = 0.5421; Fig. 5A, 5B).

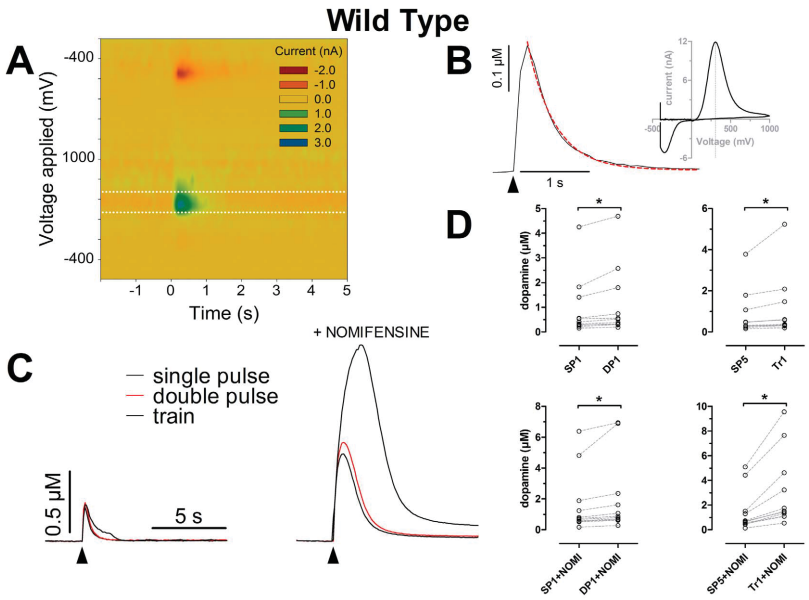

Figure 1. Dopaminergic transmission evaluated using FSCV. Electrically evoked DA transients were detected by FSCV in the dorso-lateral region of slices containing the most rostral part of the striatum. **A** Heat-map plot showing the measured current as a function of time and applied potential. **B** Extracellular DA overflow measured by the carbon fiber electrode at a sampling rate of 10 Hz (black trace) and the exponential fit (red trace) applied from the peak to the end of the signal (half-life: 0.2723 s, 95% confidence intervals: 0.2633 to 0.2821 s; R^2: 0.9646); arrow-head represents the time of stimulation. Inset: voltammogram corresponding to the peak of DA concentration, depicting maximal oxidation current at a potential of 306.12 mV (vertical dotted line). **C** Averaged 5 consecutive responses to either single-pulse, double pulse or train stimulation in normal ACSF (left) or in the presence of 5 µM nomifensine. **D** Scatter plots representing the peak DA concentration elicited by the different stimuli. Significant differences were found between the first single and double pulse stimulation in normal ACSF and between the fifth single pulse and the first train ($p = 0.0010$; $p = 0.0020$, respectively. Two-tailed Wilcoxon matched pairs test). In the presence of 5 µM nomifensine both comparisons yielded significant differences (both $p = 0.0010$. Two-tailed Wilcoxon matched pairs-test). All data presented in this figure were generated from experiments with WT animals belonging to the Parkin colony (slices n = 11; animals n = 11).
doi:10.1371/journal.pone.0094826.g001

The half-life of DA overflow responses evoked by single pulses was also not different between genotypes (0.52±0.08 s, mean ± SEM for WT and 0.49±0.07 s, mean ± SEM for LRRK2 Tg; two-tailed student t test $p = 0.7671$; Fig. 5A).

Discussion

This is the first study to provide a side by side comparative evaluation of striatal DA transmission in some of the main KO or transgenic mouse models of PD (parkin, DJ-1, PINK1 and LRRK2-R1441G Tg mice). Considering the previously reported absence of DA neuron loss in these mice and the possibility of age-dependent compensatory adaptations capable of circumventing primary impairments [3,14,16,48,49], we restricted our analysis to striatal brain slices prepared from young 6–8 week old mice. In light of the multiple studies suggesting mitochondrial dysfunction and related bioenergetic defects due to mutations in these genes [3], we examined activity-dependent DA overflow induced by graded stimuli ranging from single pulses, paired pulses and trains. Using FSCV, a technique allowing direct detection of evoked DA transients with subsecond resolution, we found that paired pulses and stimulation trains induced more extensive DA release, most likely recruiting vesicles from both the readily releasable and reserve pools. We found no evidence of impaired DA axon terminal function in any of the strains tested, thus excluding any robust effect of the genotypes on both DA release and reuptake from nigrostriatal terminals at the age range examined. Subtle impairments of DA transmission cannot be excluded in light of the present results; additional experiments such as input/output analysis, evaluations of the rate of recovery of paired pulse suppression and its dependence on extracellular [Ca^{2+}] could provide further insight into other possible alterations of the release machinery in dopaminergic neurons [50–52].

Our findings are intriguing in light of the previous reports suggesting either reduced release or enhanced reuptake in older genetically-modified mice. For example, evaluating female Parkin KO mice of 8–16 weeks using amperometry, Kitada and colleagues [12] reported reduced DA overflow in response to single pulses. In a separate study, using a different Parkin KO mouse line, Oyama and colleagues reported reduced *in vivo* DA overflow evoked by 50 Hz stimulation trains in 3 and 6 months old male mice, but not in 9 or 12 months old mice [14]. In DJ-1 KO mice, a single study

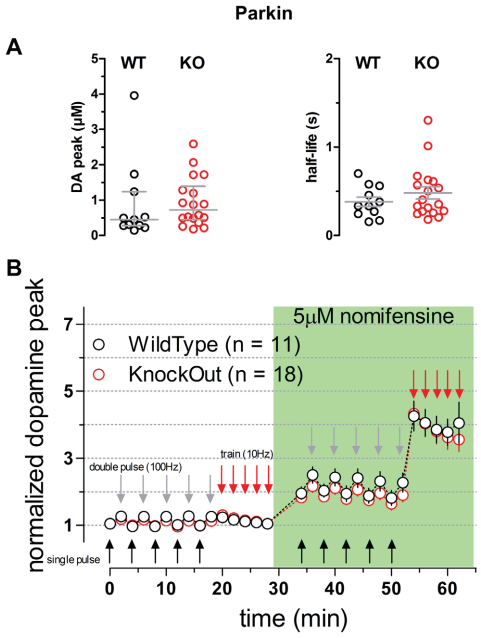

Figure 2. Dopaminergic transmission in striatal slices of parkin WT and KO mice. A Scatter plots illustrating the values of the peak [DA] (left panel) and the half-life (right panel) measured from averaged single-pulse transients. Bars represent median and 25% interquartile range (DA peak) and mean and SEM (half-life), no statistical differences were detected when comparing the WT and KO genotypes (Two-tailed Mann Whitney p = 0.2909 and two-tailed t test p = 0.3109 DA peak and half-life, respectively). **B** Time course of the normalized peak of the evoked responses to single pulses (black arrows) double pulses (gray arrows) and trains (red arrows). Genotypes were compared by means of a 2 Way Repeated Measures ANOVA yielding no significant difference (p = 0.5478; slices n = 11, animals n = 11 WT; slices n = 18, animals n = 14 KO). Green box indicates presence of 5 μM nomifensine into circulating ACSF.
doi:10.1371/journal.pone.0094826.g002

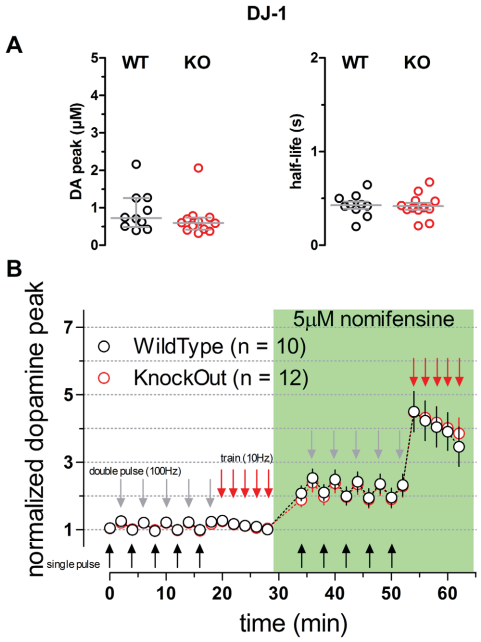

Figure 3. Dopaminergic transmission in striatal slices of DJ-1 WT and KO mice. A Scatter plots illustrating the values of the peak [DA] (left panel) and the half-life (right panel) measured from averaged single-pulse transients. Bars represent median and 25% interquartile range (DA peak) and mean and SEM (half-life), no statistical differences were detected when comparing the WT and KO genotypes (Two-tailed Mann Whitney p = 0.2225 & two-tailed t test p = 0.8562 DA peak and half-life, respectively). **B** Time course of the normalized peak of the evoked responses to single pulses (black arrows) double pulses (gray arrows) and trains (red arrows). Genotypes were compared by means of a 2 Way Repeated Measures ANOVA yielding no significant difference (p = 0.9679; slices n = 10, animals n = 9 WT; slices n = 12, animals n = 10 KO). Green box indicates presence of 5 μM nomifensine into circulating ACSF.
doi:10.1371/journal.pone.0094826.g003

reported unaltered DA release measured by amperometry and evoked by single pulses in 3 months old mice, but functional evidence for increased DAT function [33]. In 2–3 months old Pink1 KO mice, amperometric recordings suggested reduced DA overflow induced by single pulses [11]. In male LRRK2 G2019S transgenic mice, FSCV was used to show reduced DA overflow evoked by single pulses in 12 months old KO mice but not in 6 months old mice [16]. The reason for our inability to detect similar perturbations of DA axon terminal functions in the present study is unclear. The age of the mice could represent an important variable to consider. In the present study, 6–8 weeks old mice were used, which is younger than most of the previous studies. It is thus possible that deficits only appear at older ages. However, the study of Oyama and colleagues [14] illustrates that early deficits can be compensated at later ages, thus arguing for the importance of evaluating younger mice in order to identify primary, early deficits, that could be relevant to understanding cellular dysfunctions that are related to presymptomatic stages of PD. In any case, our findings highlight the fact that deleting Parkin, Pink1 and DJ-1 genes, or overexpressing LRRK2 R1441G does not cause a robust and primary deficit in DA release or DA reuptake in young mice, suggesting that other cellular stressors related to age, environmental toxin exposure or genetic background may be required to lead to robust perturbations of DA overflow. The previous demonstrations that most DJ-1 and Pink1 KO mice do not show loss of DA neurons even at an advanced age (but see [39]), but show increased loss of DA neurons in response to MPTP is compatible with this interpretation [10,37]. Finally, our findings are in agreement with previous studies showing an absence of DA neuron loss in each of the mouse lines examined here, as well as in Parkin/Pink1/DJ-1 triple knockout mice [13].

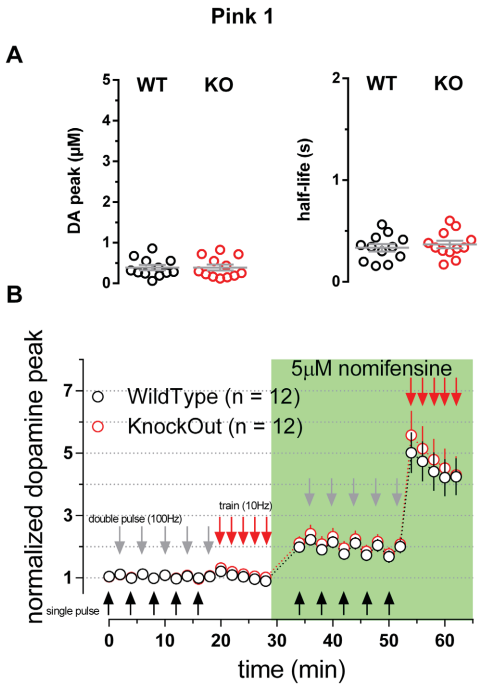

Figure 4. Dopaminergic transmission in striatal slices of Pink1 WT and KO mice. A Scatter plots illustrating the values of the peak [DA] (left panel) and the half-life (right panel) measured from averaged single-pulse transients. Bars represent mean and SEM, no statistical differences were detected when comparing the WT and KO genotypes (two-tailed unpaired t test p = 0.995 and p = 0.556 DA peak and half-life, respectively). **B** Time course of the normalized peak of the evoked responses to single pulses (black arrows) double pulses (gray arrows) and trains (red arrows). Genotypes were compared by means of a 2 Way Repeated Measures ANOVA yielding no significant difference (p = 0.2100; n = 12 WT and n = 12 KO). The green box indicates the presence of 5 µM nomifensine into circulating ACSF.
doi:10.1371/journal.pone.0094826.g004

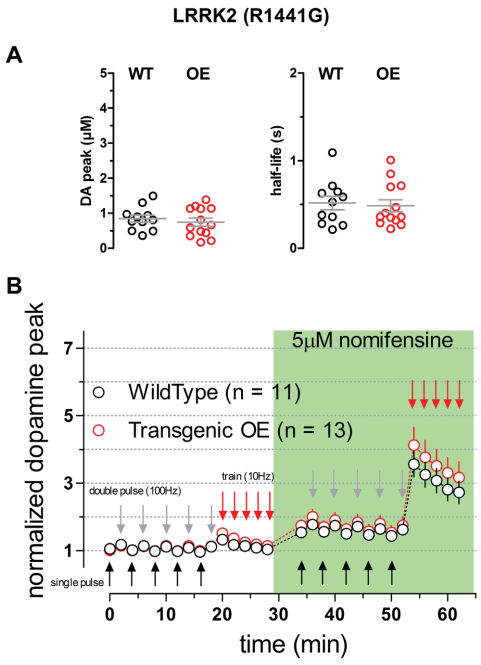

Figure 5. Dopaminergic transmission in striatal slices of WT and LRRK2(R1441G) transgenic mice. A Scatter plots illustrating the values of the peak [DA] (left panel) and the half-life (right panel) measured from averaged single-pulse transients. Bars represent mean and SEM, no statistical differences were detected when comparing the WT and transgenic genotypes (two-tailed unpaired t test p = 0.5421 and p = 0.7671 DA peak and half-life, respectively). **B** Time course of the normalized peak of the evoked responses to single pulses (black arrows) double pulses (gray arrows) and trains (red arrows). Genotypes were compared by means of a 2 Way Repeated Measures ANOVA yielding no significant difference (p = 0.4337; n = 11 WT and n = 13 Tg, animals n = 10 each). The green box indicates the presence of 5 µM nomifensine into circulating ACSF.
doi:10.1371/journal.pone.0094826.g005

Acknowledgments

We thank Marie-Josée Bourque for her help with managing mouse colonies and Dr. Edward Fon (McGill University) for his help in obtaining the *parkin* KO mice and for his help in reviewing the manuscript.

Author Contributions

Conceived and designed the experiments: LT DSP. Performed the experiments: GS RKV. Analyzed the data: GS RKV. Contributed reagents/materials/analysis tools: HB PCM DSP. Wrote the paper: GS RKV PCM HB DSP LT.

References

1. Hornykiewicz O (2008) Basic research on dopamine in Parkinson's disease and the discovery of the nigrostriatal dopamine pathway: the view of an eyewitness. Neurodegener Dis 5: 114–117.
2. Surmeier DJ, Guzman JN, Sanchez J, Schumacker PT (2012) Physiological phenotype and vulnerability in Parkinson's disease. Cold Spring Harb Perspect Med 2: a009290.
3. Dawson TM, Ko HS, Dawson VL (2010) Genetic animal models of Parkinson's disease. Neuron 66: 646–661.
4. Saxena S, Caroni P (2011) Selective neuronal vulnerability in neurodegenerative diseases: from stressor thresholds to degeneration. Neuron 71: 35–48.
5. Cannon JR, Greenamyre JT (2013) Gene-environment interactions in Parkinson's disease: specific evidence in humans and mammalian models. Neurobiol Dis 57: 38–46.
6. Exner N, Lutz AK, Haass C, Winklhofer KF (2012) Mitochondrial dysfunction in Parkinson's disease: molecular mechanisms and pathophysiological consequences. EMBO J 31: 3038–3062.
7. Picconi B, Piccoli G, Calabresi P (2012) Synaptic dysfunction in Parkinson's disease. Adv Exp Med Biol 970: 553–572.
8. Subramaniam SR, Chesselet M-F (2013) Mitochondrial dysfunction and oxidative stress in Parkinson's disease. Prog Neurobiol 106–107: 17–32.
9. Goldberg MS, Fleming SM, Palacino JJ, Cepeda C, Lam HA, et al. (2003) Parkin-deficient mice exhibit nigrostriatal deficits but not loss of dopaminergic neurons. J Biol Chem 278: 43628–43635.
10. Kim RH, Smith PD, Aleyasin H, Hayley S, Mount MP, et al. (2005) Hypersensitivity of DJ-1-deficient mice to 1-methyl-4-phenyl-1,2,3,6-tetrahydropyrindine (MPTP) and oxidative stress. Proc Natl Acad Sci U S 102: 5215–5220.

11. Kitada T, Pisani A, Porter DR, Yamaguchi H, Tscherter A, et al. (2007) Impaired dopamine release and synaptic plasticity in the striatum of PINK1-deficient mice. Proc Natl Acad Sci U S 104: 11441–11446.
12. Kitada T, Pisani A, Karouani M, Haburcak M, Martella G, et al. (2009) Impaired dopamine release and synaptic plasticity in the striatum of parkin-/- mice. J Neurochem 110: 613–621.
13. Kitada T, Tong Y, Gautier CA, Shen J (2009) Absence of nigral degeneration in aged parkin/DJ-1/PINK1 triple knockout mice. J Neurochem 111: 696–702.
14. Oyama G, Yoshimi K, Natori S, Chikaoka Y, Ren Y-R, et al. (2010) Impaired in vivo dopamine release in parkin knockout mice. Brain Res 1352: 214–222. d
15. Akundi RS, Huang Z, Eason J, Pandya JD, Zhi L, et al. (2011) Increased mitochondrial calcium sensitivity and abnormal expression of innate immunity genes precede dopaminergic defects in Pink1-deficient mice. PloS One 6: e16038.
16. Li X, Patel JC, Wang J, Avshalumov MV, Nicholson C, et al. (2010) Enhanced striatal dopamine transmission and motor performance with LRRK2 overexpression in mice is eliminated by familial Parkinson's disease mutation G2019S. J Neurosci Off J Soc Neurosci 30: 1788–1797.
17. Lu X-H, Fleming SM, Meurers B, Ackerson LC, Mortazavi F, et al. (2009) Bacterial artificial chromosome transgenic mice expressing a truncated mutant parkin exhibit age-dependent hypokinetic motor deficits, dopaminergic neuron degeneration, and accumulation of proteinase K-resistant alpha-synuclein. J Neurosci Off J Soc Neurosci 29: 1962–1976.
18. Chesselet M-F, Richter F, Zhu C, Magen I, Watson MB, et al. (2012) A progressive mouse model of Parkinson's disease: the Thy1-aSyn (''Line 61'') mice. Neurother J Am Soc Exp Neurother 9: 297–314.
19. Watson MB, Richter F, Lee SK, Gabby L, Wu J, et al. (2012) Regionally-specific microglial activation in young mice over-expressing human wildtype alpha-synuclein. Exp Neurol 237: 318–334.
20. Clark IE, Dodson MW, Jiang C, Cao JH, Huh JR, et al. (2006) Drosophila pink1 is required for mitochondrial function and interacts genetically with parkin. Nature 441: 1162–1166.
21. Cui M, Tang X, Christian WV, Yoon Y, Tieu K (2010) Perturbations in mitochondrial dynamics induced by human mutant PINK1 can be rescued by the mitochondrial division inhibitor mdivi-1. J Biol Chem 285: 11740–11752.
22. Irrcher I, Aleyasin H, Seifert EL, Hewitt SJ, Chhabra S, et al. (2010) Loss of the Parkinson's Disease-linked gene DJ-1 perturbs mitochondrial dynamics. Hum Mol Genet. 19: 3734–3746.
23. Matsuda N, Sato S, Shiba K, Okatsu K, Saisho K, et al. (2010) PINK1 stabilized by mitochondrial depolarization recruits Parkin to damaged mitochondria and activates latent Parkin for mitophagy. J Cell Biol 189: 211–221.
24. Vives-Bauza C, Zhou C, Huang Y, Cui M, de Vries RL, et al. PINK1-dependent recruitment of Parkin to mitochondria in mitophagy. Proc Natl Acad Sci U S 107: 378–383.
25. Narendra DP, Jin SM, Tanaka A, Suen D-F, Gautier CA, et al. (2010) PINK1 is selectively stabilized on impaired mitochondria to activate Parkin. PLoS Biol 8: e1000298.
26. Chen Y, Dorn GW 2nd (2013) PINK1-phosphorylated mitofusin 2 is a Parkin receptor for culling damaged mitochondria. Science 340: 471–475.
27. Vincow ES, Merrihew G, Thomas RE, Shulman NJ, Beyer RP, et al. (2013) The PINK1-Parkin pathway promotes both mitophagy and selective respiratory chain turnover in vivo. Proc Natl Acad Sci U S A 110: 6400–6405.
28. Gandhi S, Wood-Kaczmar A, Yao Z, Plun-Favreau H, Deas E, et al. (2009) PINK1-associated Parkinson's disease is caused by neuronal vulnerability to calcium-induced cell death. Mol Cell 33: 627–638.
29. Wang H-L, Chou A-H, Wu A-S, Chen S-Y, Weng Y-H, et al. (2011) PARK6 PINK1 mutants are defective in maintaining mitochondrial membrane potential and inhibiting ROS formation of substantia nigra dopaminergic neurons. Biochim Biophys Acta 1812: 674–684.
30. Heeman B, Van den Haute C, Aelvoet S-A, Valsecchi F, Rodenburg RJ, et al. (2011) Depletion of PINK1 affects mitochondrial metabolism, calcium homeostasis and energy maintenance. J Cell Sci 124: 1115–1125.
31. Hinkle KM, Yue M, Behrouz B, Dächsel JC, Lincoln SJ, et al. (2012) LRRK2 knockout mice have an intact dopaminergic system but display alterations in exploratory and motor co-ordination behaviors. Mol Neurodegener 7: 25.
32. Melrose HL, Dächsel JC, Behrouz B, Lincoln SJ, Yue M, et al. (2010) Impaired dopaminergic neurotransmission and microtubule-associated protein tau alterations in human LRRK2 transgenic mice. Neurobiol Dis 40: 503–517.
33. Goldberg MS, Pisani A, Haburcak M, Vortherms TA, Kitada T, et al. (2005) Nigrostriatal dopaminergic deficits and hypokinesia caused by inactivation of the familial Parkinsonism-linked gene DJ-1. Neuron 45: 489–496.
34. Li Y, Liu W, Oo TF, Wang L, Tang Y, et al. (2009) Mutant LRRK2(R1441G) BAC transgenic mice recapitulate cardinal features of Parkinson's disease. Nat Neurosci 12: 826–828.
35. Paterna JC, Leng A, Weber E, Feldon J, Bueler H (2007) DJ-1 and Parkin modulate dopamine-dependent behavior and inhibit MPTP-induced nigral dopamine neuron loss in mice. Mol Ther J Am Soc Gene Ther 15: 698–704.
36. Manning-Bog AB, Caudle WM, Perez XA, Reaney SH, Paletzki R, et al. (2007) Increased vulnerability of nigrostriatal terminals in DJ-1-deficient mice is mediated by the dopamine transporter. Neurobiol Dis 27: 141–150.
37. Haque ME, Thomas KJ, D'Souza C, Callaghan S, Kitada T, et al. (2008) Cytoplasmic Pink1 activity protects neurons from dopaminergic neurotoxin MPTP. Proc Natl Acad Sci U S 105: 1716–1721.
38. Tong Y, Pisani A, Martella G, Karouani M, Yamaguchi H, et al. (2009) R1441C mutation in LRRK2 impairs dopaminergic neurotransmission in mice. Proc Natl Acad Sci U S A 106: 14622–14627.
39. Rousseaux MWC, Marcogliese PC, Qu D, Hewitt SJ, Seang S, et al. (2012) Progressive dopaminergic cell loss with unilateral-to-bilateral progression in a genetic model of Parkinson disease. Proc Natl Acad Sci U S A 109: 15918–15923.
40. Harris JJ, Jolivet R, Attwell D (2012) Synaptic energy use and supply. Neuron 75: 762–777.
41. Court FA, Coleman MP (2012) Mitochondria as a central sensor for axonal degenerative stimuli. Trends Neurosci 35: 364–372.
42. Hsia AY, Masliah E, McConlogue L, Yu GQ, Tatsuno G, et al. (1999) Plaque-independent disruption of neural circuits in Alzheimer's disease mouse models. Proc Natl Acad Sci U S A 96: 3228–3233.
43. Platt NJ, Gispert S, Auburger G, Cragg SJ (2012) Striatal dopamine transmission is subtly modified in human A53Tα-synuclein overexpressing mice. PloS One 7: e36397.
44. Itier JM, Ibanez P, Mena MA, Abbas N, Cohen-Salmon C, et al. (2003) Parkin gene inactivation alters behaviour and dopamine neurotransmission in the mouse. Hum Mol Genet 12: 2277–2291.
45. Paxinos G, Watson C (2005) The rat brain in stereotaxic coordinates. 5th ed. San Diego: Academic Press.
46. Martel P, Leo D, Fulton S, Berard M, Trudeau LE (2011) Role of kv1 potassium channels in regulating dopamine release and presynaptic d2 receptor function. PLoS One 6: e20402.
47. Yorgason JT, España RA, Jones SR (2011) Demon voltammetry and analysis software: analysis of cocaine-induced alterations in dopamine signaling using multiple kinetic measures. J Neurosci Methods 202: 158–164.
48. Marder E (2011) Variability, compensation, and modulation in neurons and circuits. Proc Natl Acad Sci U S A 108 Suppl 3: 15542–15548.
49. Golden JP, Demaro JA 3rd, Knoten A, Hoshi M, Pehek E, et al. (2013) Dopamine-dependent compensation maintains motor behavior in mice with developmental ablation of dopaminergic neurons. J Neurosci Off J Soc Neurosci 33: 17095–17107.
50. Platt NJ, Gispert S, Auburger G, Cragg SJ (2012) Striatal dopamine transmission is subtly modified in human A53Tα-synuclein overexpressing mice. PloS One 7: e36397.
51. Abeliovich A, Schmitz Y, Fariñas I, Choi-Lundberg D, Ho WH, et al. (2000) Mice lacking alpha-synuclein display functional deficits in the nigrostriatal dopamine system. Neuron 25: 239–252.
52. Janezic S, Threlfell S, Dodson PD, Dowie MJ, Taylor TN, et al. (2013) Deficits in dopaminergic transmission precede neuron loss and dysfunction in a new Parkinson model. Proc Natl Acad Sci U S A 110: 4016–4025.

Copyright Permission Policy

These guidelines apply to the reuse of articles, figures, charts and photos in the ***Journal of Biological Chemistry***, ***Molecular & Cellular Proteomics*** and the ***Journal of Lipid Research***.

For authors reusing their own material:

Authors need **NOT** contact the journal to obtain rights to reuse their own material. They are automatically granted permission to do the following:

- Reuse the article in print collections of their own writing.
- Present a work orally in its entirety.
- Use an article in a thesis and/or dissertation.
- Reproduce an article for use in the author's courses. (If the author is employed by an academic institution, that institution also may reproduce the article for teaching purposes.)
- Reuse a figure, photo and/or table in future commercial and noncommercial works.
- Post a copy of the paper in PDF that you submitted via BenchPress.
- Link to the journal site containing the final edited PDFs created by the publisher.

EXCEPTION: If authors select the Author's Choice publishing option:

- The final version of the manuscript will be covered under the Creative Commons Attribution license (CC BY), the most accommodating of licenses offered. Click here for details.
- The final version of the manuscript will be released immediately on the publisher's website and PubMed Central.

Please note that authors must include the following citation when using material that appeared in an ASBMB journal:

"This research was originally published in Journal Name. Author(s). Title. *Journal Name*. Year; Vol:pp–pp. © the American Society for Biochemistry and Molecular Biology."

For other parties using material for noncommercial use:

Other parties are welcome to copy, distribute, transmit and adapt the work — at no cost and without permission — for noncommercial use as long as they attribute the work to the original source using the citation above.

Examples of noncommercial use include:

- Reproducing a figure for educational purposes, such as schoolwork or lecture presentations, with attribution.
- Appending a reprinted article to a Ph.D. dissertation, with attribution.

For other parties using material for commercial use:

Navigate to the article of interest and click the "Request Permissions" button on the middle navigation bar. (See diagram at right.) It will walk you through the steps for obtaining permission for reuse.

Examples of commercial use by parties other than authors include:

- Reproducing a figure in a book published by a commercial publisher.
- Reproducing a figure in a journal article published by a commercial publisher.

Updated March 20, 2013

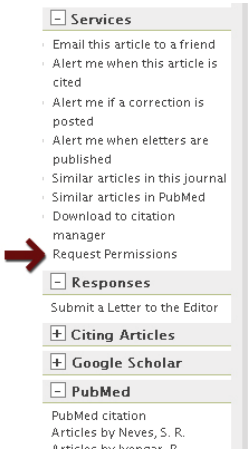

THE JOURNAL OF BIOLOGICAL CHEMISTRY VOL. 290, NO. 51, pp. 30441–30452, December 18, 2015

BAG2 Gene-mediated Regulation of PINK1 Protein Is Critical for Mitochondrial Translocation of PARKIN and Neuronal Survival*

Received for publication, July 9, 2015, and in revised form, November 3, 2015 Published, JBC Papers in Press, November 4, 2015, DOI 10.1074/jbc.M115.677815

Dianbo Qu[‡§], Ali Hage[‡§], Katie Don-Carolis[‡§], En Huang[‡§], Alvin Joselin[‡§], Farzaneh Safarpour[‡§], Paul C. Marcogliese[‡§], Maxime W. C. Rousseaux[‡§], Sarah J. Hewitt[‡§], Tianwen Huang[‡§], Doo-Soon Im[‡§], Steve Callaghan[‡§], Danielle Dewar-Darch[§¶], Daniel Figeys[§¶], Ruth S. Slack[‡§], and David S. Park[‡§1]

From the [‡]Department of Cellular and Molecular Medicine, [§]Brain and Mind Research Institute, and [¶]Ottawa Institute of Systems Biology, University of Ottawa, Ottawa K1H 8M5, Ontario, Canada

Emerging evidence has demonstrated a growing genetic component in Parkinson disease (PD). For instance, loss-of-function mutations in *PINK1* or *PARKIN* can cause autosomal recessive PD. Recently, PINK1 and PARKIN have been implicated in the same signaling pathway to regulate mitochondrial clearance through recruitment of PARKIN by stabilization of PINK1 on the outer membrane of depolarized mitochondria. The precise mechanisms that govern this process remain enigmatic. In this study, we identify Bcl2-associated athanogene 2 (BAG2) as a factor that promotes mitophagy. BAG2 inhibits PINK1 degradation by blocking the ubiquitination pathway. Stabilization of PINK1 by BAG2 triggers PARKIN-mediated mitophagy and protects neurons against 1-methyl-4-phenylpyridinium-induced oxidative stress in an *in vitro* cell model of PD. Collectively, our findings support the notion that BAG2 is an upstream regulator of the PINK1/PARKIN signaling pathway.

Parkinson disease (PD)[2] is the second most common neurodegenerative disorder, characterized by selective loss of the pigmented dopaminergic neurons of the substantia nigra pars compacta (1). Although most PD cases are sporadic in nature (2), mutations in several genes have been linked to familial forms of PD (reviewed in Ref. 3). Indeed, these familial genes serve as important vehicles to study the potential mechanisms of pathogenesis in PD. In this regard, increasing evidence suggests that mitochondrial dysfunction may play a critical role in both the inherited and sporadic forms of PD, although the precise role of mitochondrial dysfunction in PD is unclear (4). Recently, two familial recessive PD genes, PTEN-induced putative kinase 1 (*PINK1*), a mitochondrially localized serine/threonine kinase gene, and *PARKIN*, an E3 ubiquitin ligase gene, have been identified as acting along similar pathways in regulating mitochondrial quality control in mammalian systems (5–8). These findings are supported by genetic studies in *Drosophila* models of PD that show that PARKIN and PINK1 function in a common pathway, with PARKIN being a downstream player of PINK1 (9–11). A third recessive PD gene, *DJ-1*, associated with the regulation of oxidative stress, also regulates PINK1/PARKIN-mediated control of mitochondrial health (12).

PINK1 is normally shuttled to the inner mitochondrial membrane where it is processed by multiple proteases (13). The endogenous role of PINK1 at this site is unknown. However, *PINK1*-deficient cells display altered calcium homeostasis at the mitochondria as well as altered mitochondrial function (14). Processed PINK1 at the inner mitochondrial membrane has also been proposed to be shuttled to the cytosol, where it is degraded by the proteasome (15). However, under conditions of mitochondrial stress such as treatment with the mitochondrial uncoupler carbonyl cyanide *p*-chlorophenylhydrazone (CCCP) or with the complex I inhibitor 1-methyl-4-phenylpyridinium (MPP^+), PINK1 can also regulate mitophagy in a PARKIN-dependent fashion (12, 16–19). The framework by which this mitochondrial control pathway occurs has been generally delineated. PINK1 is stabilized on the outer membranes of damaged/depolarized mitochondria (8). PINK1 then recruits PARKIN to the mitochondria, where it ubiquitinates a number of substrates, including MFN1, MFN2, VDAC1, and MCL1, which, in turn, activates mitophagy (8, 16–22). More recently, recruitment of PARKIN by PINK1 to mitochondria has also been observed in primary neurons in a reactive oxygen species-dependent manner (12, 23). Interestingly, processed cytosolic PINK1 may also interact with cytosolic PARKIN, limiting its translocation to the mitochondria and mitophagy (15). Likewise, in the presence of MG-132, an inhibitor of the proteasome, the level of processed cytosolic PINK1 is increased significantly (24), indicating that turnover of PINK1 is through the proteasomal pathway. Consistent with this, PINK1 has also been shown to be ubiquitinated (25, 26). Interestingly, a recent report has indicated that BAG2 can regulate the ubiquitination of exogenous PINK1 in HEK293 cells (26). Taken together, these findings indicate that the regulation of PINK1 levels and activity is crucial to mitochondrial function and quality at a

* This work was supported by grants from the Canadian Institutes of Health Research, the Parkinson's Society Canada, the Parkinson's Research Consortium Ottawa, the Network of Centers of Excellence in Neurodegeneration, the Heart and Stroke Foundation of Ontario, and the Neuroscience Brain Canada/Krembil Foundation. The authors declare that they have no conflicts of interest with the contents of this article.

[1] To whom correspondence should be addressed: Dept. of Cellular and Molecular Medicine, University of Ottawa, Ottawa K1H 8M5, ON, Canada. Tel.: 613-562-5800, ext. 8816; Fax: 613-864-8816; E-mail: dpark@uottawa.ca.

[2] The abbreviations used are: PD, Parkinson disease; CCCP, carbonyl cyanide *p*-chlorophenylhydrazone; MPP^+, 1-methyl-4-phenylpyridinium; IP, immunoprecipitation; MTT, 3-(4,5-dimethylthiazol-2-yl)-2,5-diphenyltetrazolium bromide; FL, full-length.

number of levels, including regulation of mitochondrial health. The exact mechanism through which PINK1 activity/levels is governed is not fully understood. In addition, the biological consequences of dysregulation of PINK1 processing by ubiquitin-mediated pathways are unclear. In this study, we examined the role of BAG2 and provide evidence that it physically interacts with PINK1 *in vivo* and stabilizes PINK1 from proteasomal degradation, facilitates recruitment of PARKIN to depolarized mitochondria, and protects primary cortical neurons under stress conditions in a PINK1-dependent manner.

Experimental Procedures

Mice—Germ line-deleted *pink1* and *parkin* mice have been described previously in detail, respectively (27, 28). CD1 mice were obtained from Charles River Laboratories. All animal procedures were approved by the University of Ottawa Animal Care Committee, and animals were maintained in strict accordance with the Guidelines for the Use and Treatment of Animals put forth by the Animal Care Council of Canada and endorsed by the Canadian Institutes of Health Research.

Antibodies—The following antibodies were used: rabbit anti-BAG2 (Abcam), rabbit anti-PINK1(494) (Novus), mouse anti-FLAG (Sigma), mouse anti-MYC and rabbit anti-RAF1 (Santa Cruz Biotechnology), mouse anti-V5 and anti-complex I (Invitrogen), mouse anti-ACTIN (Sigma), rabbit anti-TOM20 (Santa Cruz Biotechnology), mouse anti-UBIQUITIN (Abcam), and anti-mouse and anti-rabbit horseradish peroxidase-conjugated secondary antibody (eBiosciences) for IP Western blots and anti-mouse and anti-rabbit horse radish peroxidase-conjugated secondary antibodies (Millipore) for regular Western blots. The secondary antibodies labeled by Alexa Fluor 564 for mouse IgG or Alexa Fluor 633 for rabbit IgG were purchased from Life Technologies. All primary antibodies were used at 1:5000 dilution, except anti-ACTIN, which was diluted 1:50,000 for Western blot analyses. All primary antibodies were diluted 1:200 for immunofluorescent staining. The secondary antibodies for IP were diluted 1:5000. The secondary antibodies for Western blots were diluted 1:10,000. The secondary antibodies for immunofluorescent staining were diluted 1:200.

Constructs—*PINK1-V5* was a gift from Dr. Mark Cookson. The *MYC-BAG2* construct was a gift from Dr. Suneil K. Kalia. *GFP-PARKIN* in the pEGFP vector was a gift from Dr. Edward Fon. *PINK1-FLAG* and *PINK1(K219M)-FLAG* were inserted into the pAdTrack vector by using NotI and HindIII. *CHIP* was cloned into the pCMV-3Tag vector by using BamHI and XhoI. The *HA-HSP90* construct was a gift from William Sessa (Addgene, plasmid no. 22487).

Cell Culture—HEK293T cells were cultured with 10% fetal bovine serum (Sigma) in Dulbecco's modified Eagle's medium (Sigma). Cortical neurons were dissected from embryonic days 14.5–15.5 WT CD1, *pink1* (C57BL/6), or *parkin* C57BL/6 mice. The primary cortical neurons were maintained in Neurobasal medium (Invitrogen) supplemented with B27 with antioxidants (Invitrogen), N2 (Invitrogen), 0.5 mM L-glutamine (Sigma), and penicillin/streptomycin (Invitrogen) as described previously (29, 30).

Proteomic Screen—HEK293T cells were transiently transfected with the *PINK1-FLAG* plasmid. The cells were then cultured in fresh medium (DMEM with 10% FBS) for 24 h. The cells were then harvested, lysed by lysis buffer (20 mM Tris-HCl (pH 7.5), 150 mM NaCl, 1 mM EDTA, 1% Nonidet P-40, 0.5% sodium deoxycholate, 10 μg/ml aprotinin, and 0.2 mM 4-(2-aminoethyl)benzenesulfonyl fluoride hydrochloride (AEBSF) (Calbiochem)), and cleared from cell debris by centrifugation at 20,000 $\times$ *g* for 30 min. The cleared cell lysate was subjected to immunoprecipitation using M2-agarose resin (Sigma-Aldrich) for 1 h. After three washes, the co-precipitated proteins were eluted by 50 mM ammonium bicarbonate containing 400 μM FLAG peptide. The purified proteins were subjected to SDS-PAGE and detected by colloidal Coomassie staining, and then protein bands from qualified lanes were excised from the gel. These proteins were treated with DTT, iodoacetamide (to alkylate the free sulfhydryl groups), and trypsin, and the digested peptides were then purified from the gel and concentrated and analyzed by mass spectrometry. As reported earlier (31), the data were generated using an LCQ Deca mass spectrometer (Thermo Finnigan). Mascot version 1.9 (Matrix Sciences) was used to analyze the obtained spectra by searching against a human protein sequence database with 122,989 entries. The settings to run the Mascot were as follows: search mode, MS/MS Ion; fixed modification, carbamidomethyl on cysteine; variable modification, oxidation on methionine; peptide mass tolerance, 2 Da; fragment mass tolerance, 0.4 Da; maximum missed cleavages, 2; enzyme, trypsin. The Mascot score is the probability of randomness of the match and is reported as $-10\mathrm{LOG}_{10}(P)$, where P is the absolute probability. In other words, a score of 30 means an absolute probability of 10^{-3}.

Assay for Mitochondrial Translocation of PARKIN and Survival—To study PARKIN translocation in HEK293T cells, 2.0×10^5 cells/well were transfected with plasmids by Lipofectamine 2000 according to the instructions of the manufacturer for suspended cells in a 24-well plate. Briefly, *GFP-PARKIN* was transfected with either the empty vector or *MYC-BAG2* at a ratio of 1:3 (0.5 μg total) with 1 μl of Lipofectamine 2000 (Invitrogen). 24 h after transfection, the cells were treated with 10 μM CCCP (Sigma) for up to 2 h to induce oxidative stress as described previously (12). For PARKIN translocation in neurons, the dissected neurons were seeded on poly-D-lysine-coated coverslips in 24-well plates at a density of 1.5×10^5 cells/well. 3 days after plating, the neurons were transfected with plasmids, *GFP-PARKIN* with empty vector or *GFP-PARKIN* with *MYC-BAG2*, at a ratio of 1:3 (0.5 μg total) with 1 μl of Lipofectamine 3000 (Invitrogen). 24 h after transfection, the neurons were treated with 10 μM CCCP (Sigma) for 2 h to depolarize the mitochondrial membrane potential, as described previously (12). After treatment, cells were fixed, permeabilized, and immunostained with the indicated antibodies and visualized by confocal microscopy.

Cell Fractionation—The mitochondrial and cytosolic fractions were isolated as described previously (13). Briefly, collected cells from one 10-cm culture dish were resuspended in 1 ml of BIB buffer (210 mM mannitol, 70 mM sucrose, 5 mM Tris (pH 7.4), 0.2 mM EGTA, 0.1 mM EDTA, 0.1% bovine serum albumin, and protease inhibitor mixture) and homogenized with 50 strokes using a 2-ml glass homogenizer. The superna-

tant, from two centrifugations at 1000 × *g* for 10 min at 4 °C, was subjected to centrifugation at 12,000 × *g* for 10 min at 4 °C to pellet mitochondria. The supernatant was used as the cytosolic fraction. The mitochondrial pellet was resuspended in 1 ml of BIB buffer for sonication to extract mitochondrial proteins. The extracts were subjected to IP.

Survival Assays—For plasmids transfection, the neurons were transfected 3 days after plating. 24 h after transfection, the neurons were treated with 20 μM MPP^+ for 48 h and assessed for survival as described previously (30). Briefly, following fixation, GFP-positive neurons were assessed for nuclear integrity as determined by Hoechst staining. Neurons with punctate or condensed nuclei were assessed as dead. For siRNA transfection, neurons were transfected with 30 pmol/well (24-well plate) siRNA to mouse *bag2*, *pink1*, or *parkin* plus 30 pmol/well of control siRNA to 60 pmol siRNA in total. For co-transfection of siRNAs, neurons were transfected with 30 pmol/well of each using Lipofectamine 2000 as described previously (32). 24 h after transfection, the neurons were treated with 20 μM MPP^+ for 48 h. The 3-(4,5-dimethyl-2-thiazolyl)-2,5-diphenyl-2*H*-tetrazolium bromide (MTT) assay was carried out. Briefly, the neurons were incubated with 10 μl of 5 mg/ml MTT for 4 h. After removal of the medium with MTT, 100 μl of solubilization buffer was applied for extracting the converted MTT for 2 h. The plate was read at 570 nm by a plate reader (30).

Determination of PINK1 Levels and Ubiquitination—For determination of levels of overexpressed PINK1, 0.1 μg of *PINK1-FLAG* was transfected with 0.4 μg of empty vector or *MYC-BAG2* using 1 μl of Lipofectamine 2000 (Invitrogen) onto 2.0×10^5 HEK293T cells/well in 24-well plates. 2 days after transfection, the total cell lysates were collected and subjected to Western blot analysis with anti-FLAG antibody for PINK1 and anti-MYC antibody for MYC-BAG2. For endogenous PINK1, empty vector or *MYC-BAG2* was transfected into HEK293T cells for 2 days, and the total cell lysates were analyzed by Western blot for PINK1. For the ubiquitination assay of overexpressed PINK1, 3.0×10^6 HEK293T cells in a 35-mm dish were transfected with 1 μg of *PINK1-FLAG* in the presence of 3 μg of empty vector or *MYC-BAG2* utilizing 8 μl of Lipofectamine 2000. 2 days after transfection, the total proteins were extracted in 200 μl of radioimmune precipitation assay (RIPA) buffer. After 10 min of boiling and 20 min of centrifugation (20,000 × *g*) at 4 °C, the supernatants were diluted twice with water for IP using 1 μg of anti-FLAG antibody and 30 μl of anti-mouse IgG beads (eBiosciences) for 2 h at 4 °C. The beads were washed four times using a wash buffer containing 20 mM Tris (pH 7.4), 300 mM NaCl, 0.1% SDS, and 1 mM EDTA. Proteins were eluted in 2× SDS sample buffer for separation by 4–15% SDS-PAGE gel (Bio-Rad) and Western blot analyses utilizing an anti-UBIQUITIN antibody. The ubiquitination assay of endogenous PINK1 was performed similar to that described above, except that HEK293T cells were transfected with empty vector or *MYC-BAG2*, and the IP was carried out with anti-PINK1 antibody.

siRNA—All siRNAs were purchased from Santa Cruz Biotechnology. For siRNA transfection, 30 pmol of siRNA/well was transfected with 1 μl of Lipofectamine 2000 in 24 wells, and 150 pmol of siRNA was transfected with 8 μl of Lipofectamine 2000 in a 35-mm dish. Twenty-four hours after siRNA transfection, plasmids were transfected as above for the protein level assay or the ubiquitination level assay.

Statistical Analysis—Statistical significance was determined using paired Student's *t* test for related samples unless stated otherwise. Two-way analysis of variance was used in PARKIN translocation and BAG2-regulated survival to determine the significance between WT and KO under control and treated conditions. All data are presented as mean ± S.E. Significance is denoted as follows: *, $p < 0.05$; **, $p < 0.01$; ***, $p < 0.001$. No significance is denoted by N.S.

Results

Physical Interaction between PINK1 and BAG2—PINK1 plays an important role in regulating dopaminergic loss (5) and in a number of critical biological processes such as mitochondrial quality control. However, the potentially diverse set of processes that regulate PINK1 function or its downstream effectors are not completely known. In particular, the mechanisms that control PINK1 levels and stability, likely important components of PINK1 regulation, are not completely clear. To identify these regulatory mechanisms, we performed a PINK1 interactomic screen to search for proteins associated with PINK1 on the basis of mass spectrometric strategy (31). One particular target of interest in the regulation of PINK1 levels was BAG2, which was identified as an interactor of PINK1 with a Mascot protein score of 99.

BAG2 has been identified previously as a chaperone protein involved in the proteasomal process (33), and we hypothesized that it might be critical for the regulation of PINK1 stability. Accordingly, we pursued this target in more detail. To confirm the physical interaction, we first co-expressed *V5*-tagged *PINK1* (*PINK1-V5*) with *MYC*-tagged *BAG2* (*MYC-BAG2*) in HEK293T cells. Cell extracts were then immunoprecipitated with IgG control or MYC antibody and probed by Western blot analyses for V5 to assess BAG2 interaction. As shown in Fig. 1*A*, *left panel*, interaction was observed with MYC pulldown but not the IgG control. We also performed the reverse interaction studies by immunoprecipitating for V5 and probing by Western blot analyses for MYC. Consistent with our initial results, an interaction between expressed BAG2 and PINK1 was also observed (Fig. 1*A*, *right panel*). As shown in Fig. 1*A*, BAG2 interacts not only with full-length PINK1 but also with processed PINK1. Previous studies have indicated that cleavage of PINK1 is processed in mitochondria (13). Therefore, the mitochondrial and cytosolic fractions from HEK293T cells transfected with *PINK1-FLAG* and *MYC-BAG2* were subjected to immunoprecipitation with MYC antibody to check where the interaction of PINK1 and BAG2 takes place. As shown in Fig. 1*B*, the interaction of PINK1 and BAG2 was observed in both fractions but predominantly in the mitochondrial fraction. Finally, to ensure that this interaction could also be observed with endogenous PINK1 and BAG2, we probed non-transfected HEK 293T cells extract by immunoprecipitating with PINK1 antibody or IgG control and immunoblotting with BAG2 antibody. HEK293T cells were utilized to study endogenous interaction because we can readily detect endogenous PINK1 with available antibodies. This interaction could not be

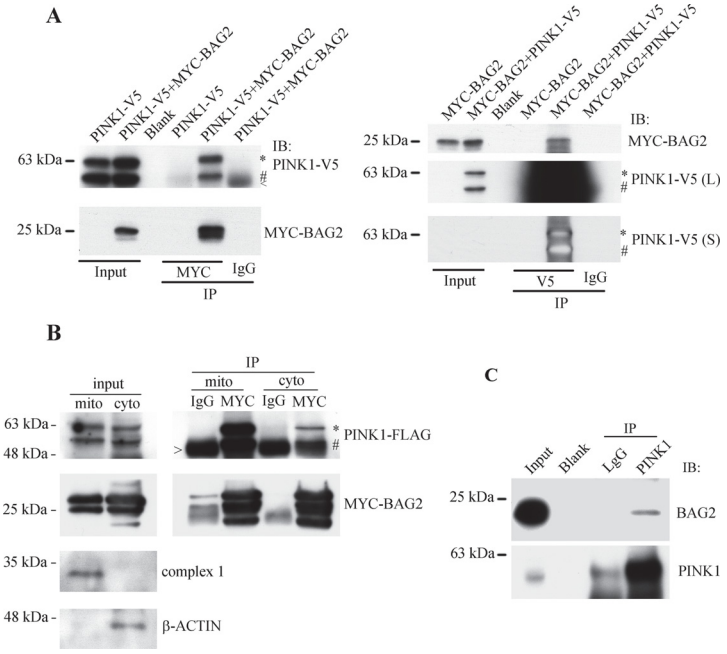

FIGURE 1. **BAG2 forms a complex with PINK1.** *A*, BAG2 interacts with PINK1 upon expression of PINK1 and BAG2 in HEK293T cells by co-immunoprecipitation. The plasmids *PINK1-V5* and *MYC-BAG2* were co-transfected into HEK293T cells. For IP of MYC-BAG2 (*left panel*), transfection of an empty vector and *PINK1-V5* was as one of the controls. For reverse IP of PINK1-V5 (*right panel*), transfection of an empty vector and *MYC-BAG2* was as one of the control. *IB*, immunoblot. *B*, mitochondrial (*mito*) and cytosolic (*cyto*) fractions from HEK293T cells transfected with *PINK1-FLAG* and *MYC-BAG2* were subjected to IP using MYC antibody. The precipitated proteins were separated by SDS-PAGE for Western blots. *C*, the total cell lysate from HEK293T was used for IP of endogenous PINK1. The endogenous BAG2 was detected from IP of PINK1. *Asterisks*, full-length PINK1; #, processed PINK1; > and <, the heavy chain of IgG.

studied in primary neurons because PINK1 antibodies do not readily recognize PINK1 from murine or rat sources. In agreement with our tagged expression interaction studies, we detected endogenous interaction between PINK1 and BAG2, confirming the validity of this interaction (Fig. 1*C*).

BAG2 Modulates PINK1 Levels through Proteasomal Degradation—To explore the functional consequences of this interaction, we first investigated whether the PINK1 level is regulated by BAG2. We initially explored the effects of expression of BAG2 on exogenously expressed tagged PINK1 levels. As shown in Fig. 2*A*, increasing amounts of *MYC-BAG2* plasmid (balanced for amounts by a control vector) was cotransfected with a constant level of *PINK1* plasmid. Increasing expression of BAG2 was confirmed by Western blot analyses. We showed that increased BAG2 expression correlates with increased levels of FLAG-tagged PINK1. Recent studies have suggested that chaperones such as HSP90 also affect PINK1 stability (34, 35). Accordingly, we checked whether expression of HSP90 may affect PINK1 stability in ways similar to that of BAG2 expression. We found that HSP90 failed to affect PINK1 levels, suggesting that BAG2 acts in ways different from that of HSP90 (Fig. 2*B*). We next performed the converse experiment, where we examined siRNA-mediated down-regulation of endogenous BAG2 on the levels of exogenous PINK1. As shown in Fig. 2*A*, *right panel*, *siBAG2*, compared with scrambled siRNA controls, led to significantly reduced levels of FLAG-tagged PINK1. siRNA mediated down-regulation of BAG2 was confirmed by Western blot analyses. Finally, we examined whether overexpression of BAG2 or siRNA-mediated knockdown of BAG2 affects the endogenous PINK1 level in HEK293T cells. Consistent with the effect of BAG2 on exogenous PINK1, expression of BAG2 increased levels of PINK1, whereas siRNA-mediated down-regulation of BAG2 reduced endogenous PINK1 levels (Fig. 2*C*).

Next we explored whether the effect of BAG2 on PINK1 protein levels is mediated via a proteasomal pathway. HEK293T cells were cotransfected with *FLAG*-tagged *PINK1* or *FLAG*-tagged *PINK1(K219M)*, a kinase-dead mutant of *PINK1*, along with *MYC-BAG2* or *PINK1* and siRNA for *BAG2* and treated with the proteasomal inhibitor MG132 to stabilize ubiquitinated PINK1. After immunoprecipitation of PINK1 with anti-FLAG antibody, ubiquitinated PINK1 was detected by Western blot analyses using an anti-ubiquitin antibody. As shown in Fig. 3*A*, *left panel*, overexpression of BAG2 dramatically reduced the level of ubiquitinated PINK1. In this experiment, it is interesting to note that MG132 treatment only slightly elevated the levels of ubiquitinated PINK1 (mostly higher molecular weight species). This may be due to the dif-

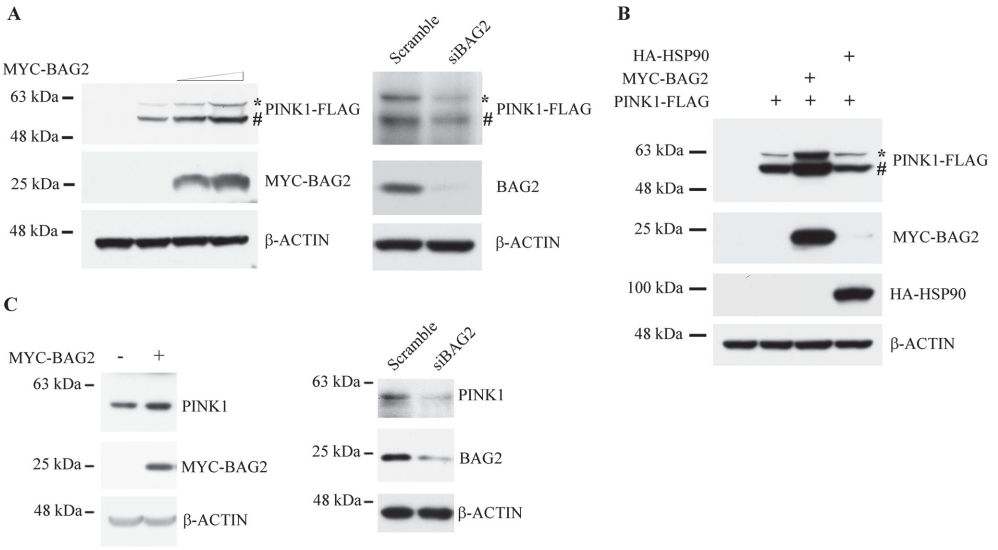

FIGURE 2. **BAG2 regulates PINK1 stability.** *A*, *PINK1-FLAG* and *MYC-BAG2* were coexpressed in HEK293T cells. Expression of PINK1-FLAG or MYC-BAG2 was observed from total cell lysates (*left panel*). *PINK1* was expressed in *BAG2* knockdown HEK293T cells. Overexpressed PINK1-FLAG and MYC-BAG2 (*left panel*) or endogenous BAG2 (*right panel*) were probed from total cell lysates. *B*, *PINK1-FLAG* alone or with *HA-HSP90* or *MYC-BAG2* was transfected into HEK293T cells. 24 h after transfection, the total cell lysates were analyzed by Western blot analysis using the indicated antibodies. *C*, endogenous PINK1 was detected in HEK293T cells with expression of MYC-BAG2 (*left panel*) or knockdown of BAG2 (*right panel*). *Asterisks*, full-length PINK1; #, processed PINK1.

ferential kinetics of turnover of ubiquitinated PINK1 species. Similarly, we also observed that BAG2 dramatically affects the level of ubiquitinated PINK1(K219M) in HEK293T cells along with overexpression of BAG2, as shown in Fig. 3*A*, *center panel*. In contrast, knockdown of BAG2 led to the converse and increased PINK1 ubiquitination, as shown in Fig. 3*A*, *right panel*. In agreement with the effect of BAG2 on exogenously expressed PINK1, overexpression or knockdown of BAG2 decreased or increased the ubiquitinated level of endogenous PINK1, respectively (Fig. 3*B*). Importantly, BAG2 expression did not significantly affect levels of total ubiquitination. BAG2 has been associated with CHIP (C terminus of HSC70-interacting protein) E3 ubiquitination activity. Previous results have shown that BAG2 inhibits CHIP E3 ligase activity (36). Accordingly, we examined whether CHIP may be involved in the BAG2-mediated effects on ubiquitination of PINK1. Expression of CHIP with exogenous PINK1 led to an unexpected increase in total PINK1 and a decrease in ubiquitinated PINK1 (Fig. 3*C*, *left panels*). Conversely, knockdown of CHIP resulted in a decrease in total PINK1 but an increase in ubiquitinated PINK1 (Fig. 3*C*, *right panels*). Although not completely conclusive, this suggests a CHIP independent pathway of regulation of PINK1 by BAG2. Increasing evidence suggests that PINK1 and PARKIN function in the same pathway in regulating mitochondrial functions (9–11, 37, 38). Therefore, we examined whether BAG2 affects the level of PARKIN. Expression of BAG2 did not cause an increase in PARKIN in HEK293T cells (Fig. 3*D*), indicating that BAG2 may regulate PARKIN mitochondrial translocation through PINK1.

BAG2 Regulates PARKIN Translocation to Mitochondria in a PINK1-dependent Manner—We next examined whether BAG2-mediated regulation of PINK1 affects known PINK1-relevant biological outcomes. Loss of mitochondrial membrane potential promotes PINK1/PARKIN-mediated mitophagy in different cell lines as well as primary cultured neurons (8, 12, 16, 18, 19). To test whether the stabilizing effect of BAG2 exerted on PINK1 translates into a functional outcome, we determined whether BAG2 influences PARKIN translocation in a PINK1-dependent manner. To this end, HEK293T cells were cotransfected with *GFP* or *GFP-PARKIN* along with *MYC-BAG2* or siRNA for *BAG2*. 1–2 days after transfection, cells were treated with CCCP to induce mitochondrial depolarization. As shown in Fig. 4, *A* and *B*, expression of exogenous BAG2 significantly increased mitochondrial translocation of PARKIN compared with controls transfected with control vector. Importantly, down-regulation of BAG2 almost significantly diminished PARKIN translocation to mitochondria (Fig. 4, *C* and *D*). In agreement with the results from the immunofluorescence assay, the biochemical fractionation studies confirmed that BAG2 significantly affects the mitochondrial translocation levels of overexpressed or endogenous PARKIN (Fig. 4, *E* and *F*).

Because mitochondrial translocation of PARKIN has also been observed recently in primary neurons (12, 23), we investigated whether BAG2 also affects mitochondrial translocation of PARKIN in primary neurons after mitochondrial depolarization. We found that BAG2 expression significantly increased mitochondrial translocation of PARKIN induced by CCCP. The BAG2-mediated increase in PARKIN translocation was

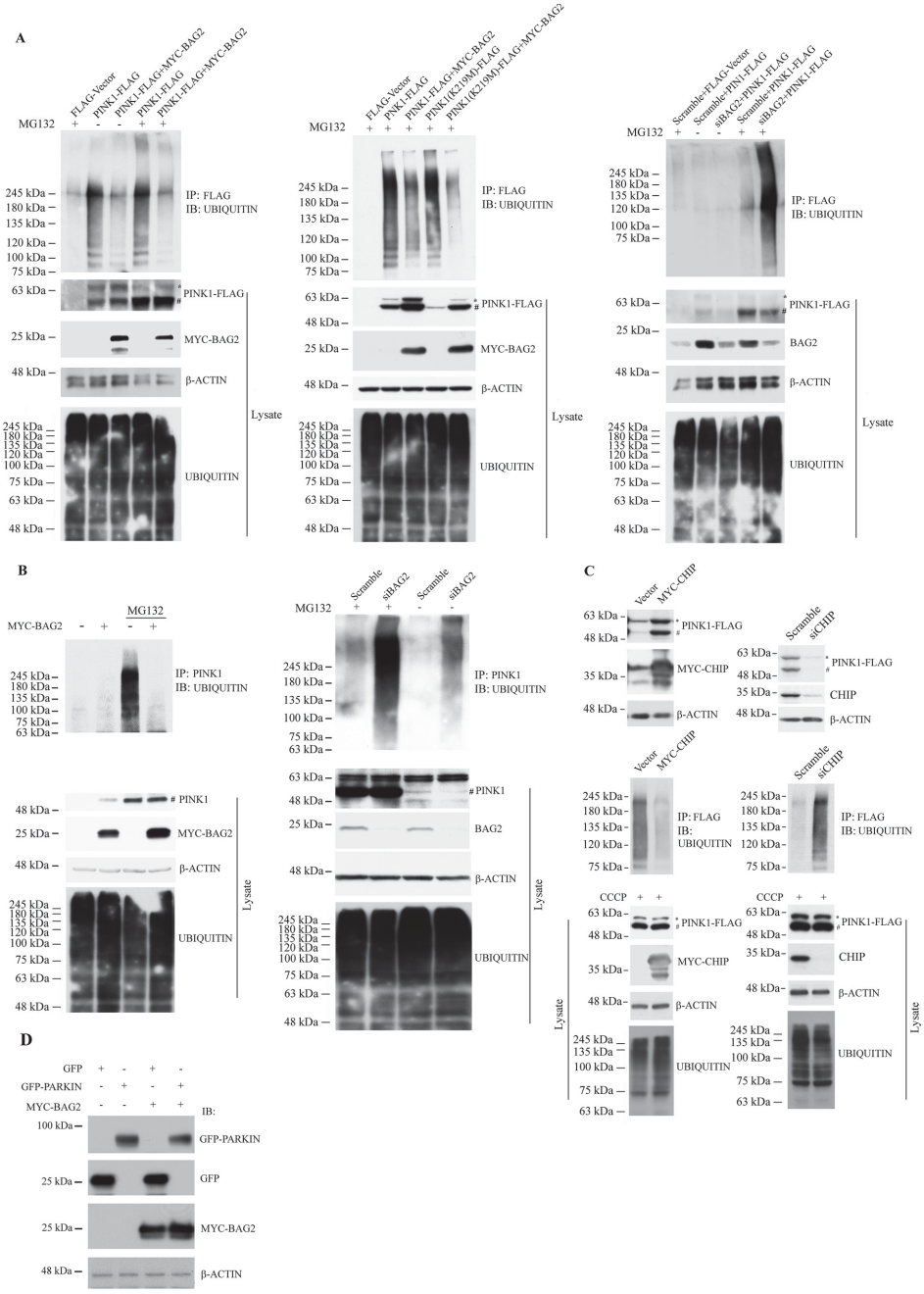

completely dependent on PINK1 because PARKIN translocation did not occur in PINK1-deficient neurons (Fig. 5). As an alternative control, we also examined whether BAG2 might affect levels of PARKIN as an alternative explanation of the observed increase in PARKIN translocation. However, the expression level of BAG2 appeared to have no effect on PARKIN levels (Figs. 3*D* and 4*D*, *top panel*). Taken together, this suggests a model in which BAG2 contributes to increased PARKIN levels on mitochondria through a PINK1-mediated pathway that is independent of any global effect on PARKIN levels.

BAG2 Protects Neuronal Death through a PINK1/PARKIN Pathway—Both PINK1 and PARKIN have also been reported to promote the survival of neurons in response to multiple stresses. Given that overexpression of PINK1 protects cells against reactive oxygen species-induced death (5, 39), and BAG2 promotes PARKIN translocation through PINK1, we investigated whether BAG2 protects neurons against oxidative stress induced by MPP^+ through the PINK1/PARKIN signaling cascade. First, we evaluated whether BAG2 itself protects cultured primary cortical neurons in an MPP^+-induced cell model of PD. As shown in Fig. 6*A*, *top panel*, overexpression of BAG2 protected neurons against MPP^+-induced neuronal death. We have reported previously that acute down-regulation of PINK1 sensitizes neurons to MPP^+ (39). We recapitulate this observation here and also confirm the same with Parkin down-regulation. Interestingly, siRNA-mediated down-regulation of BAG2 led to the same degree of sensitization to death observed with down-regulation of either PARKIN or PINK1. Furthermore, combined down-regulation of BAG2 and PINK1 or PARKIN did not further increase death when compared with either alone. This was also true of co-treatment with siRNA to both *parkin* and *pink1* (Fig. 6*A*, *bottom panel*). We also assessed whether the survival effects of BAG2 expression were dependent on PINK1 or PARKIN. We utilized *pink1*- or *parkin*-deficient neurons obtained from germ line KO animals. In this case, sensitization of death induced by loss of *pink1* or *parkin* alone was not observed, as shown with acute knockdown. This may be due to compensation resulting from long-term *pink1*/*parkin* loss. Indeed, *pink1*/*parkin* KO animals do not show dopaminergic loss (40, 41). Importantly, however, the protection observed in WT cultures with BAG2 expression is abolished with either *parkin* or *pink1* deficiency (Fig. 6*B*). Taken together, these data suggests that BAG2 can increase neuronal viability through a PINK1/PARKIN pathway.

Discussion

Previous work has shown that PINK1 is degraded by the proteasomal pathway (42, 43). After being processed by a number of proteases, PINK1 is degraded by the proteasome (13, 44–46), resulting in a low abundance of PINK1 in healthy cells. Upon loss of mitochondrial membrane potential, accumulated full-length PINK1 (FL-PINK1) on the outer mitochondrial membrane recruits PARKIN to mitochondria, leading to mitochondrial clearance via autophagy (16–19). Some reports have also suggested that cleaved PINK1 can perform the same function (46, 47). These observations indicate that regulation of PINK1 processing and turnover is critical to its biological function. Here we identify BAG2 as one mechanism by which PINK1 levels are regulated and link its effect on PINK1 with its downstream biological effects.

BAG2 is one member of the BAG family. Its members are reported to have a diverse range of effects, particularly on stimulating or interfering with ubiquitin E3 ligase activity (36, 48). For example, BAG1 stimulates chaperone-associated E3 ubiquitin ligase activity, facilitating proteasomal activity for protein degradation. BAG2 inhibits chaperone-associated E3 ubiquitin ligase activity, interrupting protein degradation (36, 48, 49). Beyond regulation of chaperone-associated E3 ubiquitin ligase activity, BAG5 also inhibits the E3 ligase activity of PARKIN through its functional interaction with PARKIN (50).

We provide evidence that BAG2 is central to the regulation of PINK1 stability. First, BAG2 expression increases the levels of both exogenously expressed and endogenous PINK1. Second, BAG2 expression reduces the ubiquitination of expressed or endogenous PINK1. These results are consistent with a recent report showing that expression of BAG2 reduces ubiquitinated PINK1, possibly through blocking ubiquitin ligase activity (26). Importantly, we also show that down-regulation of endogenous BAG2 leads to the converse observations, providing much clearer evidence that BAG2 plays a central role in regulating PINK1 levels. It is interesting that BAG2 appears to regulate the stability of full-length as well as processed forms of PINK1. This is in contrast to MG132 treatment, which stabilizes only the more processed forms. The reason for this is unclear, but BAG2 does interact with both forms of PINK1. We can only speculate that the interaction of BAG2 with full-length PINK1 may slow down the conversion of full-length PINK1 to processed PINK1 by proteases such as PARL (45).

Given the evidence that BAG2 can regulate proteasomal activity through inhibition of CHIP E3 ligase activity, we anticipated that the ubiquitinated level of PINK1 should be up-regulated upon expression of CHIP. However, we observed a decrease in ubiquitinated PINK1 and an increase in PINK1 levels as a result of CHIP expression. Furthermore, we found that HSP90, a chaperone protein important for CHIP-mediated

FIGURE 3. **BAG2 regulates PINK1 degradation in HEK293T cells.** *A*, ubiquitination of overexpressed PINK1 is inhibited by BAG2. *PINK1-FLAG* or *PINK1*(*K219M*)-*FLAG* along with *MYC-BAG2* was coexpressed in HEK293T cells. Transfection of *PINK1-FLAG* and an empty vector was used as a control. Where indicated, transfected cells were treated with MG132 for 2 h. FLAG-tagged PINK1 or its mutant was immunoprecipitated for ubiquitination analysis by Western blot (*left* and *center panels*). *Left panel*, the ubiquitination analysis was performed from HEK293T cells with expression of PINK1-FLAG and overexpression of MYC-BAG2. *Center panel*, the ubiquitination analysis was performed for detection of PINK1-FLAG or PINK1(K219M)-FLAG with expression of MYC-BAG2. *Right panel*, the ubiquitination level of PINK1-FLAG was examined with knockdown of BAG2. *IB*, immunoblot; *Ubi*, ubiquitin. *B*, expression or knockdown of BAG2 affects the ubiquitination of endogenous PINK1. The ubiquitination of PINK1 was detected by IP of PINK1 from HEK293T cells that either expressed MYC-BAG2 (*left panel*) or knockdown of BAG2 (*right panel*). *C*, the level of CHIP affects the PINK1 level through regulating the ubiquitination of PINK1. *PINK1-FLAG* was transfected into HEK293T cells along with overexpression of CHIP or knockdown of CHIP. *Top panels*, 24 h after transfection, the total cell extracts were subjected to Western blots for PINK1-FLAG. *Bottom panels*, 24 h after transfection, cells were treated with MG132 for 2 h for ubiquitination analyses. *D*, BAG2 has no effect on PARKIN level. *MYC-BAG2* and *GFP-PARKIN* were cotransfected into HEK293T cells. 24 h after transfection, cell lysates were subjected to Western blot analysis. *Asterisks*, full-length PINK1; #, processed PINK1.

proteasomal degradation (51), did not influence the level of PINK1, further indicating that CHIP-mediated protein degradation may not have a critical role in PINK1 degradation. Taken together, these results suggest that an alternative E3 ligase other than CHIP is a target for BAG2.

Importantly, we also assessed the biological consequences of BAG2 expression. We first assessed the effects of BAG2 on the Parkin-mediated mitochondrial control pathway. Given that accumulation of PINK1 recruits PARKIN to the outer membrane of mitochondria (8, 16, 18, 19), the stabilization of PINK1

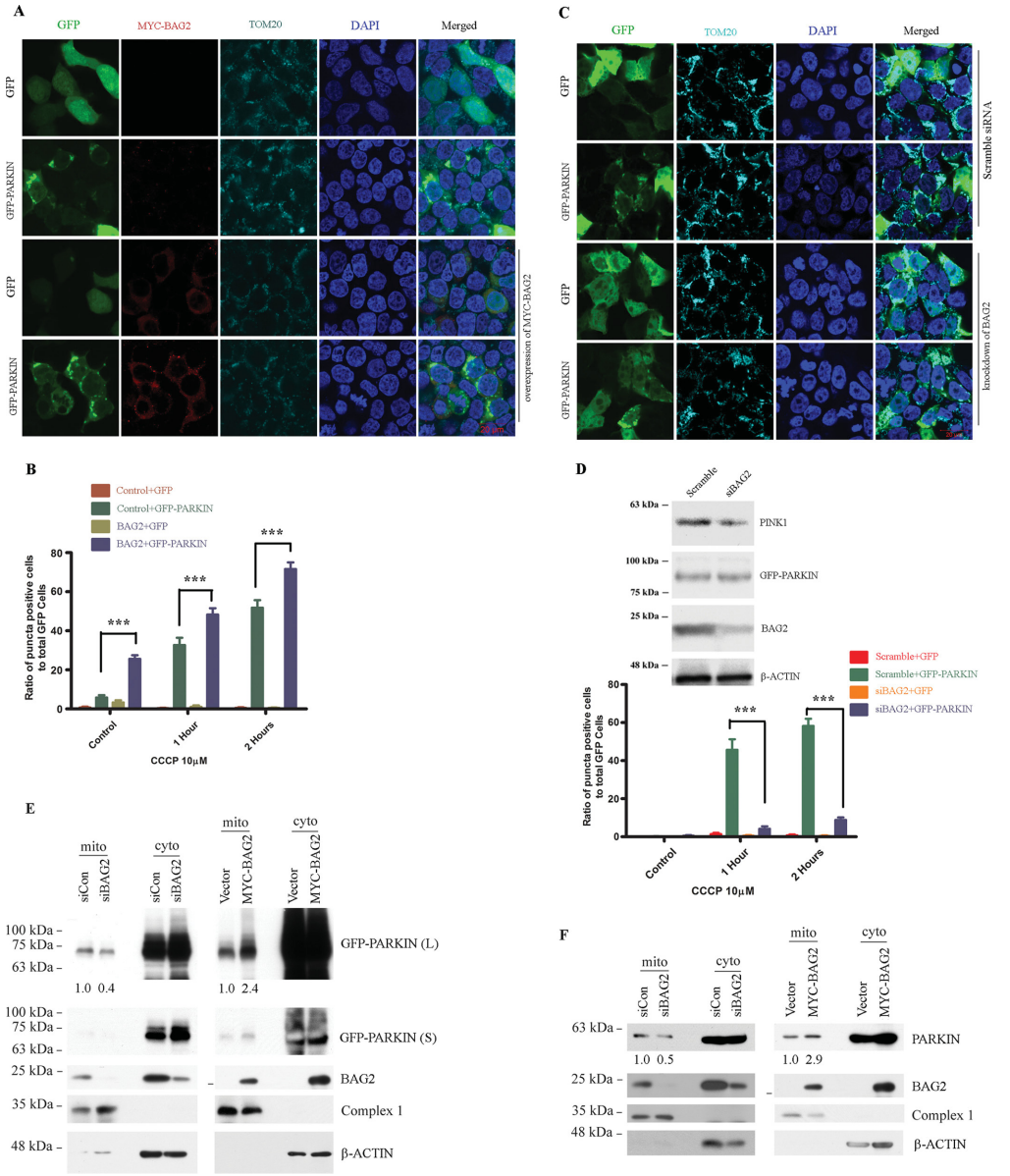

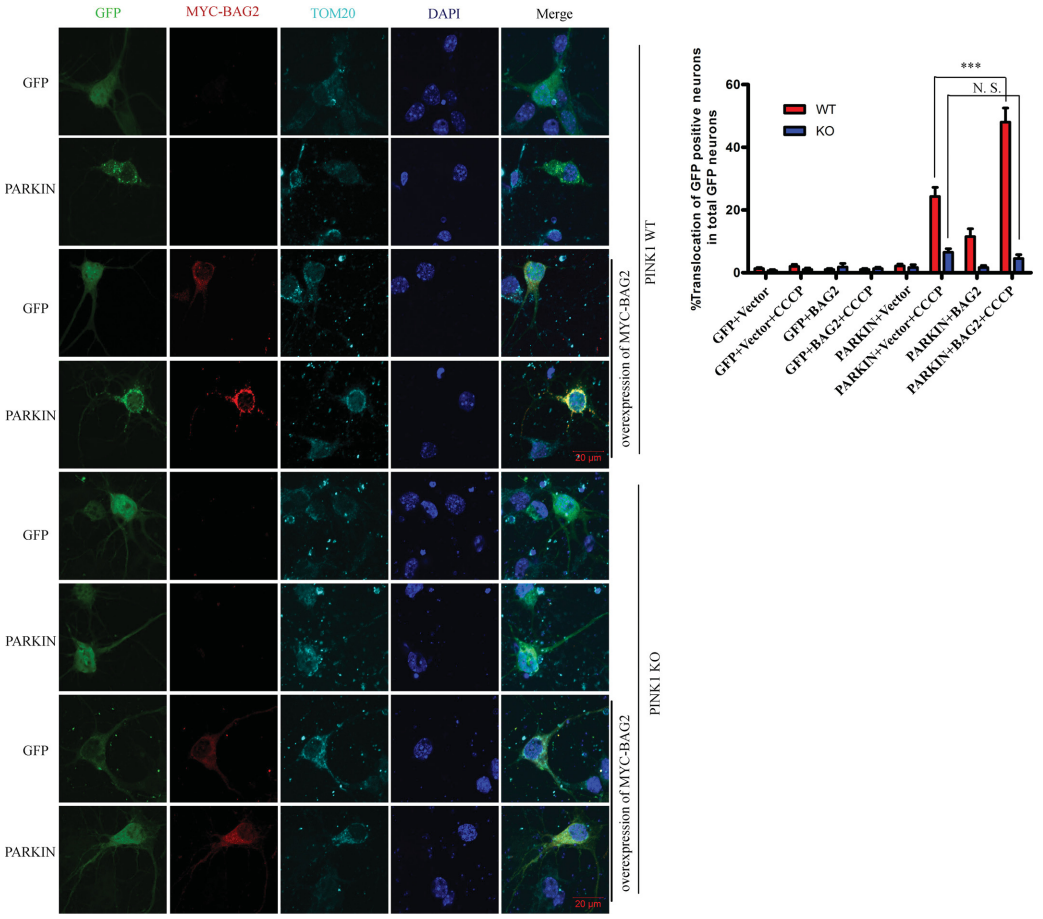

FIGURE 5. **PARKIN translocation is regulated by BAG2 via PINK1 in cortical neurons.** Primary cortical neurons were transfected with plasmids as described in Fig. 4, *A* and *B*. *A*, representative images showing the distribution of GFP or GFP-PARKIN in wild-type or PINK1-deficient neurons with CCCP treatment with and without BAG2 expression, as indicated. Shown are GFP/GFP-PARKIN (*green*), MYC-BAG2 (*red*), mitochondrial TOM20 (*cyan*), and nuclei (*blue*). *B*, the percentage of puncta in GFP-positive neurons colocalized with TOM20 was evaluated by comparing to the total number of GFP-positive neurons. Data are presented as mean ± S.E. of at least three independent experiments. ***, $p < 0.001$; *N.S.*, not significant.

should augment mitochondrial translocation of PARKIN upon depolarization of mitochondria. Indeed, expression of BAG2 significantly increased PARKIN translocation to the mitochondria. In addition, down-regulation of BAG2 by siRNA led to the converse observation, dramatically blocking PARKIN recruitment to the mitochondria. Importantly, we also assessed

FIGURE 4. **BAG2 regulates PARKIN translocation via PINK1.** *A* and *B*, BAG2 expression regulates PARKIN translocation in HEK293T cells. HEK293T cells were cotransfected with empty vector and *GFP*, empty vector and *GFP-PARKIN*, *MYC-BAG2* and *GFP*, or *MYC-BAG2* and *GFP-PARKIN* as indicated. *A*, representative images from transfected cells treated with CCCP for 1 h. Shown are GFP/GFP-PARKIN (*green*), MYC-BAG2 (*red*), mitochondrial TOM20 (*cyan*), and nuclei (*blue*). *B*, cells were left untreated or treated with CCCP as indicated. GFP colocalization with the mitochondrial marker TOM20 was analyzed under fluorescence microscopy. The percentage of GFP/mitochondria colocalization was ascertained as a ratio relative to total GFP-positive cells. ***, $p < 0.001$. *C* and *D*, *GFP-PARKIN* or *GFP* was expressed in HEK293T cell with control siRNA or *BAG2* siRNA. *C*, representative images from transfected cells, as indicated, treated with CCCP for 1 h. *D*, *top panel*, siRNA for *BAG2* significantly knocked down BAG2, resulting in a decrease of PINK1 but no effect on GFP-PARKIN. *Bottom panel*, quantification of mitochondrial PARKIN colocalized with TOM20 with and without CCCP treatment as indicated. Data are presented as mean ± S.E. of at least three independent experiments. ***, $p < 0.001$. *E* and *F*, the mitochondrial translocation of PARKIN was analyzed by Western blots after cellular fractionation. *E*, GFP-PARKIN was expressed in HEK293T cells along with overexpression of MYC-BAG2 or knockdown of BAG2 in the presence of CCCP. *F*, HEK293T cells were transfected with MYC-BAG2 or siRNA for BAG2. After CCCP treatment and cellular fractionation, the level of PARKIN was analyzed by Western blots. GFP-PARKIN or endogenous PARKIN was normalized to mitochondrial marker complex 1 for relative levels of PARKIN and then compared with control siRNA (*siCon*) or vector controls. *mito*, mitochondrial; *cyto*, cytosolic.

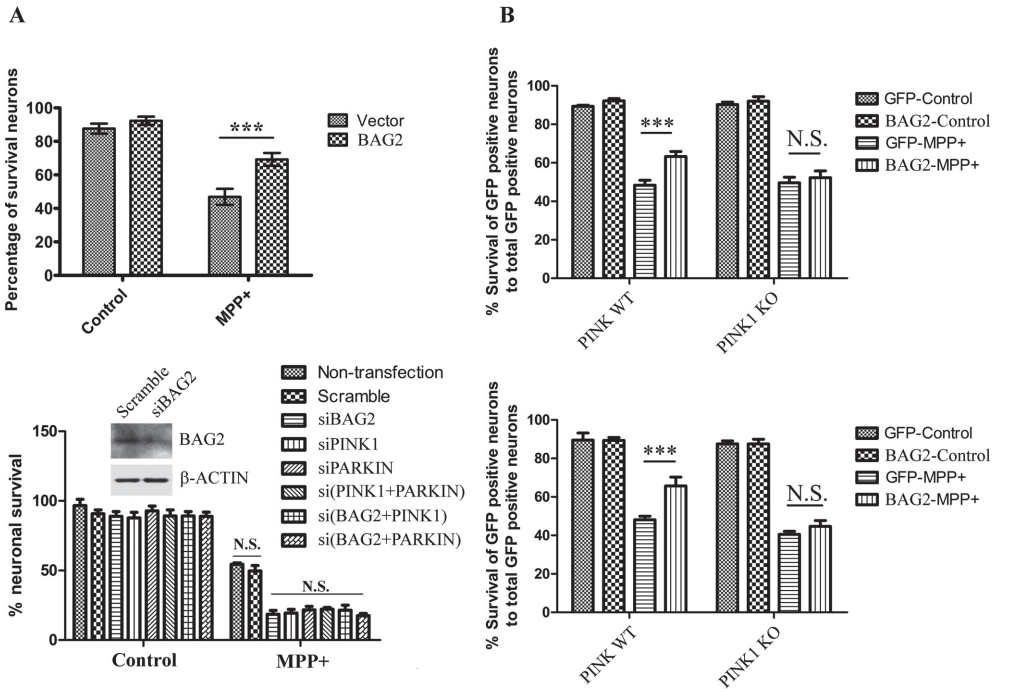

FIGURE 6. **BAG2 protects neurons through PINK1 and PARKIN against MPP^+ challenge.** *A*, expression or Knockdown of BAG2 in cortical neurons modulates neuronal viability. A plasmid expressing *GFP* or *MYC-BAG2* was transfected into primary cortical neurons. *Top panel*, the number of GFP-positive viable neurons with intact nuclei was normalized to the total number of GFP-positive neurons after MPP^+ treatment. *Bottom panel*, the neurons were transfected with control scrambled siRNA, *bag2* siRNA, *pink1* siRNA, *parkin* siRNA, siRNAs for *pink1* and *parkin*, siRNAs for *bag2* and *pink1*, or siRNAs for *bag2* and *parkin*. Viability was evaluated by MTT assay. The knockdown of BAG2 was confirmed by Western blot analyses. ***, $p < 0.001$; *N.S.*, not significant. *B*, BAG2 plays a protective role through the PINK1/PARKIN signaling pathway. *WT*, *pink1*$^{-/-}$, or *parkin*$^{-/-}$ neurons were transfected with empty vector or the *MYC-BAG2* plasmid. Neuronal viability was evaluated by normalizing GFP-positive neurons with intact nuclei to total GFP-positive neurons. Data are presented as mean ± S.E. of at least three independent experiments. ***, $p < 0.001$.

whether BAG2 might affect PARKIN levels, thereby explaining the increased PARKIN translocation observed at the mitochondria. However, expression of BAG2 had no effect on PARKIN levels, suggesting that BAG2 did not affect the mitochondrial control pathway through direct regulation of PARKIN levels. Finally, we also determined whether BAG2 might affect PARKIN translocation through a pathway unrelated to PINK1. In this regard, we assessed whether BAG2 might increase PARKIN translocation in the absence of PINK1. However, BAG2 did not increase PARKIN translocation in PINK1 KO neurons. Taken together, our results indicate that BAG2 increases PINK1 levels, which leads to increased PARKIN translocation, an important reported step in mitochondrial quality control.

We also assessed whether and how BAG2 might affect neuronal survival in the presence of mitochondrial stress. We demonstrate that BAG2 expression is protective in this model, in which down-regulation of BAG2 sensitizes neurons to death. Importantly, we showed that the protective effect is completely dependent on the presence of either PARKIN or PINK1. This latter observation is consistent with the notion that both PINK1 and PARKIN have a protective effect in neurons against mitochondria and oxidative stress (11, 39, 52). Although our data indicate that the protective effects of BAG2 rely on PINK1/PARKIN, it is important to note that we have not established that mitochondrial quality control is the mechanism by which BAG2 regulates survival. Indeed, some data have indicated that PARKIN-regulated mitophagy does not occur in the presence of mitochondrial damage induced by loss of TFAM (transcription factor A, mitochondrial) (53). However, PARKIN/PINK1-mediated pathways of mitochondrial quality control have been noted in neurons upon oxidative/mitochondrial stress (12, 23). Regardless, our data indicate that BAG2 regulates a protective response through a PINK1/PARKIN-mediated pathway. We propose a model in which this occurs through an increase in PINK1 levels.

Finally, previous works have indicated that import of FL-Pink1 into mitochondria is required for processing of FL-PINK1 to cytosolic PINK1 by different proteases (13, 44–46, 54). The constitutive turnover of PINK1 is presumably a critical regulatory machinery to inhibit the PINK1/PARKIN pathway in healthy cells. On the contrary, FL-PINK1 is accumulated on the outer surface of depolarized mitochondria to

trigger the activation of the PINK1/PARKIN pathway (reviewed in Ref. 55). Our findings demonstrate that BAG2 expression results in the accumulation of different forms of PINK1, especially FL-PINK1, suggesting that BAG2 may block the import of FL-PINK1 into mitochondria, resulting in the accumulation of FL-PINK1. Consistent with this model, we observed more mitochondrial translocation of PARKIN in cells with expression of BAG2 even under conditions lacking mitochondrial stress. We propose two possible mechanisms by which BAG2 manipulates the PINK1 level. First, BAG2 may prevent PINK1 degradation by inhibiting the proteasomal pathway. Second, BAG2 interrupts the import of PINK1 to mitochondria, which would result in inhibition of PINK1 processing and increased FL-PINK1. It will be important to distinguish between these possibilities in future studies.

Author Contributions—D. Q., R. S. S., and D. S. P. designed the study. D. Q. and D. S. P. wrote the paper. D. Q., A. H., and K. D. C. performed the majority of the experiments. E. H., A. J., P. C. M., M. W. C. R., D. S. I., F. S., S. J. H., T. H., and S. C. provided technical assistance. D. D. D. and D. F. designed and performed the proteomic screen. All authors reviewed the results and approved the final version of the manuscript.

Acknowledgments—We thank Dr. Jie Shen (Harvard Medical School) for the pink1 knockout mouse strain. We also thank Drs. Mark Cookson (National Institute on Aging, Bethesda, MD), Edward Fon (McGill University, Canada), and Suneil K. Kalia (University of Toronto, Canada) for plasmids.

References

1. Hirsch, E., Graybiel, A. M., and Agid, Y. A. (1988) Melanized dopaminergic neurons are differentially susceptible to degeneration in Parkinson's disease. *Nature* **334,** 345–348
2. Tanner, C. M., Ottman, R., Goldman, S. M., Ellenberg, J., Chan, P., Mayeux, R., and Langston, J. W. (1999) Parkinson disease in twins: an etiologic study. *JAMA* **281,** 341–346
3. Martin, I., Dawson, V. L., and Dawson, T. M. (2011) Recent advances in the genetics of Parkinson's disease. *Annu. Rev. Genomics Hum. Genet.* **12,** 301–325
4. Abou-Sleiman, P. M., Muqit, M. M., and Wood, N. W. (2006) Expanding insights of mitochondrial dysfunction in Parkinson's disease. *Nat. Rev. Neurosci.* **7,** 207–219
5. Valente, E. M., Abou-Sleiman, P. M., Caputo, V., Muqit, M. M., Harvey, K., Gispert, S., Ali, Z., Del Turco, D., Bentivoglio, A. R., Healy, D. G., Albanese, A., Nussbaum, R., González-Maldonado, R., Deller, T., Salvi, S., Cortelli, P., Gilks, W. P., Latchman, D. S., Harvey, R. J., Dallapiccola, B., Auburger, G., and Wood, N. W. (2004) Hereditary early-onset Parkinson's disease caused by mutations in PINK1. *Science* **304,** 1158–1160
6. Deas, E., Plun-Favreau, H., and Wood, N. W. (2009) PINK1 function in health and disease. *EMBO Mol. Med.* **1,** 152–165
7. Narendra, D., Tanaka, A., Suen, D. F., and Youle, R. J. (2009) Parkin-induced mitophagy in the pathogenesis of Parkinson disease. *Autophagy* **5,** 706–708
8. Narendra, D., Tanaka, A., Suen, D. F., and Youle, R. J. (2008) Parkin is recruited selectively to impaired mitochondria and promotes their autophagy. *J. Cell Biol.* **183,** 795–803
9. Yang, Y., Gehrke, S., Imai, Y., Huang, Z., Ouyang, Y., Wang, J. W., Yang, L., Beal, M. F., Vogel, H., and Lu, B. (2006) Mitochondrial pathology and muscle and dopaminergic neuron degeneration caused by inactivation of *Drosophila* Pink1 is rescued by Parkin. *Proc. Natl. Acad. Sci. U.S.A.* **103,** 10793–10798
10. Clark, I. E., Dodson, M. W., Jiang, C., Cao, J. H., Huh, J. R., Seol, J. H., Yoo, S. J., Hay, B. A., and Guo, M. (2006) *Drosophila* pink1 is required for mitochondrial function and interacts genetically with parkin. *Nature* **441,** 1162–1166
11. Park, J., Lee, S. B., Lee, S., Kim, Y., Song, S., Kim, S., Bae, E., Kim, J., Shong, M., Kim, J. M., and Chung, J. (2006) Mitochondrial dysfunction in *Drosophila* PINK1 mutants is complemented by parkin. *Nature* **441,** 1157–1161
12. Joselin, A. P., Hewitt, S. J., Callaghan, S. M., Kim, R. H., Chung, Y. H., Mak, T. W., Shen, J., Slack, R. S., and Park, D. S. (2012) ROS-dependent regulation of Parkin and DJ-1 localization during oxidative stress in neurons. *Hum. Mol. Genet.* **21,** 4888–4903
13. Greene, A. W., Grenier, K., Aguileta, M. A., Muise, S., Farazifard, R., Haque, M. E., McBride, H. M., Park, D. S., and Fon, E. A. (2012) Mitochondrial processing peptidase regulates PINK1 processing, import and Parkin recruitment. *EMBO Rep.* **13,** 378–385
14. Gautier, C. A., Kitada, T., and Shen, J. (2008) Loss of PINK1 causes mitochondrial functional defects and increased sensitivity to oxidative stress. *Proc. Natl. Acad. Sci. U.S.A.* **105,** 11364–11369
15. Fedorowicz, M. A., de Vries-Schneider, R. L., Rüb, C., Becker, D., Huang, Y., Zhou, C., Alessi Wolken, D. M., Voos, W., Liu, Y., and Przedborski, S. (2014) Cytosolic cleaved PINK1 represses Parkin translocation to mitochondria and mitophagy. *EMBO Rep.* **15,** 86–93
16. Vives-Bauza, C., Zhou, C., Huang, Y., Cui, M., de Vries, R. L., Kim, J., May, J., Tocilescu, M. A., Liu, W., Ko, H. S., Magrané, J., Moore, D. J., Dawson, V. L., Grailhe, R., Dawson, T. M., Li, C., Tieu, K., and Przedborski, S. (2010) PINK1-dependent recruitment of Parkin to mitochondria in mitophagy. *Proc. Natl. Acad. Sci. U.S.A.* **107,** 378–383
17. Geisler, S., Holmström, K. M., Skujat, D., Fiesel, F. C., Rothfuss, O. C., Kahle, P. J., and Springer, W. (2010) PINK1/Parkin-mediated mitophagy is dependent on VDAC1 and p62/SQSTM1. *Nat. Cell Biol.* **12,** 119–131
18. Matsuda, N., Sato, S., Shiba, K., Okatsu, K., Saisho, K., Gautier, C. A., Sou, Y. S., Saiki, S., Kawajiri, S., Sato, F., Kimura, M., Komatsu, M., Hattori, N., and Tanaka, K. (2010) PINK1 stabilized by mitochondrial depolarization recruits Parkin to damaged mitochondria and activates latent Parkin for mitophagy. *J. Cell Biol.* **189,** 211–221
19. Narendra, D. P., Jin, S. M., Tanaka, A., Suen, D. F., Gautier, C. A., Shen, J., Cookson, M. R., and Youle, R. J. (2010) PINK1 is selectively stabilized on impaired mitochondria to activate Parkin. *PLoS Biol.* **8,** e1000298
20. Zhang, C., Lee, S., Peng, Y., Bunker, E., Giaime, E., Shen, J., Zhou, Z., and Liu, X. (2014) PINK1 triggers autocatalytic activation of Parkin to specify cell fate decisions. *Curr. Biol.* **24,** 1854–1865
21. Burchell, V. S., Nelson, D. E., Sanchez-Martinez, A., Delgado-Camprubi, M., Ivatt, R. M., Pogson, J. H., Randle, S. J., Wray, S., Lewis, P. A., Houlden, H., Abramov, A. Y., Hardy, J., Wood, N. W., Whitworth, A. J., Laman, H., and Plun-Favreau, H. (2013) The Parkinson's disease-linked proteins Fbxo7 and Parkin interact to mediate mitophagy. *Nat. Neurosci.* **16,** 1257–1265
22. Chen, Y., and Dorn, G. W., 2nd. (2013) PINK1-phosphorylated mitofusin 2 is a Parkin receptor for culling damaged mitochondria. *Science* **340,** 471–475
23. Cai, Q., Zakaria, H. M., Simone, A., and Sheng, Z. H. (2012) Spatial parkin translocation and degradation of damaged mitochondria via mitophagy in live cortical neurons. *Curr. Biol.* **22,** 545–552
24. Zhou, C., Huang, Y., Shao, Y., May, J., Prou, D., Perier, C., Dauer, W., Schon, E. A., and Przedborski, S. (2008) The kinase domain of mitochondrial PINK1 faces the cytoplasm. *Proc. Natl. Acad. Sci. U.S.A.* **105,** 12022–12027
25. Wang, X., Guo, J., Fei, E., Mu, Y., He, S., Che, X., Tan, J., Xia, K., Zhang, Z., Wang, G., and Tang, B. (2014) BAG5 protects against mitochondrial oxidative damage through regulating PINK1 degradation. *PloS ONE* **9,** e86276
26. Che, X., Tang, B., Wang, X., Chen, D., Yan, X., Jiang, H., Shen, L., Xu, Q., Wang, G., and Guo, J. (2013) The BAG2 protein stabilises PINK1 by decreasing its ubiquitination. *Biochem. Biophys. Res. Commun.* **441,** 488–492
27. Kitada, T., Pisani, A., Porter, D. R., Yamaguchi, H., Tscherter, A., Martella, G., Bonsi, P., Zhang, C., Pothos, E. N., and Shen, J. (2007) Impaired dopamine release and synaptic plasticity in the striatum of PINK1-deficient

mice. *Proc. Natl. Acad. Sci. U.S.A.* **104,** 11441–11446
28. Itier, J. M., Ibanez, P., Mena, M. A., Abbas, N., Cohen-Salmon, C., Bohme, G. A., Laville, M., Pratt, J., Corti, O., Pradier, L., Ret, G., Joubert, C., Periquet, M., Araujo, F., Negroni, J., Casarejos, M. J., Canals, S., Solano, R., Serrano, A., Gallego, E., Sanchez, M., Denefle, P., Benavides, J., Tremp, G., Rooney, T. A., Brice, A., and Garcia de Yebenes, J. (2003) Parkin gene inactivation alters behaviour and dopamine neurotransmission in the mouse. *Hum. Mol. Genet.* **12,** 2277–2291
29. Kim, R. H., Smith, P. D., Aleyasin, H., Hayley, S., Mount, M. P., Pownall, S., Wakeham, A., You-Ten, A. J., Kalia, S. K., Horne, P., Westaway, D., Lozano, A. M., Anisman, H., Park, D. S., and Mak, T. W. (2005) Hypersensitivity of DJ-1-deficient mice to 1-methyl-4-phenyl-1,2,3,6-tetrahydropyrindine (MPTP) and oxidative stress. *Proc. Natl. Acad. Sci. U.S.A.* **102,** 5215–5220
30. Qu, D., Rashidian, J., Mount, M. P., Aleyasin, H., Parsanejad, M., Lira, A., Haque, E., Zhang, Y., Callaghan, S., Daigle, M., Rousseaux, M. W., Slack, R. S., Albert, P. R., Vincent, I., Woulfe, J. M., and Park, D. S. (2007) Role of Cdk5-mediated phosphorylation of Prx2 in MPTP toxicity and Parkinson's disease. *Neuron* **55,** 37–52
31. Ewing, R. M., Chu, P., Elisma, F., Li, H., Taylor, P., Climie, S., McBroom-Cerajewski, L., Robinson, M. D., O'Connor, L., Li, M., Taylor, R., Dharsee, M., Ho, Y., Heilbut, A., Moore, L., Zhang, S., Ornatsky, O., Bukhman, Y. V., Ethier, M., Sheng, Y., Vasilescu, J., Abu-Farha, M., Lambert, J. P., Duewel, H. S., Stewart, I. I., Kuehl, B., Hogue, K., Colwill, K., Gladwish, K., Muskat, B., Kinach, R., Adams, S. L., Moran, M. F., Morin, G. B., Topaloglou, T., and Figeys, D. (2007) Large-scale mapping of human protein-protein interactions by mass spectrometry. *Mol. Syst. Biol.* **3,** 89
32. Huang, E., Qu, D., Zhang, Y., Venderova, K., Haque, M. E., Rousseaux, M. W., Slack, R. S., Woulfe, J. M., and Park, D. S. (2010) The role of Cdk5-mediated apurinic/apyrimidinic endonuclease 1 phosphorylation in neuronal death. *Nat. Cell Biol.* **12,** 563–571
33. Takayama, S., Xie, Z., and Reed, J. C. (1999) An evolutionarily conserved family of Hsp70/Hsc70 molecular chaperone regulators. *J. Biol. Chem.* **274,** 781–786
34. Weihofen, A., Ostaszewski, B., Minami, Y., and Selkoe, D. J. (2008) Pink1 Parkinson mutations, the Cdc37/Hsp90 chaperones and Parkin all influence the maturation or subcellular distribution of Pink1. *Hum. Mol. Genet.* **17,** 602–616
35. Moriwaki, Y., Kim, Y. J., Ido, Y., Misawa, H., Kawashima, K., Endo, S., and Takahashi, R. (2008) L347P PINK1 mutant that fails to bind to Hsp90/Cdc37 chaperones is rapidly degraded in a proteasome-dependent manner. *Neurosci. Res.* **61,** 43–48
36. Arndt, V., Daniel, C., Nastainczyk, W., Alberti, S., and Höhfeld, J. (2005) BAG-2 acts as an inhibitor of the chaperone-associated ubiquitin ligase CHIP. *Mol. Biol. Cell* **16,** 5891–5900
37. Geisler, S., Holmström, K. M., Treis, A., Skujat, D., Weber, S. S., Fiesel, F. C., Kahle, P. J., and Springer, W. (2010) The PINK1/Parkin-mediated mitophagy is compromised by PD-associated mutations. *Autophagy* **6,** 871–878
38. Poole, A. C., Thomas, R. E., Andrews, L. A., McBride, H. M., Whitworth, A. J., and Pallanck, L. J. (2008) The PINK1/Parkin pathway regulates mitochondrial morphology. *Proc. Natl. Acad. Sci. U.S.A.* **105,** 1638–1643
39. Haque, M. E., Thomas, K. J., D'Souza, C., Callaghan, S., Kitada, T., Slack, R. S., Fraser, P., Cookson, M. R., Tandon, A., and Park, D. S. (2008) Cytoplasmic Pink1 activity protects neurons from dopaminergic neurotoxin MPTP. *Proc. Natl. Acad. Sci. U.S.A.* **105,** 1716–1721
40. Martella, G., Platania, P., Vita, D., Sciamanna, G., Cuomo, D., Tassone, A., Tscherter, A., Kitada, T., Bonsi, P., Shen, J., and Pisani, A. (2009) Enhanced sensitivity to group II mGlu receptor activation at corticostriatal synapses in mice lacking the familial parkinsonism-linked genes PINK1 or Parkin. *Exp. Neurol.* **215,** 388–396
41. Kitada, T., Tong, Y., Gautier, C. A., and Shen, J. (2009) Absence of nigral degeneration in aged parkin/DJ-1/PINK1 triple knockout mice. *J. Neurochem.* **111,** 696–702
42. Takatori, S., Ito, G., and Iwatsubo, T. (2008) Cytoplasmic localization and proteasomal degradation of N-terminally cleaved form of PINK1. *Neurosci. Lett.* **430,** 13–17
43. Lin, W., and Kang, U. J. (2008) Characterization of PINK1 processing, stability, and subcellular localization. *J. Neurochem.* **106,** 464–474
44. Whitworth, A. J., Lee, J. R., Ho, V. M., Flick, R., Chowdhury, R., and McQuibban, G. A. (2008) Rhomboid-7 and HtrA2/Omi act in a common pathway with the Parkinson's disease factors Pink1 and Parkin. *Dis. Model. Mech.* **1,** 168–174
45. Jin, S. M., Lazarou, M., Wang, C., Kane, L. A., Narendra, D. P., and Youle, R. J. (2010) Mitochondrial membrane potential regulates PINK1 import and proteolytic destabilization by PARL. *J. Cell Biol.* **191,** 933–942
46. Thomas, R. E., Andrews, L. A., Burman, J. L., Lin, W. Y., and Pallanck, L. J. (2014) PINK1-Parkin pathway activity is regulated by degradation of PINK1 in the mitochondrial matrix. *PLoS Genet.* **10,** e1004279
47. Jin, S. M., and Youle, R. J. (2013) The accumulation of misfolded proteins in the mitochondrial matrix is sensed by PINK1 to induce PARK2/Parkin-mediated mitophagy of polarized mitochondria. *Autophagy* **9,** 1750–1757
48. Dai, Q., Qian, S. B., Li, H. H., McDonough, H., Borchers, C., Huang, D., Takayama, S., Younger, J. M., Ren, H. Y., Cyr, D. M., and Patterson, C. (2005) Regulation of the cytoplasmic quality control protein degradation pathway by BAG2. *J. Biol. Chem.* **280,** 38673–38681
49. Demand, J., Alberti, S., Patterson, C., and Höhfeld, J. (2001) Cooperation of a ubiquitin domain protein and an E3 ubiquitin ligase during chaperone/proteasome coupling. *Curr. Biol.* **11,** 1569–1577
50. Kalia, S. K., Lee, S., Smith, P. D., Liu, L., Crocker, S. J., Thorarinsdottir, T. E., Glover, J. R., Fon, E. A., Park, D. S., and Lozano, A. M. (2004) BAG5 inhibits parkin and enhances dopaminergic neuron degeneration. *Neuron* **44,** 931–945
51. Connell, P., Ballinger, C. A., Jiang, J., Wu, Y., Thompson, L. J., Höhfeld, J., and Patterson, C. (2001) The co-chaperone CHIP regulates protein triage decisions mediated by heat-shock proteins. *Nat. Cell Biol.* **3,** 93–96
52. Petrucelli, L., O'Farrell, C., Lockhart, P. J., Baptista, M., Kehoe, K., Vink, L., Choi, P., Wolozin, B., Farrer, M., Hardy, J., and Cookson, M. R. (2002) Parkin protects against the toxicity associated with mutant α-synuclein: proteasome dysfunction selectively affects catecholaminergic neurons. *Neuron* **36,** 1007–1019
53. Sterky, F. H., Lee, S., Wibom, R., Olson, L., and Larsson, N. G. (2011) Impaired mitochondrial transport and Parkin-independent degeneration of respiratory chain-deficient dopamine neurons *in vivo*. *Proc. Natl. Acad. Sci. U.S.A.* **108,** 12937–12942
54. Becker, D., Richter, J., Tocilescu, M. A., Przedborski, S., and Voos, W. (2012) Pink1 kinase and its membrane potential ($\Delta\psi$)-dependent cleavage product both localize to outer mitochondrial membrane by unique targeting mode. *J. Biol. Chem.* **287,** 22969–22987
55. Scarffe, L. A., Stevens, D. A., Dawson, V. L., and Dawson, T. M. (2014) Parkin and PINK1: much more than mitophagy. *Trends Neurosci.* **37,** 315–324

BAG2 Gene-mediated Regulation of PINK1 Protein Is Critical for Mitochondrial Translocation of PARKIN and Neuronal Survival

Dianbo Qu, Ali Hage, Katie Don-Carolis, En Huang, Alvin Joselin, Farzaneh Safarpour, Paul C. Marcogliese, Maxime W. C. Rousseaux, Sarah J. Hewitt, Tianwen Huang, Doo-Soon Im, Steve Callaghan, Danielle Dewar-Darch, Daniel Figeys, Ruth S. Slack and David S. Park

J. Biol. Chem. 2015, 290:30441-30452.
doi: 10.1074/jbc.M115.677815 originally published online November 4, 2015